RUSSIAN ACADEMY OF SCIENCE
FEDERAL AGENCY ON EDUCATION OF RUSSIAN FEDERATION
RUSSIAN NATIONAL COMMISSION FOR UNESCO
COMMITTEE ON SCIENCE AND HIGHER EDUCATION OF THE GOVERNMENT OF SAINT-PETERSBURG
COUNCIL OF RECTORS OF SAINT-PETERSBURG HIGHER EDUCATION ESTABLISHMENTS
SAINT-PETERSBURG STATE UNIVERSITY OF AEROSPACE INSTRUMENTATION (SUAI)
UNESCO CHAIR "DISTANCE EDUCATION IN ENGINEERING" OF SUAI
RUSSIAN SECTION OF THE INTERNATIONAL SOCIETY OF AUTOMATION

ИЗВЕСТИЯ КАФЕДРЫ UNESCO ГУАП «ДИСТАНЦИОННОЕ ИНЖЕНЕРНОЕ ОБРАЗОВАНИЕ»

Сборник статей

Выпуск 7

BULLETIN OF THE UNESCO DEPARTMENT "DISTANCE EDUCATION IN ENGINEERING" OF THE SUAI

Collection of the papers

Issue 7

РОССИЯ, САНКТ-ПЕТЕРБУРГ 2022 SAINT-PETERSBURG, RUSSIA

ББК 378.1
УДК 74.58
И33

И33 Bulletin of the UNESCO department “Distance education in engineering” of the SUAI: Collection of the papers. St. Petersburg, Issue 7. – SPb.: SUAI, 2022. – 178 p.
ISBN 978-5-8088-1709-8

ISA District 12 (The International Society of Automation) and SUAI (Saint-Petersburg State University of Aerospace Instrumentation) have organized the Eighteenth ISA European student paper competition (ESPC-2022). Papers of professors and the best students were included into this issue of the Bulletin of the UNESCO department “Distance education in engineering” of the SUAI. Papers can be interesting for students, post-graduate students, professors and specialists.

ISBN 978-5-8088-1709-8

International Society of Automation
Setting the Standard for Automation™

On behalf of ISA, I would like to congratulate the ISA Russia Section and the St. Petersburg State University of Aerospace Instrumentation (SUAI) on successfully completing the XVIII ISA European Student Paper Competition.

I commend the students who contributed their time, knowledge, and expertise to prepare a paper for this competition. I also want to acknowledge the review committee, including ISA Europe, Middle East, and Africa District student volunteers, who selected the papers for publication and awards.

The students of today are the engineers of tomorrow and it's very important for them to get in contact with other professionals that could guide and mentor them. Our society welcomes their future contributions in helping us achieve our vision of "Creating a
better world through automation", and our mission of "advancing technical competence by connecting the automation community to achieve operational excellence" and the educators provide an essential role by helping prepare students for their future careers.

Whichever career path these students choose, I hope ISA will continue to play an important role in their continuing education and professional development.

I extend my best wishes to all students, lecturers, and committee members in the XVIII ISA European Student Paper Competition.

Sincerely,

Carlos Mandolesi
2022 ISA Society President

3252 S. Miami Blvd. #102, Durham, NC 27703
PHONE: +1 919-549-8411 • FAX: +1 919-549-8288 • EMAIL: info@isa.org • www.isa.org

Setting the Standard for Automation™

Congratulations to ISA Russia Section and the St. Petersburg State University of Aerospace Instrumentation (SUAI) on successfully completing the eighteenth ISA European Student Paper Competition.

The papers published in this volume, selected by the advisory committee, represent the best contributions from among an excellent group of papers. The students who committed their time to prepare a paper should be very proud to be selected for this publication.

Students today are the engineers of tomorrow. We are excited about these talented individuals who will be instrumental in "setting the standard for automation" that will enhance our lifestyle into the future. To the lecturers and professors thank you for your development of today's students.

ISA is focusing on Students Internationally, to identify how ISA can develop career paths for students to choose. I hope ISA will continue to play an important role in your and other student's continuing education and professional development.

I would like to extend my best wishes to all students, lecturers, and attendees at the 2022 ISA European Student Paper Competition.

Sincerely,

Brian J. Curtis
ISA Society President 2018

Standards

Certification

Education & Training

Publishing

Conferences & Exhibits

International Society of Automation
3252 S. Miami Blvd, # 102
Durham, NC 27703

Phone +1 919-549-8411
Email. info@isa.org
www.isa.org

Setting the Standard for Automation™

I would like to extend congratulations to the ISA Russia Section, ISA District 12, and The Saint Petersburg State University of Aerospace Instrumentation (SUAI) for successfully organizing the Eighteenth ISA International Student Paper Competition.

As an educator and a member of ISA for over 40 years, I never tire of the opportunity to share with students the amazing challenges and personal rewards that a career in automation can bring. ISA is proud to have the opportunity to nurture the next generation of automation professionals.

We look forward to continuing the close relationship we have established between ISA, the Russia Section, District 12, and the SUAI. Through distance learning classes on project management and ongoing international online forums, we are developing new understandings in the technical, cultural, and personal arenas.

Congratulations to those who developed papers for this volume and to the advisory committee who had the difficult task of making paper selections.

Sincerely,

Gerald W. Cockrell

Gerald W. Cockrell
ISA Former President

Standards
Certification
Education & Training
Publishing
Conferences & Exhibits

ISA
67 Alexander Drive
P.O. Box 12277
Research Triangle Park, NC 27709
PHONE (919) 549-8411
FAX (919) 549-8288
E-MAIL info@isa.org
www.isa.org

AUTOMATION OF VISUAL MONITORING OF LAYER-BY-LAYER SYNTHESIS PROCESSES USING ARTIFICIAL INTELLIGENCE

Alexandr Chabanenko

Saint-Petersburg State University of Aerospace Instrumentation,
Saint-Petersburg, Russia
E-mail: Chabalexandr@gmail.com

Annotation
Computer vision is designed to solve problems associated with the collection and analysis of visual information in various areas of production, while partially or completely replacing a person. Questions related to computer vision were popular back in the 60s of the XX century, but now they are in a special stage of their development. Since recently it has become possible to make available computers and software to a large number of users to process images and create software tools based on the idea of computer vision. Computer vision is understood as the theory and technology of creating artificial computer systems that detect, classify and track objects. They obtain information from images, which can be represented by a specific video sequence, images from various cameras or three-dimensional data, scanned images, etc.

The purpose of computer vision is to generate useful inferences about objects and scenes in the real world based on the analysis of images obtained using sensors.

Modern quality assurance systems tend to focus less on acceptance sampling and try to focus their efforts on statistical process control and designed experiments. Acceptance sampling tends to reinforce the idea of quality against specifications and has no feedback either in the manufacturing process or in engineering design or development that would necessarily lead to quality improvement.

For designing and predicting quality, it is possible to use artificial intelligence in video monitoring with the quality of additive manufacturing.

An artificial intelligence (AI) system is a software system that simulates the process of human thinking on a computer. To create such a system, it is necessary to study the very process of thinking of a person who solves certain problems or makes decisions in a specific area, highlight the main steps of this process and develop software tools that reproduce them on a computer. Therefore, AI methods suggest a simple structural approach to the development of complex software decision-making systems.

The third area of quality control and improvement is sample acceptance. It is closely related to product inspection and testing, which is one of the earliest aspects of quality control, long before statistical quality improvement methodology was developed. Verification can occur at many points in the process. Receiving sampling, defined as the inspection and classification of a sample of units selected at random from a larger lot or lot, and the final decision to dispose of the lot, generally occurs at two points: the incoming raw materials or components, or the final production. In the acceptance of finished products, it is also possible to use artificial intelligence mechanisms to visualize inconsistencies (Figure 2).

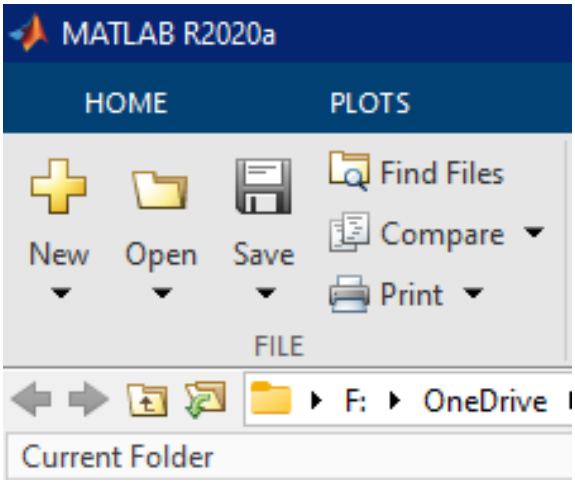

Figure 1. Program Creation Window

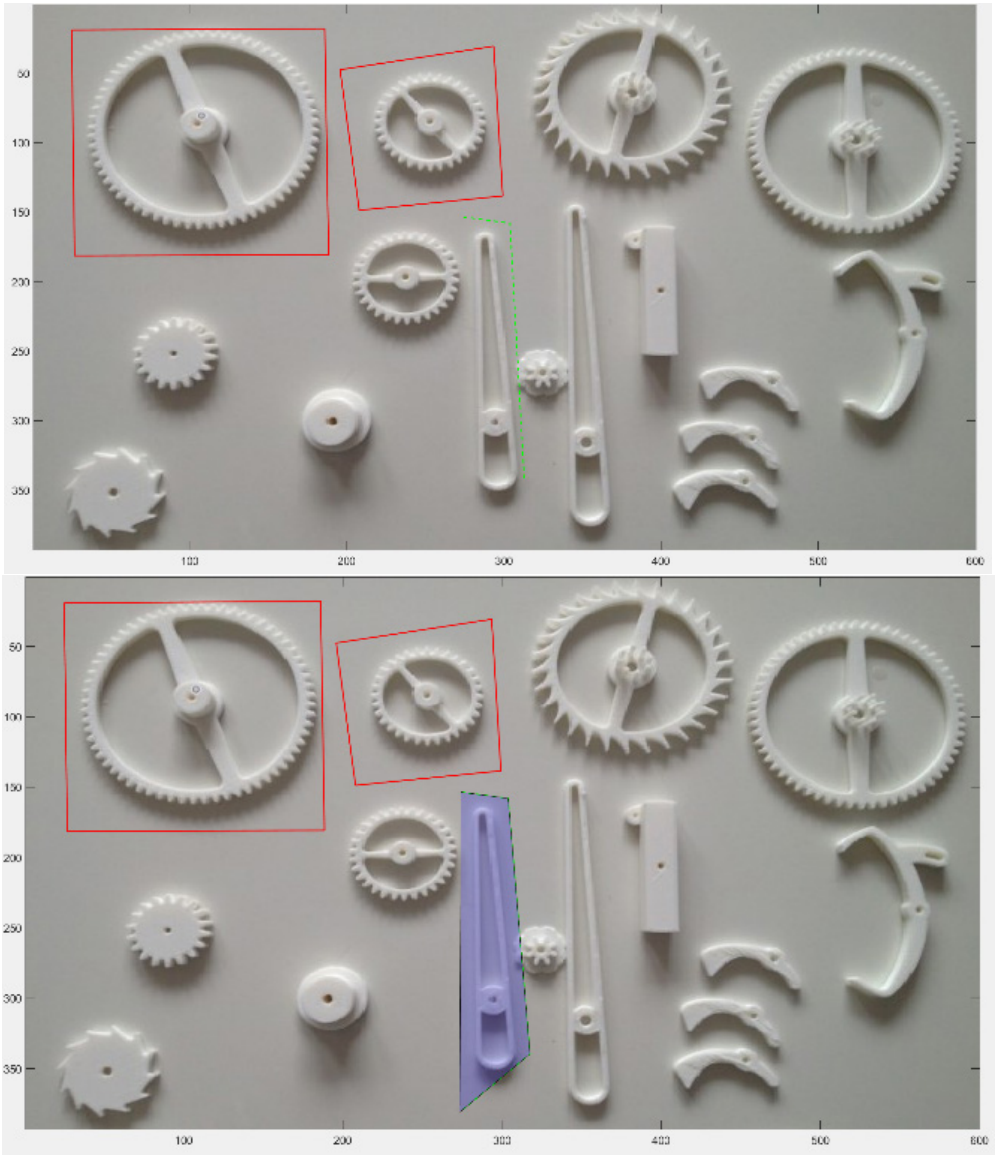

Figure 2. Additive Manufacturing Parts Detector Video

To organize monitoring, the computer mathematics program Matlab, Figure 1, is used.

IP - video surveillance is one of the new and most promising areas in monitoring and control systems. Network cameras (ip - cameras) and video servers are used to build video surveillance systems both at territorially large and small objects. IP cameras are indispensable for controlling and monitoring remote locations where there is a need to use unattended equipment. To ensure the safety and effective management of facilities and the company as a whole, it is necessary to see the whole picture. And respond to changes in the situation in real time and in the shortest possible time.

Artificial intelligence in video surveillance places increased demands on the installation of cameras.

To install video surveillance, it is possible to use a program for monitoring objects that fall into the focus of the camera.

The "smart" camera creates a dynamic 3D model of the room and all objects in it. Any change in the environment (movement, displacement, the appearance of a new object) is recorded and reflected in the model. Machine learning allows the camera to classify both objects and their actions.

The longer the camera works, the better it understands what is in front of it.

Commercial solutions are expensive. Closed source products are generally designed to run on operating systems such as Windows, they do not take into account the specific requirements that the end user of the system may have.

Open-source software products are poorly documented and not designed to work in large industrial facilities.

In view of this, it is advisable to develop our own intelligent surveillance systems.

Able to independently analyze the image depending on the needs of production.

According to GOST R 27.002–2015, an imperfect state (flaw) is a state of an object in which it does not meet at least one of the requirements established in the documentation for it. Non-compliance with at least one of the requirements can be defined as a state in which the value of at least one parameter of an object does not meet the requirements of the documentation for this object.

According to GOST R ISO 13372-2013, a fault is a state of an object when one of its elements or a group of elements shows signs of degradation or malfunction, which can lead to machine failure.

1 - A malfunction is often the result of a failure but may occur in its absence.

2 - The state of the object is not considered as faulty if it arose due to planned procedures or lack of external resources.

The $_{Qi}(t)$ function is called the failure risk (accident, hazard, or production) function. The reliability and risk functions have corresponding densities.

MTBF is the ratio of the MTBF of the object being restored to the mathematical expectation of the number of its failures during this MTBF. Statistically, the MTBF is determined by the ratio of the total operating time of the objects being restored to the total number of failures of these objects:

$$T = \sum_{i=t}^{N} t_i$$

Table 1

Registration of levels of quality indicators of control effects on polymers

Designation	Name of the control action	Value for a level		
		1	2	3
ASA-plastic	Polymer temperature	160ºC	200ºC	240ºC
ABS EG plastic	Polymer temperature	210ºC	225ºC	250ºC
ABS HG plastic	Polymer temperature	220ºC	212ºC	260ºC
ABS MP Plastic	Polymer temperature	200ºC	210ºC	220ºC
ABS 2020-plastic	Polymer temperature	190ºC	200ºC	260ºC

```
>> calibrateCamera
ans =
      1440        2560           3
  1.0e+03 *
   1.1493    0.4790
  1.0e+03 *
   1.1636    0.7516
  1.0e+03 *
   1.3974    0.8124
  1.0e+03 *
   1.5364    0.4740
  1.0e+03 *
   1.7455    0.3193
  1.0e+03 *
   1.7208    0.5247
  1.0e+03 *
   1.8663    0.5449
  1.0e+03 *
   1.9013    0.3345
 521.9815  543.6690
 527.1768  697.0493
 638.8765  659.0211
 619.3940  511.9789
  1.0e+03 *
   1.0402    0.9417
```

1.0e+03 *
1.1532 0.8555
1.0e+03 *
1.3636 0.9316
1.0e+03 *
1.2571 1.0456
1.0e+03 *
1.4493 0.4372
1.0e+03 *
1.4597 0.2978
1.0e+03 *
1.5805 0.3218
1.0e+03 *
1.5688 0.4854

Deviation from the specified temperature conditions will lead to a deviation from the specified geometric shape, which will be noticed by intelligent video monitoring.

Video monitoring of additive manufacturing will allow predicting the number of inconsistencies and allow you to predict printing deviations in advance.

Figure 3. Additive Manufacturing Products

The more small elements in the product, the more complex the video monitoring.
For video monitoring, cameras from HD resolution Figure 4 are suitable.

Figure 4. Typical camera for video monitoring of deviations in the technological process

The red stroke represents the position of the object in the scene and its designation 5.

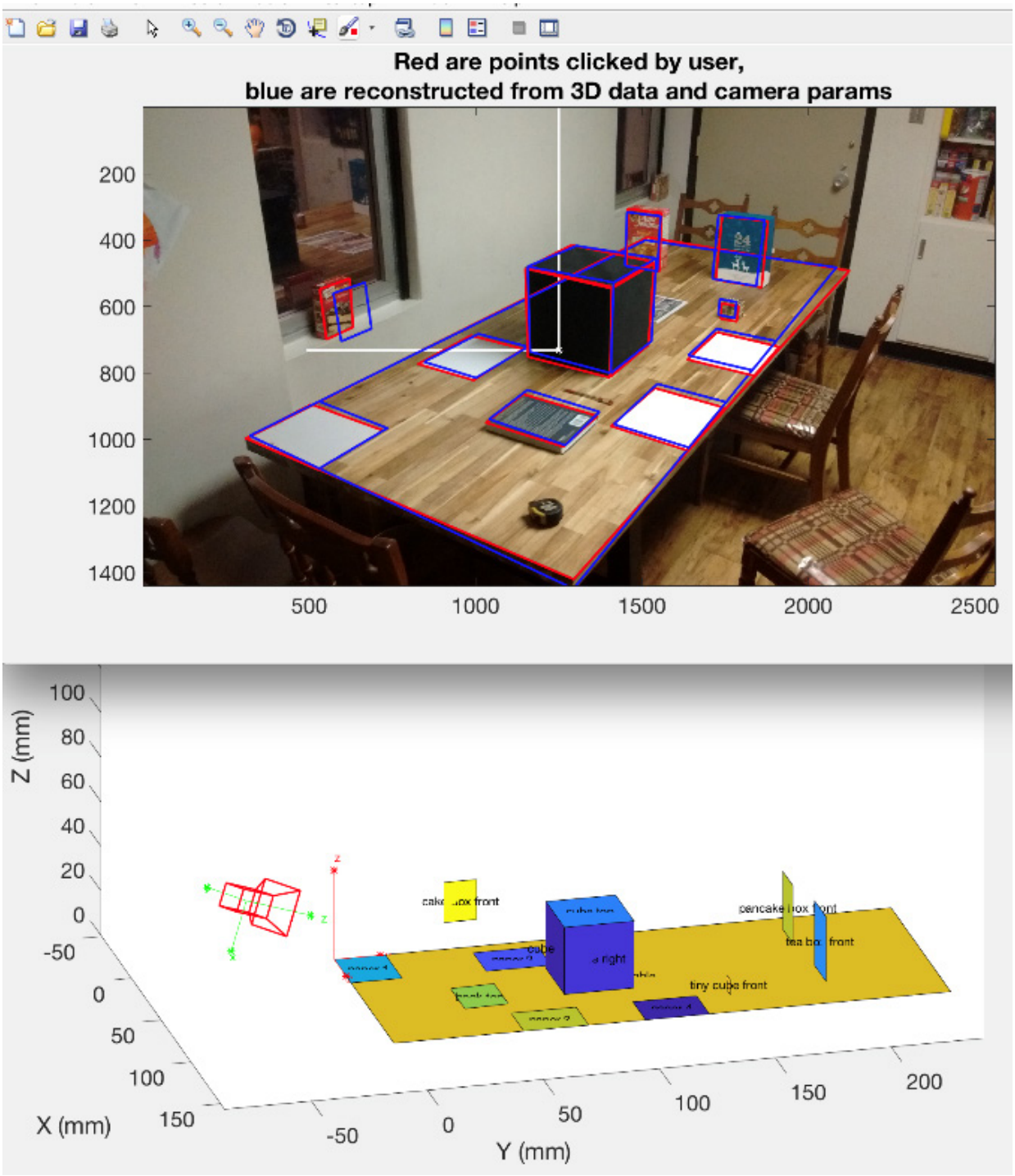

Figure 5. Detection of objects of the monitoring scene

```
function orthoc = findOrthocenter( imageFilename)
% Finds the principle point of the camera by first finding a triangle whos
% vertices are defined by the vanishing point of 3 mutually
% othogonal sets of parallel lines.  The orthocenter of this triangle is
% the principle point of the camera.
%
%  Instruction video: https://youtu.be/WEYwitb6dTo
%
% by  Aaron T. Becker, 10/30/2018
% Updated by Nima Eskandari in 2018 nima.eskandari@outlook.com such
% that draws a line from the first clicked point to the mouse position
% as you find the three sets of orthogonal lines.
if nargin<1
    imageFilename = 'CameraCalP1.jpg';%    1.0e+03 * [1.3198; 0.7816];
end
close all

%imshow(img);
f1 = figure( 'units','normalized','outerposition',[0 0 1 1]);
set(f1,'name', 'find orthocenter','MenuBar', 'none', 'ToolBar', 'none');
img = imread(imageFilename);
image(img,'Parent',gca);
set(gca,'fontsize', 18);
hold on
% % zoom in (optional
% title('zoom in: click twice to set the zone to be zoomed into')
% bb =ginput(2);
% axis([bb(1,1),bb(2,1),bb(1,2),bb(2,2)]);

%pause()
intxy1 = drawParallelLines(1);
intxy2 = drawParallelLines(2);
intxy3 = drawParallelLines(3);

%draw triangle
l1 = plot([intxy1(1),intxy2(1),intxy3(1),intxy1(1)],[intxy1(2),intxy2(2),i
set(l1,'color','k','linewidth',2);

% calculate the orthocenter (??)
orthoc = orthocenterTri(intxy1,intxy2,intxy3);
plot(orthoc(1),orthoc(2),'w*')
```

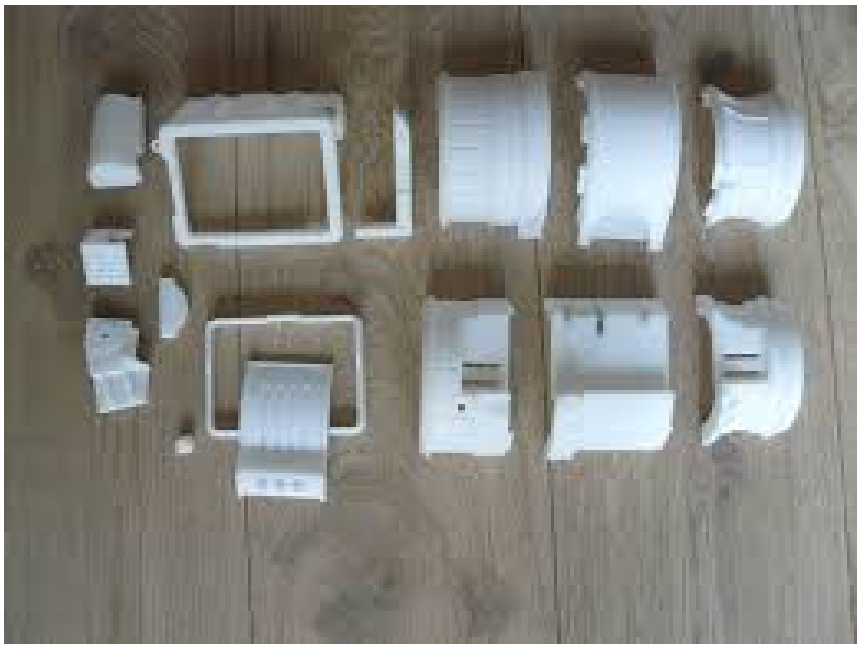

Figure 6. To simplify monitoring, it is proposed to use separate elements

Polymer indicators

The identified indicators of polymers of the ABS special type, which are used to print parts and control them with a video surveillance system.

Table 2

Polymer indicators

№	Polymer name	Mechanical properties		
		Tensile strength MPa	Vic softening temperature at 5 kg/^{cm2} in C	Density at 23 S in g/^{cm3}
26	ABS-OM-2020-30	not less than 38 MPa.	108 s.	
27	ABS plastic 0809-30	not less than 41,6 MPa	106 s.	
28	ABS plastic 0809M	not less than 40 MPa.	110	
29	ABS plastic 2020-30 of the highest grade	38,2	97	
30	ABS plastic 2020-31 of the highest grade	49	109	
31	Composite material ABS/PC Discar-L	not less than 50 MPa.	not less than 120 C.	
32	Composite material ABS/PC Discar-SL	not less than 50 MPa.	not less than 120 C.	
33	Composite material ABS/PC Discar-E	not less than 50 MPa.	not less than 115 C.	
34	ABS plastic 1030-30	not less than 35.3 MPa (360 kgf/^{cm2}).	not less than 90 C.	
35	ABS plastic 1030-31	not less than 35.3 MPa (360 kgf/^{cm2}).	not less than 88 C.	
36	ABS plastic 1106M-30	not less than 38.2 MPa (390 kgf/^{cm2}).	not less than 95 C.	
37	ABS plastic 1106M-31	not less than 38.2 MPa (390 kgf/^{cm2}).	not less than 95 C.	
38	ABS plastic 1106-30 of the highest grade	not less than 38.2 MPa (390 kgf/^{cm2}).	not less than 96 C.	
39	ABS plastic 1530-30	not less than 34.3 MPa (350 kgf/^{cm2}).	not less than 90 C	
40	ABS Plastic 2020-32	not less than 38.2 MPa (390 kgf/^{cm2}).	not less than 97 C.	
41	ABS Plastic 2020-60	29,4	80	1,03
42	ABS plastic 2802-30 of the highest grade	not less than 36.3 MPa (370 kgf/^{cm2}).	not less than 95 C.	
43	ABS plastic ABS-S	not less than 30.0 MPa (306 kgf/^{cm2}).	not less than 95 C.	

Video monitoring of additive manufacturing will allow you to predict the number of inconsistencies and will allow you to predict deviations in advance when printing.

Conclusion

At the moment, examples of the implementation of artificial intelligence in Russian industrial companies are rare, but they all confirm the effectiveness of the technology. Among the customers are large mining and processing enterprises. We have created and continue to develop systems for monitoring the industrial safety of workers, the safe movement of moving objects on the production site, video analysis to eliminate adverse situations in production, video monitoring of product quality, monitoring the performance of production equipment and optimizing the work of production personnel.

Referens

[1] Chabanenko A V, Kurlov A V 2021 Control the quality of polymers based on the model of Dzeno Journal of Physics: Conference Series

[2] Chabanenko A V, Kurlov A V and Tour A C 2020 Model to improve the quality of additive production by forming competencies in training for high-tech industries *J. Phys.: Conf. Ser.* **1515** 052065.

[3] Chabanenko A V and Yastrebov A P 2018 Quality Assurance of Hull Elements of Radio-Electronic Equipment by Means of Control System *J. Phys.: Conf. Ser.* **1515** 052065.

[4] Chabanenko A V, Kurlov A V 2019 Construction of mathematical model of training and professional development of personnel support of additive production of REA IOP Conference Series: Materials Science and Engineering

[5] Batkovskiy A M, Kalachikhin P A, Semenova E G, Fomina A V and Balashov V M 2018 Conficuration of enterprise networks *Entrepreneurship and Sustainability Issues* **6(1)** 311–28.

[6] Batkovskiy A M, Nesterov V A, S emenova E G, Sudakov V A and Fomina A V 2017 Developing intelligent decision support systems in multi-criteria problems of administrative-territorial formations infrastructure projects assessment *Journal of Applied Economic Sciences* **12(5)** 1301-11.

[7] Maiorov E E, Prokopenko V T, Mashek A C, Tsygankova G A, Kurlov A V, Khokhlova M V, Kirik D I and Kapralov D D 2018 Experimental study of metrological characteristics of the automated interferometric system for measuring the surface shape of diffusely reflecting objects Measurement Techniques **60(10)** 1016-21.

[8] Chabanenko A V, Semenova E G, Smirnova V O, Smirnov A O and Rozhkov N N 2018 Quality assurance of additive manufacturing by means of a layer-by-layer synthesis control system *Issues of radio electronics* **10** 17-24.

[9] Chabanenko A V 2018 Quality management of radioactive electronic equipment *RIA: Journal: "Standards and Quality"* **2** 90-94.

[10] Korshunov, G., Smirnov, V., Frolova, E., Nazarevich, S. Fuzzy models and system technical condition estimation criteria (2020) Advances in Intelligent Systems and Computing, 1041, pp. 179-189.

[11] Korshunov, G.I., Nazarevich, S.A., Smirnov, V.A. Fuzzy classification of technical condition at life cycle stages of responsible appointment systems (2018) CEUR Workshop Proceedings, 2258, pp. 427-437.

[12] Nazarevich, S.A., Urentsev, A.V., Kurlov, V.V., Balashov, V.M., Rozhkov, N.N. Management of development of basic structures of technological systems of machine-building production (2019) IOP Conference Series: Materials Science and Engineering, 537 (4), article No. 042024.

[13] Artjuhova, M.A., Balashov, V.M., Nazarevich, S.A., Smirnova, M.S. Evaluation of time to failure for radio transmitters under the radiation influence (2019) IOP Conference Series: Materials Science and Engineering, 537 (2), article No. 022016.

[14] Nazarevich, S., Smirnova, M., Tushavin, V. Integral criteria for evaluation of scientific and technical research (2015) International Journal for Quality Research, 9 (3), pp. 467-480.

[15] Vinnichenko, A.V., Nazarevich, S.A., Kurlov, V.V. Drifting models for evaluating the functional properties of products of innovative value (2021) Journal of Physics: Conference Series, 1889 (4), article No. 042074.

[16] Vinnichenko, A.V., Nazarevich, S.A., Kurlov, V.V. Drifting models for evaluating the functional properties of products of innovative value (2021) Journal of Physics: Conference Series, 1889 (4), article No. 042074.

[17] Vinnichenko, A.V., Nazarevich, S.A., Kurlov, V.V. Drifting models for evaluating the functional properties of products of innovative value (2021) Journal of Physics: Conference Series, 1889 (4), article No. 042074.

[18] Artjuhova, M.A., Balashov, V.M., Semenova, E.G., Nazarevich, S.A. The quality of aerospace equipment production analysis (2019) IOP Conference Series: Materials Science and Engineering, 537 (3), article No. 032023.

[19] Korshunov, G.I., Nazarevich, S.A. Parametric Models of the Product Novelty Assessment Through the Basic Structures Approach (2019) IOP Conference Series: Earth and Environmental Science, 272 (3), article No. 032142.

[20] Tushavin, V.A., Semenova, E.G., Smirnova, M.S., Frolova, E.A. Comparison of qualitative assessments of employees work by randomized indicators ARPN Journal of Engineering and Applied Sciencesthis link is disabled, 2015, 10(16), pp. 7280–7287.

THE RADIOTECHNICAL SYSTEMS SIMULATION IN CONFLICT SITUATIONS OF A COGNITIVE NATURE

A. F. Kryachko

Saint-Petersburg State University of Aerospace Instrumentation
Saint-Petersburg, Russia
E-mail: alex_k34@mail.ru

Abstract. The approaches to complex radiotechnical systems simulating in conflict situations of a cognitive nature are represented in the article. The synthesis equation, discriminating system state equations are received on the basis of the general systems theory. The experiment is carried out, on which basis the indications characterizing radiotechnical system subsystem models providing the required effectiveness of its functioning are defined.
Keywords – radiotechnical system, cognitive impact, conflict situation, functioning effectiveness.

Introduction

Modern information and telecommunications space is characterized by the active use of radio-electronic means and systems operating with different intensity degrees. In such conditions, antagonistic situations are inevitable, during which radio engineering systems (RTS) will have to fight for a limited frequency resource.

The RTS management in such conditions is a rather complicated task, which non-trivial solution stimulates the new unusual approaches search to the conflict situations resolving. This task class area solving determines the radio-electronic means development direction based on the cognitive radio systems new concept.

Domain analysis

The traditional methodology of conflict situations solution is carried out on the basis of game-theoretic modeling methods, which formalize various practical implementation algorithms, including ones on the basis of the operating frequency software adjustment. [1–4]. But these approaches make it possible to obtain acceptable solutions, subject to a priori knowledge of the conflicting parties behavior strategy. However, the modern RTS implementation based on modern technology [6-8] and the CRS (Cognitive Radio System) system platform [9, 10] is based on the artificial intelligence principles and implies non-determinism of their behavior, which is cognitive in nature, determining the reaction change not only depending on the situation, but also on the knowledge level received by the system during the conflict situation course [11].

Given these aspects, it is interesting to resolve conflict situations that arise between cognitive RTS using solutions making theory elements, which initially allows us to have a non-deterministic nature of both the destructive impact on the system and its response

Then, within the framework of this problem, we will formulate the research task in the following context: the development of a conflict situation model between RTS with cognitive properties, implementing the impact dynamic change of exposure depending on a set of informational signs about the interaction functional model and RTS reaction themselves.

Management task formalization

In the interests of this task formalization, we consider a closed-loop control scheme in which the control action is determined by the destructive influence of the external environment and the implementation system information flow (Fig. 1) [12]. The conflict topology of two cognitive RTS in fig. 1 is characterized by their interaction based on the allocated resources management in the functional-time domain, which determining the interaction dynamics.

On the generalized structural scheme, the external forming effect on the RTS 1 control system is represented by a function $F_R(t)$. This function is time dependent, characterizes the completfasr8e control function. In general, it is not clearly formalized.

The $F_R(t)$ function domain is in the $\widehat{F}_R(t)$ definition domain determining the complex 1 controlling action , taking into account the destructive influence of the external environment $S_1(t)$. The controlling decision implementation is based on the $\widehat{F}_R(t)$ control function, taking into account external factors $S_2(t)$.

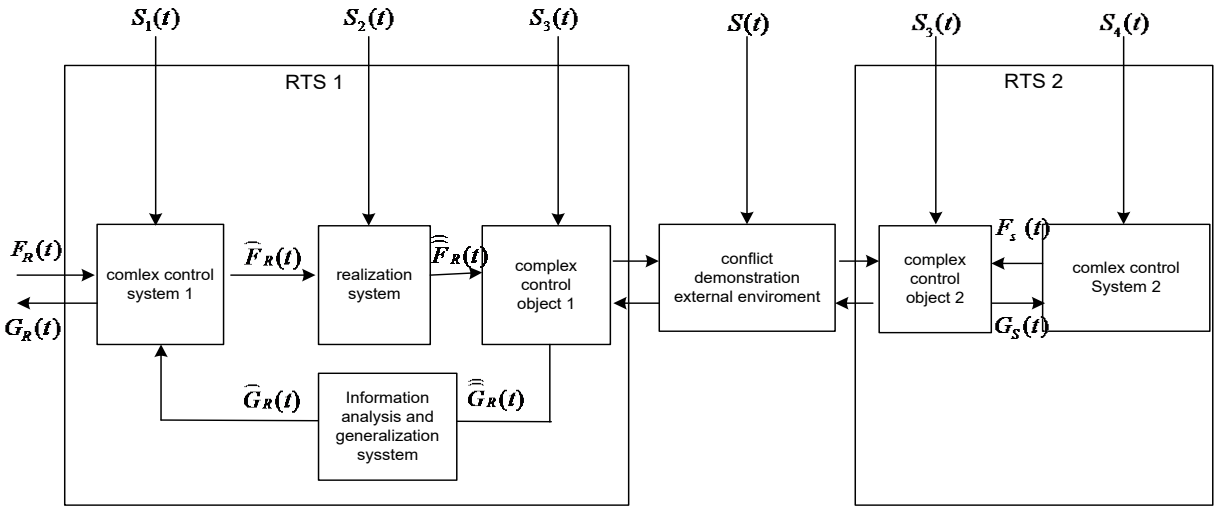

Fig. 1. RTS interaction generalized structural diagram in a conflict situation

The solution implementation system impact is determined by the $\widehat{\widehat{F}}_R(t)$ function under conditions formalized by the $S_3(t)$ impact. The external influence functions in a cognitive conflict situation are correlated. They determine the decision-making hierarchy at various interaction levels.

Given that $F_R(t)$, $\widehat{F}_R(t)$, $\widehat{\widehat{F}}_R(t)$ functions describe the control system effects, they must also be correlated in nature. Their independence indicates either the control circuit rupture or the control action absence.

The $\widehat{\widehat{G}}_R(t)$, $\widehat{G}_R(t)$, $G_R(t)$ functions close the control loop and characterize the control object state display at each conflict situation stage. They are implemented by the information analysis and synthesis system.

The control object is various parameters and characteristics that determine the RTS functioning efficiency.

Obviously, the RTS 1 and RTS 2 control goals in a conflict situation with one of the RTS dominating will not coincide. In the following, we will assume that one of the RTS, being the dominant one, takes advantage of the frequency resource, and the other RTS opposes it by implementing destructive influences on the control subsystem. In this connection, the $F_S(t)$ and $F_R(t)$ functions, characterizing the control processes and the control object information display processes have the opposite goals. The $H_R(t)$ and $H_S(t)$ functions are described similarly.

Since the considering functions strictly mathematical implementation in the conditions of the RTS cognitive interaction is not possible, then the general control theory methods can be used to solve this problem. They allow us to transform these functions as a goal vector, state vector and error vector with corresponding variation boundaries [12]. The possibility of conducting only qualitative analysis, excluding the RTS parameters quantitative estimates obtaining is this approach limitation. But it allows us to formalize the contradiction between the RTS practical implementation need in a conflict situation and their functionality based on the analyzed methods.

To solve this contradiction, let us present the RTS interaction model, possessing cognitive properties, in the form of a conflict model with a stable state, characterizing the efficiency required indicators achievement in the field of boundary values (fig. 2).

The work teserazus.Conditions and limitations.

We define the work thesis for the logical-formal approach to the conflict situations modeling of the cognitive RTS interaction in the following edition.

We take indicators that are subject to specified requirements as the RTS functioning quality. In particular, many parameters can be used determining the RTS properties at their modeling stage in order to assess the functioning quality when control tasks solving.

Taking into account the comments made, we define the RTS functioning efficiency as the quality indicators achievement degree. We take the RTS resources control strategy as the elementary control methods set. And we define the elementary method as a set of methods aimed at achieving the required value of the RTS functioning efficiency.

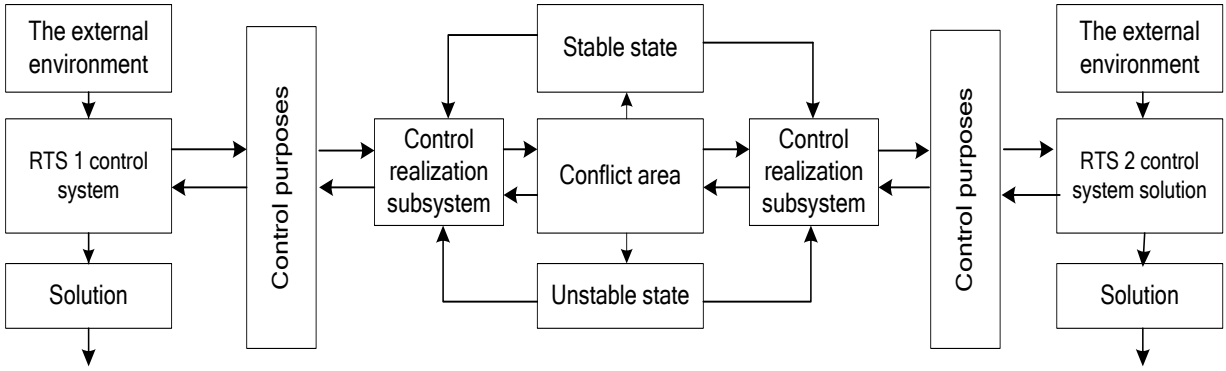

Fig. 2. The cognitive systems interaction conflict situation model

The elementary control methods distinctive properties are their further indivisibility, consistency in the RTS resources control strategy formation.

Under the elementary control methods systematic nature we take their structural and functional interconnectedness, given that uncorrelated elementary control methods form separate control strategies.

If we assume that the RTS resources control system implements m (m = 2, 3, 4, ...) of the elementary control methods, then the countermeasure system recourses control system should also implement m elementary methods. At the same time, each elementary RTS recourses control method will correspond to an elementary countermeasure system controlling, determined by its cognitive capabilities. In case of non-fulfillment of this condition, the efficiency value of the RTS models functioning goes beyond the permissible range. The conflict situations modeling of cognitive RTS interaction on the given principles means compliance with the criterion for allocating the resources required amount in the intensive control model.

In order to aggregate the RTS complexes model in deterministic conflict situations, we will assume that the countermeasure system goal is to reduce the opposite side efficiency.

Conflict situation solution

We will further elaborate the conflict on the general systems theory methods. Using the simulated systems integrity criterion, we distinguish three classes of tasks to be solved: goal-oriented, ensuring, and protecting.

The targets class is determined by the RTS model synthesis purpose and reflects its functional purpose in fact. The RTS properties formalize the supporting problems solution, based on the opposite side effects compensation.

The protective tasks class determines the RTS control strategy taking into account the conflict situation stages development. At the same time, the above-mentioned tasks class forms a complete group, mapping other tasks classes into one of the listed ones.

Based on the decisions determined this way, we present the RTS model in the conflict situation conditions of cognitive nature by means of three subsystems classes: goal-oriented, ensuring and protecting.

In order to detail the cognitive nature of the destructive impact, let us present the ensuring and protecting subsystems as identification and neutralization ones of with different service intensities (fig. 3).

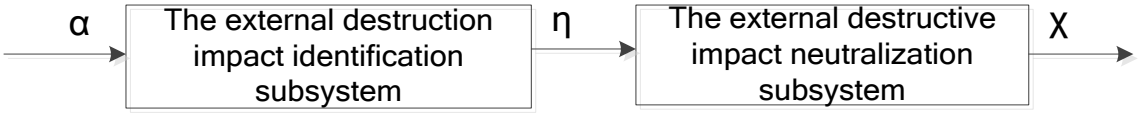

Fig. 3. Ensuring and protecting RTS subsystem model

In fig. 3:

α is the composite impact flow on the RTS;

η is the intensity of impact strategy detection by the RTS impact identification subsystem;

χ is the intensity of impact neutralization by the RTS neutralization subsystem.

Let us analyze the possible states of the model in accordance with Fig. 3:

C_{00} – the impact identification subsystem and the neutralization subsystem are free - the probability of

such a state is denoted by P_{00};

C_{10} – the identification subsystem is busy, the neutralization subsystem is free – P_{10};

C_{01} – the identification subsystem is free, the neutralization subsystem is busy by the information processing –P_{01};

C_{11} – both systems are busy – P_{11}.

Taking into account the concepts introduced, we formulate differential equations characterizing the state of the RTS.

The C_{00} condition is possible in the following incompatible cases:

– at t time, the RTS 1 identification and neutralization subsystem is free. For the time interval RTS 2 control complex 2 Δt strategy has not changed. This event probability is defined as

$$P_{00}(t)\,(1-\alpha\,\Delta t)\,; \tag{1}$$

– at t time point, the RTS 1 identification complex subsystem was in C_{01} state. During Δt, data on the sign of RTS 2 complex 2 destructive effect were revealed. This event probability

$$P_{01}(t)\,\chi\,\Delta t; \tag{2}$$

The ratio for C_{00} state is written in the form

$$P_{00}(t+\Delta t) = P_{00}(t)\,(1-\alpha\,\Delta t) + P_{01}(t)\,\chi\,\Delta t\,; \tag{3}$$

After the appropriate transformations and the transition to the limit as $\Delta t \to 0$, we obtain the differential equation

$$\frac{d}{dt}P_{00}(t) = P_{00}(t)\,\alpha + P_{01}(t)\,\chi. \tag{4}$$

C_{01} condition is possible in the following incompatible cases:

– RTS 1 identification subsystem at t time point is free. For Δt time interval, the impact strategy change did not occur, the neutralization subsystem is busy. This event probability is equal to

$$P_{01}(t)\,(1-\alpha\,\Delta t)(1-\chi\,\Delta t)\,; \tag{5}$$

– at t time point, RTS 1 identification subsystem is busy, the neutralization subsystem is free. For Δt time, the RTS 1 identification subsystem revealed data on the impact means

$$P_{10}(t)\,(\eta\Delta t)\,; \tag{6}$$

– at t time point, the RTS 1 identification subsystem is busy. For Δt, the identification subsystem is free, the neutralization subsystem is busy. Such event probability

$$P_{11}(t)\,\eta\,\Delta t\,; \tag{7}$$

The ratio for C_{01} state is defined as the following differential equation

$$\frac{d}{dt}P_{01}(t) = P_{01}(t)\,(\alpha+\chi) + P_{11}(t)\,\eta + P_{10}(t)\,\eta. \tag{8}$$

When compiling the differential equation of C_{10} state, we analyze the following incompatible events:

– at t time point RTS 1 identification subsystem was in C_{00} state. For Δt time interval, the required indication of the RTS 2 impact strategy change was identified. This event probability

$$P_{00}(t)\,\alpha\,\Delta t; \tag{9}$$

– at t time point the RTS 1 identification subsystem was in C_{10} state. For Δt time in the identification subsystem action area, the RTS 2 impact required indication appeared. No ion was detected. This event probability is defined as

$$P_{10}(t)\,(1-\eta\,\Delta t);\,; \tag{10}$$

– at t time point the RTS 1 neutralization subsystem was in C_{11} state. For Δt time the neutralization subsystem formed RTS 2 neutralization strategy. This event probability is equal to

$$P_{11}(t)\eta\Delta t. \tag{11}$$

Then the ratio for the C_{10} state is written in the form of the following differential equation

$$\frac{d}{dt}P_{10}(t) = P_{00}(t)\,\alpha - P_{10}(t)\,\eta + P_{11}(t)\,\chi\,; \tag{12}$$

The state of C_{11} is defined as follows:

– at t time point the RTS 1 neutralization subsystem was in C_{01} state. For Δt time the impact data were received

$$P_{01}(t)\alpha\Delta t; \tag{13}$$

– at t time point, the RTS 1 identification subsystem was in C_{11} state. For Δt time interval, the data on the RTS 2 impact strategy were not processed. We calculate the probability of this event as

$$P_{11}(t)\,(1-(\eta+\chi)\,\Delta t)\,; \tag{14}$$

The ratio for the C_{11} state is represented as a differential equation

$$\frac{d}{dt}P_{11}(t) = P_{01}(t)\,\alpha - P_{11}(t)\,(\eta+\chi).\,; \tag{15}$$

The equations systems characterizing the RTS 1 model state in a dynamic conflict situation of a cognitive nature is represented as

$$\begin{cases} \frac{d}{dt}P_{00}(t) = -P_{00}(t)\,\alpha + P_{01}(t)\,\chi \\ \frac{d}{dt}P_{01}(t) = -P_{01}(t)\,(\alpha+\chi) + P_{11}(t)\,\eta + P_{10}(t)\,\eta \\ \frac{d}{dt}P_{10}(t) = P_{00}(t)\,\alpha - P_{10}(t)\,\eta + P_{11}(t)\,\chi \\ \frac{d}{dt}P_{11}(t) = P_{01}(t)\,\alpha - P_{11}(t)\,(\eta+\chi) \end{cases}. \tag{16}$$

System (16) is an equations system of the RTS cognitive models synthesis in dynamic conflict situation conditions.

This system solution will allow us to synthesize various structural and functional complexes models, taking into account the possibility of obtaining the efficiency indications boundary value.

Experiment and confirmation

The system (16) practical solution is a non-trivial task, which involves the boundary regions determination of the RTS functional-temporal states.

On the basis of the developed methodological apparatus, an experiment was conducted under the selected constraints system, which determines the conditions under which the identification and neutralization subsystems were in the C_{00} state. These conditions characterize rather strict requirements for RTS complexes functional models. In practice, the restrictions system can be simplified, but RTS efficiency indications achieving probability is significantly reduced in this case.

In fig. 4, fig. 5 the experimental results are represented characterizing the dependences of the RTS 1 destructive impact identification and neutralization probabilities on the RTS 2 impact intensity. The results obtained analysis allows us to draw the following conclusion. The servicing intensity increasing by the RTS complexes identification and neutralization subsystems in conflict situation conditions of a cognitive nature ensures their functioning efficiency increase.

In particular, for the RTS model, characterized by the parameters χ=η=100 c^{-1}, its functioning efficiency does not exceed 0.2 (Fig. 5). The analyzed parameters substantial increase determines its effective performance to a value greater than 0.7. Moreover, the functional models effectiveness increase is achieved by η parameters and χ model subsystems simultaneous increase.

The developed scientific and methodological apparatus is a further decision making theory development in the case of quasi-stationary functions behavior and allows us to simulate the objects reactions in the RTS form in conflict situations conditions. It is obvious that the cognitive nature of the systems does not allow one to obtain unambiguously deterministic solutions even in special cases (Fig. 5 shows the guaranteed area

of decision making). However, if we define flow indicators in more detail, the solution space narrows down to the plane level, the center of mass of which will determine the most probabilistic solution.

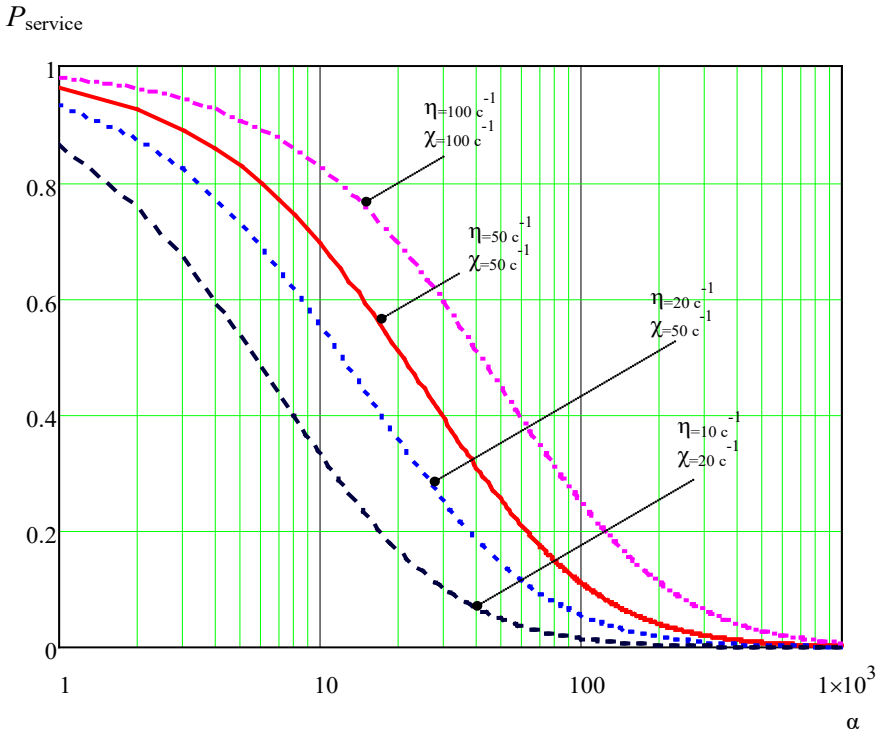

Fig. 4. The RTS destructive impacts flow identification and neutralization probability in conflict situations of cognitive nature

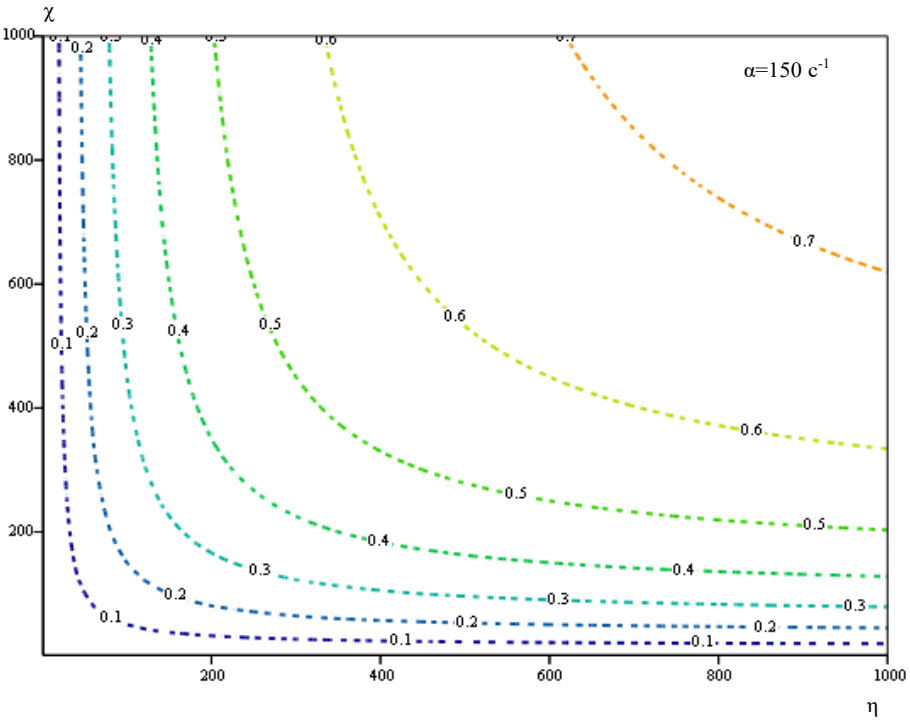

Fig. 5. RTS model performance at impact flow intensity fixed value

The further research directions are attributed by the authors to the further (16) system detailing with the conflict situations various parameters and cognitive RTS possibilities.

Referens

[1] Y. M. Lam. P. H. Wittke. Frequency hopped spread spectrum transmission with band-efficient modulations and simplified noncoherent // IEEE Transaction on circuts and systems, Vol. 45, №1, 1998, pp. 106-121.

[2] Pelechrinis K., Koufogiannakis C., Krishnamurthy S. On the efficacy of frequency hopping in coping with jamming attacks in 802.11 networks// IEEE transactions on wireless communications, 2010. №10. - pp. 3258-3271.

[3] Zander. J., Malmgren G. Adaptive frequency hopping in HF communications // IEE Proceedings Communications, Vol. 142, 1995, pp. 99-105.

[4] Naser Hossein. Frequency hopping spread spectrum: an effective way to improve wireless communication performance // Advanced Trends in Wireless Communications, 1999, Vol. 34. pp. 187-202.

[5] Interoperability and performance standards for Medium and High Frequency radio systems, MIL-STD-188-141B, 2001.

[6] Proakis J. G. Digital communications; 5th McGraw – Hill, 2008.

[7] Torrieri D. Principles of spread spectrum communications systems / Springer Science. Business Media Inc., 2005. 444p.

INVESTIGATION OF THE ALGORITHM FOR DETECTING MOVING OBJECTS IN A VIDEO SEQUENCE USING THE INTER-FRAME DIFFERENCE METHOD PROCESSED BY THE OCU METHOD

Victoria Afanaseva

Saint-Petersburg State University of Aerospace Instrumentation,
Saint-Petersburg, Russia
E-mail: victoria_afanaseva@mail.ru

Abstract
In this paper, a method for detecting and classifying moving objects by frames of a video sequence formed by a static optoelectronic surveillance system is implemented. The method of digital image processing and the method of detecting connected areas were used. The result of the work is a classified set of video stream frames, classified according to the following types of moving objects (counting the number of objects): people, cars.
***Keywords*:** object detection, counting of moving objects, binarization of images, Otsu's method.

Introduction

The detection of objects based on video sequence frames formed by a static optoelectronic surveillance system has recently become one of the most important tasks of scene analysis in automated monitoring applications for moving objects.

Processing video stream frames using automated monitoring applications allows you to select the necessary objects on the processed scene, classify them and count them.

Detection and counting of moving objects is used in various fields. These areas include: autonomous air vehicle control systems, including unmanned, as well as advanced ways of human-computer interaction, navigation of onboard unmanned systems, etc.

Based on this, we can conclude about the relevance of the topic of this work.

The objective of this study is to develop a method for automated detection and identification of moving objects with their subsequent classification according to selected characteristics.

FRAME-TO - FRAME DIFFERENCE METHOD

Detection of moving objects is often implemented using the difference method. This method is based on subtracting the video sequence of the previous frame from the current frame, the resulting difference will reflect moving objects (figure 1). When processing, those places on the frame that relate to the movement of the object are marked with a binary unit, and the rest are marked as binary zeros. As a result, the pixels of the image of a moving object are highlighted. From the resulting image, you can determine the location and parameters of the object's movement. But in order to use this method, the frames of the video stream must be binarized.

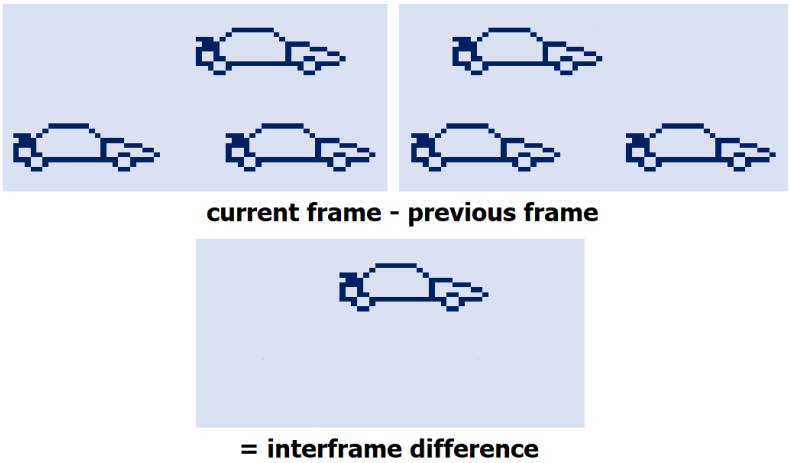

Figure 1 – The principle of the algorithm

BINARIZATION OF VIDEO SEQUENCE FRAMES USING THE OCU METHOD

Binarization is to establish the presence of objects in the image that have certain certain characteristics. Such a characteristic can be, for example, brightness. One of the simplest and most natural ways to detect an object (or objects) is to select a brightness threshold, or threshold classification. The meaning of such a threshold is to divide the image into a light object (foreground) and a dark background (background). I.e. an object is a collection of those pixels whose brightness exceeds the threshold ($I > T$), and the background is a collection of other pixels whose brightness is below the threshold ($I < T$). There are dozens of threshold selection methods. A fast and effective method is the method invented by the Japanese scientist Nobuyuki to his Father in 1979.

Let's apply the Otsu method in practice, let there be a video frame for which it is required to calculate the threshold and binarize it. The result of image binarization using this method in the MATLAB environment is shown in figure 2

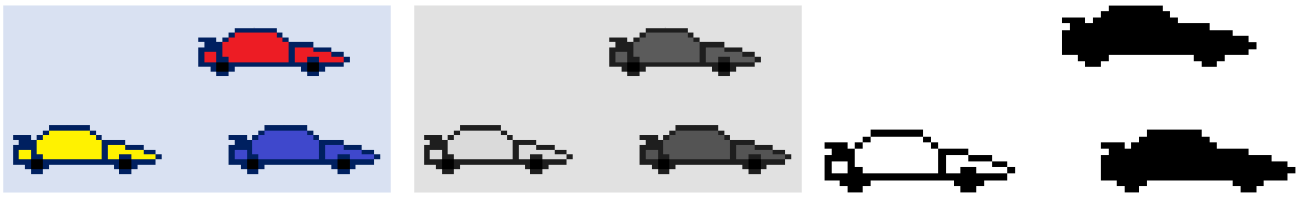

a) Original image *b) Grayscale image* *c) Binarized image*

Figure 2 - The result of binarization of the image using the Ocu method

EXPERIMENT ON DETECTING MOVING OBJECTS IN A VIDEO SEQUENCE USING THE OCU METHOD

Figure 3 (a) has a binary image of one frame. It is necessary to get a mask of moving objects in the video, for this you need to apply this transformation to each frame and use the inter-frame difference method.

In figure 3 (b), you can see the result of processing a frame of a video stream converted to binary form using the Otsu method with and without unnecessary noise.

To remove unnecessary noise from the frame, the method of morphological opening of the image was used, with the help of it, unwanted pixels of a given size and shape were removed.

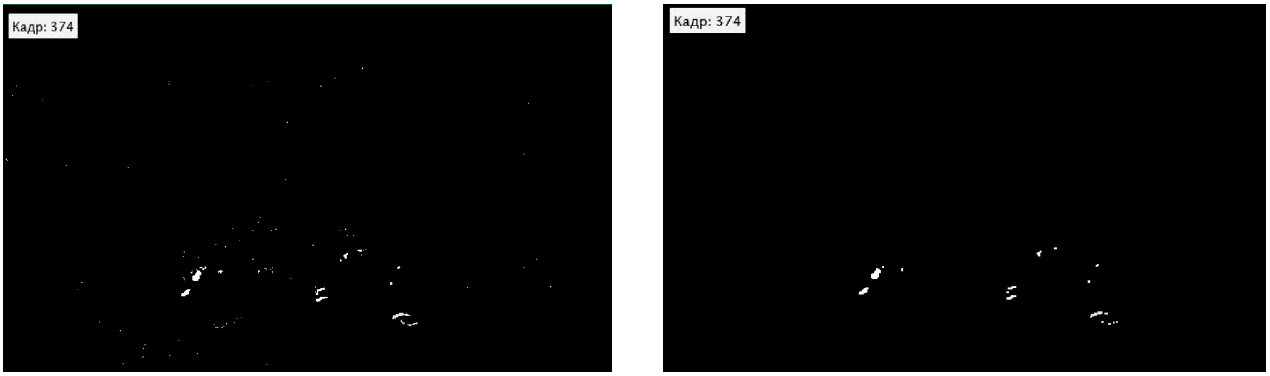

a) Mask with noise b) Mask without noise

Figure 3 – Video frame processing result

After that, using this mask, you can select objects in the frame that occupy a certain number of pixels on the frame (figure 4).

Figure 4 – Selected objects

The parameters of the object to be selected are configured using the connected areas assignment function. There can be many such parameters if we need to classify several types of objects.

Conclusions

As a result of this study, a method for detecting moving objects in a video sequence formed by a static optoelectronic surveillance system using the Ocu method is implemented and considered.

An experiment was conducted to detect cars. As part of this experiment, real video data obtained from an optoelectronic surveillance system was used. Thus, the possibility of object detection based on the use of the difference method of object detection using the Ocu method was shown.

Reference

1. Convolutional neural network, part 2: learning by error back propagation algorithm / / URL: https://habr.com/ru/post/348028/

2. Nenashev V. A., Sentsov A. A., Kuyumchev G. V. Modeling of the process of forming a high-resolution radar image in an on-board radar. 2013. Vol. 2. no. 3. pp. 48-56.

3. Nenashev, V. A., Kryachko, A. F., A. P. Shepeta, Burylev D. A. Features of information processing in the on-Board dip small radar on the basis of the UAV, SPIE Future Sensing Technologies, Tokyo, Japan, 2019, pp. 111970X-1-111970X-7.

4. Kapranov, E. A. Nenashev, V. A., Sergeev A. M., Burylev D. A., S. A. Nenashev Distributed matrix compression techniques, masking and error-correcting coding of images in high-speed network of information exchange, data processing and information aggregation, SPIE Future Sensing Technologies, Tokyo, Japan, 2019, pp. 111970T-1-111970T-7.

5. Object detection by the Ocu method / / URL: https://habr.com/ru/post/112079/

6. Nenashev, V. A., Kryachko, A. F., A. P. Shepeta, Burylev D. A. Features of information processing in the on-Board dip small radar on the basis of the UAV, SPIE Future Sensing Technologies, Tokyo, Japan, 2019, pp. 111970X-1-111970X-7.

7. Kapranov, E. A. Nenashev, V. A., Sergeev A. M., Burylev D. A., S. A. Nenashev Distributed matrix compression techniques, masking and error-correcting coding of images in high-speed network of information exchange, data processing and information aggregation, SPIE Future Sensing Technologies, Tokyo, Japan, 2019, pp. 111970T-1-111970T-7.

DEVELOPMENT OF THE AUTOMATED CARDIAC RHYTHM DISORDERS DETECTION AND CLASSIFICATION ALGORITHM

Bella Akopyan

Saint-Petersburg State University of Aerospace Instrumentation,
Saint-Petersburg, Russia
E-mail: akopyan.bella@yandex.ru

Abstract
The algorithm of classification of arrhythmias on the basis of automatic algorithm of detection of arrhythmic episodes on electrocardiogram signal is offered. The estimation of probabilities of classification errors by the method of statistical modeling is carried out.
***Keywords*:** electrocardiogram, electrocardiogram, automatic processing, classification, decision making.

Introduction

The process of classification of heart rhythm disorders can be divided into two tasks: analysis of the registered arrhythmic cardio cycles type (sorting by groups «norm»/«pathology») and analysis of the number of sequentially detected arrhythmic RR-intervals and appropriate time intervals [1]. Based on the generalized principle of heart rhythm disorders classification algorithms [2, 3], it is obvious that it is necessary to solve two problems to develop an algorithm of classification of arrhythmias:

1. Choose an arrhythmic episode detection algorithm that provides the least possible detection error;
2. Propose a decision rule for classifying rhythm disorders based on the results of the detection of arrhythmic episode.

Arrhythmic episodes detection algorithm

Based on the generalized principle of the electrocardiogram (ECG) express-diagnostics algorithms [2], it is obvious that the result of heart rhythm disorders classification will directly depend not only on the direct classification rule, but also from the quality of ECG processing algorithms at the stage of QRS-complexes detection and rhythm violations analysis. Therefore, the algorithm for detection of arrhythmias based on digital filtration of QRS-complexes with the decisive rule based on the measurement of the difference of RR-intervals standard deviation was chosen as the basis for the algorithm, described in [4], which showed suitable for practical application results on the criterion of the minimum probability of an erroneous decision.

Another advantage of this algorithm is that the results of its work are easier to analyze from the point of view of the ECG-signs of the arrhythmia in question. In particular, by the number of automatically detected consecutive episodes of rhythm disturbance and the time relationships between them, it is possible to classify the heart rate in three categories:

1. Normal sinus rhythm,
2. Single rhythm disorders (e.g., atrial and ventricular contractions),
3. Frequent rhythm disorders (for example, atrial fibrillation as one of the most common types of arrhythmia [5]).

Development of a decisive rule of classification of arrhythmic episodes

Based on the analysis of the algorithm results presented in article [4], the following classification criteria can be distinguished for the categories of signals considered in the study:

1) Single atrial contraction corresponds to one observed abnormality;
2) Single ventricular contraction corresponds to two instantaneous rhythm disturbances;
3) Atrial fibrillation corresponds to three or more consecutive rhythm disturbances (chaotic heart rate).

According to these, the following decision rule is proposed for the classification of ECG according to the recorded arrhythmic episodes. The flowchart of the proposed classification algorithm is presented in Figure 1. Based on the operation of the arrhythmia detection algorithm [3], the first five results of the decision on the state of rhythm are part of the adjustment stage and do not need classification.

Classification of detected rhythm disorders is carried out by categories:

1) single episode of rhythm disturbance is classified as an atrial contraction (state «AC», fig. 1);

2) two episodes of rhythm disturbance, followed by each other, are classified as ventricular contraction (state «VC»);

3) Three episodes of rhythm disturbance, following each other, are classified as a prolonged arrhythmic episode of atrial fibrillation (state «AF»).

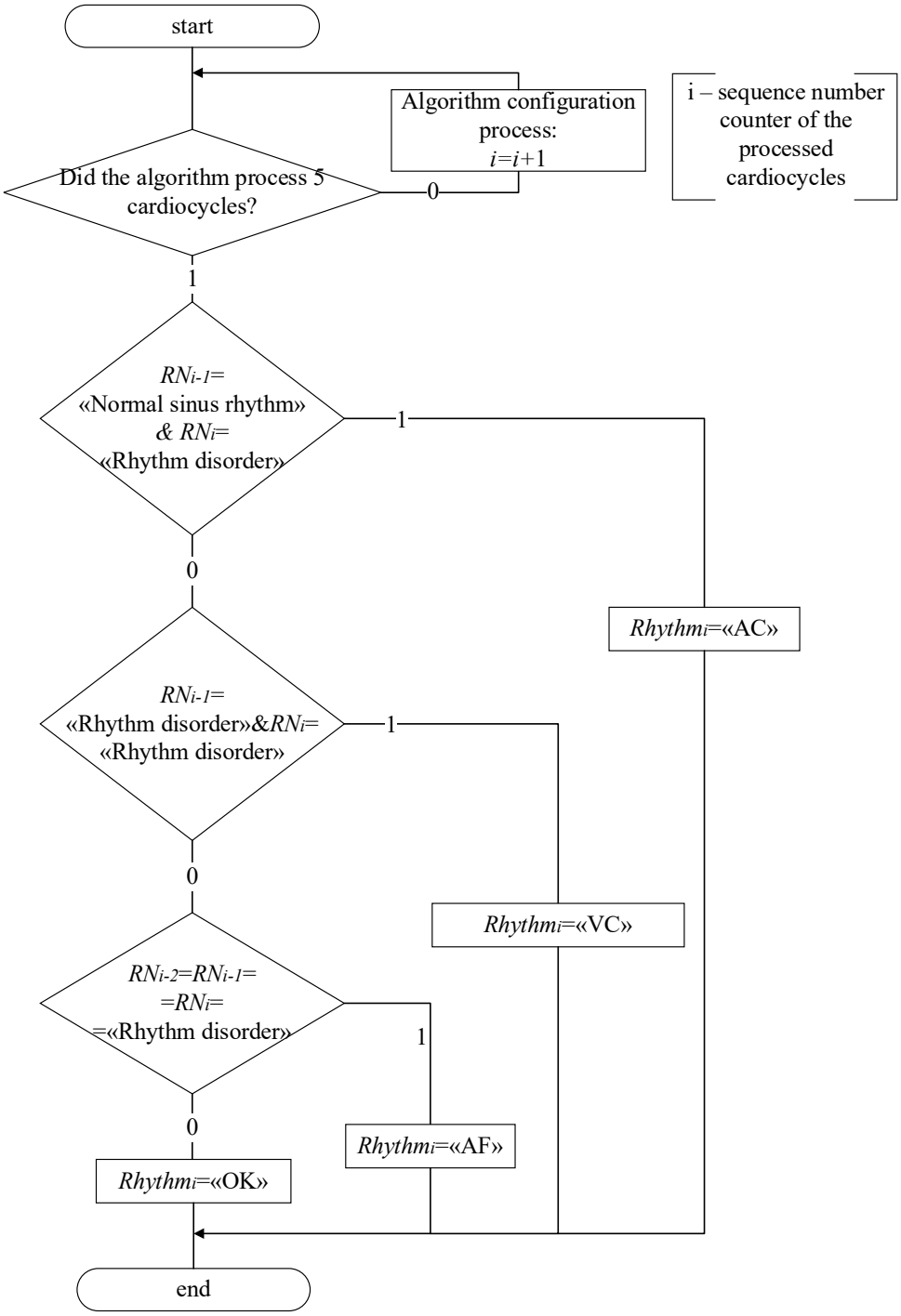

Fig. 1. The diagram of the decision rule of the automated cardiac rhythm disorders detection algorithm

Otherwise, if the rhythm disorder was not recorded, the rhythm state is defined as normal (state «OK»).

For the study, realistic ECG records were used, created using the model ECG [6] based on parameters of real ECG records presented in MIT-BIH Normal Sinus Rhythm Database [7] and MIT-BIH Arrhythmia Database [8]. A total of 1,200 records lasting 120 seconds were used, with a sampling rate of 1,000 Hz divided into three categories:

1) Normal Sinus Rhythm ECG with parameter of heart rate variability = 0-10% [9];

2) ECG with simulation of single heart rhythm disorders (atrial and ventricular contraction) constituting not more than 10% of the total number of cardiac ECG;

3) ECG of atrial fibrillation.

All of ECG from the base is categorized uniquely and cannot be assigned to another category. Therefore, to model the stage of classification of diagnosed arrhythmias it is sufficient to classify the ECG records directly. If the number of violations in an ECG record belonging to a certain category exceeds a certain threshold, the whole ECG record is classified according to this category.

Records are classified as follows:

1) If single rhythm disorders prevail (state of «AC» and «VC»), then the entry corresponds to class of contractions;

2) long-term episodes of arrhythmia (state «AF») - atrial fibrillation.

If the fraction of the classified disorders does not exceed the threshold, this entry is classified as normal, which will eliminate the influence of minor rhythm disorders on the results of the examination in a healthy person.

Simulation results

Based on the analysis of the arrhythmia detection algorithm [3], it was decided to select a threshold of 3.5% for the diagnosis of the total number of violations. The results of the classification error probability estimates are presented in table 1.

Table 1

Results of errors probabilities estimation of the proposed arrhythmia classification algorithm

True ECG State	The probability of classification as:		
	Normal Sinus Rhythm	Single Rhythm disorders (contractions)	Atrial fibrillation
Normal Sinus Rhythm	0.993	0.007	0
Single Rhythm disorders (contractions)	0.005	0.985	0.010
Atrial fibrillation	0	0.005	0.995

The resulting classification quality indicators are satisfactory for the arrhythmia detection algorithm used in practice, so the algorithm can be used to analyze the three ECG categories.

References

1. Antsiperov V.E., Zabashaev I.V., Strozhgaev D.V. Detection of heart rate disorders using analytical spectra technique/ / Journal of radio electronics, 12, 2015. URL: http://jre.cplire.ru/jre/dec15/4/text.html [Анциперов В.Е., Забросаев И.В., Растягаев Д.В. Детектирование нарушений сердечного ритма с использованием техники аналитических спектров// Журнал радиоэлектроники, №12, 2015. URL: http://jre.cplire.ru/jre/dec15/4/text.html]

2. Akopyan B.K. Review of electrocardiogram processing algorithms for decision support systems on classification of heart rate disorders// International scientific conference «Processing, transmission and protection of information in computer systems» (Saint-Petersburg, 14 - 22 April 2021) sb. Reports / SPb.: Published by GUAP, 2021. P. 7-12. [Акопян Б.К. Обзор алгоритмов обработки электрокардиограмм для систем поддержки принятия решения о классификации нарушений сердечного ритма// Международная научная конференция «Обработка, передача и защита информации в компьютерных системах» (Санкт-Петербург, 14 - 22 апреля 2021 г.): сб. докладов / СПб.: Изд-во ГУАП, 2021. С. 7-12.]

3. Heart monitors. Continuous monitoring equipment EKG: study. manual for universities/ under Ed. A. L. Baranovsky and A. P. Nemirko. M.: Radio and communication, 1993. 248 p. [Кардиомониторы. Аппаратура непрерывного контроля ЭКГ: учеб. пособие для вузов/под ред. А. Л. Барановского и А. П. Немирко. М.: Радио и связь, 1993. 248 с.]

4. Akopyan B.K. Development and research of automated arrhythmic episodes detection algorithms by electrocardiographic signal// Bulletin of the UNESCO department “Distance education in engineering” of the SUAI: Collection of the papers. St. Petersburg, Issue 6.– SPb.:SUAI, 2021. P. 29-34.

5. Ruzov V.I. Gimaev R.H., Razin V.A.. Basics of clinical electrocardiography. Practical guidance on internal diseases: training. manual/ Ulyanovsk: UlSU, 2009. 124 p. [Рузов В.И. Гимаев Р.Х., Разин В.А.. Основы клинической электрокардиографии. Практическое руководство по внутренним болезням: учеб. пособие/ Ульяновск: УлГУ, 2009. 124 с.]

6. Akopyan B.K., Zharinov O.O. Development of computer simulation model of electrocardiogram/ 1st scientific conference «Information processing, transmission and protection in computer systems» (St.-Petersburg, April 14 - 22, 2020): Sat. Reports / SPb.: Published by GUAP, 2020. P. 17-23. [Акопян, Б.К., Жаринов О.О. Разработка компьютерной имитационной модели электрокардиограммы//Первая Всерос. научная конференция «Обработка, передача и защита информации в компьютерных системах» (Санкт-Петербург, 14 - 22 апреля 2020 г.): сб. докладов / СПб.: Изд-во ГУАП, 2020. С. 17-23.]

7. MIT-BIH Normal Sinus Rhythm Database, URL: https://physionet.org/content/nsrdb/1.0.0/

8. MIT-BIH Arrhythmia Database, URL: https://physionet.org/content/mitdb/1.0.0/

9. Ivanov G.G., Dvornikov V.E., Sbeitan S. etc. Analysis of indicators of the structure of heart rhythm variability in healthy persons according to PP- and RR-intervals // Bulletin of the Russian University of Friendship of Peoples. Series: Medicine, 4, 2007. P.26-34. [Иванов Г.Г., Дворников В.Е., Сбеитан С. и др. Анализ показателей структуры вариабельности ритма сердца у здоровых лиц по данным PP- и RR-интервалов // Вестник Российского университета дружбы народов. Серия: Медицина, №4, 2007. С.26-34.]

ENVIRONMENTAL POLLUTION DETECTION SYSTEM – AN INTELLIGENT DYNAMIC SOLUTION

Andrea Pietro Arena

Computer Engineering and Networks Laboratory – Kore University of Enna - Italy
Email: andreapietro.arena@unikorestudent.it

Abstract
This document proposes a quick and targeted solution on air quality management in metropolitan cities. Pollution is the most important challenge and making decisions quickly is the priority. The EPDS system carries out periodic measurements by means of sensors and, through an appropriate logic controller, it sends the actions to be taken to the actuators, the result of the processing is shown on the screen together with the luminous indicator. The scenario is implemented in built-up urban areas with high concentrations of PM10 particulate matter. The system will consist of a wireless sensor network and other intelligent solutions that will make the system autonomous and free of any bureaucracy.

Introduction

The use of intelligent systems is a fundamental factor in the reduction of environmental pollution. The international scientific community and the WHO (World Health Organization) have determined that the most relevant urban pollution factor is road transport. The substances released into the environment are identified as type ten airborne particulate matter (PM10), the concentration of the latter has a significant impact on people's lives.

Actually, there is a higher mortality rate in built-up urban areas and diseases in the significant respiratory and cardiac systems.

The first approach used is to have intelligent surveys of the main polluting gases, assisted by environmental temperature and humidity sensors, on a regular basis.

The data collected by the sensors are evaluated in an innovative way; in addition to the measurements in percentage gas terms, the Thom index on the degree of human discomfort is taken into consideration in the face of atmospheric temperature and humidity measurements.

The sensors are placed on the roofs of buildings at a suitable operating altitude near the gates. The sensors communicate with the controller through a dedicated 802.15.4 ZigBee wireless network. The wireless network of the ZigBee sensors type was chosen for its low energy impact; that means the devices are powered by batteries and potentially rechargeable through solar panels which further reduce the emission of CO_2 deriving from energy production. The controller is a device that can be placed either near the gates or in administrative offices, it is placed in a wired CSMA / CD Ethernet network potentially interconnected with other zone controllers. The controller's task is to analyze the data and to communicate the outcome of the processing to the actuator. The actuator is the gate, it works both in standard mode referring to times established by the local authority and in pollutant detection mode. The fundamental purpose is to have a result on a regular basis and to implement immediate solutions to combat the pollution of that area without having bureaucratic deadlines on limiting traffic. In the next section some commercial solutions will be shown, while the other sections will technically describe the project and evaluate the performance impact of the latter.

RELATED WORKS

operation is similar to statistics and traffic limitation. However, these systems are not intelligent and do not make immediate decisions. The intervention should be immediate but, as usual, the judgment must be given by public administrative bodies, and this leads to an increasingly poor quality of the air breathed by the population.

A commercial solution identified as potentially competing is that of the NESA company.

The commercial solution proposed by the company can be of a fixed or mobile nature. The systems presented only carry out monitoring and do not undertake actions to prevent or reduce vehicular traffic. The fixed solution involves the installation of a controller cabin and sensors placed at a suitable measurement altitude, these systems are stand-alone developed by NESA and a datalogger capable of communicating data over the network is also provided. However, the mobile solution is worse than the fixed solution; its implementation is on a combustion vehicle which could greatly affect the data detected by the sensors and substantially does not prevent the phenomenon, on the contrary it amplifies it. These systems do not use renewable

energy as proposed, thus producing CO_2. An ideal and eco-sustainable system is the one proposed in this document.

THE PROPOSED APPROACH

The metropolitan city under observation is Milan, reference is also made to area B of the limited traffic zone. The solution proposed in this document integrates with the existing system of gates, for access to restricted traffic areas. The integral part shown in figure [1] is composed as follows:

- IP54 type temperature sensor, powered by a battery shared by all 5000mAh sensors with consumption of 100mW (360 J / h). The measurement range is -40 ÷ + 60 ° C with a resolution of 0.01 ° C. Transducer Type 1/3 Din Platinum Resistance Thermometer. Made of painted aluminium alloy and approximate weight of 700g.
- IP54 humidity sensor, battery powered with consumption of 100mW (360 J / h). The measurement range is 0 ÷ 100% with accuracy ± 1%. Type of capacitive transducer. Made of painted aluminium alloy weighing approximately 680g.
- IP54 type gas sensor, battery powered with consumption of 480mW (1728J / h). The component consists of specific gas sub-sensors which are: N_3 (Ammonia - Range 0 ÷ 100), CO_2 (Carbon Dioxide - Range 0 ÷ 10000 ppm), CO (Carbon Monoxide - Range 0 ÷ 1000 ppm), H_2S (Hydrogen Sulfide - Range 0 ÷ 200 ppm), CH_4 (Methane - Range 0 ÷ 100%), NO_2 (Nitrogen Dioxide - Range 0 ÷ 20 ppm), O_2 (Oxygen - Range 0 ÷ 25% v / v), SO_2 (Sulfur Dioxide - Range 0-100 ppm). The average operating range is -10 ÷ +45 ° C. Total weight of approximately 560g.
- Gateway, allows communication and data exchange between networks: sensor, controller and actuator.
- Controller, device useful for data processing.
- Actuator monitor, simple display useful not only as processing output but as information to motorists regarding the restrictions currently in force.

The Sensors of the B area of Milan carry out surveys at intervals of thirty minutes. The sensor network communicates the data using the 802.15.4 ZigBee protocol (Network N ° 1) to the gateway, then the information is routed to the controller using a wired communication CSMA / CD Ethernet (Network N ° 2). The controller carries out a processing of the data received and forwards the restriction level to the actuator, a wired CSMA / CD Ethernet communication (Network No. 3) is used, finally the restriction level is shown by the actuator on the screen.

SCENARIO

The simulation scenario is made possible through the Matlab / Simulink application using TrueTime. The simulation was carried out in the first days of January and it is possible to extend it for the entire calendar year.

The first level of development is to define the behavior of atmospheric sensors, making the data close to a correct operational reality. The simulink components allow you to have random values over a given interval, they were not correct for the simulation day. A basic signal was created through a spreadsheet on which then later through matlab function to determine which is the temperature close to concrete reality for that time slot [1], especially considering the season of belonging.

Regarding the second group of sensors, however, a base signal has not been created because the gas concentrations can vary following various factors, in fact the values have been randomly generated. The temperature and humidity values are related following an average of measurements made in the last thirty years in the city of Milan.

The second development level is the controller one. It receives the data from the gateway and processes the information under appropriate criteria. The data received are inputs from two distinct directions: the sensor data of the atmospheric group are the input of a fuzzy logic controller while the data of the pollutant group are the input of a matlab function. The fuzzy component imports the Thom index and through the data received it is able to classify the degree of human discomfort perceived in relation between temperature and humidity. The gas matlab function defines an output value based on the gas having a higher percentage than the relative range and also takes into account the oxygen concentration present in that area.

Finally, the degree of restriction is determined by a last fuzzy logic controller which has as input the outputs of the elaborations made by the first fuzzy component and by the second gas component matlab function. Road transport vehicles are distinguished in terms of emissions, the categories are defined by the year

of production and the type of particulate filter. On the basis of the value processed, more polluting categories can be banned rather than others.

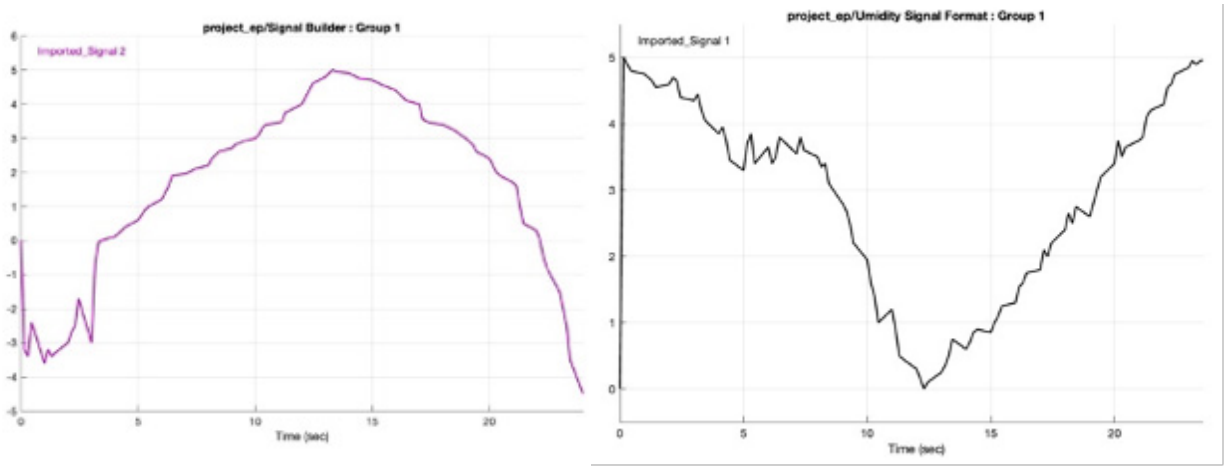

Figure 1. From left to right: Two customized basic signals of temperature and humidity. These signals simulate the environmental reality

The third level of development is the actuator one, it receives the data from the gateway and places them as an input to the Stateflow simulink. The Stateflow component is a logical control tool used to model reactive systems through state machines and flow diagrams within a Simulink model, in particular it is possible to represent the operation of the gate device in the specific scenario. The component has been internally designed to operate both in standard mode at times and at values received resulting from the processing of the controller [2].

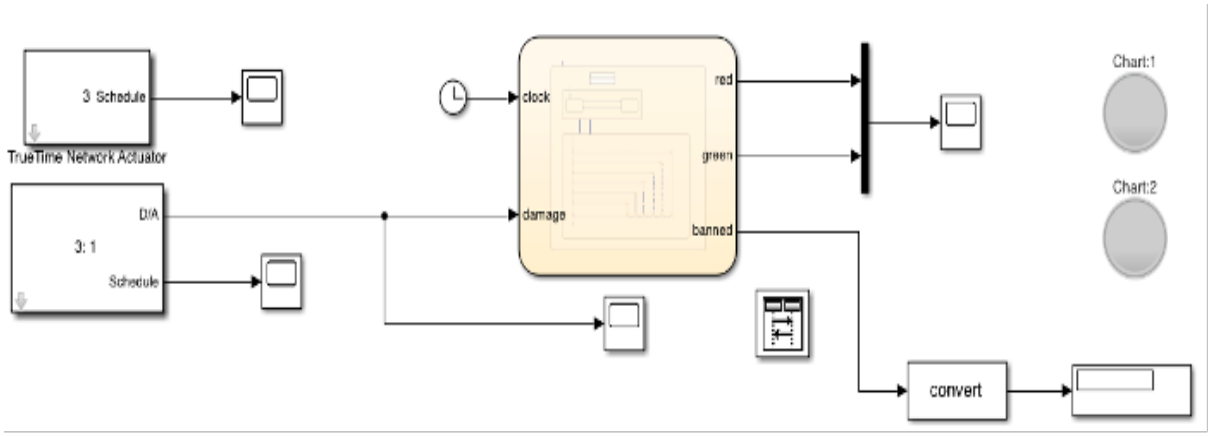

Figure 2: The kernel actuator received the directives forwards the incoming data to the stateflow. The result is shown by means of two indicator lights and a screen

The dual functioning allows to integrate this system with existing systems. Operation with pollutants has priority over normal operation, the result is shown by a Simulink display and by two green and red indicator lights.

PERFORMANCE EVALUATION

The performance aspect of the entire system is important in terms of reliability and effectiveness. The performances that have been measured are related to the delay in the propagation of information and the quantity of information (packetloss) lost in the ether. The measurement by the sensors is carried out at intervals of thirty minutes, the information is then forwarded accordingly. The measurement technique adopted is that of predicting the next enumerative of information that you think you should receive.

The calculation of the lost information is carried out every time there is an incremental value different from the one hoped for by subtracting the identifier received and the identifier hoped for, from the operation the result is stored together with the previous results of the same nature. It is estimated that for the whole du-

ration of the simulation over the 24 hours there is a loss attested to approximately 15.2% percentage points, out of a total of 46 forwardings there are only 39 receptions.

The propagation delay is the time elapsed from the forwarding of the information until the time of receipt.

The propagation delay that was measured relates to the temperature sensor, also because, for the other two sensors, an average delay very similar to that considered was attested. The report provided in the spreadsheet describes how each forwarding of about 30 minutes corresponds on average throughout the day to an average delay of 8% of about 0.08 [3].

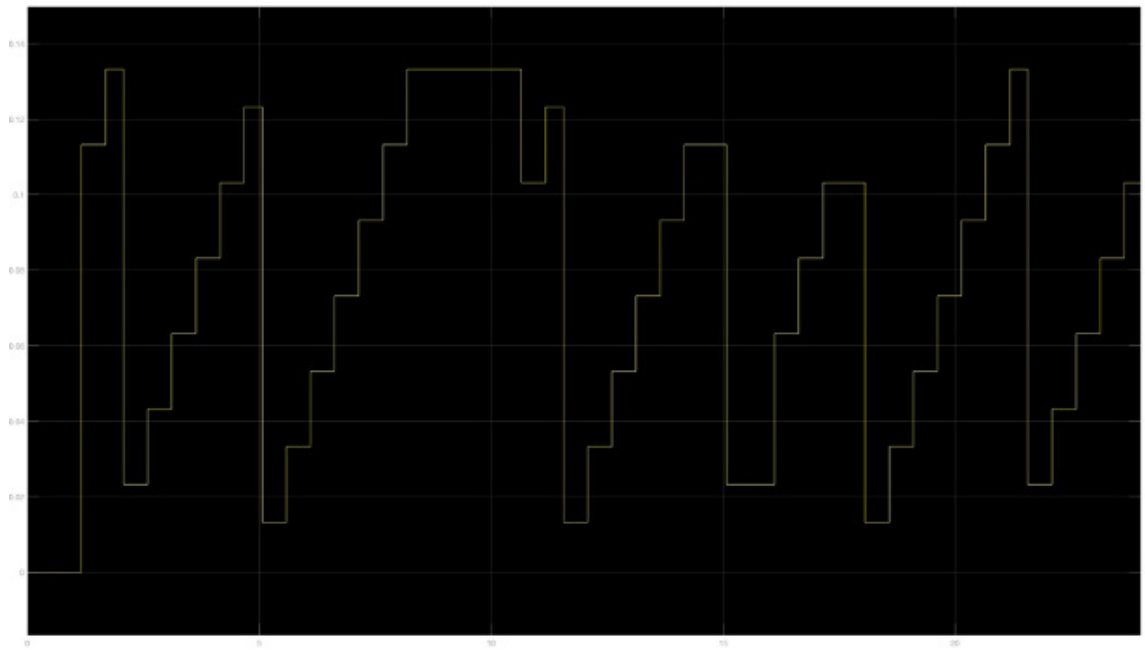

Figure 3: The report shows the time elapsed between one receipt of information and another.

Conclusions

The proposed solution is intelligent and is capable of limiting particulate concentrations immediately, possibly also carrying out a prevention function by closing certain categories of vehicles to traffic.

The interesting solution for the near future is the use of a mobile solution, using an eco-sustainable means of transport that does not affect the surveys, for example by means of an electric vehicle. The mobile solution is much more concrete than the physical solution at the gates because technologies could be used in collaboration with other companies, such as Google or Tesla for autonomous driving without a driver in order to have surveys on targeted areas or even extra-urban areas.

References

[1] Essential MATLAB for Engineers and Scientists Brian D. Hahn, Daniel T Valentine

[2] Numerical Analysis Using MATLAB and Excel Steven T. Karris

[3] Matlab Simulink documentation MathWorks https://it.mathworks.com/help/matlab/

[4] TRUETIME 2.0 – Reference Manual Anton Cervin Dan Henriksson Martin Ohlin Department of Automatic Control Lund University February 2016

[5] WHO global air quality guidelines Particulate matter (PM2.5 and PM10), ozone, nitrogen dioxide, sulfur dioxide and carbon monoxide

MACHINE-READABLE STANDARDS FOR LEAN PROCESS DESIGN

Maria Belova

Saint Petersburg State University of Aerospace Instrumentation
E-mail: marebel13@mail.ru

Annotation
Today, there is a need for full automation of all types of activities that can ensure the country's transition to a new level of economy. The past years have shown that only those enterprises that have switched to the digital environment and have realized the need for all new tools to automate most technological processes are competitive and survive. [1]

The gradual exclusion of the human factor from the technological process allows the company to increase the volume of products or services, reduce the time to perform labor-intensive operations, reduce the cost of raw materials, increase wastelessness, etc. Properly automated and well-organized operations will help not only reduce time and resources for manufacturing, as well as increase profits. [2,3]

But the current market conditions, characterized by technological changes and increasing requirements for documentation and employee skills, make most management systems obsolete. As a result, conventional automation, accompanied by the introduction of robotization, can cause a series of problems associated with the non-acceptance of new systems by personnel performing their work according to the established model, and will also incur large costs for the implementation of this scientific and technological revolution. Thus, new approaches are needed to increase the effectiveness of process improvement, eliminate additional costs and timely implementation of projects. Lean design is proposed and used as a solution to the problem.

This concept, otherwise called Lean, is built on designing a product or service with minimal costs and high consumer value.

Figure 1. Lean design concept

The Lean concept is based on the analysis of all parties interacting with the product and the processes of its manufacture and consumption, its competitiveness is also revealed by comparison with analogues, only after that the target cost design and planning of technological processes takes place. Various tools are used for its implementation: the transition from traditional logistics to the physical Internet, information modeling and digital twins are used. But many authors of scientific publications [4] see the workflow of transforming lean design of technological processes precisely on the basis of open machine-readable standards, which are moving to new technological principles in accordance with certain proposals of the market environment. The

chosen method for improving technological processes is based on social responsibility to the staff, which accepts negatively any scientific and technological revolutions.

Changing standards, their bases and information processing capabilities affect the “foundation” of the production system, which, as a result, leads to a gradual change and improvement of the entire production system. This fact is a direct proof of the transitional period corresponding to the proximity to the scientific and technological revolution on an industrial scale.

«Of course, standards should and can push the development of technologies - but today we are talking about fundamental changes. These changes require not only the content of the standards, but also their form. The standard and the document in the new conditions become not just a source of information, but a real tool at all stages of the product life cycle, from development to implementation. Namely, this is an expectation on the part of users of the standard.» [4]

To improve the standardization system and its viability, a product has been developed, called a machine-readable standard, which provides the possibility of using not only a person, but also computers. The classification of machine-readable standards is presented in Table 1.

Table 1

Classification of machine-readable standards and information systems

Level	Feature
Zero	The standard is fixed only on paper, which does not imply work with the machine
First	An open digital format (PDF-file) representing a system for publishing approved standards that allows reading and searching
Second	A machine-readable document (such as XML-standards) implemented by a user server
Third	Contains machine-readable content (standards in the form of a database or program code), reflects the life cycle of scientific and technical documentation, represents systems for managing regulatory and technical documentation and requirements management
Fourth	SMART-standards, whose systems are closely integrated with CAD / CAM, PLM / PDM, with systems based on BID technologies. This standard can be interpreted by the machine itself (computer technology) without the participation of a human operator. These standards are inherently information models capable of building independent relationships between elements.

Thus, a machine-readable standard goes through 5 levels of development, the key of which is a fundamentally new product, the work with which is possible without human intervention. SMART standard is a complex digital structure that can contain containers of textual, graphical and numerical data, as well as digital models. On the one hand, it has "smart" human-readable components that form expert and analytical systems that help the professional make a decision.

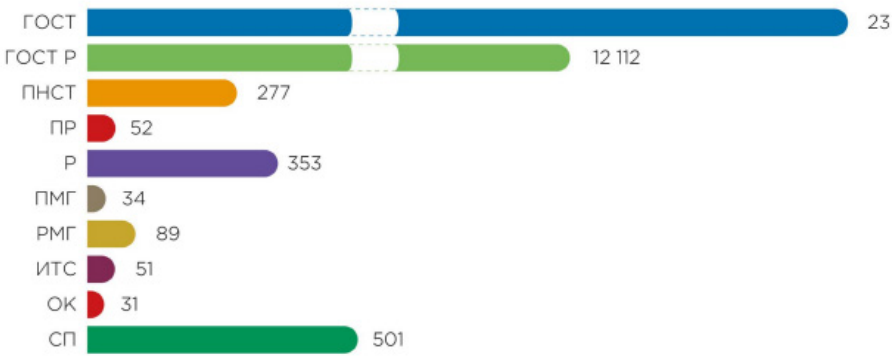

Figure 2. Composition of the Federal Standards Fund (data as of 01/01/2021)

The use of machine-readable standards in lean design of technological processes is built on the basis of the Lean concept itself: since this design requires a complete analysis of technological processes, the development of machine-readable requirements for the manufacture of products will be able to control the produc-

tion and operation process on-line with the help of correct reading by any information systems, while using artificial intelligence, digital twins, the Internet of things and other possibilities of Industry 4.0.

The transfer of the fund (Fig. 2) to the digital XML format will help at this stage to create a documentation base, the search and analysis of which will already be more accessible to employees. Adding to this system the ability to search for the required documentation using artificial vision analyzing the manufactured product, as well as reading the standard by a machine and setting an automatic operation command, all this can reduce waste in raw materials, time and knowledge. reduce the risks associated with quality, missed deadlines, and product overpricing, and manage the life cycle of a high value product or service.

Thus, the above possibilities of machine-readable standards in the future will help to make the design of technological processes more economical, since the possibility of automated interaction throughout the entire life cycle with all the necessary documentation for manufactured products, as well as the possibility shifts or adjustments of technological operations based on identified standards and communicating information systems will prevent manufacturers from unnecessary losses and establish processes without equipment downtime.

Conclusion

There is a real opportunity to observe the next round of development of complex technical and information systems, in which it will be possible to see the standards not in the usual paper form, but already in the form of a program code or a set of symbols that create an orderly activity. Of course, there is a certain kind of difficulty in implementing such systems, since they will cause widespread conservative resistance from personnel related to the execution of technological processes. Entire industry structures that are engaged in the repair and maintenance of technological complexes will have to switch to new principles for organizing work and adapt to existing realities. The introduction of typewritten standards will avoid a high number of defective products, due to the absence of the influence of the human factor. Fully standardize all technological operations, as well as achieve the unification of most assembly units and parts in industrial production. [1]

Literature

1. Problems of integration of machine-readable standards into reproducible production processes of scientific and industrial complexes / S.A. Nazarevich for the conference of the III International Forum in the framework of the celebration of the 80th anniversary of the St. Petersburg State University of Aerospace Instrumentation, 2021, p.399-400

2. Korshunov G., Frolova E., Nazarevich S., Smirnov V. Fuzzy models and system technical condition estimation criteria. Advances in Intelligent Systems and Computing . 2020. T. 1041. C. 179–189.

3. Nazarevich S.A., Vinnichenko A.V., Kurlov V.V. Applicability of the reverse engineering model for unification tasks in systems engineering processes of engineering enterprises. In the collection: JOP Conference Series: Metrological Support of Innovative Technologies. Krasnoyarsk Science and Technology City Hall of the Russian Union of Scientific and Engineering Associations. Krasnoyarsk, Russia, 2020. C. 52076.

4. V. P. Kupriyanovsky, O. N. Pokusaev, D. E. NAMIOT, A. A. Klimov, M. G. Zhabitsky Digital concrete: open BIM, machine-readable standards, IOT, digital twins, logistics 4.0, lean building and other industrial approaches using the examples of transport infrastructures In the collection: INTERNATIONAL JOURNAL OF OPEN INFORMATION TECHNOLOGIES, 2021, p. 133-173

ANALYSIS OF REGULATORY DOCUMENTATION ON THE USE OF COLLABORATIVE ROBOTIC SYSTEMS IN THE TECHNOLOGICAL PROCESS

Aleksey Bobryshov

Saint-Petersburg State University of Aerospace Instrumentation,
Saint-Petersburg, Russia
E-mail: ap.bobryshov@mail.ru

Abstract
A collaborative robot is an automatic device capable of performing technical operations together with humans without causing them any harm. Such devices are implemented in industries where the process is designed in such a way that a human and a manipulator need to function in the same area. For example, the system of automated verification of control and measuring devices implies the use of a robot as a body, which sets the measuring devices in the connection cells of the measuring stand. The task of a human is to control the verification process, and to correct the connection of the equipment under test, which implies a temporary location in the working area of the manipulator. Therefore, in order to implement a collaborative robot in the process of verification of testing and measuring equipment, it is necessary to comply with all regulatory requirements. This article analyzes and studies the safety requirements for the introduction of collaborative robots in the production process.

Regulatory documents

For industrial robots and robotic systems, "Safety Requirements for Industrial Robots", ISO 10218-1 and 10218-2 committee dated 2011 [1] have been developed. Due to the emergence of a new type of robotic manipulator designed to work together with humans, the committee developed ISO/TS 15066:2016 [2] based on previous GOSTs. This is the first specification in the world, which describes all safety requirements for collaborative robots, these requirements have been developed since 2010. The ISO committee consisted of experts from twenty-four countries, and leading companies manufacturing industrial robots. It focuses on the additional requirements and recommendations in collaborative industrial robotics which are described in ISO 10218-1 and ISO 10218-2. The main objective of ISO/TS 15066 is to establish safety requirements for collaborative robotic systems and humans (Figure 1), collaborative workspace - collaborative workspace, operation space - workspace.

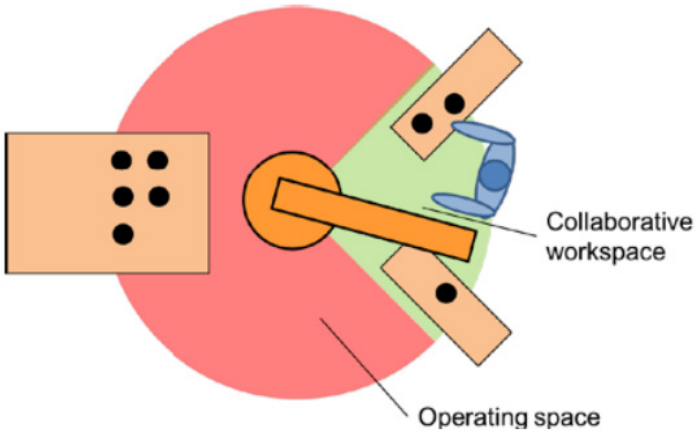

Fig. 1. Divided workspace areas

The document is also a guideline for technicians performing risk assessment of human-robotic collaboration. The main requirements in ISO/TS 15066:2016 for CR and robotic systems when working with humans are: speed of operation at close proximity to humans, human distance estimation, applied force at physical contact, and speed of response to contact.

Manipulator workspace

According to the established norms, the joint workspace of the CR with a human, is divided into several zones with different speeds of the collaborative robot. Figure 2 shows their main types [2]. The first two zones, in which a person enters when it is necessary to interact with the manipulator, are the areas of the beginning of the average speed and slow speed, at their intersection the speed of the collaborative robot begins to gradually decrease. The first zone is the interaction between the robot and the human, with the speed of the manipulator remaining the same, then comes the second zone, in which the pace of operation begins to decrease to a minimum set value. The next areas of space are, the control stop area with nominal safety and the safety stop. The control stop area implies the reduction of the speed of the manipulator to a minimum value of about one to two centimeters per second, the safety stop area implies a complete stop of the robot when crossing this area. If during the process of work the workers do not have to be close to the robot's working area most of the time, then the distance requirement and reaction to its change will be enough for the collaborative robot.

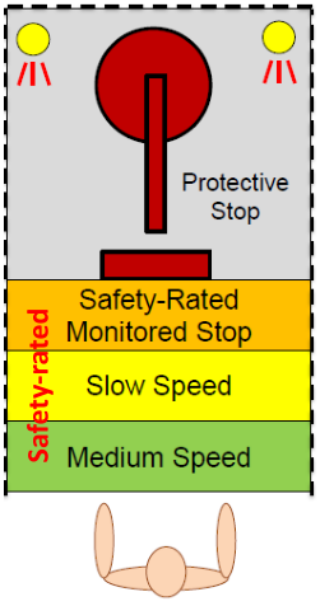

Fig. 2. Collaborative workspace areas of a collaborative robot with a human

Safety-rated - nominal safety zone, protective stop - protective shutdown zone, safety-rated monitored stop - controlled nominal safety stop zone, slow speed - slow operating speed zone, medium speed - medium operating speed zone. The whole area of the working space is called the safety separation distance and can be calculated according to the following formula:

$$S_p(t_0) = S_h + S_r + S_s + C + Z_d + Z_r$$

Where in this formula: $S_p(t_0)$ - protective separation distance; S_h - change of operator's location; S_r - change the location of the robot; S_s - protective braking distance; C – the distance a person can go into the area of the danger zone; $Z_d + Z_r$ – uncertain facts of "intrusion" for robot and human.

The listed zones are set as follows. The change of location of the robot is the working area equal to the area in which the collaborating robot operates. The next protective braking distance, equal to half the area of the working area. The area of the danger zone in which a person can enter is one fourth of the area of the working area. The operator's change of location is set equal to the protective braking distance. The last undefined area, is set equal to 20% of the working area value. These zone values are the minimum values, in the design. Figure 3 shows a graph of the dependence of the speed of operation of the CR on the distance to the working personnel [2].

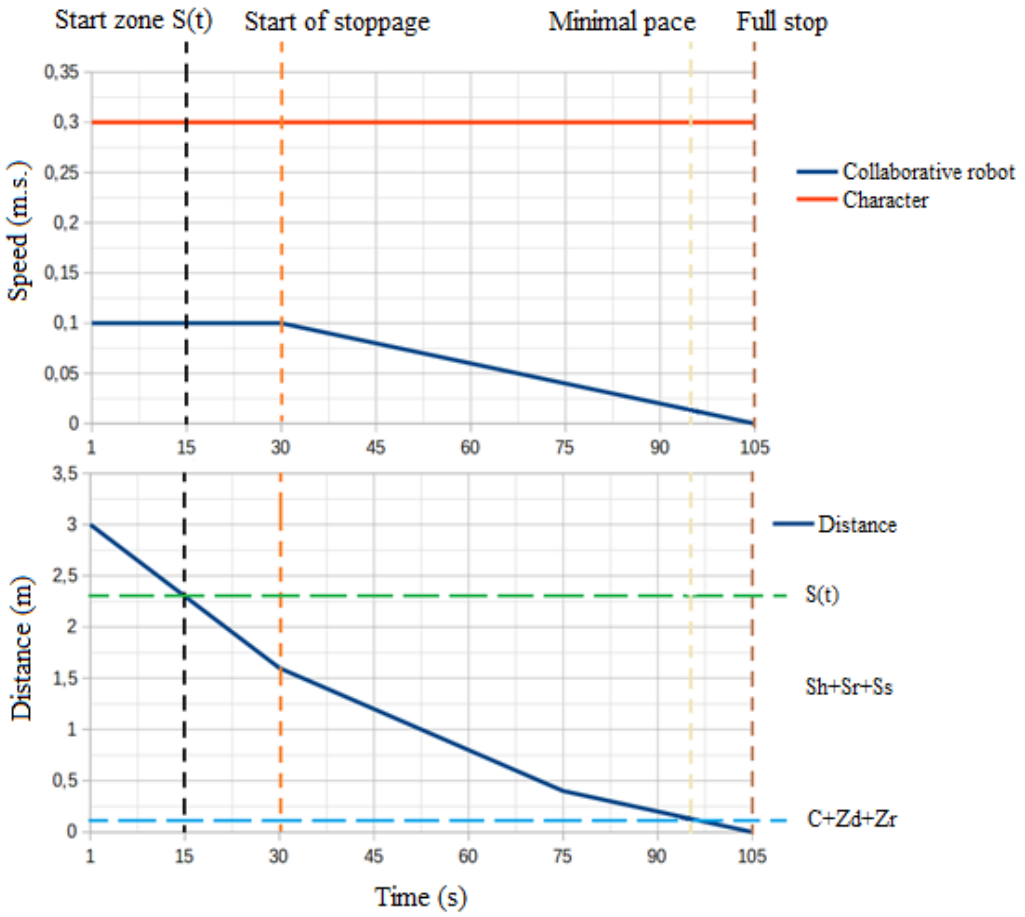

Fig. 3. Diagram of the speed of the collaborative robot on the distance to the workforce

There are five main time zones that can be noted on the graph. The first region up to the guard separating distance, can constitute absolutely any time interval, as long as the worker does not cross the boundaries of the first zone. The next region is from the beginning of the zone $S_p(t_0)$ to the beginning of the stop zone, as described above, in this region the robot's operating tempo is maintained. The zone from the beginning of the stop to the minimum ramp is the immediate zone of the manipulator speed reduction. The fourth area shows the time of ramp reduction from minimum to full stop. The last time interval shows a complete stop of the crane. These time intervals are calculated, the speed of the working personnel is taken as a conventional value of 3 m/s.

Interaction at human contact

Physical contact between the collaborative robot and operator can occur either intentionally or unintentionally, which is why the robot system must be designed with power and force limitation. Normal contact is detected by means of force sensors mounted on the collaborative robot itself. If the constant presence of the working personnel in a close area, and sometimes in the area itself, of the workspace is necessary, equipping the robot with contact sensors is necessary [2]. It is also necessary to determine the conditions under which contact can occur, assess the potential risk of these contacts, intelligently design a joint workspace to reduce the probability of collision. If the nature of the work does not allow to avoid contact between the robot and a person it is necessary to take into account the areas of the operator's body exposed to contact with the collaborative robot. The probability of collision of the robot's organs with the head, throat and neck must be avoided [3]. When writing the standard ISO/TS 15066:2016 were taken into account the study of human pain threshold, when in contact with different parts of the body. Table 1 presents these values. The values are divided from 1 to 30, the lower the score, the lower the pain threshold on contact. It is also necessary to take into account the established time of reaction of the person on contact, the given value is equal 0,3 - 0,5 seconds.

Table 1

Results of the study of human pain threshold

Body area	Exact area	Evaluation
Head and forehead	Center of forehead	1
	Temple	2
Face	Chewing muscles	3
Neck	The whole area	4 - 5
Back and shoulders	The whole area	6 – 7
Breasts	The whole area	8 – 9
Belly	Abdominal muscle	10
Pelvis	The whole area	11
Forearms and elbow joints	The whole area	12 – 16
Lower area and joints of the arm	The whole area	14 – 15
Palms and fingers	The whole area	17 – 25
Hips and knees	The whole area	26 – 27
Shins	The whole area	28 - 29

Conclusion

According to the requirements of ISO/TS 15066:2016 normative documentation, when introducing a collaborative robot into a technological process, important points of requirements must be fulfilled. Initially, the safety separation distance $S_p(t_0)$ must be calculated, in other words, the boundaries of the collaborative workspace must be established. When calculating the separation distance, the anticipated contact between man and machine, the initial access paths (route or worker movement), the risk of slipping or falling due to touching the work leads must be taken into account. The human factor, such as possible loss of concentration, fatigue, mistakes of the worker in interaction with the manipulator, human reflexive behavior, the level of training of the worker must be taken into account, as this condition will also help to comply with the admission of specially certified workers to work together.

Manipulator installation also plays an important role. Considering the technological process in the form of installing measuring devices in the test bench and keeping in mind that the upper region of the human body has a lower pain threshold, it is recommended to install the collaborative robot in such a way that the head, face, neck and chest do not fall into the contact zone of the robot and the person. According to the results of the pain threshold study, and considering the decrease in the robot's speed when the separation space is reduced, collision with human body parts below the thorax will not be significant. It is also always worth keeping in mind the probable failure of the manipulator or failure of the work program, in which case it is necessary to provide for a manual shutdown of the robot.

It is advisable to introduce a collbar robot into the technological process designed for an average flow of produced or verified products. This solution allows you to place the manipulator in a small area without the use of a fencing cage to restrict personnel access to it [4]. Of course, such a solution will allow to carry out joint labor activity of a person with a manipulator without the risk of injury to the latter, which is an undoubted advantage.

References

1. GOST ISO 10218-1 и 10218-2. Safety requirements for industrial robots;
2. GOST ISO/TS 15066 Safety requirements for collaborative robots and robotic systems;
3. Modeling and control of trust in human and robot collaborative manufacturing. URL: https://www.researchgate.net/publication/288362883_Modeling_and_control_of_trust_in_human_and_robot_collaborative_manufacturing (Date of request: 20.02.22);
4. Manufacturing Perfomance Increase by application of a transformable assembly system using collaborative robots. URL: https://cyberleninka.ru/article/n/povyshenie-proizvoditelnosti-truda-za-schet-primeneniya-transformiruemoy-sborochnoy-sistemy-s-ispolzovaniem-kollaborativnoy/viewer (Date of request: 01.03.22).

STARTUP DEVICE FOR AUTOMATED CONTROL OF THE GEOMETRIC PARAMETERS OF AN ADDITIVE PRODUCT

Daniele Casadio

Saint-Petersburg State University of Aerospace Instrumentation,
Saint-Petersburg, Russia
E-mail: kazdanila@gmail.com

Annotation
The implementation of measuring systems for additive processes is hampered by the problem of the lack of systems for diagnosing and controlling the products being created. The quality of parts manufactured by additive technologies deviates greatly from the specified standards due to inapplicable dimensional tolerances, defects in surface roughness, and the presence of mechanical stress fields. For this reason, minimal deviations in external conditions that occur during the manufacturing process cause a discrepancy in the final product in terms of properties or shape. A huge advantage will be the fact that the measuring system has the ability to be integrated into an agreed production complex. This is due to the fact that the final measurements of the geometric parameters of certain products must be compared with the mathematical model developed in the CAD system, and the measurements associated with defects, latent stresses, product structures must be transferred to the CAE system in order to make a decision about suitability of the product or preparation of technology and algorithm for further work with it. In order to control the parameters of products created on the basis of additive technologies, certain measures were proposed related to the methods of structured light and shearography (Figure 1).

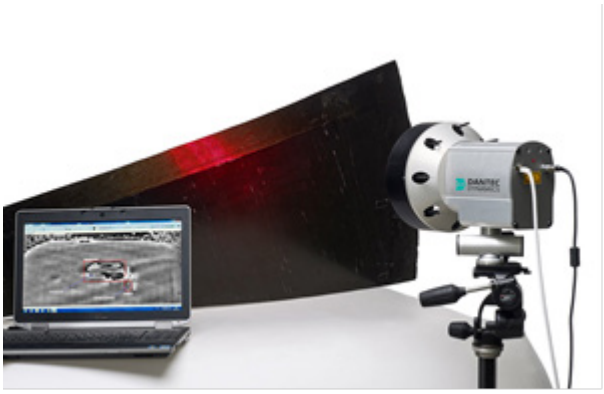

Figure 1. Sherography

Additive technologies are becoming one of the main links that determine the current state of the country in the field of digital technologies, and ensure the modernization of established industries and the development of new generation industrial production. This technology of "3D printing" began its development in the late 80s of the last century. The pioneer in this field is 3D Systems, which in 1986 developed the first Stereolithography Apparatus.

The first stereolithographic (SLA) and powder (SLS) machines had little popularity due to high cost and a limited choice of materials used. They were mainly used in the field of development and research work, intersecting with the defense industry until the mid-90s. With the further development and spread of digital technologies in the fields of detailed modeling, machining and 3D modeling, technology has made a huge leap in development.

From 2010 to 2015, the global additive technology market grew by an average of 27% per year and reached a volume of $5.1 billion, of which about 40% is for equipment and materials, and 60% for engineering services (development of mathematical models, technologies and synthesis of details).

For the production and modeling of products, it is necessary to use computer technologies and programs in order to develop a layer-by-layer synthesis technology. They use systems such as CAM (Computer-Aided Manufacturing) and CAD (Computer-Aided Design). The list of these automated systems has recently included CAE (Computer-Aided Engineering). All of them were created with the aim of evaluating when observing a real product in the conditions of use for its intended purpose using mathematical modeling methods using calculation methods (finite difference method, finite element method, finite volume method)

in order to be able to evaluate and monitor the behavior of a computer product models in the initial and previously established conditions. These technologies have a broad and direct impact on accelerating innovation as well as cutting costs and significant cost reductions for new product development, in turn leading to increased competitiveness (Figure 2).

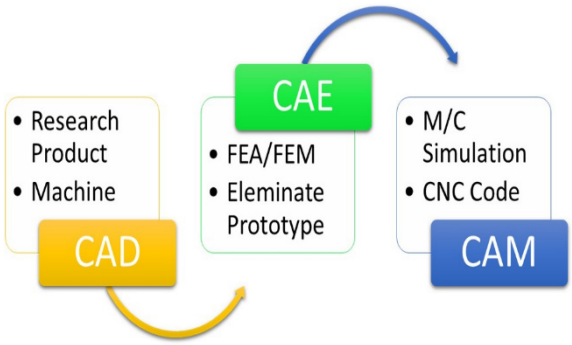

Figure 2. Computer simulation technologies

CAD / CAM / CAE systems are used by all industries in which it is necessary to create products using additive technologies. Their capabilities include the synthesis of details of various technical and not only systems (development of 3D models, distribution and manufacture of supports) and control over the synthesis technology (scanning strategy, radiation power, scanning speed and step, etc.). This takes into account the process of formation of the structural-phase state of metal, ceramic and polymeric materials of a new generation in the process of additive technologies with subsequent thermal and barothermal processing of parts.

Devices called 3D scanners are used to capture 3D measurements of real objects, which are then processed and analyzed digitally. These devices have gained immense popularity due to their capabilities. They do not need to be in direct contact with the object being scanned, they can be used for partial or full three-dimensional measurement of any material object. Most of these devices generate points of extremely high density compared to traditional contact measuring devices, which gives much more information about the object being measured (Figure 3).

Figure 3. 3D scanner

The most popular models of metrological equipment are Creaform's MetraSCAN and HandyPROBE. MetraSCAN is a 3D laser scanner designed for high-speed scanning and precision measurements of large, complex objects. HandyPROBE is a portable coordinate measuring machine that replaces traditional measuring hands, it allows you to measure simple objects (planes, cones, cylinders) and save the measurement results as CAD data. The principle of operation of a laser scanner is based on the triangulation method of measuring the distance to an object. The essence of this method is as follows: the laser beam emanating from the source, which differs from ordinary light by the high parallelism of the beam, falls on the surface. Further, part of the incident beam is reflected from this surface and enters the receiver.

At the receiver, a lens focuses the reflected beam onto the CCD, where the position of the bright spot on the array indicates the direction of the incoming beam, i.e. the angle between the laser beam and the returned light.

The angle of reflection of the laser changes depending on the distance to the object and thus the position of the laser point on the receiver changes. Given that the laser beam source and receiver are fixed and located at a certain distance, we can measure the angle of reflection with a simple geometric construction.

As a result, we know three parameters: the distance from the receiver to the source, the angle between the emitted laser beam and the receiver-laser line, and the angle between the reflected beam and the receiver-laser line. Using these three parameters, you can restore all sides and angles of the triangle, including the distance to the object.

Table 1

Comparison of portable 3D scanners

Comparable characteristics	Creaform Go!SCAN 50	Creaform Go!SCAN 20
Permission	0,5 мм	0,2 мм
Accuracy	100 мкм	100 мкм
Depth of field	250 мм	100 мм
Scanned object size	0,3-3 м	0,05-0,5 м
Working distance to object	400 мм	380 мм
Texture resolution	50 to 150 DPI	50 to 250 DPI
Light source	white LED	white LED

The main problem that hinders the widespread introduction of additive technologies is the lack of diagnostic and control systems for manufactured products. The quality of AM parts varies greatly due to inadequate dimensional tolerances, surface roughness, and defects, thus limiting the wide application of these technologies. This variability can be minimized by process control, but there are no adequate measurement processes available today. This leads to the fact that the slightest deviations of external conditions that occur during the manufacturing process cause inconsistencies in the final product in shape or properties.

It is also extremely important to check parts formed using additive technologies for defects. Due to the peculiarities of the physical processes that occur during the formation of such products, not only defects usually characteristic of the materials used, but also fields of mechanical stresses can occur in them (Figure 4).

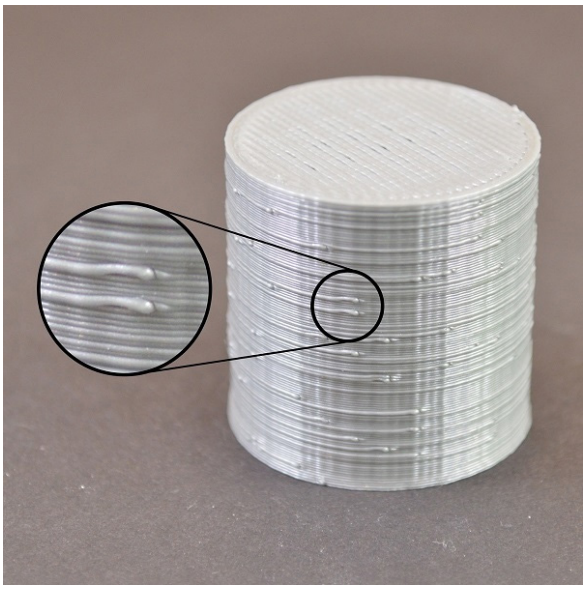

Figure 4. Part defect

Considering that the use of additive technologies is most appropriate in the manufacture of expensive products of complex shape and with desired properties, control over technological processes and diagnostics of final products are one of the key links in the wide distribution of these technologies.

At the same time, it should be noted that the result of measurements of the geometric parameters of specific products must be compared with the mathematical model developed in the CAD system, and measurements of defects, hidden stresses, product structures must be transferred to the CAE system to make a decision on the suitability of the product or develop an algorithm and technology for its further processing. Thus, the measuring system should have the potential to be built into a single production complex.

When creating measuring systems for additive technologies, a combination of various methods of reliable non-destructive testing can be used, which in the general case requires solving the following problems: first, in each specific case, it is necessary to determine the list of characteristics of additive manufacturing products that need measurements; secondly, to determine the most adequate measurement methods that allow creating a system for assessing the quality of additive manufacturing products. An analysis of modern industrial technologies makes it possible to formulate the basic requirements for measuring and diagnostic equipment that are used in their implementation. These include: non-contact measurements, high productivity, on-site measurements, high detectability of defects, real-time measurement of characteristics, forming effects on the material; thirdly, to develop methods and equipment for non-destructive testing of products obtained using additive technologies with the required level of reliability. Create appropriate measuring instruments and develop a system for their metrological support.

Conclusion

Develop methods for metrological control and testing of products made by layer-by-layer synthesis; Finally, what may be the most important thing is to integrate the created measuring systems as much as possible into an integrated system of digital production. This requires the creation of specialized software interfaced with modern CAD / CAM / CAE systems.

List of used literature

[1] Chabanenko A V, Kurlov A V 2021 Control the quality of polymers based on the model of Dzeno Journal of Physics: Conference Series

[2] Pavel Kosushkin Edition: Vector High Technologies No. 2 (23) 2016

[3] Batkovskiy A M, Nesterov V A, S emenova E G, Sudakov V A and Fomina A V 2017 Developing intelligent decision support systems in multi-criteria problems of administrative-territorial formations infrastructure projects assessment Journal of Applied Economic Sciences 12(5) 1301-11.

[4] Maiorov E E, Prokopenko V T, Mashek A C, Tsygankova G A, Kurlov A V, Khokhlova M V, Kirik D I and Kapralov D D 2018 Experimental study of metrological characteristics of the automated interferometric system for measuring the surface shape of diffusely reflecting objects Measurement Techniques 60(10) 1016-21.

[5] A V 2018 Quality management of radioactive electronic equipment RIA: Journal: "Standards and Quality" 2 90-94.

[6] V. L. Minaev, G. N. Vishnyakov, A. D. Ivanov, G. G. Levin Methods of control of geometrical parameters and internal stresses of products of additive technologies 2020.14.1.42.54

HOSPITAL'S NETWORK FOR COVID-19 MANAGEMENT

Corrado Picone,
Marco Severino,
Matteo Tornabene

Computer Engineering and Networks Laboratory – Kore University of Enna - Italy
Email: {corrado.picone, marco.severino5, matteorino.tornabene }@unikorestudent.it

Abstract
After the global health emergency of SARS-CoV-2 virus that has devastated the global society and economy, there is the need to create new structures that can offer the main health services, with specific tasks, to fight the pandemy.

Introduction

The project was based and developed on the Italian hospital system. The simulation was ran on a town of 30,000 inhabitants that fight the virus in a year (where a second of simulation corresponds to a day). However the simulation analyzes and processes data using risk indicators provided by "Ministero della Salute" (Italian Ministry of Healt), as mentioned: "Il monitoraggio dell'epidemia dei casi di COVID-19 in Italia viene effettuato attraverso [...] il flusso dei dati aggregati inviati dalle Regioni coordinato da Ministero della Salute, con il supporto della Protezione Civile e dell'Istituto superiore di sanità, per raccogliere informazioni tempestive sul numero totale di test positivi, decessi, ricoveri in ospedale e ricoveri in terapia intensiva in ogni Provincia d'Italia"[1] .

THE PROPOSED APPROACH

The system is clearly divided into five sections connected to each other by five wired networks and three gateways:

1) Vaccines Center (Network 1)

The Vaccines Center is in charge of the vaccines daily somministration to the whole population during all the simulation time. For a realistic results, the vaccines somministration begins after one month.

2) Covid-Tests center (Network 2)

The Covid-Tests center provides the number of daily positive covid tests. This is influenced by zone value and vaccination rate.

3) Intensive Care (Network 3)

The Intensive Care provides the daily number of hospitalized patients in intensive care. This is influenced by vaccination rate and number of daily positives.

4) ASP (Network 4)

The ASP (Azienda Sanitaria Provinciale) is the entity that is responsible of data management and processing, from the previous Networks, for determine zone value to adopt. The concept of zone value is linked to epidemiological dissemination. The zone values are:

- White, minimal diffusion
- Yellow, moderate diffusion
- Orange, high diffusion
- Red, maximum diffusion

5) Comune (Network 5)

The Comune is a municipal organization that defines and decides the limitations to adopts in relation of the zone value, for the following sections:

- Public services
- Catering
- Education
- Entertainment
- Sport

SCENARIO

This scenario was simulated using Matlab/Simulink - TrueTime software. The created networks are of wired networks CSMA/CD (Ethernet) type, and communication through the networks was made by three gateways. Below are analyzed the networks elements of the project:

Vaccines Center (Network 1)

(Image 1 in the Appendix) The Vaccines Center takes from the input a uniform random value between 95 and 115 that simulates the daily injections. This value was calculated to get the 100% of vaccinated population within 286 days. Using a delay block (30 sec) it simulates the vaccine release after a month. A Matlab function calculate the total injections day by day.

2) Covid-Tests Center (Network 2)

(Image 2 in the Appendix) The covid-tests center takes from the input two different values: vaccinated percent and zone value. A Fuzzy Logic Controller decides the percentage of positive covid tests. A Matlab function, that takes from the input a uniform random value between 100 and 1000 and the exit of the Fuzzy Logic Controller, decides the finite number of daily positive covid tests.

3) Intensive care (Network 3)

(Image 3 in the Appendix) The Intensive care takes from input two values: the daily positive covid tests and the vaccinated percent. By using a Fuzzy Logic Controller are determined the Intensive care patients. Through a Matlab function that takes in input a uniform random value between 0 and 60 (that represents the number of patients that have successfully recovered), the number of current patients, and the exit of the Fuzzy Logic Controller added to the patients waiting to have access to the intensive care, it gets the daily intensive care patients.

4) Gateway ASP 1

(Image 4 in the Appendix) This section sends data into the networks (vaccines center, covid-tests center, intensive care and ASP) through the use of two gateways: node 2 (node of networks 1-2-3-4) and node 4 (node only of the 4th network).

5) ASP (rete 4)

(Image 5 in the Appendix) The ASP takes from the input the number of vaccinated, the number of daily positives and the number of hospitalized patients in intensive care. The system uses a block of MBSD (Model Based System Design) named “Positivi totali” for summing daily positives to those not yet healed. In particular it uses a uniform random number to denote the viral load of a positive covid-test and determinates the remaining number of positives (this process is carried out individually for each positive).

A Matlab function calculates the percentage of vaccinated in relation to the number of the population, the percentage of positives in relation to the number of the population and the percentage of hospitalized patients in intensive care in relation to the number of places available. Using the first and second percentages, into a Fuzzy Logic Controller followed by a Matlab Function, is determinate the zone value.

6) Gateway ASP 2

(Image 6 in the Appendix) This section forwards zone value data from ASP (Network 4) to Comune (Network 5).

7) Comune (Network 5)

(Image 7 in the Appendix) Comune receives zone value data and uses a Matlab Function to defines and decides the limitations to adopts in relation of the zone value.

PERFORMANCE EVALUATION

In the simulation there has been done

Three types of Performance Metrics:

1) Responsiveness in ASP, calculated as

the difference between the transmission time and the receiving time of the packets from the ASP’s kernel. From measurements taken the latency found was 3 seconds;

2) Control of correct and complete reception of packets in an orderly way by using an ID, assigned in ascending order. From measurements taken there aren’t packets loss;

3) Responsiveness in Comune, calculates the time between the new zone value choosen (in ASP) and the restrictions actuation by the Comune. From measurements taken the latency found was 2 seconds;

Conclusions

At the end of simulation, we can infer that in absence of vaccine and restrictions the curve of infections increases linearly. After 30 seconds (days) at the release of vaccines, the curve of infections begins to be influenced by vaccinated rate, equally also the hospitalizations in intensive care. After 312 seconds (when the percentage of vaccinated population is 100%) the curve of infections, the number of patients in intensive care and the restriction adopted, drop dramatically (Image 8 in Appendix).

In conclusion, the difficult situation that all we are living it's far more complicated than the one shown by the simulation. Anyway, the proposed work wants to send a message purposeful and of hope, aimed to encourage the population to get vaccinated, proving the effectiveness of vaccine on the evolution of global pandemy. In addition, the system tends to highlight how a good synergy between organs and bodies, responsible of the virus management, permits the use of optimal standards and safety measures for the containment of the epidemic from Covid-19.

References

[1] Website Ministero della Salute - www.salute.gov.it - 24 January 2022 (data updated when the report is drawn up)

APPENDIX

(IM.1) Network 1 (Vaccines center) in Matlab-Simulink

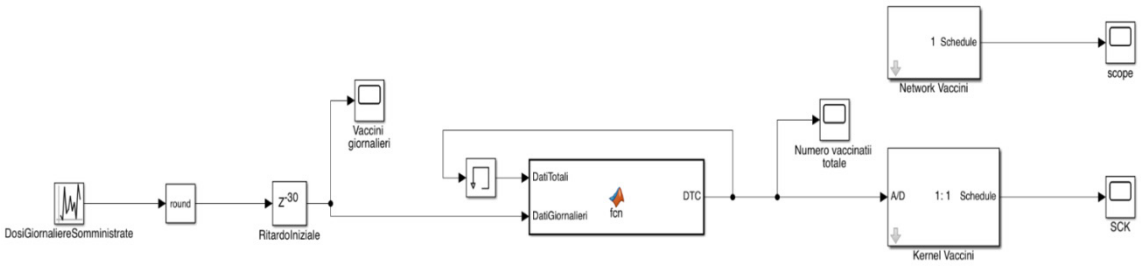

(IM.2) Network 2 (Covid-Tests center) in Matlab-Simulink

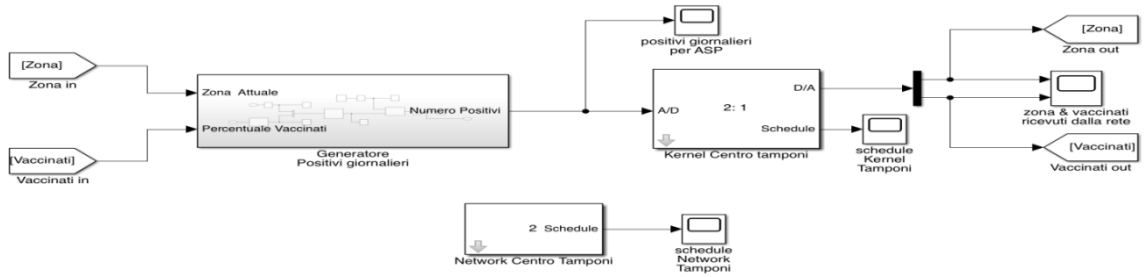

(IM.3) Network 3 (Intensive care) in Matlab-Simulink

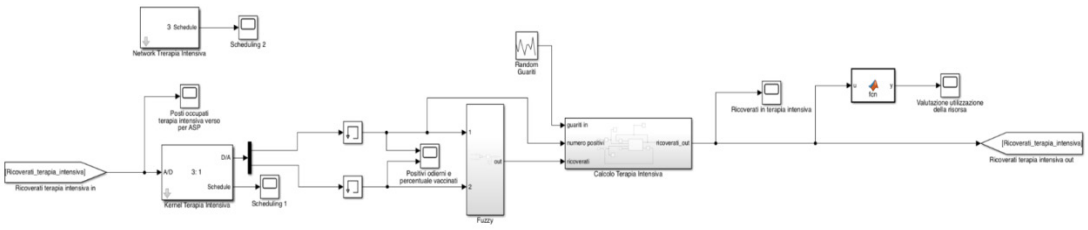

(IM.4) Gateway ASP 1 in Matlab-Simulink

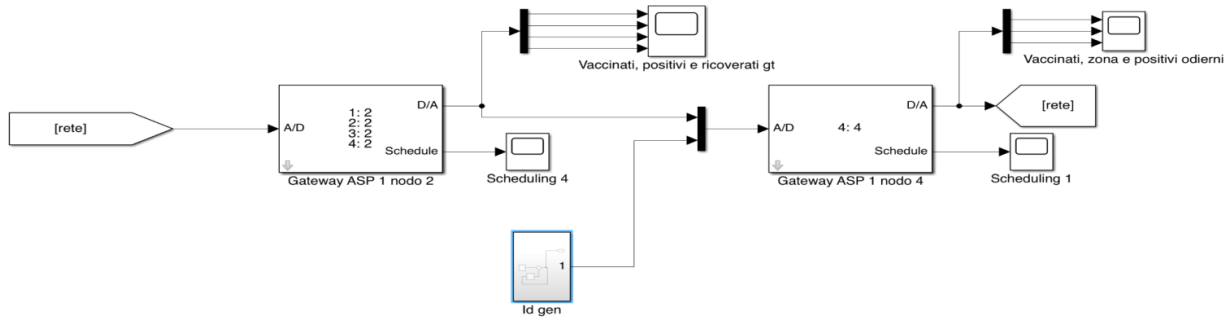

(IM.5) Network 4 (ASP) in Matlab-Simulink

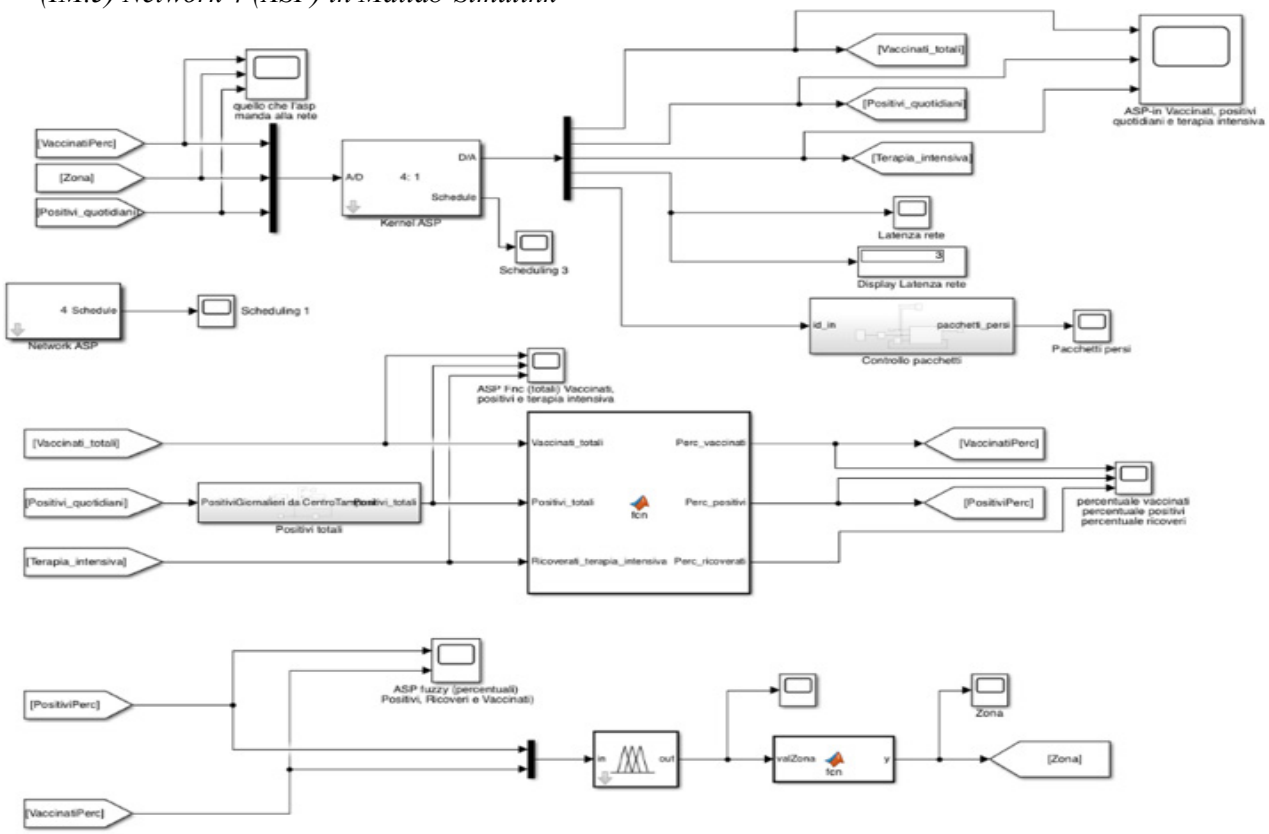

(IM.6) Gateway ASP 2 in Matlab-Simulink

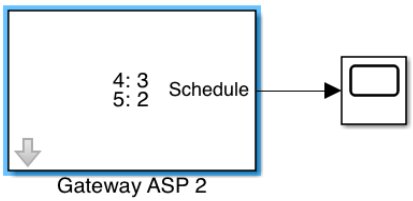

(IM.7) Network 5 (Comune) in Matlab-Simulink

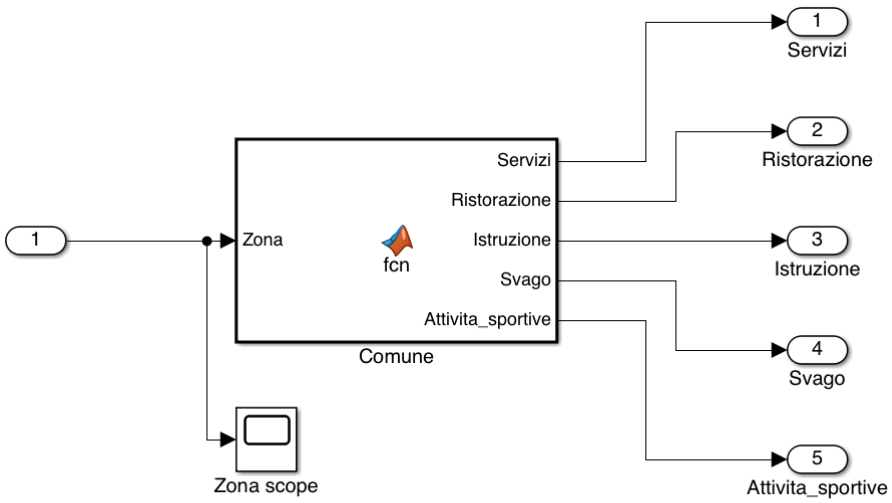

(IM.8) Rate of vacciantes, positives and intensive care in Matlab-Simulink

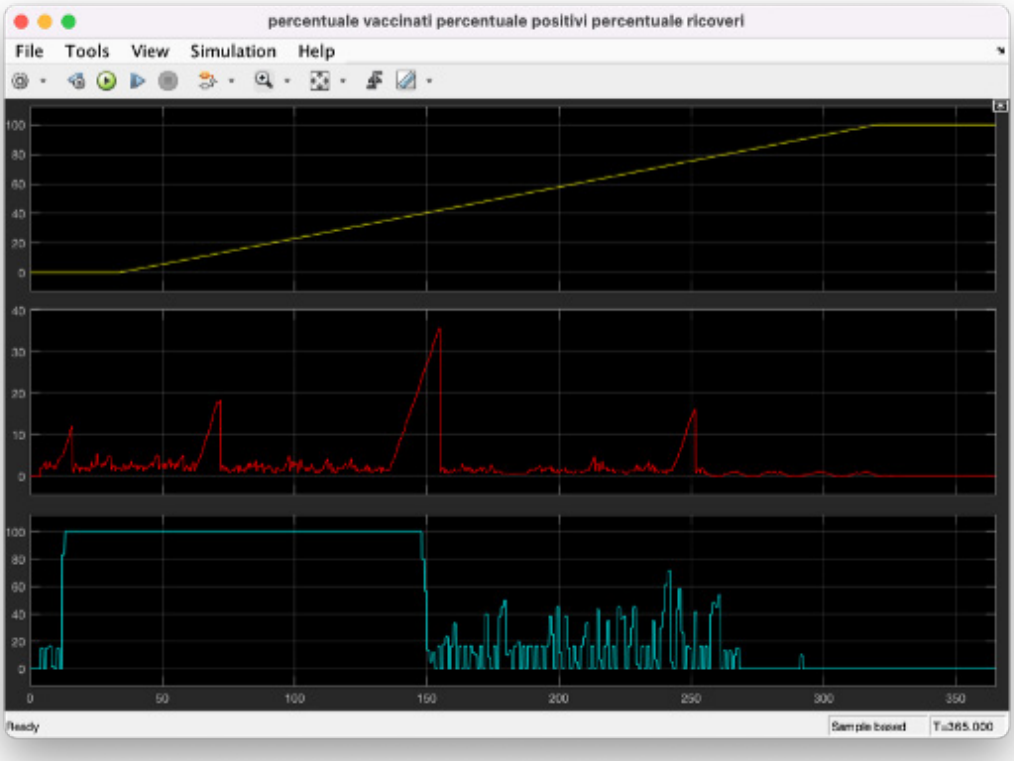

KOREHOME

Daniele Maria Bonadonna e Riccardo Russo

Computer Engineering and Networks Laboratory – Kore University of Enna – Italy
E-mail: danielemaria.bonadonna@unikorestudent.it
riccardo.russo9@unikorestudent.it

Abstract
The usage of home automation has been increasing in recent years thanks to the popularity of the Internet of Things. It can improve the quality of life by automating daily actions, thanks to the use of various sensors capable of conversing and exchanging information between them. Specifically, our project proposes the ideal scenario of a house, equipped with various sensors and switches allowing the activation of automation related to safety or quality of life. In particular, each room of the house has thermal and motion sensors, able to detect the presence of a person inside the room itself, thus being able to activate the automations. All the sensors are connected using LAN and wireless networks. In addition, the sensors in each room are wireless and battery-powered, recharged by a small solar panel.

INTRODUCTION

The KOREHome project represents our interpretation of home automation, applied to a realistic scenario.

Our project has the following features:

- **2 networks**: LAN and Wireless.

- **8 wireless nodes**: one per room, each connected to a battery.

- **1 LAN node**: a solar panel that sends production data to the gateway.

- **1 shared node**: the gateway, shared between the two networks.

Each node has the following sensors:

- **HC-SR501 PIR SENSOR** (Motion Sensor)
- **AMG88 GRID-EYE** (Thermal Camera)

The LAN node has the following solar panel:

- **GTIWUNG Solar Panel**

Each wireless node is connected to the following battery:

- **PANASONIC CR-P2L**

The choice of the components is the result of careful reflection on the realism and feasibility of the project. These components are available at very low costs and have a low power consumption.

We chose the batteries and the solar panel, so that we can physically guarantee a battery life of over 24h with a single charge having sensors always active.

The following sections will cover the following topics:

- **II: Related works**

- **III: Proposed approach** - detailed explanation of the networks

- **IV: Scenario** - detailed explanation of the Simulink implementation with slides

- **V: Performance** - detailed explanation of performance metrics and power consumption.

RELATED WORKS

Many years have passed since the diffusion of home automation, but it has yet to become a standard in every home, due to problems related to feasibility and costs. But in the last few years, thanks to the technological advancement, the costs of microprocessors have become more affordable and it is possible to arrive at excellent solutions at low cost. As written in [1] we can see that the introduction of wireless battery sensors

can help the feasibility of home automation in an easy and fast way, with consequent reduced costs, since you will not have to do any work on the structure of the house, as the sensors are movable. The authors of [2] illustrate the services that can be implemented in home automation nowadays, in fact the various types of services include security services, medical services, entertainment services, work services and so on.

Based on this, our project has tried to cover as many types of automation as possible. For example, speaking of security services, we have implemented anti-burglar systems and systems for gas leakage. We also decided to implement automations that aim to improve the quality of life, such as the automatic switching on of the lights and the automatic adjustment of the room temperature.

The following paragraph illustrates how the above-mentioned ideas are implemented.

THE PROPOSED APPROACH

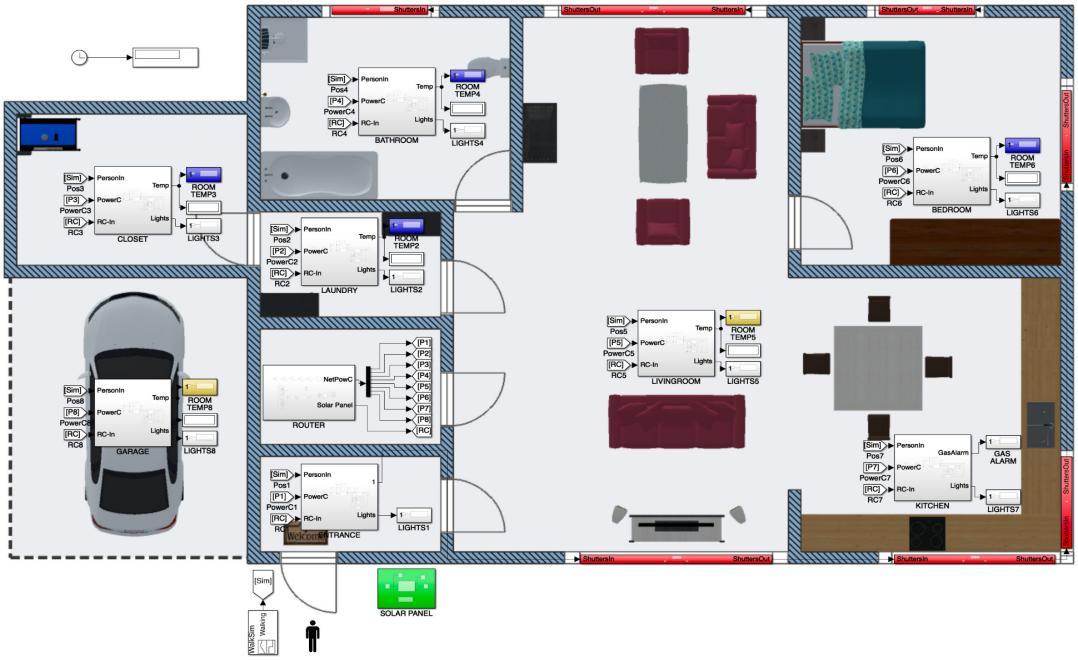

Figure 1: Structure of the Simulink model, made using a floor plan of a house. In our case, each room of the house corresponds to a node of the network.

The project makes use of a router, as seen in *Figure 1*, equipped with wireless antennas (network 1) and LAN ports (network 2).

The technical specifications of the Wireless network are:

- Type: 802.11b (WLAN)
- Data Rate: 0.8Mbit/s
- Transmit Power: 20dBm
- Packet Loss Probability: 1%

The technical specifications of the LAN network are:

- Type: CSMA/CD (Ethernet)
- Data Rate: 1.0Mbit/s
- Packet Loss Probability: 5%

In order to make the project consistent and realistic in all its parts, we calculated the positions of the wireless nodes in the various rooms of the house, based on the floor plan. Specifically, the position of the nodes is relative to the Wireless Network (positioned in x=0 and y=0).

With a transmission power of 20dBm the maximum range is about 87 meters.

The calculation of the distance between a node and the gateway is equal to the hypotenuse of the triangle formed by the coordinates.

SCENARIO

The system in *Figure 2* is common to all the wireless nodes.

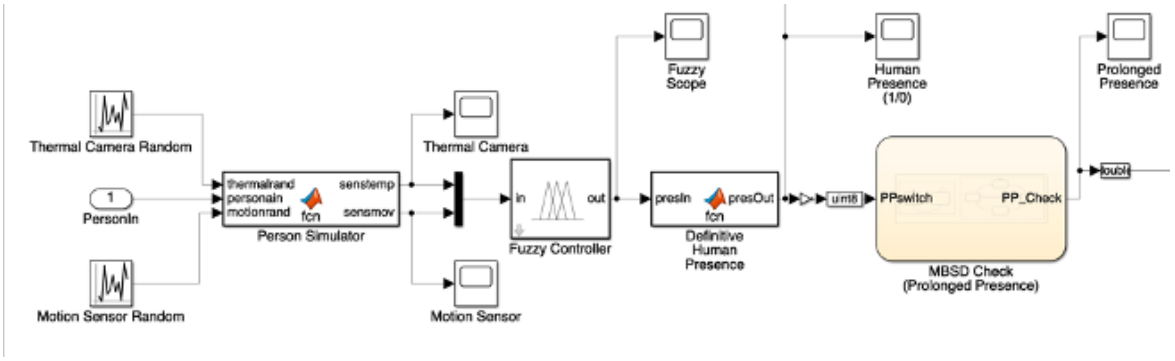

Figure 2: From left to right: random number generators (thermal and motion sensor values), a fuzzy controller and an MBSD used to determine if a person is in the room.

To simulate a realistic scenario, the two sensors receive data only in moments of time defined by the signal builder, which will be passed to a fuzzy controller to determine if the motion detected was human. This movement is sent to an MBSD controller to check how many seconds it lasted. If the duration exceeds 2 seconds, then the output of the MBSD will be equal to 1. This will allow us to enable all the automations, sending this data into the network.

Subsequently, each node has different functions, depending on the automation it will have to perform. For example, the entrance node is structured as shown in *Figure 3*.

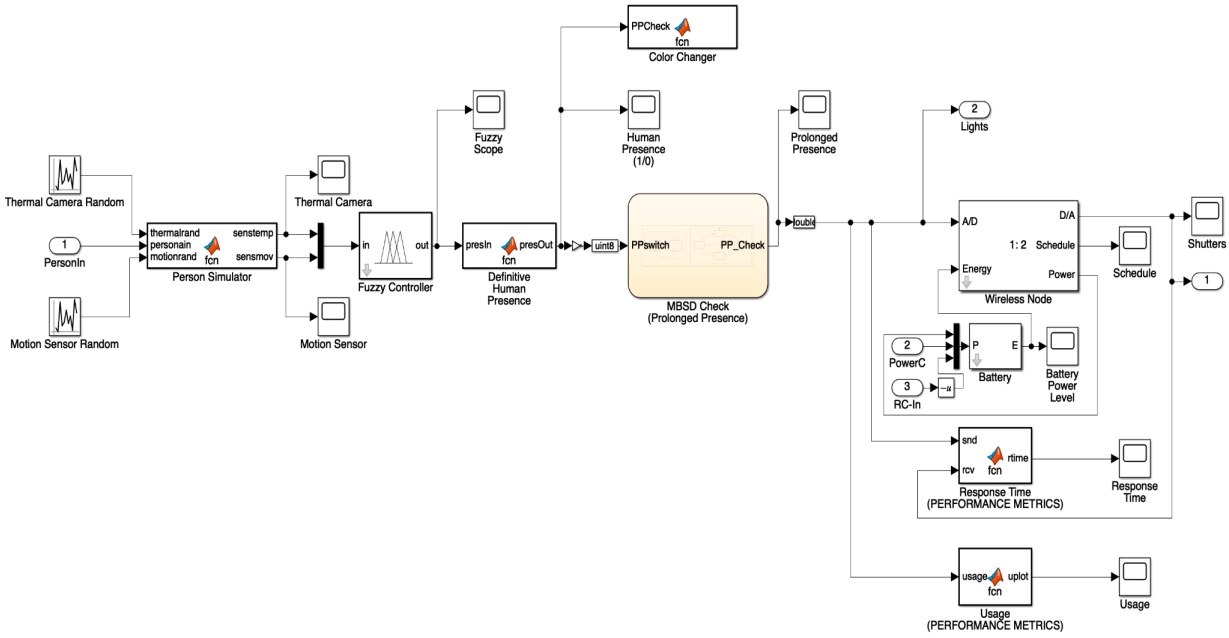

Figure 3: This specific node, after sending the prolonged presence to the gateway, will decide whether the shutters should be opened or closed throughout the house.

There are also two MATLAB functions to check the Response Time of a request and the Usage of this node throughout the duration of the simulation.

As for the signal builder, we decided to use it to simulate the realistic movement of a person inside the house.

The system would still work by simply using random generators, but we opted for the use of a signal builder to make the simulation more realistic. We gave an ID to each room, and created a signal that simulates the movement of a person in all the rooms of the house, and also simulates the intrusion of a burglar when the person is not at home, as shown in *Figure 4*.

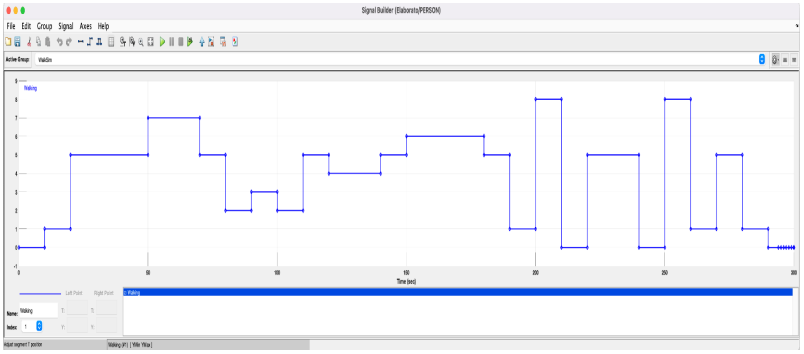

Figure 4: This is the arbitrary signal used to simulate the movement of a person inside the house, each value corresponds to the ID of a room, the duration of the value represents in seconds the presence of the person in the room.

Basically, what happens is that, as seen in the previous figures, the first Matlab Function of each node has 3 inputs, the two random generators and the signal builder. When the signal builder value is equal to the room ID, the Matlab Function outputs will be equal to the random generator inputs.

The router structure is shown in *Figure 5*.

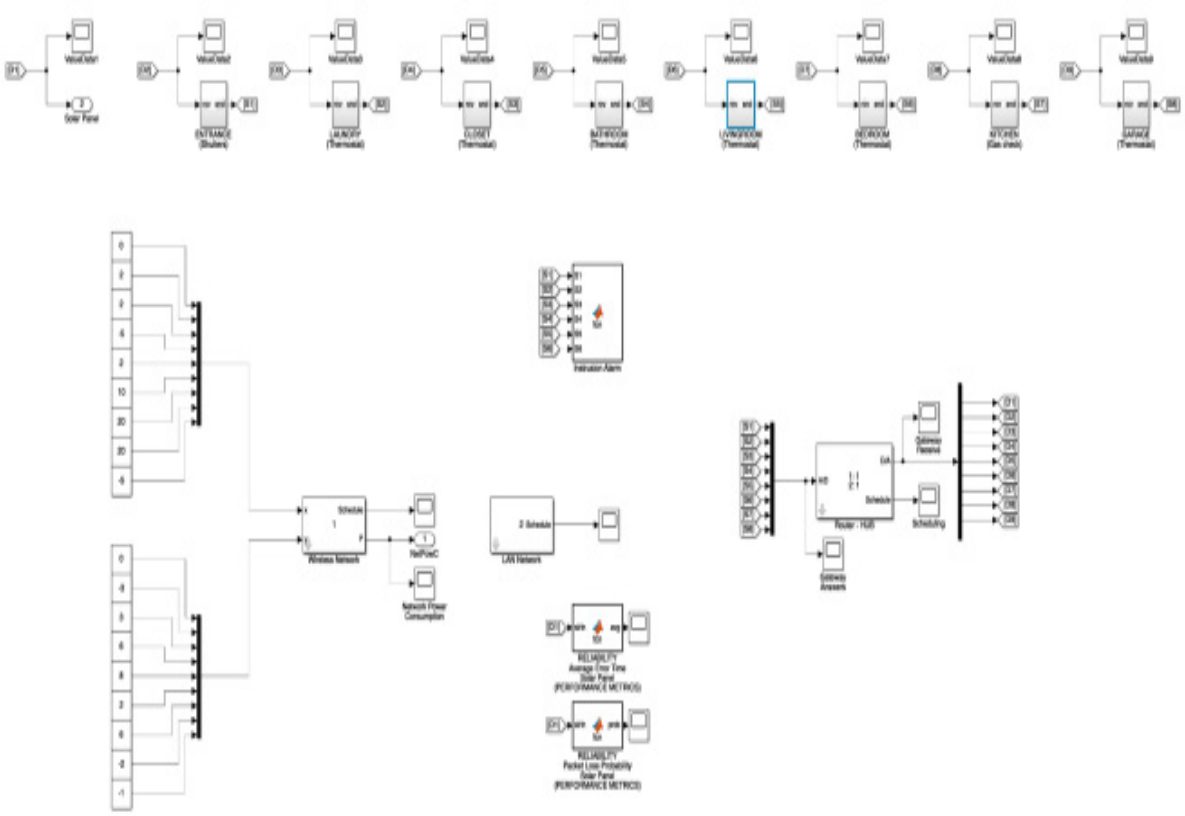

Figure 5: The router has a subsystem to manage each connected node, since they may have different automations.

For example, the subsystem of the Living Room has a thermostat, which works by inserting the "target" temperature in the constant block. The subsystem, receiving the temperature of the room every second, will decide whether the temperature should rise or fall and then it sends the information to the node.

The node of the Living Room, once it has received the information from the router, if there's someone inside the room will lower or raise the temperature based on the information it has received. If there's no one in the room the automation is turned off and the room will change temperature according to the environment, as shown in *Figure 6*.

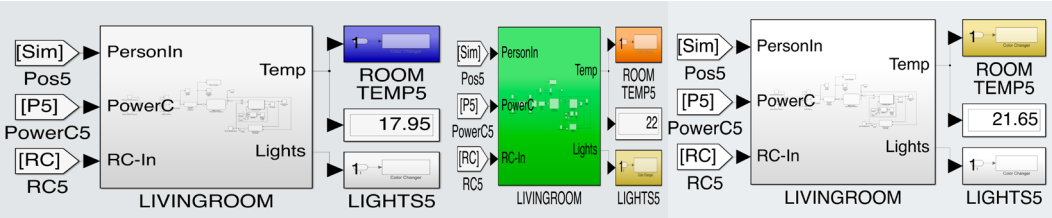

Figure 6: From left to right, at first the room is empty and the temperature is low. During the simulation someone enters the room and the temperature is raised accordingly. Eventually, the person leaves the room and the temperature starts to fall again.

In our case, we assumed the temperature would slowly go down.

About the burglar alarm, the Matlab Function at the center of the *Figure 4* will check if there's data flow into the network when the shutters are closed. If you are inside the house, the shutters are open, so the router will send the signal 1 to the node of the entrance, ignoring the function of the alarm.

If you are not at home, the shutters are closed, so the router will send the signal 0 to the entrance. As a result, if someone were to enter the house, for example from a window, the router would start to activate the automations. It would immediately trigger the alarm, as the signal sent at the entrance is 0 but the other signals sent by the router are not.

The automation of the gas leak alarm is developed by using an MBSD controller in the Kitchen subsystem inside the router. If the gas is turned on in the room, and then left on for over 30 seconds after leaving the room, an alarm will be sent to the kitchen node. If you are inside the room, the MBSD will never trigger because the person is supposed to be there to actually use the kitchen. In this case the node will not send any information.

PERFORMANCE EVALUATION

Each wireless node has some sensors and is connected to a battery. The specifications of sensors and batteries are the following:

- AMG88 GRID-EYE SPECIFICATIONS

Operational voltage: 5V
Active consumption: 4.5mA / 0.0225W
Passive consumption: 0.8mA / 0.04W

- HC-SR501 PIR SPECIFICATIONS

Operational voltage: 5V
Active consumption: 65mA / 0.325W
Passive consumption: 0.05mA / 0.00025W

Our goal is to make the battery of each node last at least 24h at full load with active nodes.
The sensors we're using have an operating voltage of 5V, which means we should be using a 5V battery.
We suppose the use of a 6V battery and a voltage regulator is connected to it to have the 5V output.

Active consumption: 0.35Wh / 0.07Ah
Standby consumption: 0.005Wh / 0.001Ah

The battery specifications are the following:

- PANASONIC CR-P2L SPECIFICATIONS

Operational voltage: 6V (5V output regulator)
Capacity: 1550mAh
Active node estimated duration: ~22h
Standby node estimated duration: ~150h

We decided to make use of a small low-end solar panel, which allows you to recharge the batteries of the nodes when they are not being used. Below are the solar panel specifications:

- GTIWUNG SOLAR PANEL SPECS

Operational voltage: 1.5V
Output: 430mAh
Active node charging: -16,25mAh (slow discharge)
Standby node charging: +52,75mAh (~28h)

To simulate the behavior of a real photovoltaic panel, energy generation is not always at its maximum. We use a random number generator to simulate different levels of production.

Figure 7 is an example of the battery and human presence in the Living Room

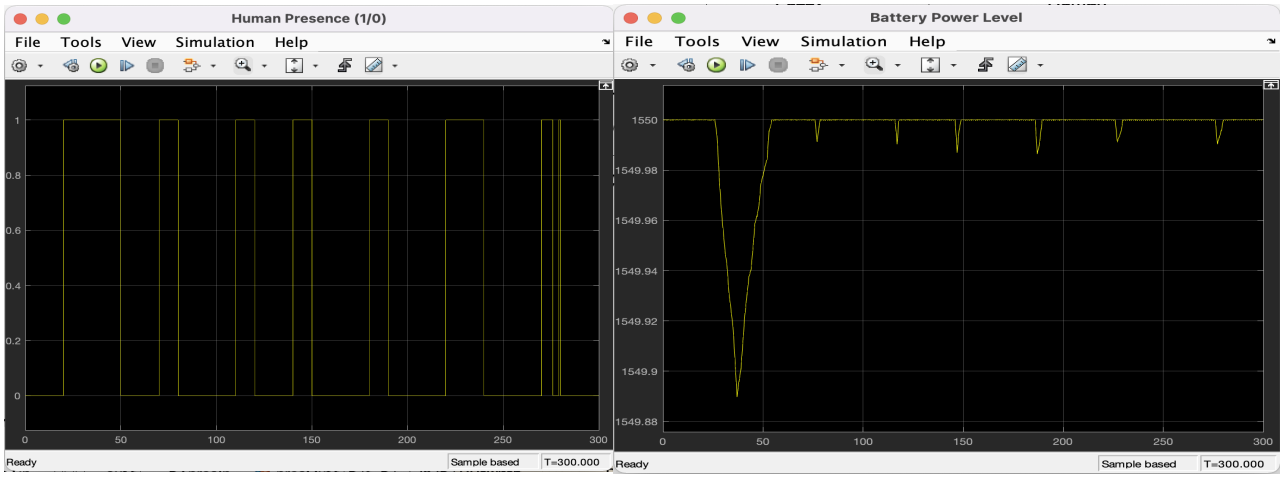

Figure 7: The graph on the left represents the human presence, the graph on the right the relative battery charge and discharge.

Figure 8 is an example of the performance metrics of the entrance node

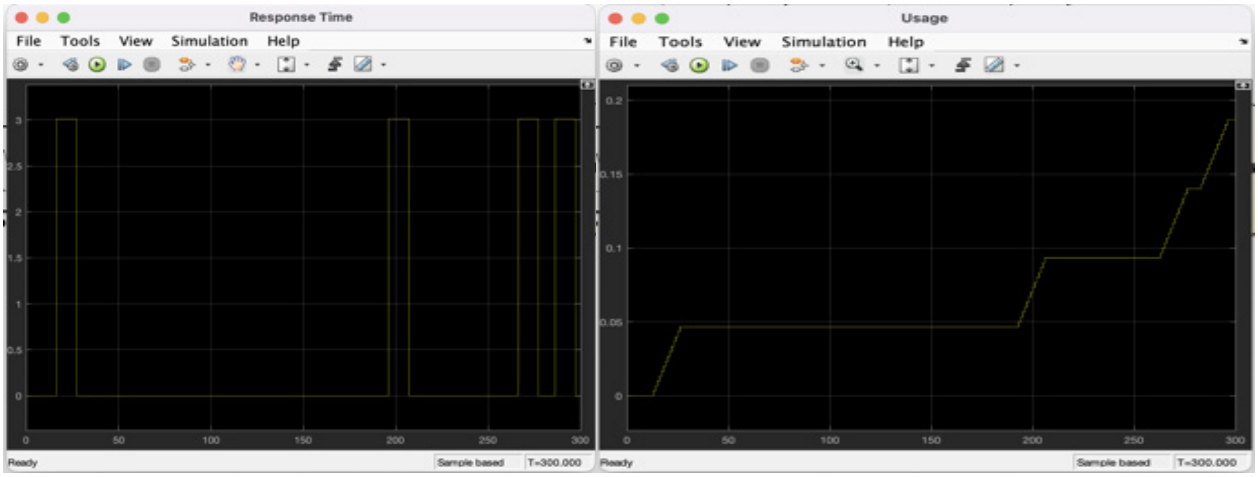

Figure 8: The graph on the left represents the Response Time, the graph on the right the Usage of the node during the simulation.

Figure 9 is an example of the performance metrics of the router

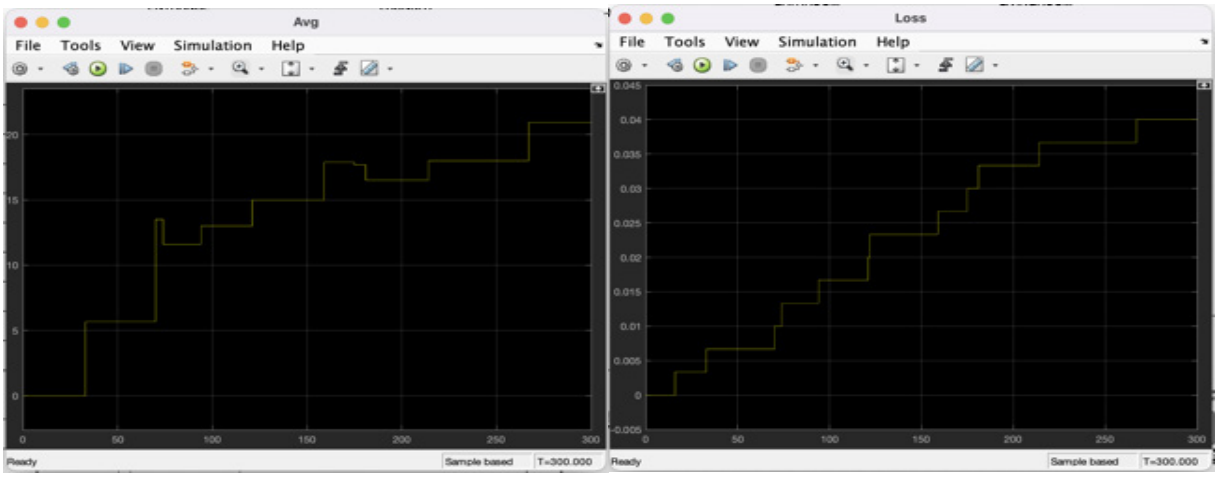

Figure 9: The graph on the left represents the Average Error Time, the graph on the right the Packet Loss of the LAN network.

Conclusions

The acquired knowledge has allowed us to come up with a possible realization of a system that makes our homes "smart". A system of this type allows us to maximize the efficiency of your homes without the request of particular knowledge from the end user. This type of automation, in addition to helping us increase the safety of the environment in which we live and improve the quality of life, using a renewable energy source, such as solar, also allows us to save economically and to live a more sustainable lifestyle. We decided, for convenience in the possible installation of sensors, to use the wireless network as a communication network. This type of system could be optimized and sped up using only Ethernet networks previously arranged in the house. This would allow us to not use batteries and to have a better response time, sacrificing, however, the ease of installation.

References

[1] Diponkar Kundu, Md. Ebrahim Khallil, Tushar Kumar Das, Abdullah Al Mamun, Ahmmad Musha, “Smart Home Automation System Using on IoT”, Year: 2020, International Journal of Scientific & Engineering Research.

[2] Baoan Li, Jianjun Yu. “Research and application on the smart home based on component technologies and Internet of Things”, Year: 2011, Elsevier LTD.

INVESTIGATION OF THE POSSIBILITY OF MEASURING PULSE OXIMETRY IN WATER

Boris Davidovich

Saint Petersburg State University of Aerospace Instrumentation
E-mail: davidovichborisvladimir@yandex.ru

Abstract
The ability of measuring pulse and saturation in an aquatic environment is investigated. An experiment of measuring and saturation in water was conducted. The results of the experiment were evaluated.
Keywords: pulse, saturation, microcontroller, sensor, processing, calculation.

Thermometer and a sound-amplifying tube for listening to heart and breathing noises were the only medical diagnostics devises to assess human health for the long time. The methods of medical diagnostics have improved with the development of modern electronics.

The physiological processes in human body could be represented as electrical signals, mechanical movements and chemical reactions.

One of the devices that can evaluate the physiological state of the human body is a pulse oximeter. Continuous monitoring of human health can be provided by pulse oximeter systems. Nowadays most of pulse oximeter systems are used only in the air environment. The use of a pulse oximeter in water could increase the effectiveness of swimmers training. It could also help to diagnose various disorders of divers' body. The process of pulse and saturation measurement is based on the principles of photoplethysmography (from the Greek "φωτός" — light, "πληθύς" – set and "γράφω" – write), which allow to isolate the arterial component of light absorption to determine arterial blood oxygenation. The area where the blood flow is examined is located between the light source and the photodiode (Figure 1) [2].

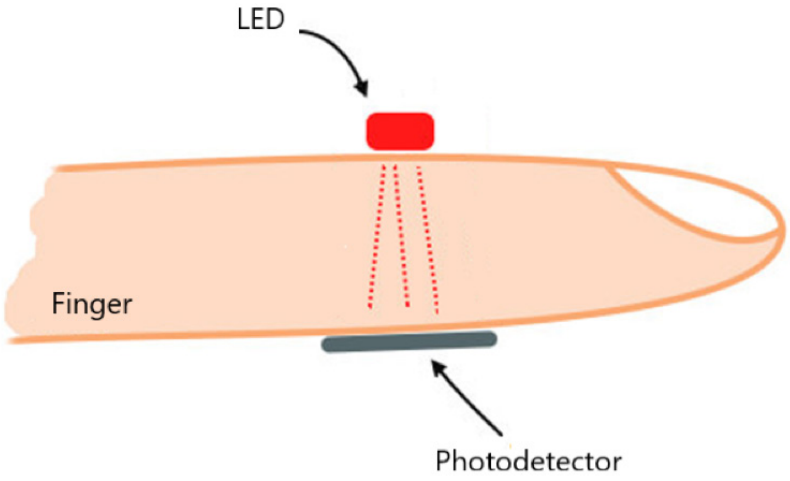

Figure 1 - Pulse Oximeter

The absorption of light by the medium can be calculated according to the Booger-Lambert-Beer law (1),

$$I(l) = I_0 \mathrm{e}^{-k_\lambda l} \quad (1)$$

In this formula $I(l)$ is the intensity of light that has passed through a layer of substance with a thickness of l, I_0 is the intensity of light at the entrance to the substance, k_λ is the absorption index [5].

It follows from the Booger-Lambert–Beer law that the smaller the thickness of the layer through which light passes, the less light absorption.

If the light-emitting diode and the photodiode are tightly attached to the body surface, then the absorption of light by the external environment can be neglected. By ensuring the proper fit of the sensor to the surface pulse and saturation could be record regardless of the environment. It should be borne in mind that if the pressure on the sensor is excessive, then arterial blood flow will be disturbed, and venous pulsation will be

observed. The pulse oximeter is not able to distinguish between arterial and venous pulses. Thus, the absorption of light by venous blood can be included in the calculation and the result could be underestimated. Venous pulsation can also be observed in various diseases of tissues and the cardiovascular system.

The pulse calculation of the pulse can be conducted for each interval between the waves of the photoplethysmogram. When information is presented in this form, it will not be possible to obtain accurate data. Nevertheless, average value for the observation period is taken. In general, these observation periods vary from 3 to 20 s [1].

The Arduino UNO platform and the KY-039 pulse oximeter were chosen for the experiment. The sensor circuit is shown in Figure 2 [5].

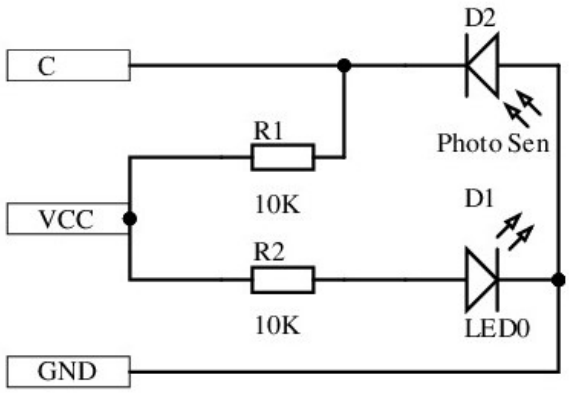

Figure 2 – KY-039 circuit

The sensor was connected to the ADC input of the microcontroller, the connection diagram is shown in Figure 3.

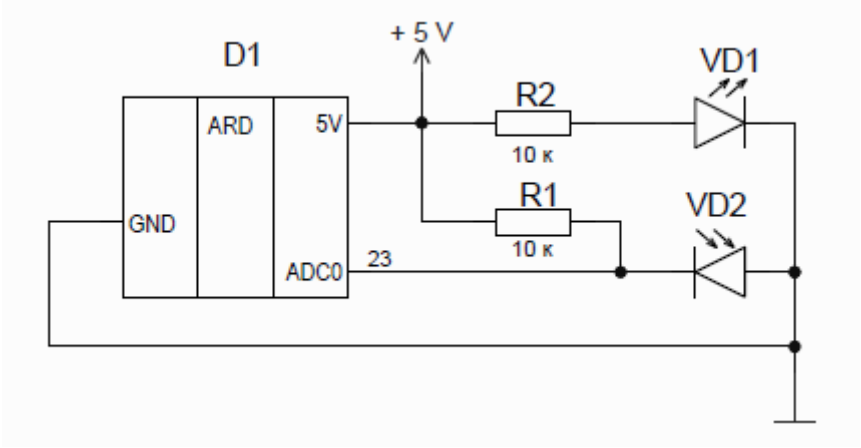

Figure 3 – Connection diagram of the KY-039 sensor to the ARDUINO UNO microcontroller

A program was developed in the ARDUINO IDE environment to take an experiment. The program takes data from the sensor every 5 s and displays it on the computer monitor via the serial port. The pulse measurement experiment was carried out on a person at rest at room temperature. The sensor was isolated from sunlight and artificial light for stability of readings [5].

It was necessary to consider that the readings of the ky-039 sensor are read by the built-in ADC of the ARDUINO UNO microcontroller during the experiment. The accuracy of the inner 10-bit ADC is determined by the formula:

$$V=5/1024*ADC \quad (2)$$

In this formula ADC is the value applied to the input of the ADC [6].

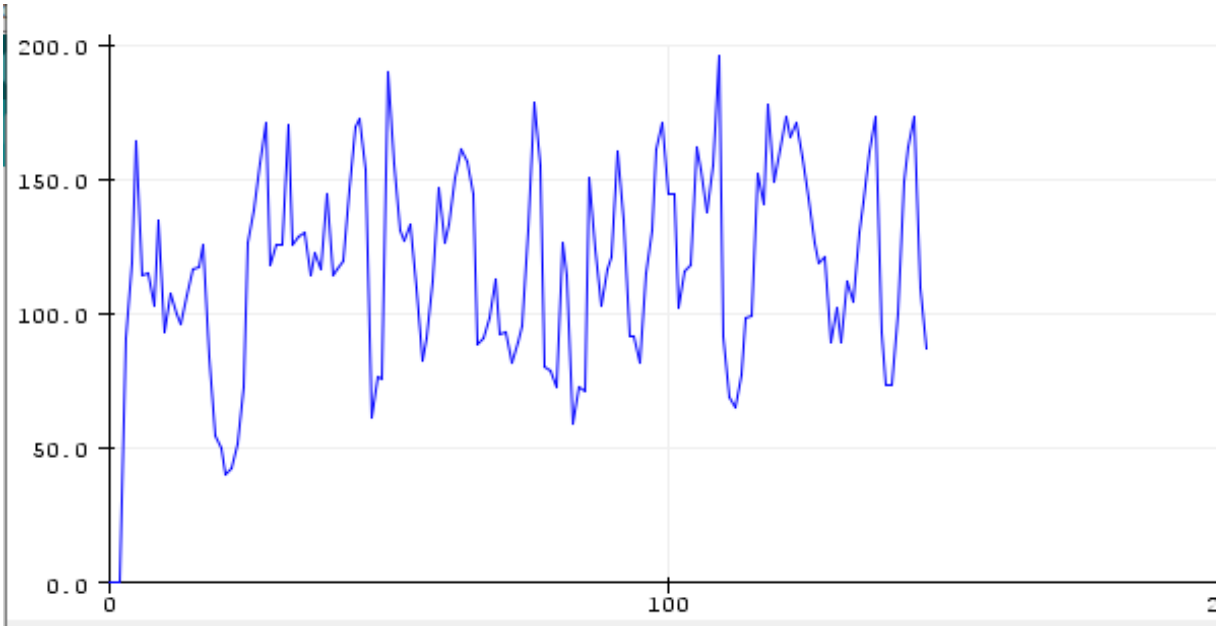

Figure 4 - Pulse in the air environment

As a result of measuring the pulse in the air, the following graph was obtained (Figure 4). Vertical pulse values, horizontal number of measurements, measurements were taken every 5 seconds. According to the principles of pulse oximetry, the measurement result is the average value of all of them [7]. During the experiment, a value of 126 beats / min was obtained.

Then the finger with the sensor was placed in the aquatic environment, not below the heart location. All contact pads, smd-resistors and the PLS-3 connector with the cable were isolated in order to prevent malfunctions of the sensor and violation of its integrity. The sealing was carried out using a non-conductive hot melt adhesive. Figure 5 shows the sensor prepared for the experiment.

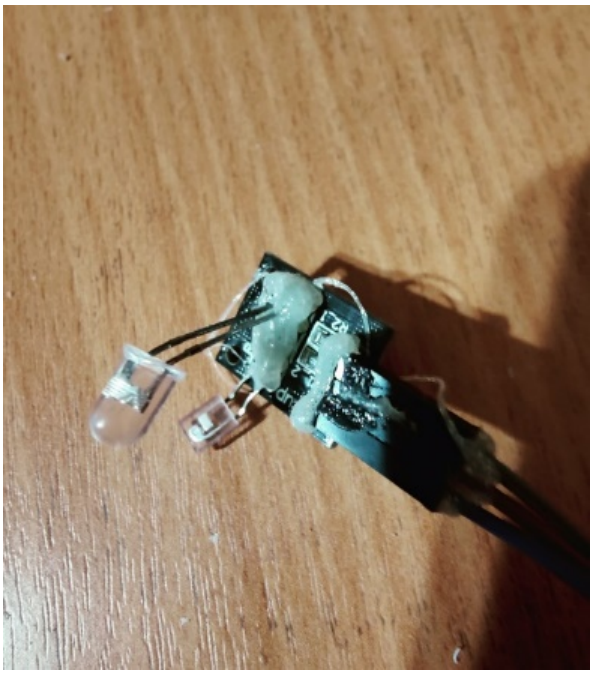

Figure 5 - Sealing the sensor

The result of the experiment is presented as a graph in Figure 6.

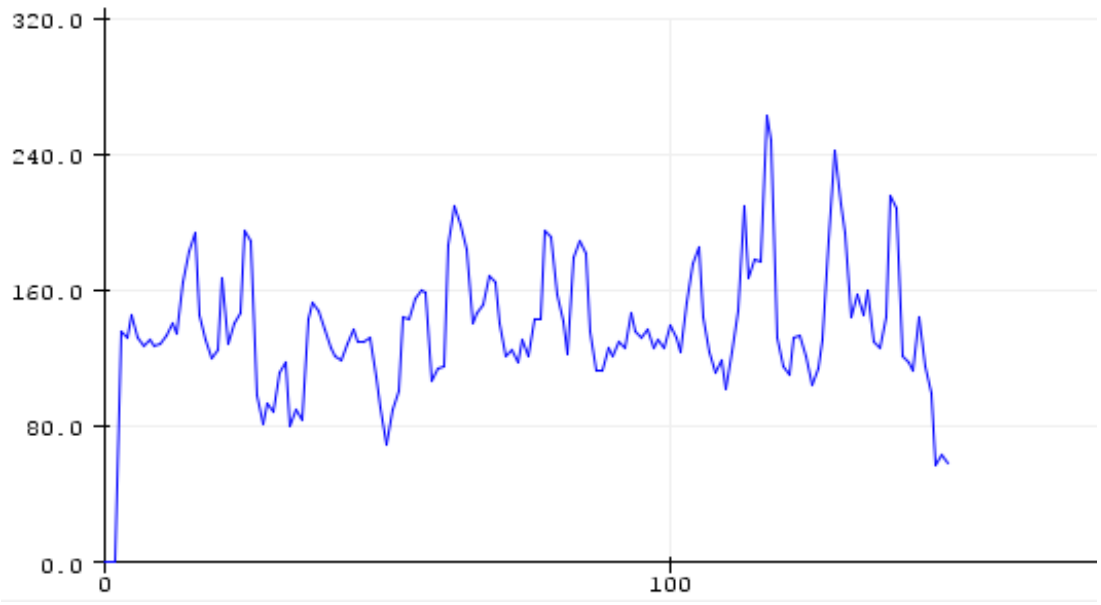

Figure 6 - Pulse in the aquatic environment

High single peaks are excluded from the calculation. As a result of the experiment, there are about 9 such bursts in water. According to the results of measurements, the pulse turned out to be 136 beats / min. During the measurements, the pulse was measured from the smart watch Samsung galaxy gear s3. During measurements in water, the pulse according to the readings of the smart watch was 134 beats / min.

According to theoretical calculations and the experiment, the pulse measurements in aquatic environment are possible. However, the appearance of "outliers" in the measurements carried out in the aquatic environment should be considered. For more accurate measurements in water and in air, a different sensor, such as the MAX30100, is required. This sensor could also measure saturation. Moreover, it is not required to cover the sensor with external rays due to its design features. It is also necessary to improve the software to avoid “outliers” in the measurements.

Measuring saturation and pulse in the aquatic environment could improve the safety of scuba diving, allow divers to determine in advance the onset of nitrogen anesthesia in divers and make it possible to develop an automatic ascent system in case of loss of consciousness. Also, it can help to calculate the minimum decompression pause time individually for each diver.

References

1. Мониторинг дыхания: пульсоксиметрия, капнография, оксиметрия/ И.А. Шурыгин. СПб.: "Невский Диалект", 2000. 301с.

2. Московский государственный университет им. М.В.Ломоносова физический факультет/ кафедра медицинской физики/ Специальный практикум/ Пульсоксиметрия: физические принципы и применение в медицине. Москва, 2008. 15с.

3. Аналого-цифровые преобразования — АЦП URL:// https://robotclass.ru/tutorials/arduino_adc/ [Дата обращения 20.11.21]

4. POLITECNICO DI MILANO Scuola di Ingegneria Industriale e dell’Informazione Corso di Laurea Magistrale in Ingegneria Biomedica/ Sviluppo e validazione di un pulsossimetro a riflettanza indossabile al dito/ Relatore: Prof. Andrea Aliverti Correlatore: Ing. Paolo Patete Correlatore: Ing. Massimiliano Torregian / Anno Accademico 2014 – 2015.

5. Закон Бугера — Ламберта — Бера URL:// https://ru.wikipedia.org/wiki/Закон_Бугера_—_Ламберта_—_Бера [Дата обращения 20.11.21]

6. Датчик сердцебиения KY-039 Ардуино URL:// https://роботехника18.рф/ky-039-arduino/ [Дата обращения 20.11.21]

STUDY OF GENETIC ALGORITHMS FOR POLAR CODE CONSTRUCTION OPTIMIZATION

Anna Fominykh

Saint-Petersburg State University of Aerospace Instrumentation,
St. Petersburg, Russia
E-mail: aawat@ya.ru

Abstract
The paper studies different genetic algorithm variants and their application to polar code construction optimization. Simulation results with a comparison of non-optimized and optimized polar code construction are presented in additive white Gaussian noise channel with successive cancellation list decoding.
***Keywords*:** genetic algorithm, convergence, polar codes

Introduction

Nowadays, information processing and transmission systems are widespread. Due to such systems' properties, the information transmitted is subject to errors. Therefore, the task of information integrity appears. For this purpose, coding theory uses methods of error-correcting coding. More specifically, the coding theory proposes introducing redundancy to the information that may be exploited after the transmission to correct errors. The redundancy is introduced using error-correcting codes. Different types of error-correcting codes were proposed, namely, low-density parity-check (LDPC) codes, turbo codes, convolutional codes, polar codes and etc. In this work, polar codes will be investigated because they can overcome the state-of-the-art LDPC codes on short lengths.

Polar codes are a class of capacity-achieving codes introduced by Arıkan [1]. Polar codes have attracted significant attention and research efforts in academia and industry over the last decade. Polar codes have been adopted as channel coding for uplink and downlink control information for the enhanced mobile broadband communication service as part of the ongoing 5th generation wireless systems (5G) standardization process of the 3rd generation partnership project (3GPP) [2].

The channel polarization phenomenon is defined as a transformation that generates N synthetic bit-channels from N independent copies of a binary-input discrete memoryless channel, as described in [1]. The new synthetic channels are then polarized in the sense that each one can transmit a single bit with a different degree of reliability, i.e., with a different chance of being correctly decoded. If N is large enough, the synthetic channels' mutual information is either near to zero (totally noisy channels) or close to one (absolutely noiseless channels), resulting in extremely high-capacity channels. Since some channels are entirely unreliable, it is reasonable to transmit the data only through reliable channels and set the unreliable ones to some known predefined value. These two types of channels are named frozen and unfrozen sets of polar codes that fully determine their construction. Polar codes may have different bit error rate performance based on their structure. Construction of the polar code requires choosing frozen and unfrozen sets, which comprehensive computations or algorithmic approaches. For instance, using density evolution and Gaussian approximation, an optimization procedure based on Bhattacharya parameter [3], construction proposed by 3GPP congress obtained by computer simulations [2]. In [4] an optimization procedure using neural networks was first proposed. Usage of a genetic algorithm to polar code construction was presented in [5]. However, currently, there is no research on the analysis of different genetic algorithm techniques applied to polar codes. In this work, the convergence of various genetic algorithms is observed, and its application to polar code construction optimization is investigated.

Polar codes

Polar codes are linear block codes of length $N = 2^n$ and rate $R = K/N$. The polar code encoding procedure is based on the effect of channel polarization, which is described by a linear transformation using the matrix $\mathbf{G}^{\otimes n}$, $n = \log_2 N$, $\otimes n$ – n-th Kronecker product of the polarizing kernel, $\mathbf{G}$ is a polarization kernel [1]:

$$\mathbf{G} = \begin{bmatrix} 1 & 0 \\ 1 & 1 \end{bmatrix}.$$

Transformation of vector $\mathbf{u} = (u_1, \ldots, u_N)$ into the codeword $\mathbf{x} = (x_1, \ldots, x_N)$ is obtained by multiplying $\mathbf{u}$ by $\mathbf{G}^{\otimes n}$, i.e., $\mathbf{x} = \mathbf{u}\mathbf{G}^{\otimes n}$. For example, a generator matrix $\mathbf{G}$ of a polar code with a code length equal to 8 is

$$\mathbf{G} = \begin{bmatrix} 1 & 0 & 0 & 0 & 0 & 0 & 0 & 0 \\ 1 & 1 & 0 & 0 & 0 & 0 & 0 & 0 \\ 1 & 0 & 1 & 0 & 0 & 0 & 0 & 0 \\ 1 & 1 & 1 & 1 & 0 & 0 & 0 & 0 \\ 1 & 1 & 0 & 0 & 1 & 1 & 0 & 0 \\ 1 & 0 & 1 & 0 & 1 & 0 & 1 & 0 \\ 1 & 1 & 1 & 1 & 1 & 1 & 1 & 1 \end{bmatrix}.$$

And the corresponding polar code graph is presented in Fig. 1.

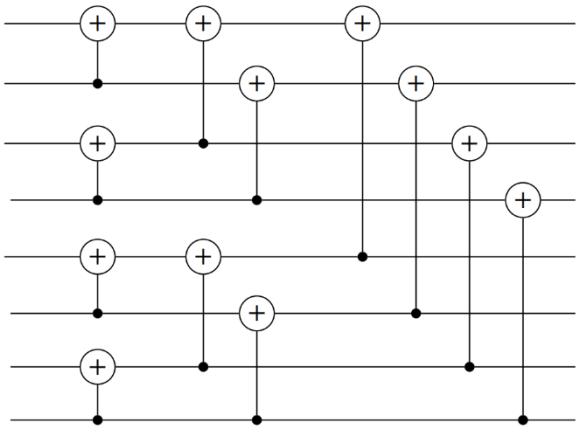

Figure 1 – (8,4) polar code graph

Genetic algorithms

Genetic algorithms are among the most used evolutionary algorithms in terms of application diversity [6]. Genetic algorithms (GA) have been used to solve the most well-known optimization issues. Furthermore, genetic algorithms are population-based, and many recent evolutionary algorithms are directly based on or have strong similarities to genetic algorithms. A genetic algorithm is a heuristic search based on Charles Darwin's natural selection hypothesis. Genetic algorithms mimic natural selection, during which the fittest individuals are chosen for reproduction to create the following generation's children.

The main steps of the genetic algorithm are population initialization, fitness function calculation, parent selection, crossover operation, mutation, survivor selection, and termination with the best offspring returning [7]. Implementation of every step may vary depending on the type of the algorithm or desired optimization goal. Population initialization may be done in a random or heuristic manner, and the latter is the initialization with some a priory known as "good" population. A fitness function is a specialized objective function for evaluating the relative effectiveness of potential solutions in a given application. The selection process is an essential part of the genetic algorithm. Selection is the process of choosing parents who will mate and recombine to produce offspring for the next generation. The choice of parents is critical to the genetic algorithm convergence rate, as good parents motivate their children to seek out better and more suited solutions. Reproduction and biological crossover are similar to the crossover operator. More than one parent is chosen, and one or more offspring are generated utilizing the parents' genetic information. A mutation is a minor random change in the chromosome that results in a new solution. Different types of mutation exist, namely, bit flip mutation, random setting, swap, scramble, and inversion mutations.

Simulation results

Different selection techniques will be observed: uniform selection, stochastic-uniform selection, roulette wheel selection, and tournament selection. Also, several crossover functions including single point crossover, double point crossover and uniform crossover will be investigated. Since the simulation for polar code construction is computationally hard, it requires a vast number of accurate simulations with decoding steps, and it is difficult to provide accurate results for each algorithm. Here the convergence of the presented algorithms for a computationally simpler problem of finding a vector with minimum Hamming weight, i.e., a vector with a minimum number of nonzero elements, will be considered. And the best genetic algorithm variant in terms of convergence will be used to optimize polar code construction.

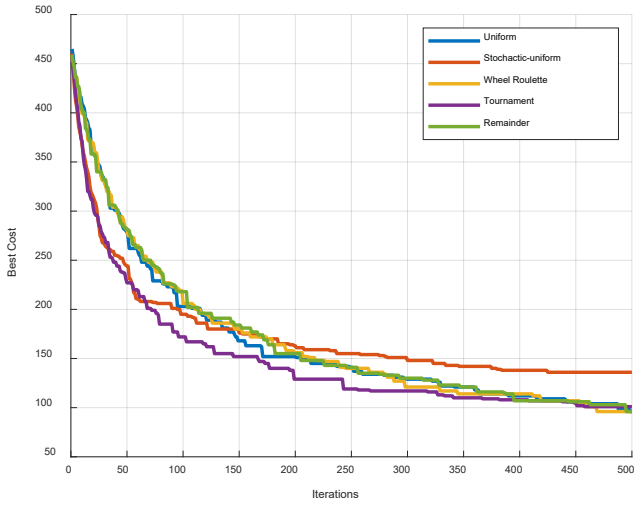

Figure 2 – Convergence for different selection functions

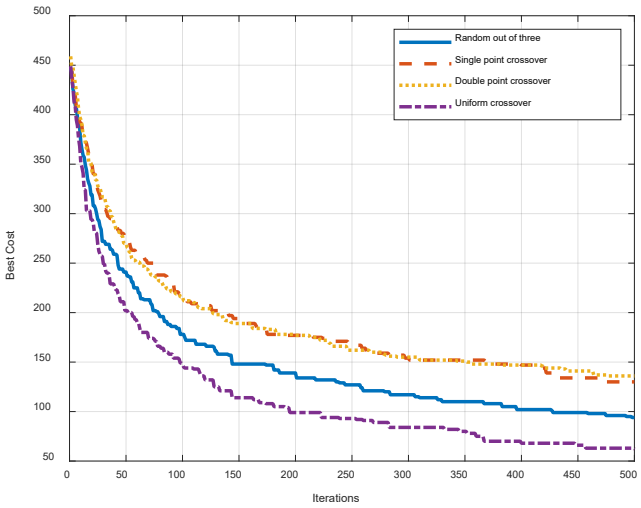

Figure 3 – Convergence for different crossover functions

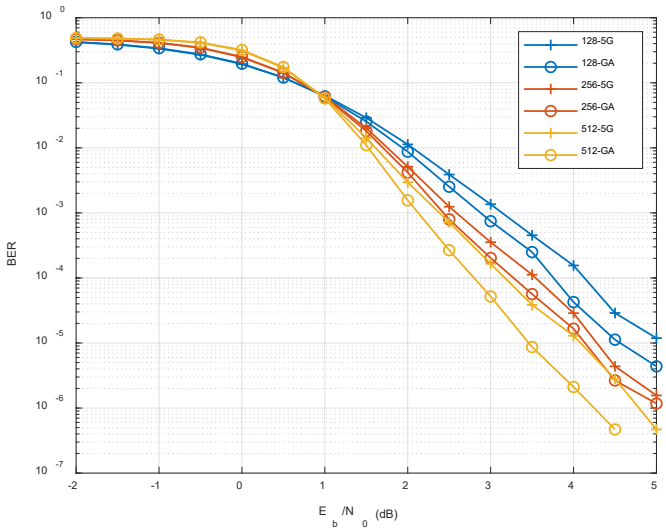

Figure 4 – BER comparison

The simulations are conducted for vectors with length 1000 with 500 epochs, population size is 50. The comparison between different parent selection techniques is presented in Fig. 2. It may be observed that the tournament selection shows the fastest convergence in the beginning, but to the end all the curves (apart from stochastic-uniform) selection curve begin to coincide. In Fig. 3 the genetic algorithm convergence with different crossover functions is presented. It may be seen that the uniform crossover shows the best convergence rate. Based on the obtained simulation results for genetic algorithm convergence, the optimization with tournament selection and uniform crossover for polar codes with different lengths with successive-cancellation list decoding was carried out. The population was initialized with 5G reliability sequence and its modifications using random bit flipping. Bit error rate results presented for additive white Gaussian noise channel in Fig. 4 shows that the optimization using genetic algorithm allowed to achieve BER improvement over non-optimized code construction.

Conclusion

The paper examined the convergence of different genetic algorithm variants and its application to polar code construction optimization. It was observed that genetic algorithm with tournament selection and uniform crossover led to the fastest convergence. This genetic algorithm set up was used to optimize a polar code construction in additive white Gaussian nose channel with successive cancellation list decoder. From a simulation results it may be observed that the genetic algorithm allowed to achieve an improvement over 5G polar code reliability sequence.

References

[1] Arikan E. Channel polarization: A method for constructing capacity-achieving codes for symmetric binary-input memoryless channels // IEEE Transactions on information Theory, T. 55, №. 7, 2009. – P. 3051-3073.

[2] 3rd Generation Partnership Project (3GPP) / Multiplexing and channel coding. 3GPP 38.212 V.15.3.0, 2018.

[3] Li H. Polar codes: construction and performance improvement //The University of New South Wales. – 2003. P. 118.

[4] Ebada M., Cammerer S., Elkelesh A., Brink S. Deep Learning-Based Polar Code Design // 2019 57th Annual Allerton Conference on Communication, Control, and Computing. – 2019. – P. 177-183.

[5] Elkelesh A., Ebada M., Cammerer S., Brink S.t. Genetic Algorithm-based Polar Code Construction for the AWGN Channel //SCC 2019; 12th International ITG Conference on Systems, Communications and Coding. – 2019. – P. 1-6.

[6] Holland, J.H. Adaptation in Natural and Artificial Systems //MIT Press. – 1992. – P. 211.

[7] Whitley, D. A genetic algorithm tutorial //Stat Comput 4. – 1994. – P. 65–85.

GAS NETWORK: IOT PROPOSAL FOR THE MANAGEMENT OF GAS PIPES

Gabriele Nicolosi

Computer Engineering and Networks Laboratory – Kore University of Enna - Italy
Email: gabriele.nicolosi@unikorestudent.it

Abstract
The nature of the interventions on gas systems differs in the type of pipes, which can be exposed or hidden. In the case of interventions on exposed pipes, the operator has an easy accessibility to the conduction and therefore an adequate ease of intervention. Actions on underground pipes, on the other hand, follow specific procedures and are not always easy to perform. One of the first objectives of pipe maintenance is certainly to maintain the integrity of the pipes and limit damage to the surface. This article aims to demonstrate how with the advent of the IoT it is possible to create a control network consisting of sensors, controllers, actuators and flow regulators in order to perform periodic measurements aimed at managing a small / medium-sized gas distribution network. belonging to a city.

Introduction

The gas pipeline, in compliance with what reported by the Gazzetta Ufficiale[1], will consist of a high pressure pipeline operating at a variable operating pressure between 12 and 24 bar (known as type II pipeline) and two smaller branches , III species, operating at a pressure between 5 and 12 bar with the purpose of offering the gas supply service to the city through the proposed technology and managing anomalous operating situations. The ultimate goal of guaranteeing the correct functioning of the network will be achieved thanks to Gas Sensiting Solution [2] and Remote Terminal Unit (RTU) [3] techniques. Thanks to these solutions it will be possible to interface physical objects of measurement and calibration of parameters to a distributed control system costing of elements that interact with each other through the network. The project combines commercial solutions that make the most of the progress made in microelectronic systems and a hybrid wired / wireless network [3] in order to minimize both the latency of the data measurement and mechanical intervention of the actuators and of the data exchange for an optimal result in terms of general performance. In particular, the commercial solutions adopted will be:

- StartBox Lx2 sensors useful for measuring gas pressure
- Gas flow rate meter FlowSic100 FlareXT Model.

The choice of these sensors rests on the fact that knowing the section of the pipe it will be possible to calculate the flow rate of the pipe itself as a product of speed and pressure which must never exceed the threshold value. In order to cope with the high operating pressures of the main gas pipeline, the following will be used:

- Actuators with high pressure 3-way ball valve SS304 HB23 with pneumatic actuator AT75 .

Each actuator will be equipped with a GLog + network device [4]. GLog + is an RTU designed for real-time monitoring and control of gas pressure reduction systems. This device, operates according to the most adopted network protocols and does not require a connection to the electricity network, but also operates through lithium batteries with a high duration range. The solution presented for a network aimed at controlling the pipeline arises from the need to perform self-diagnosis routines and reports of malfunctions of plants subject to high wear caused also by extreme pressures, a necessary action given the dangerousness of the transported material.

RELATED WORKS

Traditional solutions, for management gas, are mostly monitoring stations employed by the government, they are large and expensive and usually analyze limited air samples. Such monitoring systems have long relied on existing gas detection technologies for both environmental quality monitoring and leak detection. However, these sensors, where they exist, are quite bulky and generally consume a lot of energy. An example are networks equipped with magnetorestrictive sensors [5] that offer sensory control based on ultrasonic waves, a method that is as complex and expensive as it is effective. In the work cited, an analysis is carried out on the circumference of the duct using ultrasonic waves in order to detect anomalies. An innovative proposal that would require the production of ultrasonic waves by special devices to add to the need for network devices with high computational capabilities.

Other proposals relating to the monitoring of gas pipelines are not based on the observation and measurement of the quantities of gas transported, but rather on techniques aimed at prevention through the observation of environmental conditions. This approach does not require the use of Gas Sensiting Solution techniques, but the implementation of seismic sensor networks aimed at monitoring seismic and microsmic activity around the gas storage network [6]. It is reasonable to question the use of this type of sensor when applied to a gas distribution network since the risk factors can be multiple and not only at the seismic level. The presentation of the project aims to show how, thanks to the advancement of networks and hardware devices, it is possible to implement minimally invasive solutions with minimum environmental impact.

THE PROPOSED APPROACH

The pipeline is managed through a hybrid wired/wireless network. The network consists of the following nodes:

- 3 pressure sensors
- 2 network controllers
- 2 local actuators
- 1 speed sensor
- 1 regional actuator (flow regulator)
- 1 gateway

for a total of 5 subnets.The network topology is strongly influenced by the pipeline topology. Assuming the long-distance regional section not covered by a wireless network, a wired CSMA / CD (Ethernet) approach was chosen for it; unlike the local routes, inside the city, I suppose they can be easily interfaced with an 802.11b wireless network. The implementation of local networks is associated with two distinct wireless networks. The proposed approach for the implementation of the control network focuses on the use of the following main techniques:

- Soft Computing: for the evaluation, control and decision of the actions taken by the regulation devices.
- Model-Based Software Design (MBSD): to model the management system of logical operations through stateflow, therefore state machines and flow diagrams.
- Multiplexing and demultiplexing techniques: for regulating the transmission capacity of the input and output signals in the functional blocks used.
- Multiple network handlers for single nodes: for the management of network interrupts and a parallelization of incoming and outgoing data traffic in a subnet by activating aperiodic tasks.
- Matlab Function: for the implementation of control algorithms.
- Network gateway: for forwarding data to one of the two types of network.

The regional network will consist of a total of 4 nodes. Two nodes will be represented by the sensors, respectively a Starbox LX2 for detecting the gas pressure inside the duct and a Model A2G-20 air velocity meter for measuring the gas velocity inside the duct. The intermediate node to the network will be a GLog + network controller. The network controller will have the dual function of guaranteeing an incoming data flow to the regional network and an internal data flow to the regional network itself. The network controller performs a computation of the data detected by the sensors through functional blocks with Fuzzy logic; thanks to the use of the analogue gas speed and pressure signals, knowing a priori what the section of the duct is, the GLog + device will be able to determine a percentage of valve closure based on the maximum operating values allowed by the standard given a type II pipe [1]. In the event that the pressure values and speed of movement of the quantity of gas are regular, the calculated closing percentage will be tending to 100% as surely then the entire system including the branches will have reached optimal pressure. If the pressure drops, then the actuators for command of the controller and activation of the appropriate aperiodic task activated by the appropriate handler open the valves by a variable percentage from 0% to about 100% by injecting pressure and gas displacement speed in the pipeline.

The terminating node is represented by an SS302 HB23 actuator which will receive data from the network controller and will manage the closing and opening of the valves. The two intermediate networks see a gateway at the center of the topology. The gateway will have the crucial role of sorting data from one network to another; two network handlers, one local and one regional, will perform this task by starting tasks for entering data on the appropriate mailboxes. The gateway node will exchange data with the two network controllers. The two local networks will each consist of three nodes: a sensor, an actuator and a network controller. The local network controller, placed at the center of the local network topology, acts as a node for

both local sections. The local sensors will be LX2 Starbox for gas pressure detection. Given the logic implemented at simulated level, presented in point IV, it was decided to create aperiodic tasks for data management by the sensors. The pressure data detected by the sensors will be processed using Soft Computing techniques, as was the case for the regional network, with the difference that the values in question will be those of the pressure and pressure drop recorded in the pipelines for reasons highlighted in point IV. As it is logical to think a valve closure in one of the branches, even if slight, will result in an increase in pressure upstream that must be appropriately managed by exchanging signals between the actuators, controllers, gateway and regional sensors, therefore every time the regional network transmits 'ping' signals the local network will respond with appropriate 'pong' signals. The commercial solution adopted also offers the possibility of using software configurable alarms. A Model-Based Software Design (MBSD) approach through the evaluation indicating the pressure drop in the pipelines will allow the activation of an alarm if the pressure drop value detected by the network is abnormal compared to the permitted levels. This will imply a total closure of the valve and indeed a closure of the section itself; then the algorithm implemented through Matlab Function will allow the regional network to report the values within a certain range thanks to the management action by the network controller and the regional flow regulator. All message exchange activities between the network nodes will be monitored through the Matlab View Diagnostics.

SCENARIO

The simulated scenario is that of a gas pipeline with the ultimate aim of supplying a city. In particular, the gas pipeline, as can be seen from its topology shown above, is made up of three sections. The main section, known as the regional section, operating at a variable pressure in a range between 12 and 24 bar. This section is branched into two secondary sections, known as local and type III sections, operating at operating pressures between 5 and 12 bars. One of the following scenarios is possible:

1. The pressure values in the entire system are optimal then the system remains under pressure by completely closing the valves.
2. The pressure values are not optimal. We distinguish the following sub-cases:

• The pressure recorded upstream of the system is low, then the flow regulator opens the valves through the appropriate task generated, allowing a greater input of gas quantity managed by a Matlab function, supplying and restoring pressure also the local sections which a in turn they will start their own tasks open to us by the action of the handlers and will open the valves to allow a larger quantity of gas to enter.

	Data Rate	Frame Size	Loss Probability
Regional Network	1 GigaBit/s	512 Bits	1%

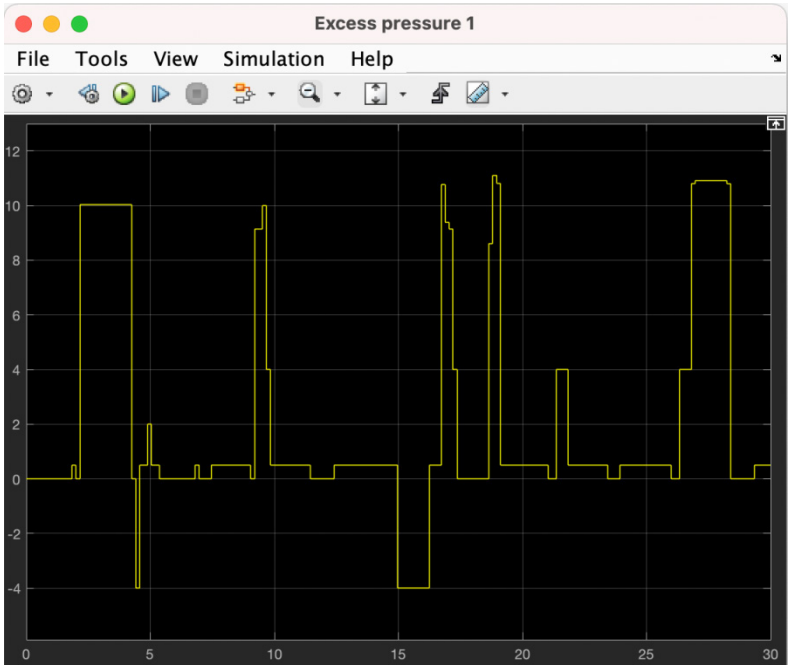

Figure 1: the excess pressure values recorded during the simulation

• The pressure recorded upstream is optimal but the local sensors through the activation of their tasks reveal a pressure drop probably due to the normal use of gas in the city (detected by fuzzy logic), then the local actuators open the valves allowing the further injection of gas which will be provided by the flow regulator due to the cascade effect.

• The pressure recorded upstream is optimal but the local sensors record high operating pressure values, then the actuators close the valves by the necessary percentage, this action will result in a coin pressure increase due to the cascade effect. An excess pressure value (figure 1) will be recorded to be reported to the regional controller.

• The pressure recorded upstream is optimal but the local sensors record an anomalous and sudden pressure drop. A failure in the network coming from the city is then assumed, in all probability a loss of pressure due to a leak or rupture of the pipeline. Then the sensors activate the alarm.

PERFORMANCE EVALUATION

We will now evaluate the performance of the network in terms of reaction time, in particular, the data of the regional network will be analyze, as it greater control action. The analyzes of these performance metrics were carried out considering the following network performances:

In order to carry out the measurements, 12 sample values were taken in a simulation interval of 9 seconds for a total of 66 samples. For the calculation of the reaction time the following values were recorded and used:

Speed sensor (sec) DATA SENDING TIME	Pressure sensor (sec) DATA SENDING TIME	Flow regulator (sec) EXECUTION START TIME
6.64	0.05	6.72
6.65	1.05	6.85
6.86	2.05	7.00
6.97	6.72	7.15
7.05	6.83	7.3
7.1	6.88	7.45
7.19	6.99	7.60
7.30	7.04	7.75
7.41	7.09	7.90
7.52	7.15	8.02
7.63	7.20	8.35
7.69	7.23	8.41

$$REACT = \frac{\sum_{i=1}^{12}(SV + SP)}{2 \cdot 12} - \frac{\sum_{i=1}^{12} ERF}{12} = 1.15sec$$

NOTE: REACT reaction time, SV speed data sending time, SP pressure data sending time, ERF flow regulator execution start time

Conclusions

The project presented has achieved the desired purpose, keeping the gas pressure values within the predetermined ranges in the regional duct and in the local ducts despite the closure of the local ducts due to faults (pressure zeroing). The solution presented not only meets the needs of designers, but also makes it easy to integrate these improved sensing capabilities into compact form factors, indispensable for battery-powered

devices. They also include calibration capabilities and upgradeable software that are critical to efficiently configure - and reconfigure - the quality monitoring projects of a gas distribution plant. Using this network, coupled with cloud connectivity, designers can work within highly supportive hardware and software ecosystems to meet current and future design requirements.

References

[1] Gazzetta Ufficiale, (all. 1 - art. 1) allegato A, Regola tecnica per la progettazione, costruzione, collaudo, esercizio e sorveglianza delle opere e degli impianti di trasporto gas naturale con densità non superiore a 0.8.

[2] Review on Smart Gas Sensing Technology Shaobin Feng, Fadi Farha, Qingjuan Li, Yueliang Wan, Yang Xu, Tao Zhang and Huansheng Ning.

[3] MASSERA, ETTORE, FORMISSANO, FABRIZIO, Progettazione realizzazione e test preliminari di prototipi di nodi sensoriali per gas ambientali “TinyNose”.

[4] Fast A Piero Fiorentini company, G-log+ E G-log Evo, RTU per la gestione dei gruppi della riduzione finale della pressione.

[5] Diagnostica e Monitoraggio di Condutture ad Onde Guidate con un Nuovo Sensore Magnetostrittivo: Misura della componente Flessurale e Caratterizzazione dei Difetti, F. Bertoncini, C. Oprea, M. Raugi, F. Turcu, Università di Pisa - Dipartimento di Sistemi Elettrici e Automazione.

[6] Priolo, Enrico & Romano, Maria Adelaide & Romanelli, Marco & Plasencia Linares, Milton P. & Garbin, Marco & Bernardi, Paolo & Zuliani, David & Fabris, Paolo & Peruzza, Laura. (2014). Rete di rilevamento sismico finalizzata al monitoraggio della sismicità naturale e microsismicità indotta presso la concessione di stoccaggio gas metano denominata “Collalto Stoccaggio” (TV) Anno di esercizio 2014 - Seconda relazione annuale.

SOLVING THE STRUCTURE OF THE FERRIELECTRIC PHASE INDUCED BY ELECTRIC FIELD IN $PBZRO_3$ THIN FILMS

Aleksandr Ganzha

Peter the Great St.-Petersburg Polytechnic University,
St. Petersburg, Russia
E-mail: alexander.ganzha@gmail.com

***Abstract*:**
In-situ x-ray diffraction shows an unusual structural response of $PbZrO_3/SrRuO_3/SrTiO_3(001)$ heterostructures appears at precritical (lower than required for switching to FE phase) electric fields. This new field-induced structure forms gradually upon increasing the applied field. The field-induced structure is similar to the antiferroelectric parent phase in octahedral-tilt pattern but differs from it in the lead-ion displacement pattern. Structural factor modeling shows the latter can be encoded as ↑↑↑↑↓↑↑↓ provided that the antiferroelectric structure is encoded as ↓↓↑↑.
***Keywords*:** x-ray, ferrielectric, AFE, thin films.

Introduction

Ferroelectrics occupy a significant niche in modern industry. For a wide class of such materials, practically significant properties are determined by the presence of structural phase transitions. In thin-films of such materials due to atom-to-atom correspondence between the film and substrate it is possible to of build high-quality and defect-free heterostructures for miniaturized devices and tailor the material properties by a set of size effects specific to films. Antiferroelectric films are much less studied than ferroelectric films but nevertheless they are interesting due to prospective applications in memory, energy storage and electrocaloric devices. Among the most thoroughly studied samples of this sort $PbZrO_3/SrRuO_3/SrTiO_3$ stands out [1–3]. The large lattice mismatch (about 5%) between $SrTiO_3$ and $PbZrO_3$ leads to the strain in these films which is quickly relaxed via dislocations in the near-interface layer [3]. Experimentally, the properties of $PbZrO_3/SrRuO_3/SrTiO_3$ heterostructures are substantially different from those of bulk $PbZrO_3$. Namely, heterostructures show a modified behavior with respect to switching between the antiferroelectric and the field-induced polar structures by electric field. The mechanism of this film-specific smearing in antiferroelectrics has not yet been established but the changes in switching behavior should lead to some structural changes occurring under the field.

Experimental

In this work we characterize (001)-oriented $PbZrO_3$(50 nm)/$SrRuO_3$(20 nm)/$SrTiO_3$ heterostructure grown by pulsed laser deposition at the University of California at Berkeley. The experiment was performed using a SuperNova (Rigaku) single-crystal diffractometer with in-situ application of electric field. Due to the specifics of the method, the field values are pre-critical, that is smaller than those needed to induce the transition to the ferroelectric phase.

Diffraction results

When no field is applied, the film is populated with antiferroelectric domains with *c*-axes parallel to the film. The related reciprocal space map is plotted in Fig. 1 a (we have plotted the pattern E ≈ 75 kV/cm instead of basically identical zero-field map because of its better quality). The diffraction pattern consists of superstructural reflections with reduced wavevectors $\vec{q} = \frac{1}{4}(1,0,1)$ in pseudocubic coordinates where [001] points along the normal Σ-points), reflections at $\vec{q} = \frac{1}{2}(1,1,1)$ (*R*-points) and at $\vec{q} = \frac{1}{2}(1,0,1)$ (out-of-plane *M*-points) and $\vec{q} = \frac{1}{2}(1,1,0)$ (in-plane *M*-points).

The Σ-point reflections are due to lead-ion displacements organized in a transverse wave with pattern ↓↓↑↑. The *R*-point reflections are expected to be due to anti-phase octahedral tilts according to the bulk

PbZrO3structure [4], although a part of the *R*-point intensity could be also due to the anti-phase lead displacements, as considered by Ricote *et al.*[5] for PZT.

The *M*-point reflections are less well understood. In PZT they have been considered by Ricote *et al.*[5] as being due to either in-phase octahedral tilts or due to anti-phase lead-ion displacements, while stressing that they are not compatible with the average rhombohedral R3c ferroelectric structure and should be related to structural inhomogeneities in rhombohedral PZT.

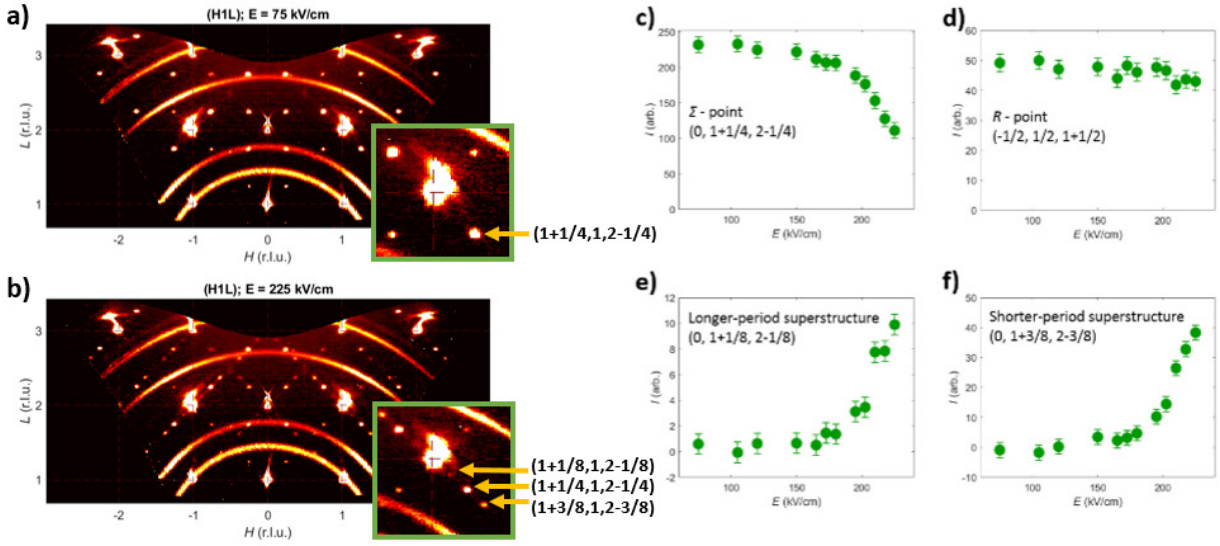

Fig. 1. Diffraction evidence for the gradual formation of long-period structure upon field increase in PbZrO3/SrRuO3/SrTiO3 heterostructure. Panels (a,b) show reciprocal space maps at E ≈ 75 kV/cm and E ≈ 225 kV/cm, respectively. The latter is still below the critical field for AFE-FE transition. Panels (c,d) show field dependence of intensity at Σ- and R-points, respectively. Panels (e,f) show field dependences for reflections emerging on field increase. Powder rings correspond to the scattering by gold electrodes.

Larger fields result in the appearance of superstructure reflections at $\vec{q}=\frac{1}{8}(1,0,1)$ and $\vec{q}=\frac{3}{8}(1,0,1)$ (Fig. 1 b, e, f). These types of reflections in $PbZrO_3$ have not been previously observed. The intensity of these reflections increases gradually with the field, while the intensity of reflections at $\vec{q}=\frac{1}{4}(1,0,1)$ decreases (Fig. 1 c). The *R*-point peak is nearly field-independent (Fig. 1 d), which should be interpreted as oxygen octahedral tilt subsystem being largely unaffected in this field range. The *M*-point reflections also remain intact.

Structure solving

Identification of the actual structure that is responsible for the diffraction pattern is not straightforward, because no well-established crystallographic workflows are available for thin films. We have used the following approach, which is based on the brute-force enumeration of qualitatively different possible displacement patterns and evaluating their potential suitability for reproducing the observed intensities.

First, the unit cell has been identified on the basis of the observed superstructural reflections. It has dimensions $\sqrt{2}a_{pc}\times 4\sqrt{2}a_{pc}\times 2a_{pc}$, which corresponds to the size of the antiferroelectric Pbam unit cell that is twice enlarged along the *b* axis. Then the intensities of superstructure spots have been used to identify the ionic displacements. Since the *R*-point reflections do not react considerably to the field, the tilt pattern should remain qualitatively intact, namely $a^-a^-c^0$[6], where tilts occur around the *a* axis. As long as zirconium ions are not expected to shift considerably, it remains to identify the lead-ion displacements. These displacements are nearly parallel to the *a* axis, as the observability conditions for the superstructure reflections indicate (no visible reflections where the reduced and the total wavevector transfers are nearly parallel). Therefore, lead-ion shifts pattern can be parametrized by eight real numbers, u_i (the number of lead-ion positions along the *b* axis). For that, one invokes an assumption that all u_i are equal in magnitude but can be different in their signs. This reduces the problem to finding those spin-like values, $s_i=u_i/|u_i|$, that allow reproducing the diffraction pattern qualitatively. This task turns out to be well conditioned, because diffraction pattern is very sensitive to s_i, while the experimental diffraction pattern is quite specific and unusual one. Based on the

above considerations, there are $2^8 = 256$ possible configurations of the lead subsystem. However, many of them are irrelevant or redundant, so an initial screening is used based on the considerations below:

1) The structure should not have a period less than eight. Otherwise, reflections in $\vec{q} = \frac{1}{8}(1,0,1)$ will not be observed.

2) A number of structures can be obtained from each other by changing the direction of the modulation wave vector.

3) A number of structures can be derived from each other by moving along the modulation wave vector.

4) A number of structures can be obtained from each other by changing the sign of lead displacements.

Points 2 and 4 correspond to a change in the state of the orientation region, but does not change the intensity of the superstructure, and point 3 corresponds to a change in the state of the translational region, and also does not change the intensity of the superstructure.

After removing irrelevant and redundant configurations, we get only 14 structures listed in Table 1.

Table 1

14 unique lead offset patterns remaining after taking in account all irrelevant or redundant configurations calculated around $\vec{Q}=(-102)$ in the $[101]$ direction

Structure number	Lead offset configuration	$\lvert F_{(-1+\xi\ 0\ 2+\xi)}\rvert^2/10^4$ (number of electrons)^2			
		ξ = 1/8	ξ = 1/4	ξ = 3/8	ξ = 1/2
1	↑↓↑↑ ↓↑↓↓	1.23	0	6.97	0
2	↑↑↑↑ ↓↑↑↓	0.61	2.07	3.48	0
3	↑↑↓↑ ↑↓↓↓	2.1	4.14	2.04	0
4	↑↑↓↑ ↓↑↓↓	0.61	2.07	3.48	4.01
5	↑↑↑↑ ↓↓↓↓	7.16	0	1.2	0
6	↑↑↑↑ ↑↓↓↓	6.11	1.04	0.18	1
7	↑↑↑↑ ↓↑↓↓	3.14	1.04	3.06	1
8	↑↑↑↓ ↑↑↓↓	1.05	5.17	1.02	1
9	↑↑↑↓ ↑↓↑↓	1.05	1.04	1.02	9.03
10	↑↑↓↑ ↑↓↑↓	0.18	1.04	5.95	1
11	↑↑↑↑ ↑↑↓↓	3.58	2.07	0.6	0
12	↑↑↑↑ ↑↓↑↓	2.1	0	2.04	4.01
13	↑↑↑↓ ↑↓↓↓	3.58	2.07	0.6	4.01
14	↑↑↑↑ ↑↑↑↓	1.05	1.04	1.02	1

The structure factor has been calculated as $F = \sum_{j=1}^{8} f(Q) exp\left(i\vec{Q}\vec{r}_j\right)$, where j enumerates lead ions in the cell, $f(Q)$ is the atomic factor for lead. Lead ion positions were assumed as if all the displacements were by 0.28 $\dot{A}$ in magnitude (as in pure $PbZrO_3$), while the signs were determined by the displacement pattern. To be potentially consistent with the experiment, the structure has to result in zero intensity for $\xi=1/2$ and provide the intensity for $\xi=3/8$ larger than for $\xi=1/8$. This is true only for config-urations numbered 1 and 2. Among those, only the structurenumber 2 has non-zero net polarization, which makes it thelikely structure that is experimentally observed.

Discussion

This field-induced structure is likely responsible for unusually large effective dielectric constant deduced from P-E loops between more sharp switching events to the ferroelectric phase. Explaining the reason for

this phase is a non-trivial task, at least the homogeneous strain, which we have considered similarly to the works [7, 8], does not seem responsible for it. Apparently, this is because the real polydomain and heterophase (antiferroelectric andferrielectric-like phases coexist) configuration sets out a problem of a different kind, which is more related to the considerations of multi-phase states in perovskites mediated by mechanical and electrical effects [9, 10], as well as to the considerations of purely local interactions at $PbZrO_3$–vacuum interface [11]. An explanation for the appearance of exactly the observed ferrielectric phase instead of the multitude of structural alternatives is obtained upon accounting for the energy of heterophase domain walls, which is important in dense nanostructures due to high surface-to-bulk ratio of nanodomains.

Conclusion

Epitaxial films of $PbZrO_3$ on $SrRuO_3/SrTiO_3$ substrate react peculiarly to the relatively small constant electric fields. Instead of keeping the antiferroelectric phase until reaching the critical field for switching, a heterophase state forms and develops gradually with changing field.

The unusual commensurateness between the modulation periods of host (↑↑↓↓) and guest (↑↑↑↑↓↑↑↓) phases can be explained upon accounting for the energy of heterophase boundaries, which is important in dense nanostructures due to high surface-to-bulk ratio of nanodomains.

The results point to the mechanism leading to the smearing of polarization-field loops in such heterostructures and suggest a perspective for controlled creation of delicate dipolar orderings for ferroic-based memory.

Acknowledgments

Aleksandr E. Ganzha acknowledges the Roman G. Burkovsky, Georgiy A. Lityagin, Alexander F. Vakulenko, Ran Gao, Arvind Dasgupta, Bin Xu, Alexey V. Filimonov and Lane W. Martin for their help in writing the article. This work has been supported by the Russian Science Foundation (Grant 20-72-10126).

References

1. K. Boldyreva, D. Bao, G. Le Rhun, L. Pintilie, M. Alexe, and D. Hesse, Microstructure and electrical properties of (120) O-oriented and of (001) O-oriented epitaxial antiferroelectric $PbZrO_3$ thin films on (100) $SrTiO_3$ substrates covered with different oxide bottom electrodes, Journal of Applied Physics **102**, 044111 (2007).

2. L. Pintilie, K. Boldyreva, M. Alexe, and D. Hesse, Coexistence of ferroelectricity and antiferroelectricity in epitaxial $PbZrO_3$ films with different orientations, Journal of Applied Physics **103**, 024101 (2008).

3. A. R. Chaudhuri, M. Arredondo, A. Hahnel, A. Morelli, M. Becker, M. Alexe, and I. Vrejoiu, Epitaxial strain stabilization of a ferroelectric phase in $PbZrO_3$ thin films, Physical Review B **84**, 054112 (2011).

4. D. Corker, A. Glazer, J. Dec, K. Roleder, and R. Whatmore, A Re-investigation of the Crystal Structure of the Perovskite $PbZrO_3$ by X-ray and Neutron Diffraction, Acta Crystallographica Section B: Structural Science **53**, 135 (1997).

5. J. Ricote, D. Corker, R. Whatmore, S. Impey, A. Glazer, J. Dec, and K. Roleder, A TEM and neutron diffraction study of the local structure in the rhombohedral phase of lead zirconate titanate, Journal of Physics: Condensed Matter **10**, 1767 (1998).

6. A. Glazer, The classification of tilted octahedra in perovskites, Acta Crystallographica Section B: Structural Crystallography and Crystal Chemistry **28**, 3384 (1972).

7. S. E. Reyes-Lillo and K. M. Rabe, Antiferroelectricity and ferroelectricity in epitaxially strained $PbZrO_3$ from first principles, Physical Review B **88**, 180102 (2013).

8. K. Patel, S. Prosandeev, B. Xu, C. Xu, and L. Bellaiche, Properties of (001) $NaNbO_3$ films under epitaxial strain: A first-principles study, Physical Review B **103**, 094103 (2021).

9. V. Y. Topolov, A. Turik, O. Fesenko, and V. Eremkin, Mechanical stresses and three-phase states in perovskite-type ferroelectrics, Ferroelectrics Letters Section **20**, 19 (1995).

10. N. A. Pertsev and V. Koukhar, Polarization instability in polydomain ferroelectric epitaxial thin films and the formation of heterophase structures, Physical review letters **84**, 3722 (2000).

11. B. K. Mani, C.-M. Chang, S. Lisenkov, and I. Ponomareva, Critical Thickness for Antiferroelectricity in PbZrO3, Physical Review Letters **115**, 097601 (2015).

VARIOUS TYPES OF APPROXIMATION OF NONLINEAR LINKS OF AUTOMATIC CONTROL SYSTEMS

Viktoria Goncharova

St. Petersburg State University of Aerospace Instrumentation
Saint - Petersburg, Russia
E-mail: goncarovav344@yandex.ru

Abstract
The paper discusses various methods for approximating the characteristics of nonlinear automatic control systems in order to study the accuracy of the system. Approximation parameters other than tabular values are calculated. Based on the parameters found, the optimal approximation method is selected.
Keywords: approximation, nonlinear automatic control systems, linear approximation, quadratic approximation, cubic approximation, exponential approximation, hyperbolic approximation, power function approximation, logarithmic approximation, exponential approximation.

To solve the problem of synthesis and analysis of an automatic control system (ACS), it is necessary to build an adequate mathematical model. In solving this problem, it is necessary to correctly idealize the parameters of the synthesized system. It is important to take into account that when constructing a mathematical model, the main characteristic features and properties of the ACS under study should be preserved, at the same time, the idealization of the system consists in the need to neglect secondary factors that have little effect on the correctness of the ACS operation. It follows that when constructing mathematical models of systems that contain elements with nonlinear characteristics, they often tend to simplify the real characteristics and approximate them.

There are various approaches and methods of approximation. Piecewise linear approximation is most often used, since it has the greatest versatility, as well as polynomial, Lagrange approximation, etc. [1,2,4,5].

The paper considers linear, quadratic, cubic, exponential, hyperbolic, power, logarithmic and exponential approximation methods [6].

It is necessary to find a function of a given form (linear, quadratic, etc.) y = F(x), which takes at given points the values closest to the real (obtained experimentally) values. As a result, we obtain an approximating expression for a nonlinear static characteristic, which makes it possible to construct an appropriate mathematical model.

To obtain the parameters of the approximating function, we use the least squares method. Thus, in each case it is required to find a function F such that the sum of the squares of S is the smallest [6].

$$S = \sum_i (y_i - F(x_i))^2 \to \min \qquad (1)$$

So, for example, in the case of linear approximation F =ax+b, expression (1) is a function of two variables a and b. To find its minimum, it is necessary to use the extremum condition, namely, the equality of partial derivatives to zero.

In this case we get

$$\begin{cases} \sum \left[y_i - F(x_i, a, b) \right] \cdot F_a^{'}(x_i, a, b) = 0 \\ \sum \left[y_i - F(x_i, a, b) \right] \cdot F_b^{'}(x_i, a, b) = 0 \end{cases}$$

Where

$$F_a^{'} = x,$$
$$F_b^{'} = 1$$

As a result

$$\begin{cases} \sum (y_i - ax_i - b) \cdot x_i = 0 \\ \sum (y_i - ax_i - b) = 0 \end{cases}$$

Therefore

$$\begin{cases} \sum y_i x_i - a\sum x_i^2 - b\sum x_i = 0 \\ \sum y_i - a\sum x_i - nb = 0 \end{cases}$$

And finally we have

$$a = \frac{\sum x_i \sum y_i - n\sum x_i y_i}{(\sum x_i)^2 - n\sum x_i^2} \tag{2}$$

$$b = \frac{\sum x_i \sum x_i y_i - \sum x_i^2 \sum y_i}{(\sum x_i)^2 - n\sum x_i^2} \tag{3}$$

Similarly to the above, relations were obtained for the coefficients of approximating functions:
Quadratic

$$\hat{y} = ax^2 + bx + c$$

Using the Kramer method , the coefficients are found *a,b,c*

$$\begin{cases} a\sum x_i^2 + b\sum x_i + nc = \sum y_i, \\ a\sum x_i^3 + b\sum x_i^2 + c\sum x_i = \sum x_i y_i, \\ a\sum x_i^4 + b\sum x_i^3 + c\sum x_i^2 = \sum x_i^2 y_i; \end{cases} \tag{4}$$

cubic

$$\hat{y} = ax^3 + bx^2 + cx + d$$

Using the Kramer method , the coefficients are found *a,b,c* and *d*

$$\begin{cases} a\sum x_i^2 + b\sum x_i + nc = \sum y_i, \\ a\sum x_i^3 + b\sum x_i^2 + c\sum x_i = \sum x_i y_i, \\ a\sum x_i^4 + b\sum x_i^3 + c\sum x_i^2 = \sum x_i^2 y_i; \end{cases} \tag{5}$$

power - law

$$\hat{y} = a \cdot x^b$$

$$b = \frac{n\sum(\ln x_i \cdot \ln y_i) - \sum \ln x_i \cdot \sum \ln y_i}{m\sum \ln^2 x_i \cdot (\sum \ln x_i)^2} \tag{6}$$

indicative

$$\hat{y} = a \cdot b^x$$

$$a = \exp\left(\frac{1}{n}\sum \ln y_i - \frac{b}{n}\sum \ln x_i\right) \tag{7}$$

indicative

$$\hat{y} = a \cdot b^x$$

$$b = \exp\frac{n\sum x_i \ln y_i - \sum x_i \cdot \sum \ln y_i}{n\sum x_i^2 - \left(\sum x_i\right)^2} \tag{8}$$

$$a = \exp\left(\frac{1}{n}\sum \ln y_i - \frac{\ln b}{n}\sum \ln x_i\right) \tag{9}$$

logarithmic

$$\hat{y} = a + b\ln x$$

$$b = \exp\frac{n\sum(y_i \ln x_i) - \sum \ln x_i \cdot \sum y_i}{n\sum x_i^2 - \left(\sum x_i\right)^2} \quad (10)$$

$$a = \frac{1}{n}\sum y_i - \frac{b}{n}\sum \ln x_i \quad (11)$$

hyperbolic

$$\hat{y} = a + \frac{b}{x}$$

$$b = \frac{n\sum \frac{y_i}{x_i} - \sum \frac{1}{x_i}\sum y_i}{n\sum \frac{1}{x_i^2} - \left(\sum \frac{1}{x_i}\right)^2} \quad (12)$$

$$a = \frac{1}{n}\sum y_i - \frac{b}{n}\sum \frac{1}{x_i} \quad (13)$$

exponential

$$\hat{y} = e^{a+bx}$$

$$b = \frac{n\sum x_i \ln y_i - \sum x_i \cdot \sum \ln y_i}{n\sum x_i^2 - \left(\sum x_i\right)^2} \quad (14)$$

$$a = \frac{1}{n}\sum \ln y_i - \frac{b}{n}\sum x_i \quad (15)$$

where a,b,c,d – approximation coefficients, n – number of static characteristic points, x_i – x coordinates of static characteristic points, y_i - y coordinates of static characteristic points, $\hat{y}_i$ – approximated values y_i.

It is necessary to estimate the degree of approximation of the approximating function to the real static characteristics of the nonlinear link, which can be done by calculating the average approximation error. Thus, it is determined which of the methods most accurately approximates the static characteristic of the system [1-4].

As a criterion of proximity of the approximating function to the specified function uses the sum of squared differences table of y-values and the theoretical calculated by the equations (2-15).

The object of the study was taken of the mechanical characteristics of single-phase asynchronous motor with squirrel cage rotor and shielded poles of ДКЭ-1,6-3 [7], shown in figure 1, for each approximation are presented the values of the coefficients a, b, c and d according to equations (2-15) in table 1.

Table 1

Approximation coefficients of the ДКЭ-1,6-3engine at ten points

	a	b	c	d
Linear approximation	-6.0807	3050.0340	-	-
Quadratic approximation	-0.0362	-0.0850	2855.1135	-
Cubic approximation	-0.0003	0.0296	-4.5214	2935.3955
Approximation by a power function	4745.8833	-0.1465	-	-
Indicative approximation	3102.1976	0.9976	-	-
Logarithmic approximation	4123.8061	-368.3403	-	-
Hyperbolic approximation	2314.8815	14136.8898	-	-
Exponential approximation	8.0399	-0.0024	-	-

It is advisable to determine the optimal number of points that define a static characteristic. Figures 1-8 show different types of approximation for n=3, 6 and 10. In this case, the calculated coordinate x corresponds to ω (the speed of rotation of the motor shaft), and y corresponds to M (moment). As follows from Figures (1-8), when determining the coefficients (2-15), by 6 or 10 points, the mathematical model of a nonlinear element gives an approximation result sufficient for practical use.

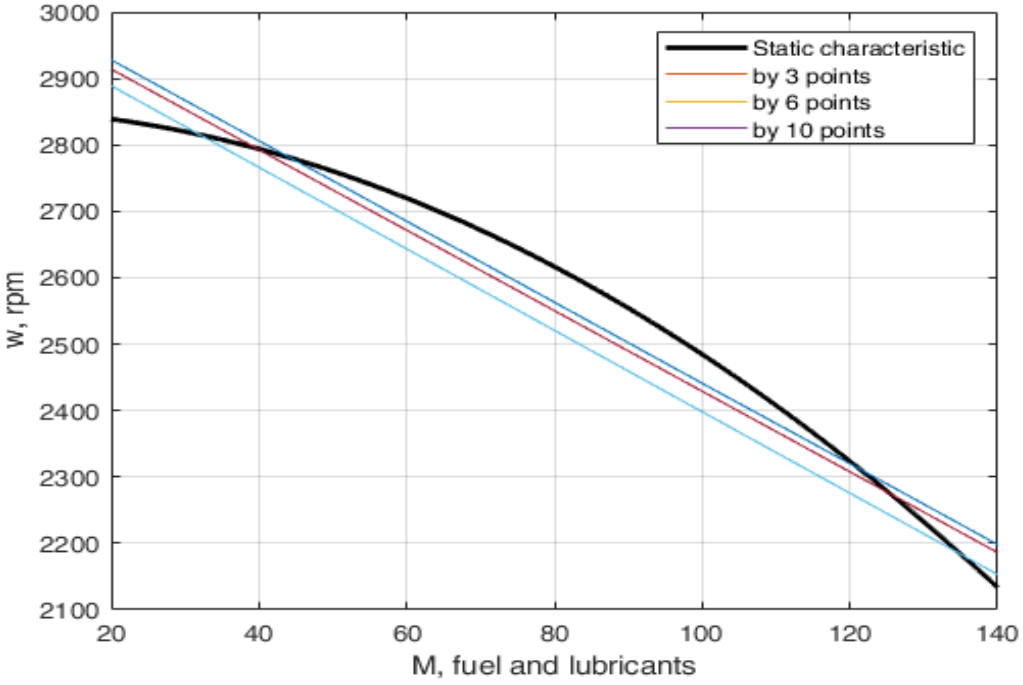

Figure 1 - Linear approximation with different number of points

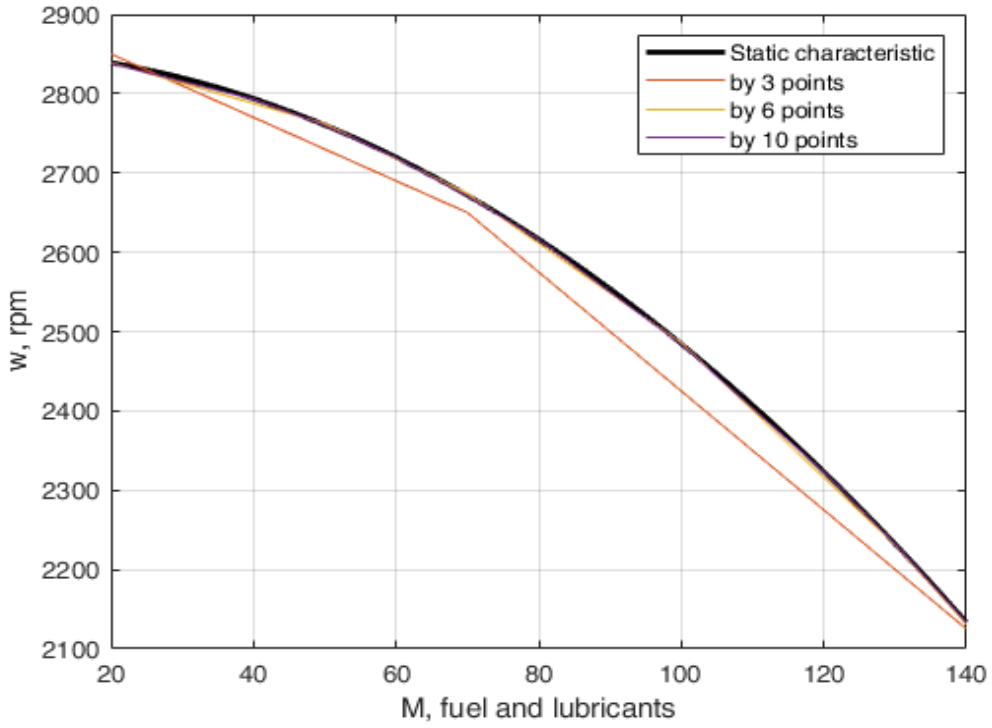

Figure 2 - Quadratic approximation with different number of points

The cubic approximation at n=3 is erroneous, in this case the minimum possible number of points is n=6.

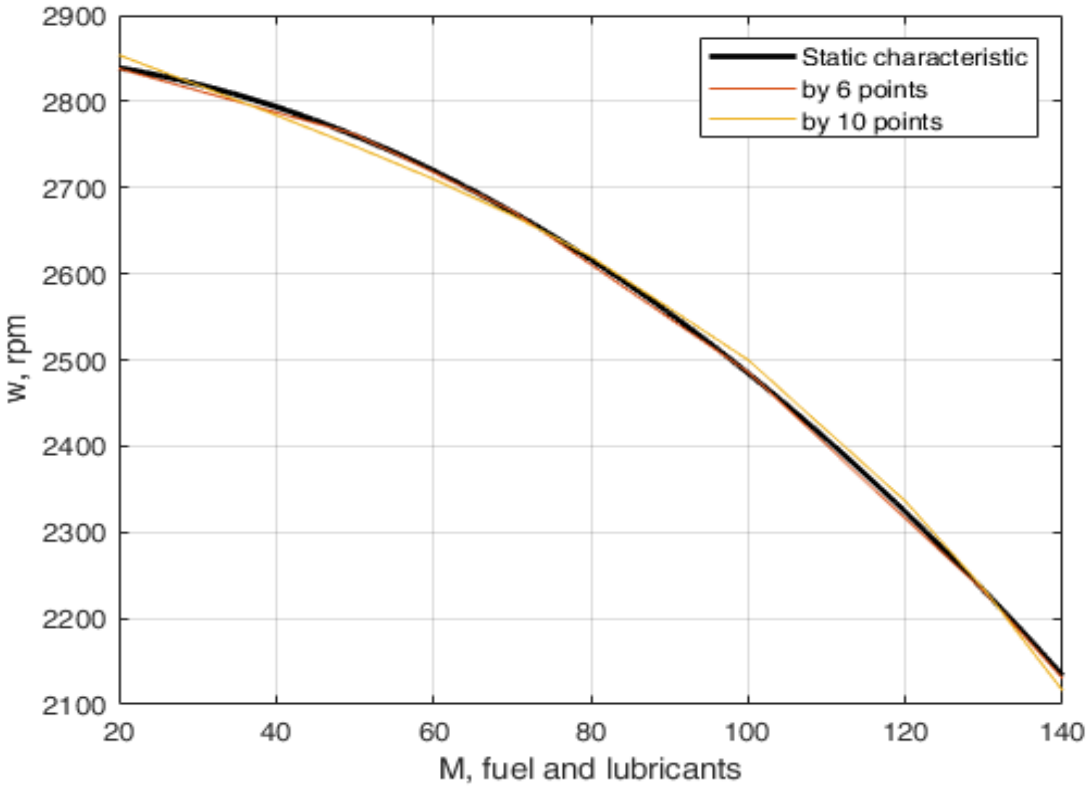

Figure 3 - Cubic approximation with different number of points

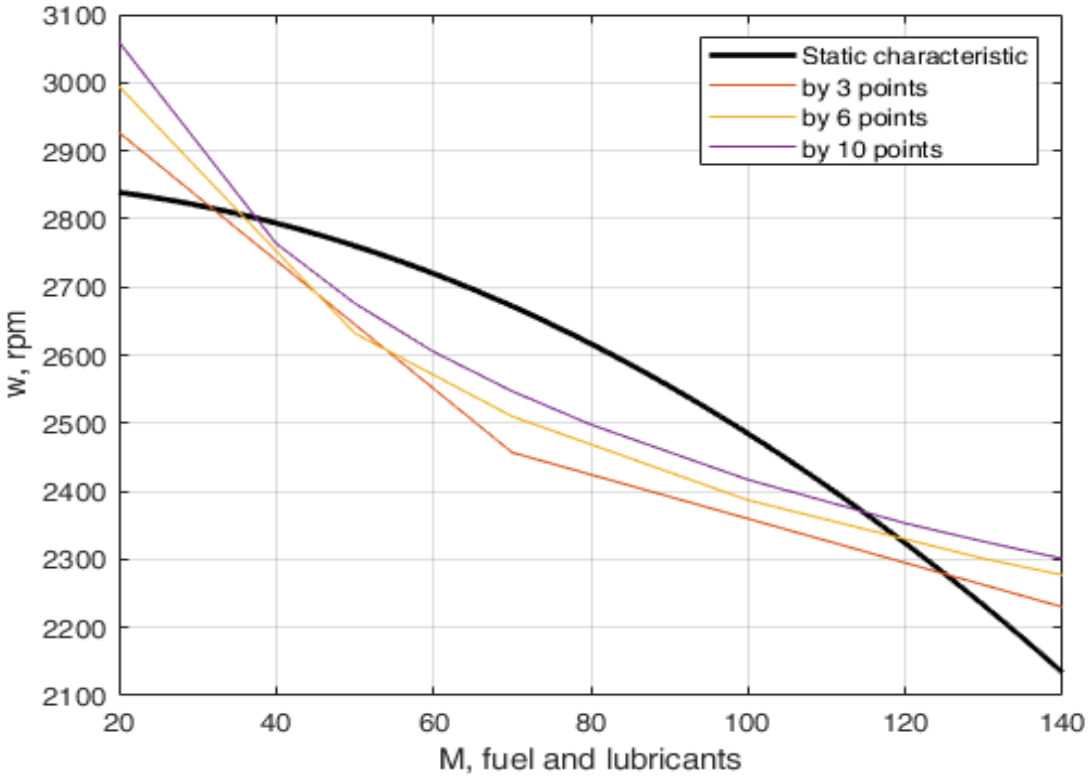

Figure 4 - Power approximation with different number of points

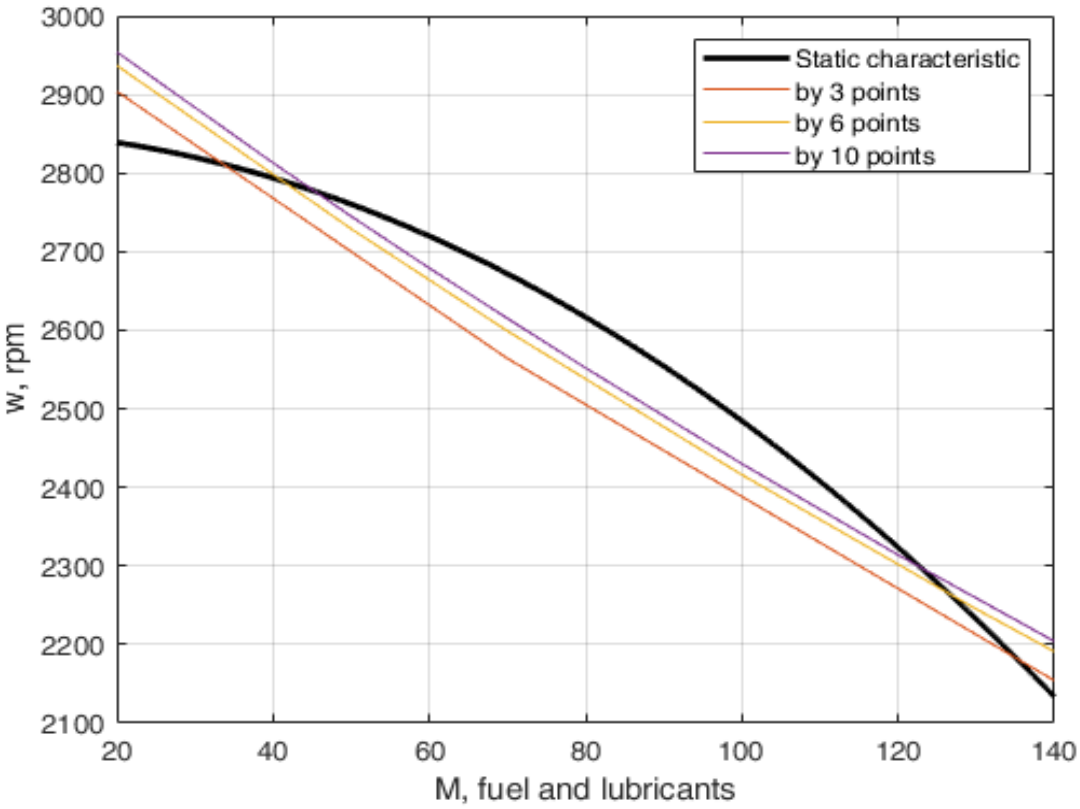

Figure 5 - Indicative approximation with a different number of points

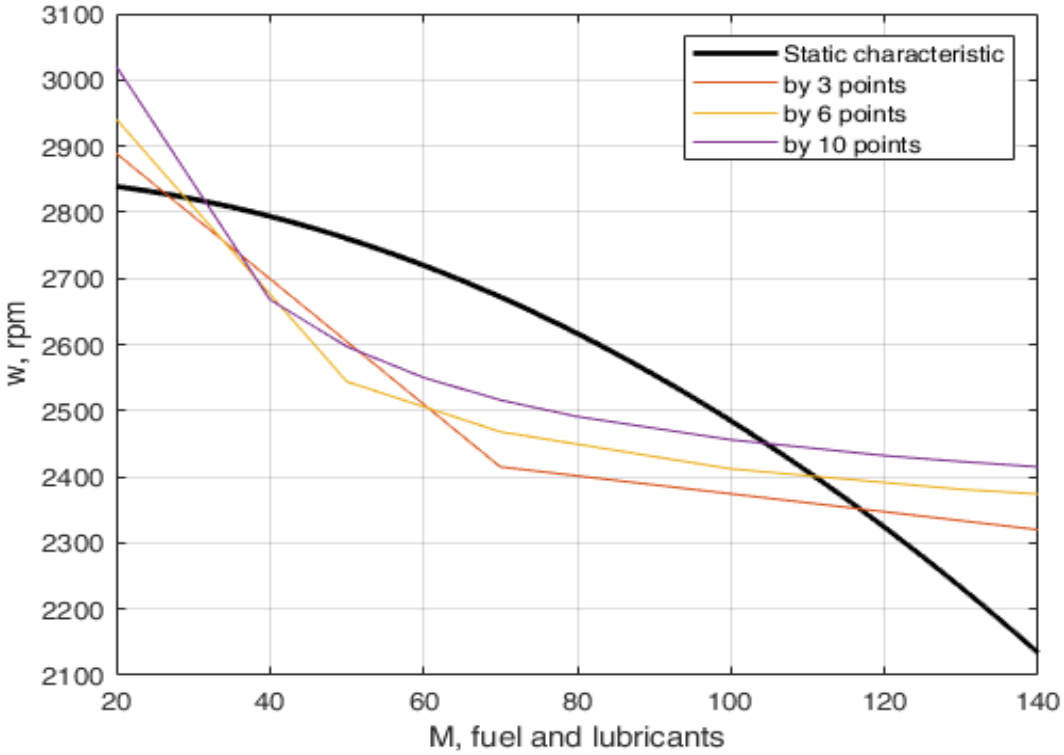

Figure 6 - Hyperbolic approximation with different number of points

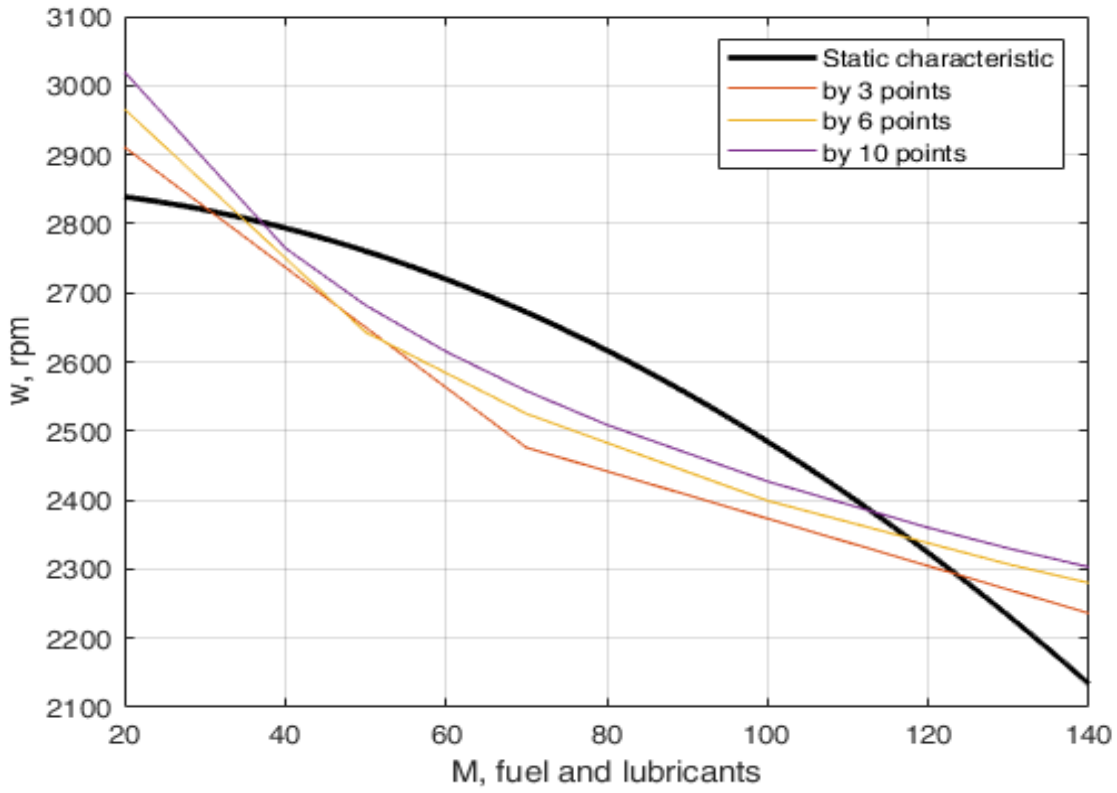

Figure 7 - Logarithmic approximation with different number of points

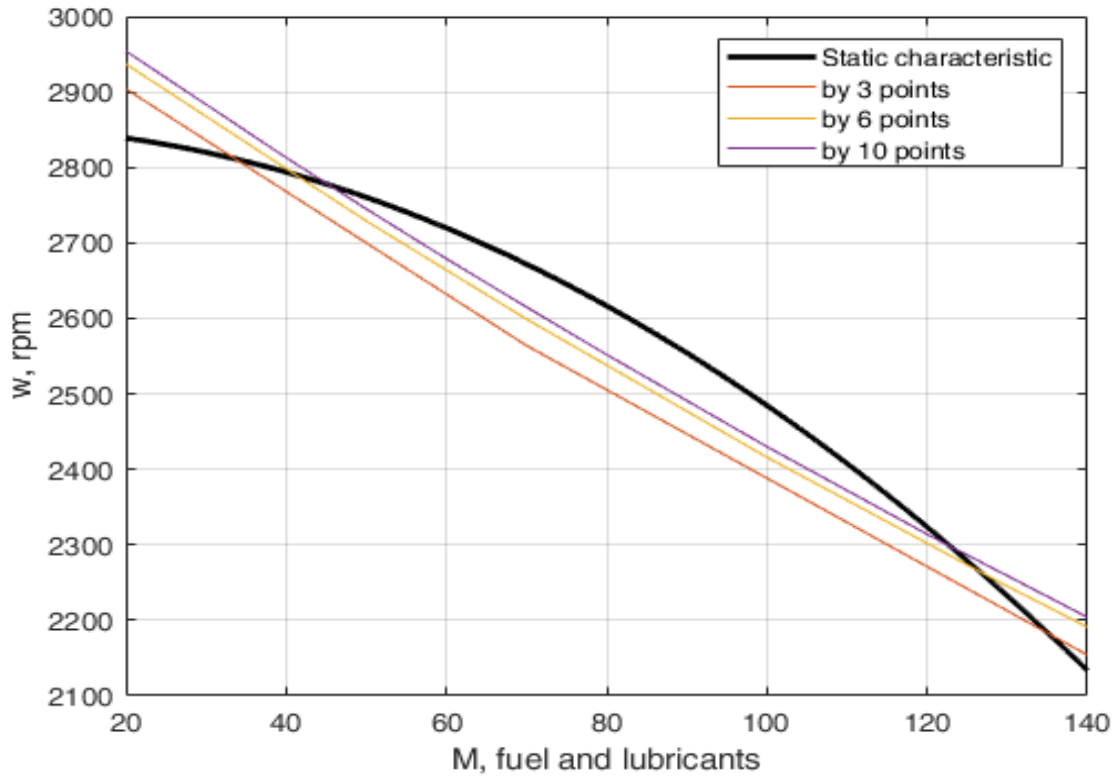

Figure 8 - Exponential approximation with different number of points

Approximation graphs are constructed based on the obtained expressions (Figure 9).

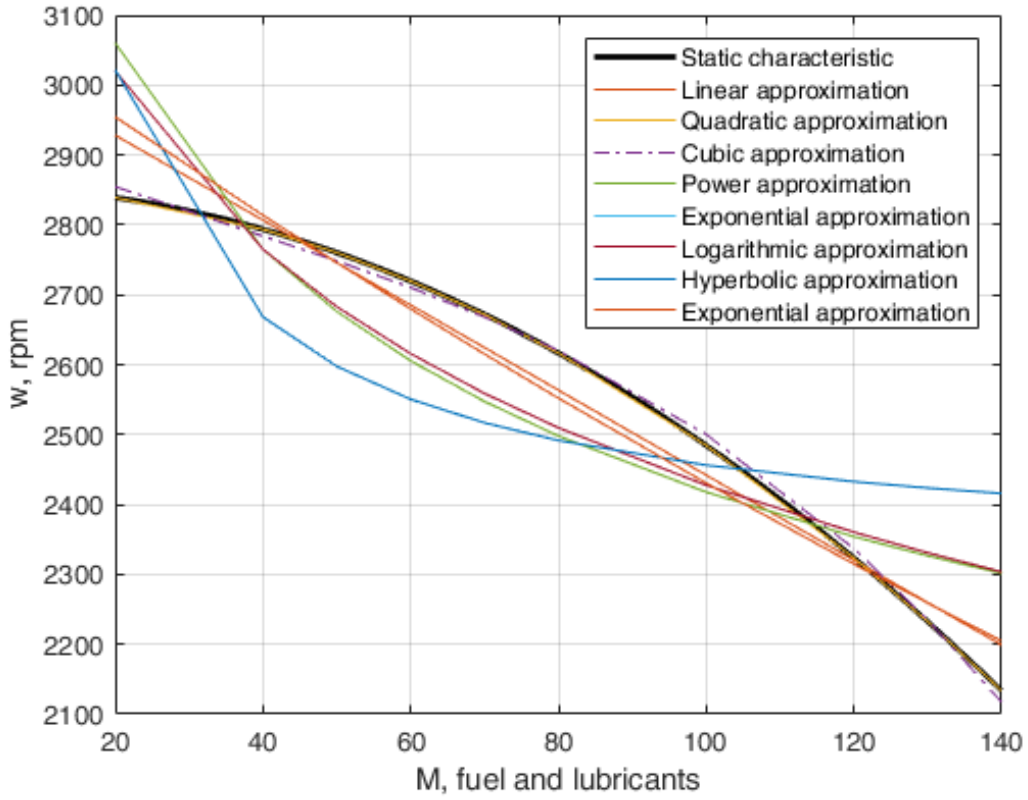

Figure 9 - different types of approximation

Approximating the static characteristic of the engine, the average values of the approximation error were obtained using the expression (16), which are summarized in Table 2.

$$\overline{A} = \frac{1}{n}\sum\left|\frac{y_i - \hat{y}_i}{y_i}\right| \cdot 100\%, \qquad (16)$$

Table 2

Average engine approximation errors ДКЭ-1,6-3

	$\overline{A}$ (average approximation error), %
Linear approximation	1.5506
Quadratic approximation	0.5248
Cubic approximation	0.4357
Approximation by a power function	4.1898
Indicative approximation	1.8596
Logarithmic approximation	3.9164
Hyperbolic approximation	6.1883
Exponential approximation	1.8596

Table 2 shows that the average approximation error for the ДКЭ-1,6-3 engine is less with cubic approximation, it is 0.4357 %.

The approach considered in this paper can be used for various types of characteristics of nonlinear elements, for constructing mathematical models that adequately reproduce the fundamentals of physics of the functioning of control systems of various classes.

Conclusion

Table 2 shows that the average approximation error for the ДКЭ-1,6-3 engine is less with cubic approximation, it is 0.4357 %.

The approach considered in this paper can be used for various types of characteristics of nonlinear elements, for constructing mathematical models that adequately reproduce the fundamentals of physics of the functioning of control systems of various classes.

References

1. Besekersky V.A., Popov E.P., Theory of automatic control: Ed. 4th edition. and additional - St. Petersburg, Publishing house "Profession", 2003 - 752 p. – (Series: Specialist)
2. Nikitin A.V., Shishlakov V. F. Parametric synthesis of nonlinear automatic control systems: monograph / Edited by V. F. Shishlakov. St. Petersburg: SPbGUAP, 2003.
3. Feldbaum A.A. Introduction to the theory of nonlinear circuits. M.:Energoizdat, 1948. 324 p.
4. Overview of approximation methods, Viktoria Goncharova, Bulletin of the UNESCO department «Distance education in engineering» of SUAI: Collection of the papers St. Petersburg Issue 6. – SPb.:SUAI, 2021.p.51-56
5. Synthesis of ACS parameters with polynomial approximation of nonlinear characteristics, Shishlakov V.F., Vataeva E.Yu., Reshetnikova N.V., In the collection: Innovations in science and practice. Collection of articles based on the materials of the VII International Scientific and Practical Conference. In 5 parts. 2018. pp. 92-98.
6. Comparison of the accuracy of approximation of experimental data by the method of least relative squares with the method of least squares, Golovanchikov A.B., Doan M.K., Petrukhin A.V., Merentsov N.A. Modeling, optimization and information technology. 2020. Vol. 8. No. 1 (28). pp. 38-39.
7. Reference manual.DKE-1,6-3, TU 16.510.412-73

ANALYSIS OF WINDOW FUNCTIONS TO REDUCE THE LEVEL OF AUTOCORRELATION FUNCTION SIDE LOBES OF A COMPRESSED CHIRP SIGNAL

Ivan Gordeev

Saint-Petersburg State University of Aerospace Instrumentation,
190000, St. Petersburg, st. B. Morskaya, 67
E-mail: ivangordeev110@gmail.com

Abstract
This article presents a comparative analysis of existing signal modulation methods. An algorithm for matched filtering of a linear frequency modulated signal using window functions is considered as the most common of side lobe reduction. The characteristics of the LFM-signal at the output of the matched filter is given. The results obtained in this work show the expediency of using weighting functions in signal processing in order to reduce the impact of external noise.
***Keywords*:** LFM-signal, window function, matched filtering.

Introduction

At present, there is often a need for efficient signal transmission with the lowest possible distortion. To carry out the transmission of information signals over a distance, it is necessary to convert the original information into a form that can be physically transmitted over the air or cable.

Nowadays, broadband signals, also called noise-like signals, have found application. With the help of these signals, the most serious problems of radar, information transmission and communication are solved [1]. A noise-like signal (NLS) is a signal in which the product of the signal duration T and the width of its spectrum F is much greater than unity [2]. This product is called the base of signal B.

$$B = F*T \gg 1.$$

The use of complex signals in radar provides high resolution in terms of range, speed, and also makes it possible to increase the information content of radio systems [3]. There are more types of NLS that are currently in use. The following can be distinguished: amplitude modulated (AM) signals; frequency modulated (FM) signals; phase modulated (PM) signals; discrete frequency (DF) signals; signals with linear frequency modulation (LFM signals or chirp signals). Combined modulation methods are also possible, when several signal parameters are simultaneously changed, for example, amplitude-frequency modulation.

Amplitude modulation, in which the change in the amplitude of the carrier wave varies in accordance with the information signal, is widely used for transmitting information over long distances, and amplitude modulation is also used in radio communications for aircraft control.

Unlike amplitude modulation, frequency modulation allows you to receive a signal with virtually no interference. FM modulation allows for high quality sound during transmission, due to which it is widely used in radio broadcasting. The scope of FM signals is quite large: broadcasting, radar, telemetry, video transmission systems, seismic exploration, medicine, etc. The disadvantages of frequency modulation include the fact that it requires a wider frequency range than amplitude modulation.

It should be noted that an important parameter in signal transmission is the signal energy. The more energy, the greater the range of the radar system. Problems in creating a signal with high energy are due to the following factors: limitations of generating and amplifying devices in terms of their allowable power; an increase in the pulse duration leads to a deterioration in the resolution of the object in range [4]. These limitations are removed by using signals with intra-pulse modulation, such as chirp and PM.

In phase modulation, the phase of the carrier signal is modulated according to the amplitude of the message signal. Phase modulation is close in characteristics to frequency modulation. If a sinusoidal signal is used as the information signal, then the result of frequency and phase modulation will be the same. The main advantages of FM signals include: high resistance to noise; at a sufficiently high transmission rate, information is transmitted without distortion. However, phase modulation has a number of disadvantages, such as more complex receiver hardware; two signals with different phases are needed [5].

The most widely used chirp signals. One of the main advantages of such signals is the possibility of achieving a large frequency deviation and a significant tuning speed. In [3], the following advantages of chirp signals over PM signals are given:

1) relative ease of correction of distortions introduced by external factors;

2) the ability to convert broadband chirp signals into narrowband ones, which can be converted into digital form for further research, for example, in an FFT processor to highlight information of interest;

3) microwave generators based on transistors, Gunn generators, have been created, which make it possible to cover bands of several gigahertz with a high tuning rate.

Recently, the scope of complex wideband signals with linear frequency modulation has expanded. LFM signals are used in many areas of radio engineering and not only. They are actively used in the tasks of detecting objects and estimating their parameters, recognizing space objects, geolocation, medicine, sonar, etc.

The expansion of the scope of chirp signals, as well as their advantage over other types of broadband signals, makes it relevant to study the properties of this type of signals.

SIMULATION OF THE PROCESS OF SIGNAL COMPRESSION

When modeling the process of matched filtering of the LFM signal, the following procedure was carried out:

1. initial data are entered and additional parameters are calculated;
2. the signal is sent and demodulated;
3. formation of signal samples at the ADC output;
4. matched filtering of the received signal;
5. processing the received signal using a window function;
6. output of the filtering result.

The block diagram of the signal compression algorithm is shown in figure 1.

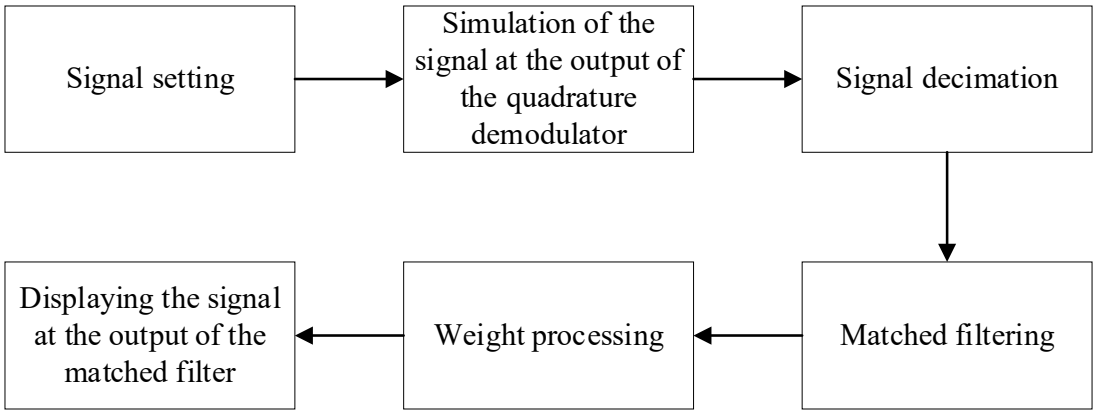

Figure 1 - The procedure of matched filtering

Parameters of the studied LFM signal:

1) Amplitude $A_0 = 0.25$

2) The initial frequency of the signal $f_0 = 10\,MHz$

3) End frequency of signal $f_1 = 50\,MHz$

4) Pulse duration $\tau_p = 2*10^{-6}\,s$

5) The duration of the pulse repetition period $\tau_{prp} = 4*10^{-5}\,s$

6) Signal delay $t_d = 8*10^{-6}\,s$

7) The initial phase of the signal $\varphi_0 = \pi/4$

A graph of the signal with these parameters and the result of matched filtering in the absence of noise are shown in figure 2 and 3.

However, as discussed in references [6–10], the chirp has a high level of side lobes. The most preferred method of interaction with side lobes in the case of chirp signals is weight processing [11, 12]. In the sources

[13 - 17], it becomes possible to use various weight functions, however, at a given number of moments of function consumption, the functions were significantly expanded, so it was decided to study window functions on a chirp signal at the end of the filter. On the subject of beautiful side lobes.

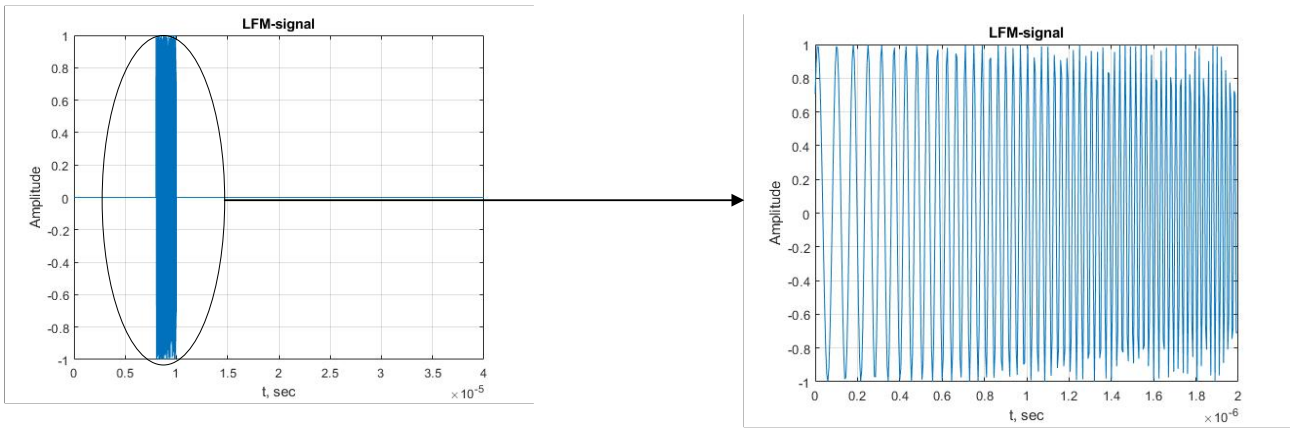

Figure 2 – Original signal

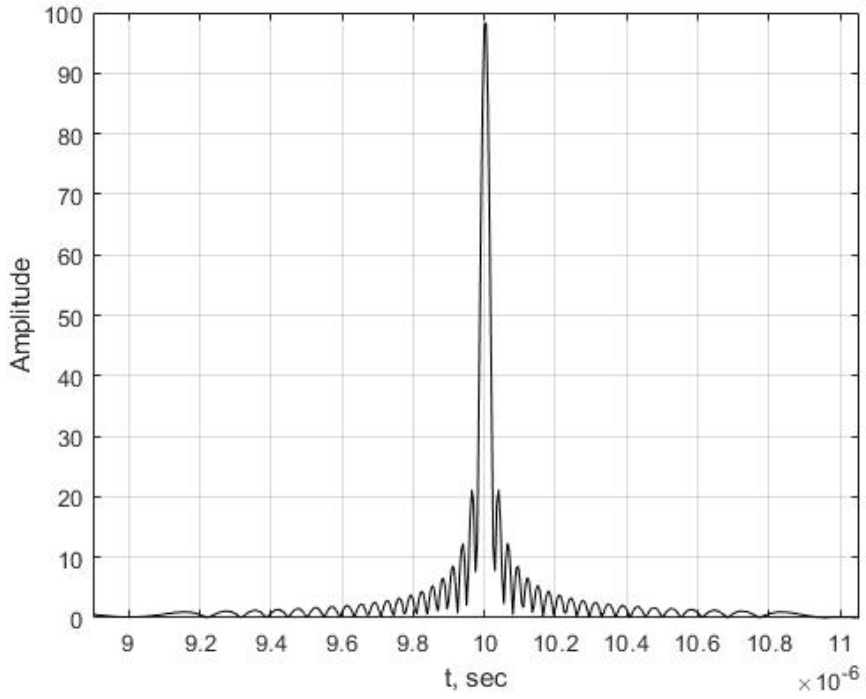

Figure 3 - Result of matched filtering

WEIGHT PROCESSING OF A COMPRESSED LFM SIGNAL IN THE ABSENCE AND PRESENCE OF INTERFERENCE

Hamming, Blackman, Kaiser, Hann, Bartlett, Chebyshev, Tukey, Bohmann, Taylor, Blackman-Harris, Bartlett-Hann windows and rectangular windows were chosen as window functions. Table 1 presents the results of the study of the parameters of the chirp signal.

Table 1

Analysis of the parameters of the chirp signal at the output of the match filter

Window function	Noise level	The ratio of the main peak to the level of the maximum sidelobe	Main lobe peak level	The average value of the ratio of the main peak to sidelobe level
Rectangular	0	4.65	98.36	40.8
	0.05	4.5	98.54	55.3
	0.1	4.36	98.73	30.2
	0.15	4.23	98.92	20.6
Hamming	0	102.19	53.46	137.8
	0.05	22.91	53.43	53.5
	0.1	11.45	53.41	27.8
	0.15	7.63	53.38	18.7
Blackman	0	96.11	41.69	96.4
	0.05	21.39	41.56	46.5
	0.1	10.26	41.43	23.1
	0.15	6.63	41.30	15.4
Kaiser	0	66.54	27.71	66.7
	0.05	17.15	27.45	38
	0.1	8.12	27.19	19
	0.15	5.25	26.93	12.5
Hann	0	38.06	49.56	128.7
	0.05	19.77	49.51	49.7
	0.1	11.06	49.47	24.9
	0.15	7.29	49.42	16.7
Bartlett	0	20.26	49.47	90.4
	0.05	17.92	49.44	52.4
	0.1	11.08	49.41	26.6
	0.15	7.39	49.39	17.8
Chebyshev	0	86.43	36.81	86.7
	0.05	20.36	36.63	44.5
	0.1	9.53	36.45	22.1
	0.15	6.17	36.27	14.7
Tukey	0	5.65	74.08	33,2
	0.05	5.51	74,93	47.3
	0.1	5.36	75.78	25.1
	0.15	5.22	76.62	17.2
Bohman	0	93.65	40.24	128.2
	0.05	21.16	40.10	45.8
	0.1	10.05	39.96	23
	0.15	6.5	39.82	15.2
Taylor	0	29.18	98.95	102.1
	0.05	20.22	99.00	58.4
	0.1	11.94	99.05	30.4
	0.15	7.96	99.11	20.5
Blackman-Harris	0	83.97	35.65	84.2
	0.05	19.9	35.46	43.9
	0.1	9.34	35.27	21.9
	0.15	6.05	35.07	14.5
Bartlett-Hann	0	60.25	49.53	128.6
	0.05	22.23	49.49	50.7
	0.1	11.11	49.45	25.6
	0.15	7.39	49.41	17

Comparison of the signal at the output of the matched filter in the absence of noise allows us to draw the following conclusions.

In case of using window functions the level of main peak has decreased:

1) for the Hamming window by 1.8 times (sidelobe level (SLL) is less than the peak level by about 102 times)

2) for Blackman window by 2.4 times (SLL is less than the peak level by about 97 times)

3) for Kaiser window by 3.6 times (SLL is less than the peak level by about 66.5 times)

4) for Hann window by 1.98 times (SLL is less than the peak level by about 38.6 times)

5) for Bartlett window by 2 times (SLL is less than the peak level by about 20.26 times)

6) for Chebyshev window by 2.7 times (SLL is less than the peak level by about 86.4 times)

7) for Tukey window by 1.3 times (SLL is less than the peak level by about 5.65 times)

8) for Bohman window by 2.4 times (SLL is less than the peak level by about 93.7 times)

9) for Blackman-Harris window by 2.76 times (SLL is less than the peak level by about 84 times)

10) for Bartlett-Hann window by 1.99 times (SLL is less than the peak level by about 60.3 times)

The use of the Taylor window made it possible to slightly increase the maximum of the main lobe (by a factor of 1.006).

Comparison of the results of chirp signal compression with the addition of noise showed the following results.

With an increase in the noise level from 0 to 0.15, the use of the Tukey window, in contrast to the other window functions, reduced the ratio of the main lobe level to the maximum SLL by only 1.08 times, the level of the side lobes increased by about 1.11 times. The use of other weight functions reduces the ratio of the main peak to the maximum SLL by tens of times, and the value of the maximum SLL decreases by up to 50 times. At a noise level of 0.15, the decrease in the maximum sidelobe level reaches 4.5 times.

Also, when noise is added, the level of the main lobe either decreases slightly or also increases slightly.

Conclusion

The paper considers the modeling of chirp signals, as well as their advantage over signals with other types of modulation. A procedure for matched filtering of a chirp signal using various window functions in order to reduce the level of side lobes is considered.

A comparative analysis of the results of matched filtering of this type of signals using weight functions is carried out. The use of weight processing makes it possible to increase the probability of detection against the background of external interference.

The use of the window functions of Hamming, Blackman, Kaiser, Chebyshev, Bohman, Blackman-Harris, Bartlett-Hann made it possible to reduce the maximum SLL by almost 50 times. In terms of the ratio of the peak value to the SLL, the Hamming, Hann, Taylor and Bartlett-Hann windows have the best results.

Of interest are the results of using Tukey's window. When filtering the signal using this weight window, it was noticed that the ratio of the peak to the maximum SLL decreases rather slowly, in contrast to other window functions.

The results obtained prove the justification for using window functions for chirp signals in radar systems.

References

1. Gantmaher, V.E. Noise-like signals / V.E. Gantmaher, N.E. Bystrov, D.V. Chebotarev // Analysis, synthesis, processing. – Saint-Petersburg: Science and technology, 2005. – 400 p. (in Russian)

2.Varaklin L. E. Communication systems with noise-like signals. – Moscow: Radio and communication, 1985. -384 p (in Russian)

3. Dogmatyrko D. G. Simulation of chirp signals and their advantages over other complex signals. // Vestnik of VSTU, 2010. – 6 p.

4. Evgeniy K. Grigoriev, Vadim A. Nenashev, Alexander M. Sergeev, and Sergey A. Nenashev "Research and analysis of methods for generating and processing new code structures for the problems of detection, synchronization and noise-resistant coding", Proc. SPIE 11533, Image and Signal Processing for Remote Sensing XXVI, 115331L (20 September 2020); https://doi.org/10.1117/12.2574238

5. Aleksandrov V.A., Krivaltsevich P.S. Frequency and phase modulation in radio receivers. Advantages and disadvantages. SSTC-75, BSTU, 2019, 128-133 p.

6. Sergeev M.B., Sentsov A.A., Grigoriev E.K., Nenashev S.A. Simulation model of the radar environment of an intelligent control system for distributed radar facilities. Modeling, Optimization and Information Technology. 2020;8(3). Available from:

https://moit.vivt.ru/wpcontent/uploads/2020/08/SergeevSoavtors_3_20_1.pdf DOI: 10.26102/2310-6018/2020.30.3.038 (In Russ).

7. Baskakov A.I., Boldinov R.O. Sidelobe correction of the autocorrelation function of complex radar and hydroacoustic signals. // Radio engineering and telecommunication systems. 2015. No. 1. pp. 21-25.

8. Zakharov A.I. Influence of the integral level of the side lobes of the RAS signal on the quality of measurements // Proceedings of the V All-Russian Scientific Conference "Radiophysical Methods in Remote Sensing of Environments", Murom: Izd. printing center MI VlSU, 2012. -567 p. ISSN 2304-0297 (CD-ROM), p.462-466.

9. Adithya Valli Nettem, D. Elizabath Rani. Modified PWNLFM signal for side-lobe reduction. International Journal of Engineering & Technology. 2019. 7(4): 4-7. DOI: 10.14419/ijet.v7i4.20.22110.

10. Guofu Wang, Tiantian Tang, Jincai Ye, Faquan Zhang. Research on Sidelobe Suppression Method in LFM Pulse Compression Technique. IOP Conf. Series: Materials Science and Engineering 677 (2019) 052104 IOP Publishing doi:10.1088/1757-899X/677/5/052104

11. Lam G. Analog and digital filters. Moscow. Mir, 1982. -592 p.

12. Kulikov A.L. Application of weighing algorithms for digital processing of relay protection signals. // Vestnik ISPEU. 2007. 1-5 p.

13. Parmar, Poonam N., Rahul Dubey and Karuna Markam. “Improvement in Side Lobe Reduction in FIR Filter Design Using Proposed Hybrid Blackman Window.” (2019).

14. Al-Ani, Muzhir Shaban. “Study the Characteristics of Finite Impulse Response Filter Based on Modified Kaiser Window.” (2017).

15. Chandrosha, Yogesh, Nirmala Maheshwari and Pranay Kumar Rahi. “Efficient Design of LOE Pass FIR Filter by Hamming, Kaiser and Blackman Window Techniques.” *International Journal of Advanced Research in Computer and Communication Engineering* 6 (2017): 896-901.

16. Raza, Ghulam Ahmad and Jafir Alam. “DESIGN AND PERFORMANCE ANALYSIS OF BAND PASS FILTER USING BLACKMAN, HAMMING AND KAISER WINDOWS.” *International Journal of Research in Engineering and Technology* 03 (2014): 211-214.

17. Ahmed, Suhaib, Mudasir Bashir and Ashish Suri. “Low Pass FIR Filter Design and AnalysisUsing Hamming, Blackman and Kaiser Windows.” *International Journal of Advanced Research in Electrical, Electronics and Instrumentation Energy* 3 (2014): 8676-8683.

ON ENSURING THE RELIABILITY OF ONLINE REMOTE MONITORING SYSTEMS

Mikhail Gordeev

St. Petersburg State University of Aerospace Instrumentation,
Saint-Petersburg, Russia
E-mail: gordeevm2019@internet.ru

Abstract
The author considers the issue of building global systems for remote online monitoring of patients' condition, which are in demand especially in the context of pandemics. Monitoring is carried out "transparently" for the patient, without involving her in the intricacies of the process of interaction with a medical institution. Threats to the normal functioning of such systems are considered, including existing problems of a general nature, related mainly to global communications. Provides solutions to ensure reliable operation of wearable devices.
Keywords**:** online monitoring, IoMT, global communications, patient mobility, patient engagement and satisfaction.

Introduction

Today, in cardiology, surgery, etc., multifunctional stationary monitors are used that can store large amounts of data and have visualization tools, a large number of measurement data collection channels, interfaces for connecting external sensors and devices, and built-in power supplies for a long period of autonomous operation. Such devices are designed, as a rule, for use in stationary conditions or on specialized automotive equipment.

With the introduction of network technologies into monitors, as well as the emerging Internet of medical things (IoMT) technology, a direction has been developed related to the development of mobile small-sized monitors and distributed systems based on them. Such monitors, which are in constant communication with the servers of medical institutions, including through global communications, are called online monitors [1].

The COVID-19 pandemic has required healthcare systems to change their approach to working with patients with chronic diseases, people with disabilities, pregnant women and children under constant medical supervision. In particular, the periods of self-isolation and quarantine clearly showed the aggravation of the problems of obtaining objective information about the condition of patients, the values of the measured and controlled parameters of their body, including unique ones.

In the aspect of these problems, online monitoring can be considered as a way to create medical systems that can not only register a number of body parameters, but also accumulate and process them, exchanging control results and signs of the development of unfavorable processes based on the processing results with the server of a medical institution.

Wearable devices that are in constant communication via Internet communications with the server of a medical institution and a developed structure of interaction between a doctor and experts are a recent trend in the creation of a new type of patient monitoring systems [2]. This technology, allowing the patient to be under long-term / constant observation, frees him from the need to visit a medical institution or save his location, being located in close proximity to a personal computer connected to Internet communications. It increases the involvement of patients in technological innovations in healthcare and their satisfaction, since interaction with doctors becomes easy and effective [1 – 3], and the process of access to such innovations becomes transparent.

However, for all the seeming simplicity of the implementation of such systems, the task of ensuring their continuous and reliable operation remains relevant. Therefore, the **purpose of this work is** to develop solutions that ensure the correct functioning and reliability of the data collected by wearable devices of online remote monitoring systems.

Online monitoring and its features

The combination of global communication technologies and IoMT largely determines the appearance of remote monitoring systems for the functioning of the vital systems of the human body, for its condition while ensuring the mobility of both the observed and the doctor.

The main purpose of using such systems is to minimize the requirements for the patient-user in terms of serving their own needs in the monitoring process, without territorial restrictions. From a healthcare perspective, this is an important aspect of implementing healthcare principles and managing the next generation of healthcare facilities.

The simplest solution in this area, as practice has shown, is the use of smartphones for these needs [4, 5]. A modern smartphone, reliable in operation, includes acceleration sensors, a positioning system, Bluitooth, WiFi, 802.11 data exchange channels, a connector for a wired interface, etc. and passivity, the intensity of physical activity. Connecting additional sensors to a smartphone using Bluetooth or a wired channel makes it a convenient tool on the basis of which, for example, an online cardiac monitor is built [6].

Another option for implementing the system is to supplement smartphones with specialized wearable devices that are connected to them wirelessly. This allows you to expand the functionality of the online monitor by increasing the number of data collection channels, connecting unique sensors and actors.

In fig. 1 shows the composition of the system, including a wearable device - a storage device for measuring information from several channels and its recording on an SD card.

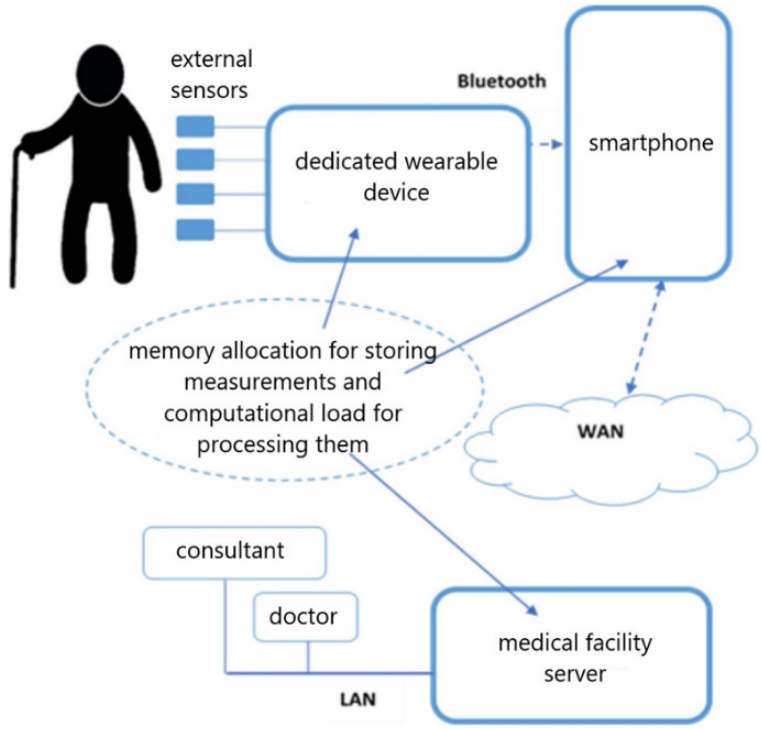

Fig. 1 – Scheme of the implementation of the online monitoring system

The wearable device as part of the system is a monolithic design similar to that developed by ASK Laboratory Ltd. (Russia) [7] and shown in Fig. 2.

Fig. 2 – External view of a wearable device for storing measurement information

It is made on the basis of an Analog Devices Inc. microprocessor with an energy-efficient interface based on Bluetooth, with the ability to independently connect via WiFi to the Internet and, accordingly, to the server of a medical institution. The graphic display with resistive touch-screen provides both viewing of completed recordings and device configuration. The body of the wearable device contains a rechargeable power supply, which significantly increases its dimensions.

In such an implementation, unique wearable devices that solve specific problems have been created with the provision of optimal consumption of the battery resource [8] and the distribution of the computing load and memory between them and the smartphone during the processing of measurement information and its accumulation.

The devices provide connection of various external sensors [9, 10] and contain multichannel biopotential amplifiers with analog-to-digital converters.

The implementation of such online monitors and the volumetric preprocessing of the controlled parameters of the patient performed by them is facilitated by:

- development and expansion of the line of ultrasensitive microminiature sensors and analyzers for medical purposes;
- a significant increase in the specific capacity of memory, power supplies [8] and the computing capabilities of microprocessors [11];
- an increase in the number of hardware solutions and software developments for IoMT, including in the Russian Federation [12].

Initialization of the device and the online monitoring process

It is obvious that the introduction of the considered systems into medical practice is based on strict adherence to methods and regulations. The regulation involves initially conducting a test survey of the patient to clarify his condition, anamnesis, her anxieties and concerns.

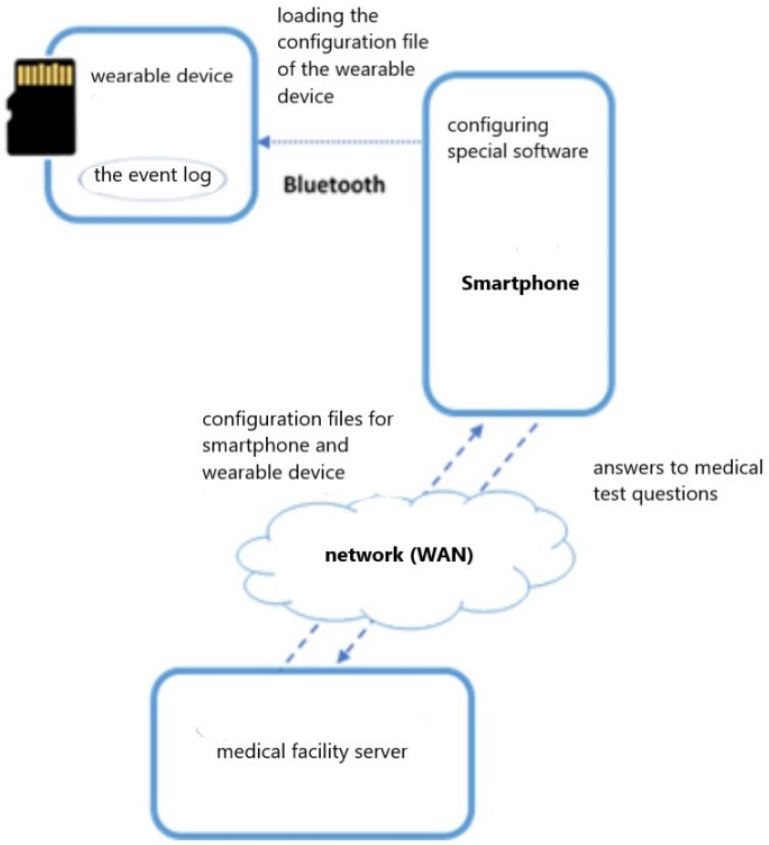

Fig. 3 – Interaction of elements of the online monitoring system during initialization

The polling process is implemented on the basis of the client-server technology "Smartphone" - "Server of a medical institution" or "Home computer" - "Server of a medical institution". Depending on the answers to the questions, the requirements for the monitoring process are formed.

For the online monitoring system, the result of the poll is the generated configuration file of the wearable device and the configured open-source software for the smartphone, transmitted over the Internet to the smartphone (Fig. 3). This solution allows the functions of collecting and accumulating measurements to be divided between a wearable device and a smartphone using built-in or external connected sensors.

Solutions aimed at ensuring the reliability of the system

The main threats to the functioning of the system of the considered configuration are used and its own elements on which it is built.

The system elements used include communications and data transfer protocols. Communications should provide the system with continuous and reliable communication, switching between WiFi, 3G/4G/5G, Wi-Max, etc. technologies, as well as seamless roaming when moving a patient in transport. The protocols, in turn, must provide secure data transmission.

Today, in favor of ensuring these requirements, one can note a significant improvement in the quality of communications in the networks of mobile operators: increasing the reliability of connections, increasing bandwidth, reducing packet transmission delays, supporting various connection technologies, which together contribute to improving the reliability of the online monitoring systems. In particular, the introduction of 5G technology makes it possible to hope that in the most difficult conditions - in crowded places with mobile devices, the connection of online monitors to the network will be guaranteed [13, 14], as well as the continuity of monitoring the patient's biometrics even when switching from one transmission technology data to another.

The reliable functioning of the wearable module is based on the prevention of the following threats:

– failures in its operation and the operation of its components: mobile communication module, interfaces, removable memory modules, etc .;

– emergency shutdowns of work due to overheating due to placement on the patient's body or in the pocket of the patient's clothing (lack of heat sink);

– errors of functioning in case of incorrect actions of the patient.

The task of protecting against the first threat should be solved at the stage of manufacturing a wearable device by choosing components that meet the required reliability parameters, MTBF probability, temperature ranges, etc.

To protect against the second threat, it is proposed to build a temperature sensor into the wearable device, which monitors the temperature and turns off / on the device periodically to prevent overheating and breakdown.

The protection against the third threat is the elaborated detailed instruction and its exact execution by the patient.

To ensure control of the correct functioning, it is proposed to implement the mandatory formation of an internal file called an "event log" in the wearable device. This log, implemented on a separate EEPROM, should be saved as event records. Writing to the event log should be done cyclically. Operations for erasing or rewriting cell values are not provided in any operating mode. Only the open source software of the medical institution's server has access to the event log.

In the event log, the wearable device should record information that captures the user's actions, as well as the state of the device for subsequent analysis and identification of incorrect actions that can disrupt the collection of statistics and distort the readings. Each record must contain at least 7 fields.

For example, in Fig. 4 shows the format of the event log record, 5 bytes in size, which are distributed as follows: Y – year [4 bits], Mo – month [4 bits], D – date [5 bits], H – hour [5 bits], Mn – minute [6 bits], S – seconds [6 bits], EC – event code [8 bits].

Y	Mo	D	H	Mn	S	EC

Fig. 4 – Format of recording in the event log of the wearable device

Some (basic) wearable device event codes are shown in Table 1.

Table 1

Event codes in the device

Event name	Binary value of the EC field
Wearable device on / off events	
"The device turned on from the clock (power failure)"	10000011
"The device turned on from the timer signal"	10000100
"The device was turned on by external power-on"	10000101
"Device turned on after reset"	10000110
"The device turned on after overheating"	10000111
"Regular shutdown of the device"	10001100
"Switching off the device due to overheating"	10001010
"Turning on the device after returning to temperature mode"	10001011
Wearable thermal events	
"System overheating"	00001000
"The system has returned to temperature mode"	00001001
Events related to errors in working with SD card	
"Error starting recording (peripheral failure)"	01111101
"Peripheral error during recording"	00001110
"Error initializing SD memory card"	00001111
"File system error on memory card"	00010000
"Error inside file on memory card"	00010001
"Error while working with memory card"	00010010
"Application initialization error Write"	00010011
"Error working with memory card"	00100101
"An internal application error has occurred."	00101111
Events related to the process of recording measurement results	
"Recording started"	00010100
"Recording stopped"	00010101
"File on memory card is full"	00111100
"Started a new recording fragment"	01111011
Wearable Device Self-Test Events	
"Memory card missing"	10011010
"There is no signal from sensor 1"	10011011
"There is no signal from sensor 2"	10011100
"The device tamper flag has been cleared"	10100100
"Change in signal state"	11010011
"Error initializing the Supervisor application"	10011001
Patient-related events	
"Detected opening of the device"	10100101
"The battery is completely discharged"	11010100
"The record file was erased"	00010110
"The memory card has been formatted."	00010111
Events related to network connections	
"Network settings have changed"	10000001
"Software update command received"	10001001

This incomplete list of conditions that indicate the operation of the wearable device helps to identify malfunctions or incorrect actions of the patient and contribute to the development of recommendations for the further use of the online monitor.

The status indication on the touch screen allows you to make a decision on the hint for the reliable storage of information on the media and its further correct functioning.

Conclusion

The technology of remote online monitoring is promising for creating medical systems for monitoring the condition of patients with anomalies, disabled people and pregnant women who remain mobile.

The use of such systems not only increases the involvement of patients in the field of remote monitoring, but also becomes decisive in monitoring them in emergencies and pandemics.

The development of communication technologies allows us to hope that they will have the least effect on the reliability of the system as a whole.

The use of the event log increases the reliability of the operation of the wearable device and the system as a whole.

Gratitude

The author expresses his sincere gratitude to his supervisor, Associate Professor A. M. Sergeev for his help and valuable advice in the preparation of this article.

Bibliography

1. IoT in Healthcare Expectations for 2020 – URL: https://www.digitalinformationworld.com/2020/02/iot-in-healthcare-expectations-for-2020.html (02.09.2021)

2. Wurzer D., Spielhagen P., Siegmann A. and etc. Remote monitoring of COVID-19 positive high-risk patients in domestic isolation: A feasibility study. *PLOS One.* 2021. September 24. DOI: 10.1371/journal.pone.0257095

3. Taiwo O., Ezugwu. A. Smart healthcare support for remote patient monitoring during covid-19 quarantine, *Informatics in Medicine Unlocked*. Vol. 20. 2020. 100428. DOI: 10.1016/j.imu.2020.100428

4. Bringing the Internet of Things to healthcare – URL: https://www.medicaldevice-network.com/comment/bringing-internet-things-healthcare/ (05.09.2021)

5. What can IOT do for HealthCare – URL: https://www.wipro.com/business-process/what-can-iot-do-for-healthcare-/ (07.09.2021)

6. Smartphone as a diagnostic device. Opportunity Overview – URL:https://evercare.ru/smartfon-kak-diagnosticheskoe-ustroistvo-obzor-voz (07.09.2021).

7. CardioSecur. URL: https://www.cardiosecur.com/ (07.09.2021)

8. Kardimonitor CardioQVARK. – URL: https://cardioqvark.ru/ (07.09.2021)

9. Spicing up your ideas. We develop and create electronic devices of any complexity – URL: https://ask-lab.com/ (10.09.2021)

10. Vostrikov A., Kurtyanik D., Sergeev A. Power Supplies for Mobile Optical Information Systems, *Universum: technical science*. 2017. № 4 (37). P. 40–45.

11. Yuldashev Z. M., Ragheb M. A. Method and Hardware-Software Complex for Assessment of Functional State and Effectiveness of the Portable On-Line Cardio Monitors, *Biotechnosphere*. 2019. №6 (64). P. 10–15. DOI:10.25960/BTS.2019.6.10.

12. Anisimov A. A., Glazova A. Yu., Pustozerov E. A., Yuldashev Z. M. Sistemy udalennogo monitoringa zdorov'ya lyudej s hronicheskimi zabolevaniyami [Remote health monitoring systems for people with chronic diseases]. *SPb.: Izd-vo SPbGETU «LETI»,* 2019. 172 p.

13. Yoshimoto M., Izumi S. Recent Progress of Biomedical Processor SoC for Wearable Healthcare Application: A Review, *IEICE Trans. Electron*., Vol. E102–C. No. 4. April 2019245. P. 245–259.

14. Analytical studies. Internet of Things: potential of Russian companies. – URL: https://www.instel.ru/izdaniya/inform-material/internet-veshchey-potentsial-rossiyskikh-kompaniy/ (09.09.2021)

15. Sergeev A. M., Blaunstein N. Sh. Evolution of Multiple-Access Networks – Cellular and Non-cellular – in Historical Perspective. Part 1, *Informatsionno-upravliaiushchie sistemy* [Information and Control Systems]. 2018. № 4. P. 86–104. doi:10.31799/1684-8853-2018-4-86-104

16. Sergeev A. M., Blaunstein N. Sh. Evolution of Multiple-Access Networks – Cellular and Non-cellular – in Historical Perspective. Part 2, *Informatsionno-upravliaiushchie sistemy* [Information and Control Systems]. 2018. № 5 (96). P. 94-103. DOI: 10.31799/1684-8853-2018-5-94-103

STUDY OF CODE SEQUENCES FOR MODULATING THE PHASE OF A RADIO SIGNAL

Evgeniy Grigoriev

Saint-Petersburg State University of Aerospace Instrumentation,
190000,St.Petersburg, st. B. Morskaya, 67
E-mail: ev.grig95@gmail.com

Abstract
The article considers the correlation characteristics of code sequences, namely m-sequences and Gold codes used in multiple access systems and distributed radar systems. In addition, the correlation characteristics of modified m-sequences, which were modified on the basis of a new theory of quasi-orthogonal matrices, were studied. It is shown that the use of modified sequences obtained from the rows of quasi-orthogonal matrices can be used to solve the problems of improving the characteristics of compression, detection, accuracy, resolution, and noise immunity.
***Keywords*:** Gold sequences, m-sequences, correlation function, quasi-orthogonal matrices.

Introduction

Currently, MIMO technology (Multiple Input - Multiple Output) is widely used in communication and radar systems [1-3]. The use of this technology in relation to radar systems makes it possible to increase the noise immunity, resolution and accuracy of these systems. However, the use of distributed radar systems imposes requirements on the probing signals used. The highest requirements for distributed radars are achieved most fully when using broadband/ultra-wideband and orthogonal probing signals [4]. In this regard, the problem of choosing a specific type of complex transmitting signals is topical.

At this time, in the practice of radar, communications and navigation, phase-shift keyed signals [4, 5] are actively used, which are a sequence of pulses with a phase changing from element to element. The phase can take on any value, but the two most common phase values are 0 and π. In this case, the law of change of the manipulated parameter is completely determined by the code sequence used [6]. In this regard, the problem of studying the properties and choosing a code sequence suitable for solving a particular problem is relevant.

When choosing a signal system, it is important to know not only the correlation properties of the selected ensemble, but also the degree of mutual influence of the signals on each other, which is determined from the cross-correlation properties.

The most popular code sequences for solving the discussed problems are:
- Sequences of maximum length (m-sequences);
- Gold sequences;
- Walsh-Hadamard sequences;
- Kasami sequences;
- Orthogonal codes.

These codes are used in radar and communication systems to improve noise immunity, privacy and multiple access. The purpose of this work is to consider generation methods and analyze the correlation properties of m-sequences and Gold codes.

M-SEQUENCES AND GOLD SEQUENCES

Sequences of maximum length, or m-sequences, are built on the basis of the theory of Galois fields [7]. m-sequences are generated using linear feedback shift registers (LFSR). Since there are two types of LFOS - Galois LFSR and Fibonacci LFSR, we will immediately make a reservation that the first ones will be used in this work. The scheme for generating a polynomial of order k over the Galois field GF(2) is shown in Figure 1.

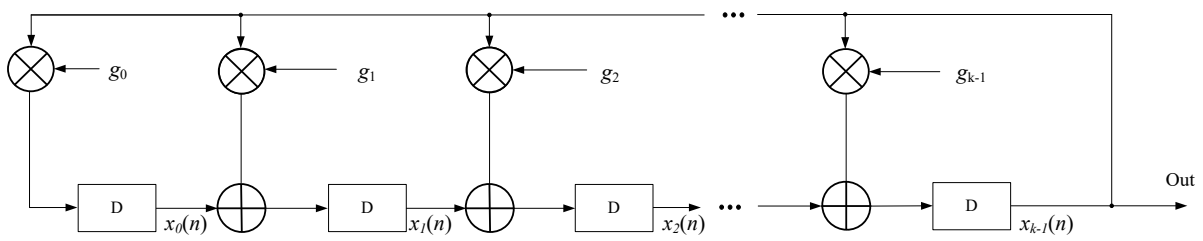

Fig. 1 – Basic architecture of LFSR.

The integer value k denotes the number of delay elements, and g_0, g_1, ..., g_k are the coefficients of the polynomial. The polynomial has the following form:

$$g(x) = g_0 + g_1 x + g_2 x^2 + ... + g_{k-1} x^{k-1} + g_k x^k \qquad (\mathrm{mod}\, 2)$$

where g_0, g_1, …, $g_{k-1} \in$ GF(2), i.e. accepts only binary values.

To generate a sequence of maximum length, the characteristic polynomial that determines the feedback coefficients must be primitive; information about primitive polynomials is widely known from the literature [7,8].

It is known that m-sequences are distinguished by good autocorrelation and cross-correlation properties, but currently there are works [9-11] that propose to modify the properties of m-sequences and are based on the theory of quasi-orthogonal matrices.

Gold sequences, named after Robert Gold, with low cross-correlation are widely used in code division multiple access (CDMA) systems, multi-position radar, and radio navigation due to the low complexity of their production [4,12-14].

Pairs of preferred m-sequences are used to generate Gold sequences. of the same length, which are summed modulo 2. The search for preferred pairs has already been covered in the scientific literature, for example, in [15]. The scheme for generating Gold codes is shown in Figure 2..

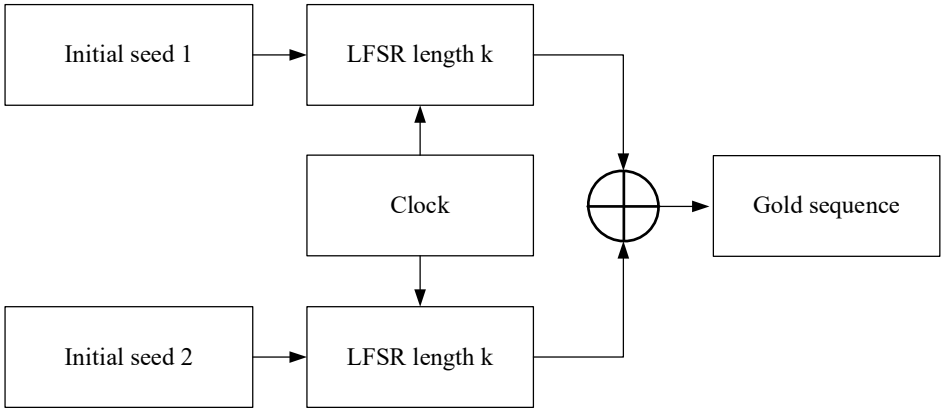

Fig. 2 – Gold sequences generation scheme.

ANALYSIS OF CORRELATION CHARACTERISTICS OF M-SEQUENCE CODES, MODIFIED M-SEQUENCES AND GOLD SEQUENCES

Let's carry out a comparative analysis of the considered code sequences for the aperiodic autocorrelation function (AACF), periodic autocorrelation function (PACF) and cross-correlation function (CCF). Additionally, together with the m-sequence, consider a modified m-sequence. Modification issues have been discussed in the scientific literature [9–11, 16].

It should be noted that further reasoning was studied for m-sequences of orders up to order 2047, however, as an illustration, we give 2^5-1 = 31 orders.

The initial data of the first m-sequence, which was used to illustrate PACF, AACF, as well as modifications:

Polynomial: x^5+x^2+1, initial conditions: [0 0 0 1 0];

The initial data of the second m-sequence, which together with the first sequence was used to calculate the CCF:

Polynomial: x^5+1, initial conditions: [0 0 0 0 1];

Figure 3 shows the periodic autocorrelation functions of the original and modified sequence.

Figure 4 shows the aperiodic autocorrelation functions of the original and modified sequence.

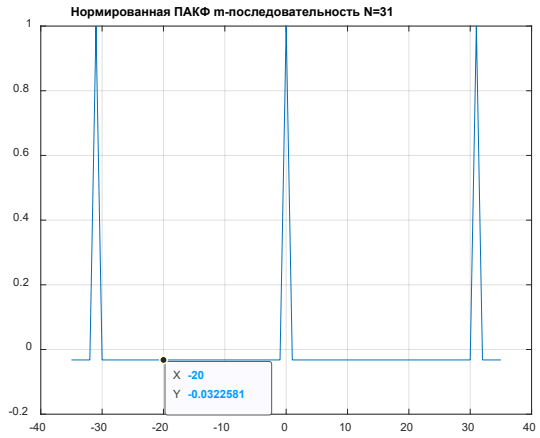

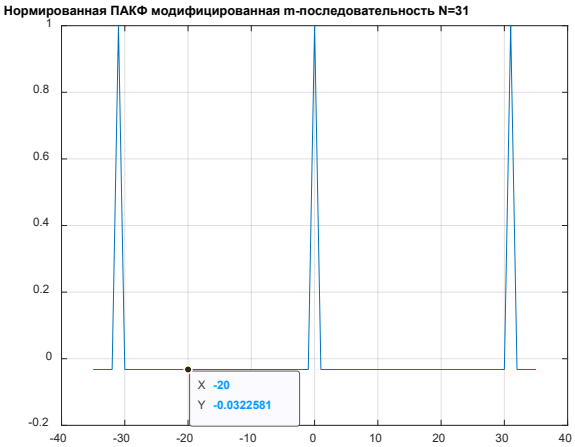

a) Initial *b) Modified*

Fig. 3 - PACF of the studied m-sequences.

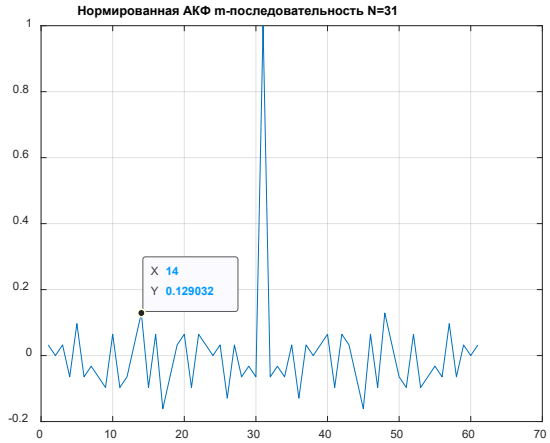

a) Initial *b) Modified*

Fig. 4 - Aperiodic ACF of the studied m-sequences.

Figure 5 shows the cross-correlation functions of the original and modified sequences

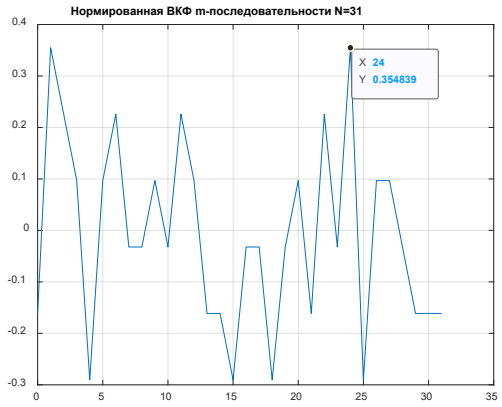

a) Initial *b) Modified*

Fig. 5 - CCF of the two studied m-sequences.

Thus, the results illustrated in Figures 3-5 show the following, the modified m-sequences are better than the original ones in terms of the minimum-maximum side-lobe criterion of the aperiodic autocorrelation function, while the modification does not violate the ideality of the periodic autocorrelation function and does not affect the cross-correlation characteristics.

Next, we will illustrate the results obtained for Gold codes. Initial data for generating the first Gold sequence:

1) m-sequence - polynomial: $x^5+x^3+x^{2+}x+1$ initial conditions: [0 0 0 0 1];
2) m-sequence - polynomial: x^5+x^3+1 initial conditions: [0 0 0 0 1];

The m-sequence data was used in the illustrative example to calculate the AACF and PACF.

Initial data for generating the second Gold sequence, which was used to analyze the CCF:

1) m-sequence - polynomial: $x^5+x^3+x^{2+}x+1$ initial conditions: [0 0 0 1 1];
2) m-sequence - polynomial: x^5+x^3+1 initial conditions: [0 0 0 1 1];

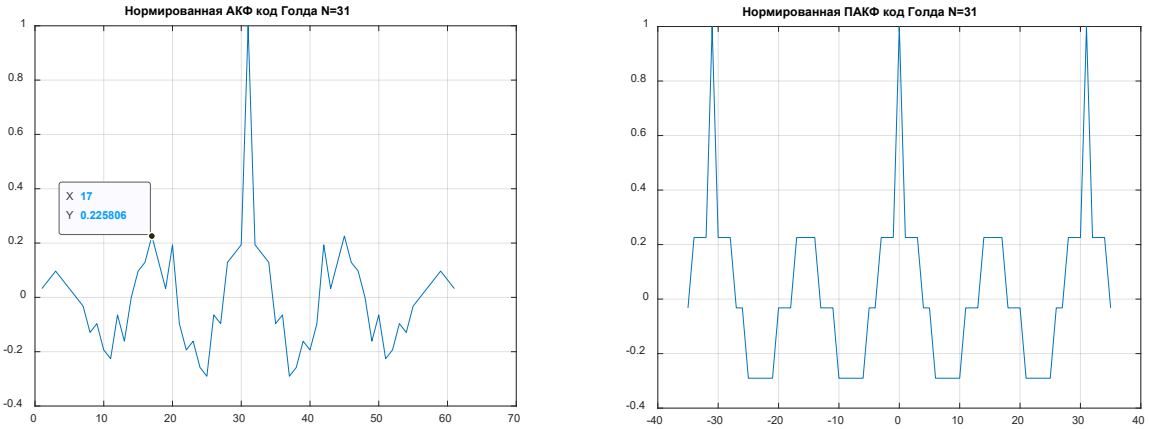

a) Aperiodic ACF *b) Periodic ACF*

Fig. 6 - Aperiodic and periodic correlation functions of the investigated Gold sequence.

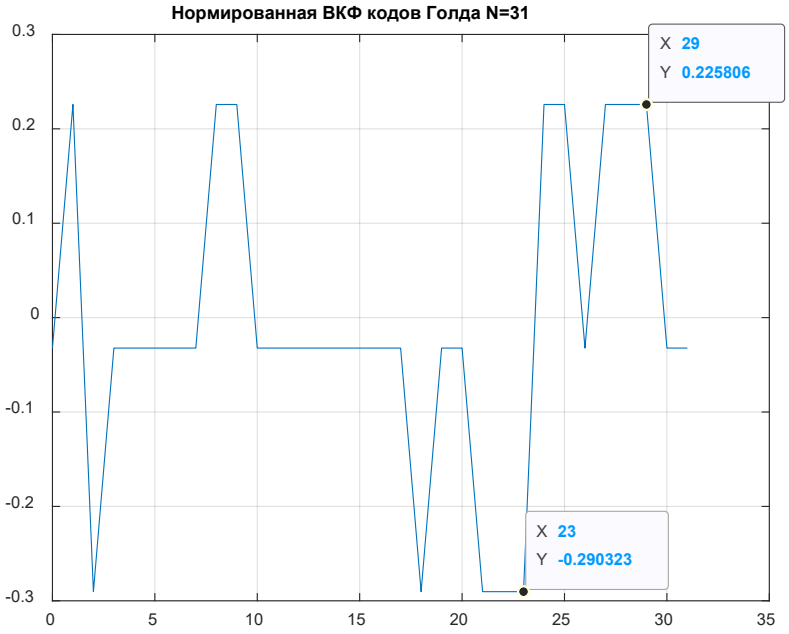

Fig. 7 - Normalized CCF of the two investigated Gold sequences.

The results shown in Figures 6-7 illustrate the well-known properties of the Gold sequences - the three-level cross-correlation function, the violation of the ideality of the periodic autocorrelation function, and the high level of side lobes of the aperiodic autocorrelation function compared to generating m-sequences.

Conclusion

The paper considers the correlation characteristics of code sequences, namely m-sequences and Gold codes used in multiple access systems and distributed radar systems.

In addition, the correlation characteristics of modified m-sequences were studied, the modification of which was carried out on the basis of a new theory of quasi-orthogonal matrices.

The results of the study show that the issues of choosing the code used depend on the characteristics of the system being designed, for example, m-sequences perform better in terms of AACF and PACF, which affects the detection of signals against the background of noise and interference and is applicable to probing signals in radar, it should also be It should be noted that the modification of m-sequences further improves the properties of the aperiodic autocorrelation function - the maximum level of the sidelobe decreases, while the cross-correlation characteristics do not worsen. Gold sequences have the best CCF properties, which can be critical when using several radar stations as part of a multi-position system.

The results obtained in the work once again prove the relevance of the use of the discussed code sequences, as well as the prospects for the use of modified m-sequences and allow us to conclude that it is expedient to use them in modern distributed radar, telecommunications, ultra-wideband, optical, acoustic and "smart" detection and transmission systems. data.

Further development of this study will be the analysis of the functions of uncertainty and mutual uncertainty of the specified code sequences.

References

1. Varakin L.E. Communication systems with noise-like signals. Moscow.: Radio and communications. 1985 [In Russ.]

2. Sergeev M.B., Sentsov A.A., Grigoriev E.K., Nenashev S.A. Simulation model of the radar environment of an intelligent control system for distributed radar facilities. Modeling, Optimization and Information Technology. 2020;8(3). DOI: 10.26102/2310-6018/2020.30.3.038 (In Russ).

3. Klemm, R. (ed.): Novel Radar Techniques and Applications. Vol 1: Real Aperture Array Radar, Imaging Radar, and Passive and Multistatic Radar, p. 1. Scitech Publishing, London (2017). Available from: https://doi.org/10.1049/sbra512f_pti

4. Verba V.S. et al. Radar systems for aerospace monitoring of the earth's surface and airspace / Ed. V.S. Verba, B.G. Tatarsjiy. Monograph. Moscow.: Radiotec, 2014. – 576 p.

5. Mahafza, B.R.: Radar Systems Analysis and Design Using MATLAB, vol. 3, p. 743. Chapman and Hall/CRC (2016). Available from: https://doi.org/10.1201/b14904

6. Gantmacher V.E., Bistrov N.E., Chebotarev D.V. Noise-like signals. Analysis, synthesis, processing – Saint-Petersburg.: Science and Technology, 2005. – 400 p.

7. S. W. Golomb, Shift-register sequences and spread-spectrum communications, Proceedings of IEEE 3rd International Symposium on Spread Spectrum Techniques and Applications (ISSSTA'94), Oulu, Finland, 1994, pp. 14-15 vol.1.

8. R. L. Peterson, R. E. Ziemer, and D. E. Borth, Introduction to Spread Spectrum Communications, Prentice Hall, Inc., 1995.

9. Evgeniy K. Grigoriev, Vadim A. Nenashev, Alexander M. Sergeev, and Sergey A. Nenashev "Research and analysis of methods for generating and processing new code structures for the problems of detection, synchronization and noise-resistant coding", Proc. SPIE 11533, Image and Signal Processing for Remote Sensing XXVI, 115331L (20 September 2020); https://doi.org/10.1117/12.2574238

10. Nenashev V.A., Grigoriev E.K., Sergeev A.M., Samohina E.V. Strategies for calculating persymmetric cyclic quasi-orthogonal matrices as bases of codes // Electrosvyaz. 2020. №10. P. 58-61

11. Search and modification of code sequences based on persymmetric quasi-orthogonal circulants / E. K. Grigoriev, V. A. Nenashev, A. M. Sergeev, E. V. Samohina // Telecommunications. – 2020 (10). – pp. 27-33.

12. Gold, R. (1967), Optimal binary sequences for spread spectrum multiplexing, IEEE Transactions on Information Theory, 13 (4), pp. 619-621.

13. Mathuranathan Viswanathan, Wireless Communication Systems in MATLAB: Second Edition, p. 382. Independently published (2020).

14. Nenashev V.A. Analysis, processing and modeling of broadband signals: / V.A. Nenashev, E.K. Grigoriev. St. Petersburg: GUAP, 2021. - 87 p.

15. Kuznetsov, V.S., Shevchenko, I.V., Volkov, A.S., and Solodkov, A.V., Generation of ensembles of Gold codes for systems of direct spectrum extension, Trudy MAI. - 2017. - No. 96. - P. 17.

16. Certificate of state registration of the computer program No. 2019664813. The program for generating special quasi-orthogonal matrices formed on the basis of modified m-sequences / V.A. Nenashev, M.B. Sergeev, A.M. Sergeev et al. Application No. 2019663534. Received October 30, 2019. Registered in the Register of Computer Programs on November 13, 2019.

THE FUNCTION OF MANAGING NATURAL SYSTEMS IN AUTOMATED MONITORING OF THE ENVIRONMENT THROUGH ARTIFICIAL INTELLIGENCE

Lidiya Klimochkina

Saint-Petersburg State University of Aerospace Instrumentation,
Saint-Petersburg, Russia
E-mail: B1T2K3@yandex.ru

Annotation
Monitoring the state of the environment is the most important task in the context of global climate change and the rapid growth of urban agglomerations. The collection and analysis of environmental data is as important in the process of studying and preserving it as the early diagnosis of a disease in its treatment. The information obtained as a result of the collection is indispensable for the prevention, localization and investigation of environmental disasters and incidents.

In order to make timely management decisions, it is necessary to quickly identify areas of pollution and predict the speed of movement and the concentration of harmful substances, depending on the current situations. The environmental monitoring system allows you to continuously monitor the environmental situation and control all the main sources of pollution for subsequent management decisions. Measured and processed data from all technical means and control points should automatically arrive at the environmental monitoring center around the clock for final processing in order to form a common database, generate and provide reports in tabular and graphical form. The software of all parts of the system must be compatible with each other, which will ensure “conflict-free” operation and allow increasing the composition of technical means without limitation.

The organization of effective control over the state of environmental pollution can be carried out using an automated system for environmental monitoring of pollutants, the block diagram of which is shown in figure 1.

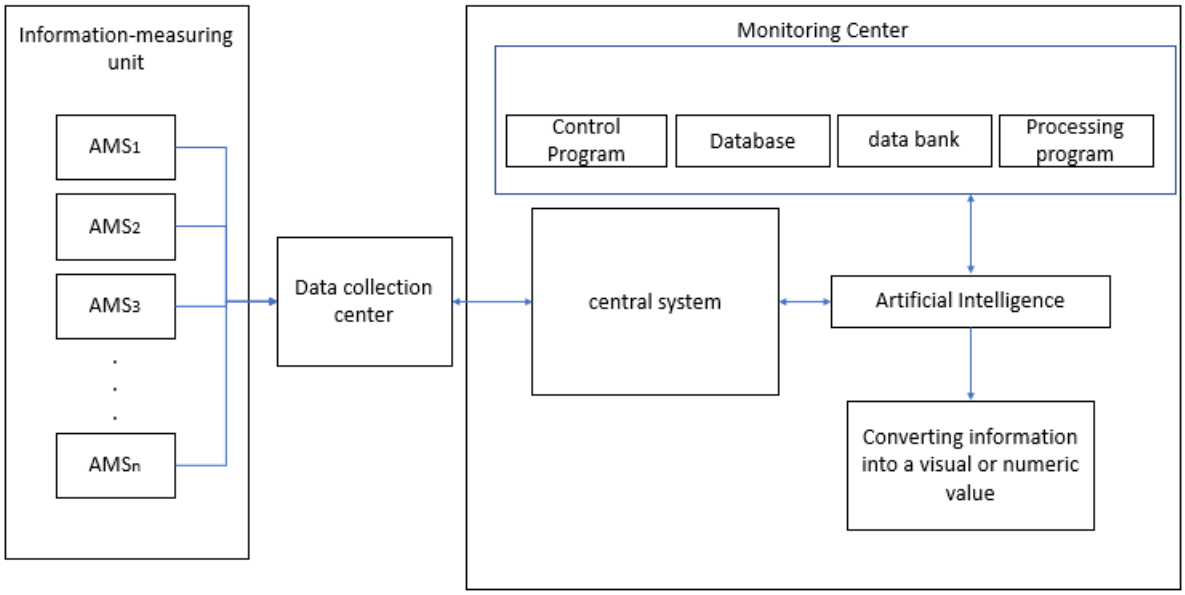

Figure 1. Structural diagram of the automated environmental monitoring system

From the point of view of system analysis, the regional automated environmental monitoring system (ASEM) belongs to the class of complex ones, because has all five features of complex systems:

1. It is hierarchical on a regional basis and consists of interdependent municipal subsystems, which, in turn, can also be divided into subsystems for measuring, transmitting data, processing and storing them, etc. down to the lowest level.

2. The choice of "elementary" constituent components in a given system is relatively arbitrary and is largely left to the discretion of the developer and researcher.

3. Intra-component communication is usually stronger than communication between components. This circumstance makes it possible to separate the "high-frequency" interactions within the components from the "low-frequency" interaction dynamics between the components.

4. Different complex systems contain the same structural parts. Hierarchical systems usually consist of a few types of subsystems, combined and organized in various ways. Thus, the subsystems of measurement, data transmission, their processing and storage, as well as municipal ones, can be arranged and organized in various combinations depending on the observed parameters, methods of transmitting information to upper hierarchical levels, etc.

5. Any working complex system is the result of the development of a working simpler system. A complex system designed from scratch will never work. You should start with a working simple system.

The effect of the total impact of many local point sources of environmental pollution has a territorial character. Therefore, it is necessary to observe and assess the state of the environment, as well as to implement measures to protect it, in a specific area. Observation programs are formed according to the principle of choosing priority (subject to priority determination) pollutants and integral characteristics. A similar amount of information in real time with minimal time can be processed by artificial intelligence.

Thus, modern environmental monitoring systems and the information and control systems that support them are complex multifunctional distributed systems that correspond to all the features of complex systems. In such systems, joint processing of complex data and knowledge is carried out. Only modern information technologies can provide them with a significant increase in the level of information and intellectual support.

One of the features of environmental monitoring and management systems is their specific feature, due to the fact that "direct management" of the environment cannot be carried out, because it is impossible to change, for example, the strength and direction of the wind, humidity, cause rain, etc., in order to reduce the concentration of harmful substances in the atmosphere. In addition, the existing environmental monitoring systems today perform the functions of observation and quite rarely - forecasting the development of the environmental situation. For the above reasons, the control function is not implemented in them.

In order to develop a "control action" in a timely manner, i.e. inform the “decision maker” (DM) about the environmental situation and propose solutions, it is necessary to use advanced information technologies, such as the Internet and the organization of remote access to OS monitoring points based on it. The block diagram is shown in figure 2.

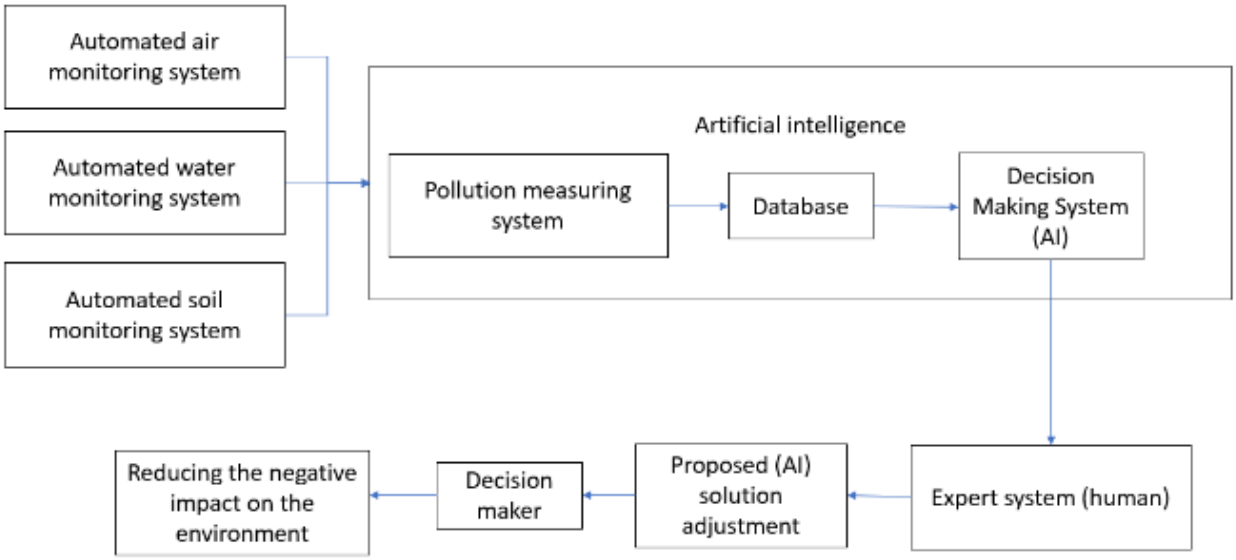

Figure 2. Structural diagram of the intelligent automated system of environmental monitoring and decision management

After preliminary processing, data on the state of the environment enter the expert system (ES), which is a complex software package that accumulates the knowledge of specialists in specific areas and replicates this empirical experience for consultations of less qualified specialists. The basic structure can be imagined as consisting of the components repentant in figure 3.

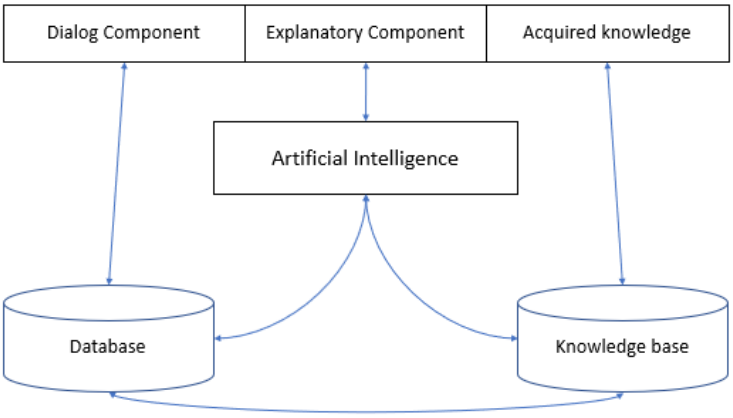

Figure 3. Basic structure of the expert system

The knowledge base (KB) in the expert system is designed to store long-term data that describes the area under consideration (rather than current data) and rules that describe appropriate data transformations in this area. The solver, using the initial data from the working memory and knowledge from the knowledge base, forms such a sequence of rights and, being applicable to the initial data, leads to the solution of the problem. The dialog component is focused on organizing friendly communication with the user. The explanatory component is designed to explain the results of the work and the process of deriving decisions. The knowledge acquisition component automates the process of filling the ES with knowledge. The database (DB) is designed to store the initial and intermediate data of the problem being solved at the current moment.

Thus, the general block diagram of the intelligent ASEM looks like shown in figure 4.

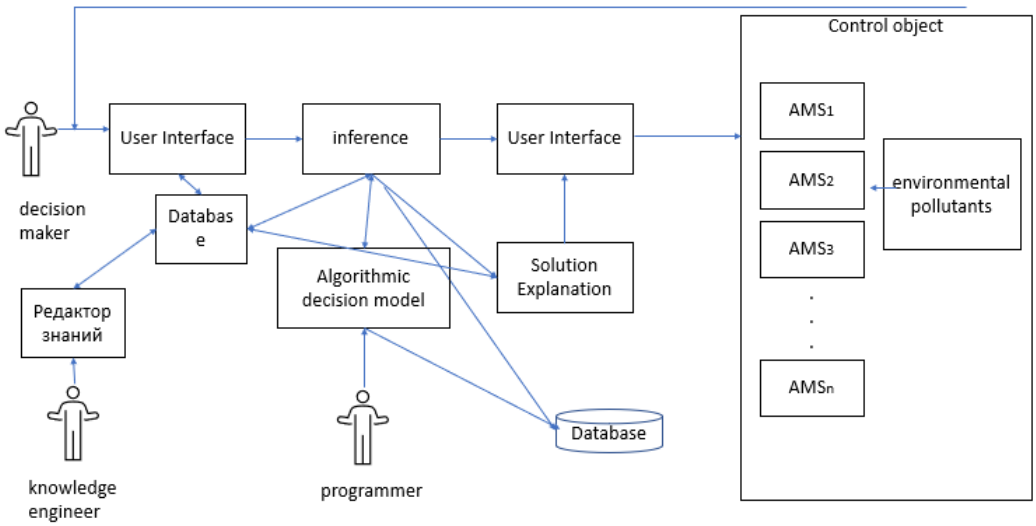

Figure 4. General structure diagram of intelligent ASEM

To replenish the knowledge base, the authors can use modern information Internet technologies.

The environmental monitoring system (Center for Environmental Monitoring), using artificial intelligence, provides a solution to the entire range of tasks of collecting, accumulating, processing and distributing monitoring information. The information-measuring system is represented by a network of automatic stationary monitoring stations and mobile observation laboratories (if necessary).

Conclusion

The Center for Environmental Monitoring using artificial intelligence in a short time solves the following tasks: collection and accumulation of information coming from the information-measuring network; mathematical modeling of environmental processes (study of the transfer and transformation of pollution, analysis and forecast of pollution dynamics); identification of sources, the reduction of emissions of which leads to a

decrease in the increased level of pollution; accumulation and archiving of measurement data and monitoring results; formation and issuance of output documents on the ecological state of the environment; prompt presentation of pollutant concentration fields on a computer display; organization of dialogue between the operator and the system; information service for users; managing the operation of all elements of the monitoring center.

Referens

[1] Chabanenko A V, Kurlov A V and Tour A C 2020 Model to improve the quality of additive production by forming competencies in training for high-tech industries *J. Phys.: Conf. Ser.* **1515** 052065.

[2] Batkovskiy A M, Kalachikhin P A, Semenova E G, Fomina A V and Balashov V M 2018 Conficuration of enterprise networks *Entrepreneurship and Sustainability Issues* **6(1)** 311–28.

[3] Batkovskiy A M, Nesterov V A, S emenova E G, Sudakov V A and Fomina A V 2017 Developing intelligent decision support systems in multi-criteria problems of administrative-territorial formations infrastructure projects assessment Journal of Applied Economic Sciences 12(5) 1301-11.

[4] Smirnov V.N. Modular software system for automated process control systems // Sat: Problems of software for automated process control systems. - 1979. - Part 1. - S. 32-35.

[5] Simon H. The Sciences of the Artificial / H. Simon. - Cambridge, MA: The MIT Press, 1982. - 218 p.

[6] Went, D. P., Volkov, V. Yu., & Barkhum, I. (2008). Intelligent automated systems in ecology. News of the Tula State University. Engineering Sciences, (4), 268-273.

DEVELOPMENT OF A METHODOLOGY FOR MEASURING THE LIGHT OUTPUT OF A LOW-POWER LED LIGHTING DEVICE

Vladimir Kuzmenko

Saint-Petersburg State University of Aerospace Instrumentation,
Saint-Petersburg, Russia
E-mail: mr.konnny@gmail.com

Abstract.
The article describes the main mechanisms of dependence of the characteristics of a low-power LED lighting device and their influence on the light intensity and the magnitude of the luminous flux. The developed method of measuring the light output of a low-power LED lighting device and the obtained experimental dependences of the decrease in illumination on the passage of the on-off cycles of a low-power household LED lamp are presented.

Introduction

In LED lighting devices, the value of the light output depends on the mode of operation of the LEDs. [1, 2] This parameter, as well as the luminous flux, is one of the determinants of the energy efficiency of the lighting device [1, 2]. As a rule, the manufacturer in the passport data for the LED shows the dependences of the relative luminous flux on the temperature at a given supply current, as well as the dependence of the required value of the supply current on a certain fixed temperature of the p-n junction.

Obviously, each of the dependencies has a different effect on the intensity of light and the magnitude of the luminous flux.

To determine the optimal operating modes of an LED lighting device, it is necessary to independently determine the influence of the temperature of the p-n junction, the temperature of the phosphor, as well as the strength and density of the current flowing through the p-n junction.

METHODOLOGY

To obtain the dependence of the luminous flux on the temperature of the p-n junction, when the LED power supply is in pulse mode, single pulses should be used to prevent the LEDs from self-heating. The pulse duration time should be selected no more than 1 second, since with a pulse duration of 1 sec. and more self-heating of the p-n junction was observed. Measurements of the luminous flux should be carried out in a given temperature range from room or average daily (average annual outdoor) to a temperature 25% higher than the nominal value in increments of 5-10 ° C. The setting and regulation of the current strength should be carried out depending on the nominal values of the LED bandwidth and the properties of the applied phosphor. Usually, the current values take from 150 mA to 1A in increments of 50 mA.

In order to assess the influence of the temperature of the p-n junction and the current density on the intensity of the luminous flux, when powered by pulsed current, it is important to observe the conditions under which the light source is placed in a thermal chamber with an optical window and receives single pulses from the power source with a duration of no more than 1 sec.

The LED radiation is fed through a set of neutral filters to a photoelectronic multiplier, the signal from which is transmitted to an oscilloscope that can display the radiation intensity in Volts.

As mentioned above, in addition to the temperature, it is necessary to regulate the current of the LEDs, if the power source does not allow you to get a current on the LED greater than the nominal, you should use an amplifier.

The main methods for measuring the photometric characteristics of LEDs are set out in the documents and standards of the state system for ensuring the uniformity of measurements, which describe mainly the prescriptions, without specifying a specific method for measuring the spectral characteristics of the radiation of an LED lighting device [4].

The measurement of spectral characteristics should be carried out in the following order: a current in the range from 150 mA to 1 A should be applied to the LED light source in a light-tight casing from the power supply, while the temperature should be recorded with a thermocouple or similar means, immediately after the power supply, the current values should be kept unchanged until the substrate temperature and the volt-

age at the terminals reaches fixed values. After that, you can fix the value of the spectral distribution, then changing the value of the current strength and repeating the measurements for the following values.

It makes the most sense to evaluate the relative radiation of the LED and phosphor in the wavelength ranges corresponding to the blue and blue glow from 400 nm to 780 nm, since this range has the greatest effect on the lens of the eye.

Based on the curves of the spectral distribution of the energy of the light source with a change in current and temperature, it is possible to calculate the values of the radiation intensities according to the formula [4]:

$$\Phi_e \approx \int_{380}^{780} \Phi_e(\ )\mathrm{d},$$

where Φeλ (λ) - is spectral density of the radiant flux at the wavelength λ.

To simplify the procedure for measuring the luminous flux of lighting devices, you can use the procedure for measuring the illumination of the site (Fig. 1) under or above the lamp and recalculating the results into the luminous flux [3].

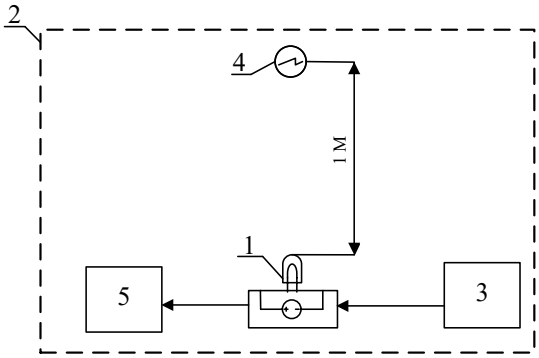

Fig. 1 *The block diagram of the measurement of the LED lightbulb luminous flux, where 1 - is a lighting device, 2 - is a dark box or a black box, 3 - is a power source, 4 - is a luxmeter, 5 - is a thermocouple.*

The method of measurement, the following:

The studied light (led lamp) 1, placed in a dark box 2 so that the distance from the light sensitive element of the meter was 1 m, power source 3 to the lamp to apply a constant current of 150 mA to 500 mA with the accepted limits depending on these the light measured by the light meter 4, after the transition of the lighting unit in steady-state operation according to the manufacturer, the case temperature measured using thermocouple 5 or TV.

Fixing the results is carried out as follows: after the supply current is applied to the lighting device, record the first values of illumination and temperature, after 1-5 minutes, then record the temperature of the substrate and the body of the product every 5 minutes

Measurements should be continued until the illumination indicators decrease by 30% relative to the initial ones.

Comparison of measurement results is carried out by comparing the data obtained with the illumination generated by a control or light-measuring lamp according with known light fluxes [4].

The easiest way to judge the dynamics of the luminous flux is by an indirect indicator - illumination with an additional measurement of the temperature of the housing and the "hot" points of the LED. The magnitude of the decrease in illumination indirectly reflects the magnitude of the temperature of the p-n transition of the LEDs in the lamp and, accordingly, the level of reduction in light output. Therefore, this parameter can be considered as informative.

It is known that it is relatively easy and not expensive to measure the illumination, unlike the luminous flux. When measuring the luminous flux, one option is to prepare a photodetector with a hollow sphere shape and the same light sensitivity in any part of the surface of this sphere, which will require time-consuming calibration.

Another option for measuring the light slope can be the measurement of the radiation pattern and its subsequent integration. But this is not easy either: it becomes necessary to place the light source in a dark room of a sufficiently large size with walls close to absolute darkness, and also to use a goniometric head with two

axes and an automatic drive-in order to avoid significant error when manually setting angles for multiple points. In this case, it becomes necessary to apply various kinds of assumptions, for example, one of the most common special cases is the assumption of the possibility of using such an emitter, the brightness of which will not depend on the angle between the normal to its surface and the direction to the observer.

This assumption is called a special case of using a cosine emitter.

The radiation pattern of such an emitter will be determined only by the visible surface area.

The ratio between the luminous flux and the intensity of light in the direction of the normal to the plane in this case will have the form:

$$I_{\upsilon} = \frac{\Phi_{\upsilon}}{\pi}.$$

Thus, to obtain the magnitude of the luminous flux, it will be necessary to calculate the product of the illumination value measured at a distance of one meter from the source and the number π.

This method can also be used in cases where the distance is not equal to one meter, then it will be necessary to take into account the surplus or shortage according to the inverse square law. However, there are also limitations, since the light source must be significantly smaller than the distance to the luxmeter, otherwise the application of the inverse square law will be impossible.

In the case of small LED light sources such as SMD 5730, 2835, 5050, 30, etc., recalculation by the cosine emitter method can achieve accuracy up to 85-09%. It should be noted that for any LEDs with a lens, as well as for LEDs without a phosphor with the ability to change the color based on RGB, this method is not suitable due to the fact that the radiation pattern of these light sources has significant differences from the cosine [5].

In most cases, the procedure can be divided into two main cases of changes in the LED light flux over time. The first is the stabilization of the luminous flux in a relatively short period of time. In the first seconds of switching on and during the first 60 minutes, the LED luminous flux can drop to 5-10% of the nominal value. The stabilization of the luminous flux is completed in about an hour and a half. However, it is very difficult to establish the exact time of complete stabilization, since random events in the form of background fluctuations in the mains voltage constantly occur in the network. In order to conduct studies with higher accuracy, it is necessary to provide for the stabilization of the mains voltage and the placement of the LED in a chamber with a stable temperature independent of the heating of the LED. Thus, before conducting research tests of the LED light characteristics, the stabilization time ($t_{stab.}$) of the luminous flux equal to at least 60 minutes from the moment of switching on the LED should be taken into account, and the measurement of the initial value should be carried out no earlier than 2-5 seconds due to the inertia of the equipment used.

When measuring illumination from LED light sources with a luxmeter, the correctness of the spectral sensitivity curve should be checked.

It is obvious that in real operating conditions, both steady-state LED operating modes are possible, for which a formula can be used to determine the magnitude of the illumination decline in the form of:

$$\partial_{decrease} = \frac{E_{initial} - E_{final}}{E_{initial}} \cdot 100\%,$$

So are the operating modes with the presence of a certain number of LED lightbulb on and off cycles, then the formula for determining the magnitude of the decrease in illumination will look like:

$$\partial_{decrease} = \frac{\sum_{i=1}^{n} E_{i\_on.} - E_{i+1\_on\cdot}}{\sum E_{on.}} \cdot 100\%.$$

The error in determining the decrease in illumination can be determined by the formula:

$$\delta_{decrease} = \left(1 - \frac{\partial_E}{\partial_E + 1}\right) \cdot 100\%.$$

where ∂_E – the relative value of the decrease in illumination of the lamp, measured over time.

Using these expressions, it was found that the error in detecting a decrease in the illumination level by 5% of the nominal is 20%. With a decrease in the luminous flux of 10%, the error in determining the level of illumination decline decreases to 10% and only at its limit values can we talk about more accurate measurements.

Based on the developed methodology, research tests of low-power household LED lamps were carried out, for which operating temperatures and luminous flux radiation are critical parameters in the quality management of the production of products of this type. Studies were conducted on the level of illumination decline depending on the passage of the household LED lamp on and off cycles, as a result of which the light output of the lighting device deteriorated.

The results of the tests are the obtained light decay curves shown in Figure 2. The measurements were carried out according to the developed methodology and repeated for ten household LED lamps with a power of 8 watts of the same design, but from different manufacturers. [5, 6]

The model was tested by comparing the calculated and experimental dependences of the thermal resistance of the structure of the LED lighting device [3].

The experimental sample described in the previous section was used to measure the parameters of thermal models of the LED.

As a result of the work, the efficiency of heat dissipation in plastic cases of LED lamps was evaluated [7]. Based on this thermal model, one can judge the dependence of the maximum temperature at the places where the LEDs are mounted on the printed circuit board of the lamp on the thermal conductivity of the housing material or the radiator, if the latter is present.

Based on the data obtained, it can be concluded that the thermal conductivity of the housing elements of the lamp under study is insufficient and the required increase in the thermal conductivity of the housing materials.

Also, these results show that the main obstacle in ensuring the thermal regime of the LED lamp is the forced elongation of the structure, due to the need to mount the driver inside the LED. This is a determining factor in the choice of the shape of the case and its base, which leads to high thermal resistances between the far ends of the fins, imitating some kind of radiator (if any) and the place where the LEDs are mounted, as well as the place where the lamp is mounted in the base, where, due to the high According to statistics, accelerated aging of the insulation of the supply wires is observed.

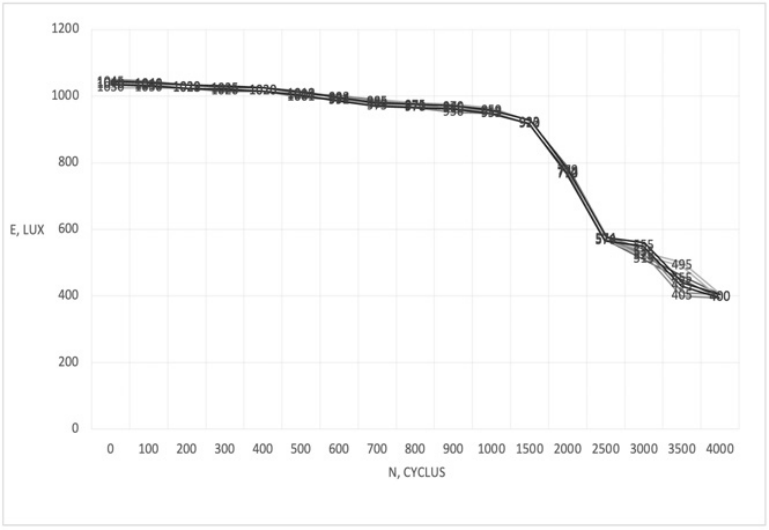

Fig. 2 *Experimentally obtained light change curves*

The most noticeable changes in illumination occurred after passing approximately 800-900 on/off cycles, in a specially selected "gentle" mode.

Conclusions

The current norms and requirements regarding natural, artificial and combined lighting of residential and public buildings are described in such standards as the code of construction and sanitary norms and rules,

and limit the pulsation of lighting devices at a pulsation frequency of up to 300 Hz. For example, in the playrooms of kindergartens, as well as classrooms, classrooms, classrooms of educational institutions, this indicator should not exceed 10%. The same standards apply to supermarket salesrooms, hairdressers, some industrial and medical premises.

The conducted research, the developed methodology and the experimental curves obtained will allow us to build a regression line for predicting the level of illumination decline depending on the number of cycles of switching on and off the LED lamp. However, it should be borne in mind that the value of the predicted illumination obtained using these coefficients should be adjusted for the magnitude of the standard error and measurement errors of equipment and laboratory conditions.

References

[1] Schubert, E. (2006). *Light-Emitting Diodes* (2nd ed.). Cambridge: Cambridge University Press. doi:10.1017/CBO9780511790546

[2] Vybor standartnogo rezhima raboty svetodiodnykh izluchateley / T.A. Barbasova, Ye.V. Vstavskaya, V.I. Konstantinov, V.O. Volkov // Vestnik YUUrGU. – 2010. – №2. – S. 48-51.

[3] Kuzmenko V.P., Solyoniy S.V., Shishlakov V.F., Kvas E.S., Solenaya O. Ya. Research tests of LED light sources / Izv. universities. Instrumentation. 2019.Vol. 62, No. 7, pp. 1-10.

[4] Lampy svetodiodnyye s tsokolem bez vstroyennogo ustroystva upravleniya. Chast' 2. Ekspluatatsionnyye trebovaniya. Razrabotka GOST R. Pryamoye primeneniye proyekta 34/A/1353/NP (2009-06) MEK 62663-2.

[5] Light sources are electric. Methods for measuring light and electrical parameters. (Instead of GOST 17616-82 on the territory of the Russian Federation).

[6] GOST R 8.749-2011 Gosudarstvennaya sistema obespecheniya yedinstva izmereniy (GSI). Svetodiody. Metody izmereniya fotometricheskikh kharakteristik.

[7] V. P. Kuzmenko, S. V. Solyonyj, A. V. Rabin, O. Ya. Solenaya, and A. V. Rysin (2020). Definition and approximation of the light flux degradation of a LED lamp. IOP Conference Series: Materials Science and Engineering. 734. 012197. 10.1088/1757-899X/734/1/012197.

INTELLIGENT MONITORING SYSTEM FOR SMART GRID BASED ON THE WIRELESS PASSIVE TEMPERATURE SENSORS

Nikita Miroshnichenko, Anastasia Raskopina, Mikhail Sinkin

Saint-Petersburg State University of Aerospace Instrumentation,
Saint-Petersburg, Russia
E-mail: Nikitos_mir.1997@mail.ru, raskopina.nastia@yandex.ru, aweekw@gmail.com

Abstract
The Smart Grid (SG) system is considered as near future of power networks because of fault identification and self-healing capabilities. Energy sustainability, renewable energy integration and an efficient control system are the key factors for developing process of the SG system [1]. Among various SG concepts, the term virtual power plant (VPP) integrates renewable energy to the grid and provides higher operational flexibility. Thus, the VPP requires extra capital costs for control systems and software. The operational activities of a smart grid largely depend on the active customer demands [2]. This paper defines various methods of intelligent monitoring systems for SG based on the wireless passive temperature sensors and presents their advantages over other systems.
Keywords: *Smart Grid, monitoring system, wireless passive sensors*

Introduction

There is an increasing demand for continuous asset monitoring in the evolving world-wide Smart Grid. One of the key factors is the contact temperature of critical electrical connections throughout the T&D infrastructure [3].

Common approaches of the HV contact temperature measurements have required IR thermal imaging or active wireless sensor systems with the power source inside. IR is a periodic asset monitoring method and is unable to alert the operator to a real time event. Wired and optical fiber methods fail to a short circuit, resulting in flash-over paths in medium voltage systems. Battery-powered active sensors require periodic maintenance especially in the medium voltage cabinets [4].

The more promising way to control temperature is an approach that offers using wireless sensors which are installed at the HV and MV connections inside cabinet (for this paper term passive means batteryless) with the further integration to user's SCADA systems [5].

The temperature monitoring of tools, industrial equipment and other mechanical parts faces some different challenges. Such issues might be resolved by using systems with a real-time wireless remote control [6]. Common methods of temperature measuring based on the Temperature dependence of resistance (thermistors or Resistance Temperature Detectors - RTDs), a variety of different types of thermometers, the temperature dependence of a diode junction (silicon), or the emission of infrared radiation from heated objects (IR thermometers). For the applications considered herein, passive devices, e.g. thermocouples, RTD and quartz thermometers, for example, have historically required cabled connections, slip-ring contacts, rotating connections, or battery-powered transmitters to communicate information [7-9].

Similarly, measuring the temperature of contacts and connections in high voltage switchboxes and transmission lines presents challenges. A standard requirement for these structures is that there be no metallic or fiber optic cabling from the contact or connection of interest to the supporting structure or frame, as this can cause a dangerous and potentially explosive path to ground.

Infrared thermometry is sometimes employed, but this requires direct line of sight to the area of interest, which should be clean for the best accuracy. IR is usually used for spot checking on a periodic basis and therefore not continuous monitoring. Typically, the infrared measurement systems used for this type of monitoring are cost prohibitive. Battery-powered temperature transmitting systems have drawbacks related to typical physical size and the need for oftentimes rather inconvenient periodic replacement of the battery. In general, batteries are not well suited for high temperature operation, especially above 150 ˚C.

In these types of applications, passive wireless temperature sensing technology offers distinct advantages over these traditional measurement methods [10-13].

The problem of overheating of electrical equipment can be solved by installing monitoring systems. There are 3 types of monitoring systems:

1. Thermosensor system for continuous monitoring of temperature contact connections;
2. Pyrometric system for continuous monitoring of tire temperature;

3. Radio channel temperature control systems [14].

Thermosensor system for continuous monitoring of temperature contact connections - the system consists of gas-generating stickers, a gas sensor and a control and receiving device. Stickers are placed on contacts. When heated, the stickers change color and emit a signal gas marker, which is fixed by the sensor [15].

Pyrometric system for continuous tire temperature monitoring is an embedded system for measuring tire temperature in a non-contact way. With the help of a pyrometric system, the power of thermal radiation is measured, after which the data obtained is processed and output to the visualization system [16].

Wireless temperature control systems. The most promising systems for temperature control of high-voltage equipment, it is advisable to consider temperature control systems based on passive acousto-electronic sensors on surface acoustic waves (surfactants) with the function of radio frequency identification. Passive sensors used in such systems have increased resistance to electromagnetic interference, have high stability of characteristics. The average service life of such sensors is up to 20 years [17].

USING WIRELESS MONITORING SYSTEMS BASED ON THE PASSIVE SENSORS

In recent days, the application of Phasor Measuring Units (PMUs) and Wireless Sensor Networks (WSN) for monitoring electrical grid parameters has been observed as a developing area. For making the operation of the grid smarter and smoother, a sensing device that observes the functioning of PMU and intimates it to the Online Monitoring System (OMS) is essential. Therefore, this way of smart integration paves the way for preventing critical grid situations such as excessive loss of power consumption. Even though the global positioning system (GPS) receiver is present, it can only track the position of PMUs. In addition, all the measurements which are provided by the PMU will be transferred to the satellite and then to the control center. While transferring the parametric data, the occurrence of a fault may be present, and there is no way to detect faults such as wrong measurement data with temperature. Moreover, the errors in measurement can only be controlled after detecting the type of problem that persists in PMU. This requires the help of a large amount of manpower, and immediate remedial actions cannot be taken. As a result, there might be a huge loss of energy where more blackouts can occur within a short period of time.

Therefore, the communicating PMU device requires a wireless device for supervision which will be able to detect the faults quickly and report them to the control center. In a modern trend, wireless sensors which can sense the fault data in PMUs with less energy consumption can be integrated with PMUs for better control operations [18-20]. The block diagram of the proposed method is indicated in Figure 1.

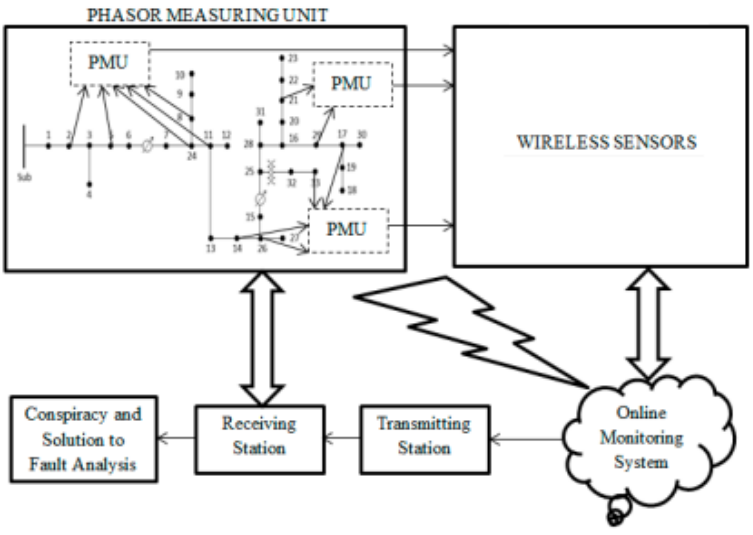

Figure 1 - Incorporation of sensors with Phasor Measuring Units (PMU) for fault detection

Passive acousto-electronic sensors based on surface acoustic waves (surfactants) will be used as wireless sensors.

The SenGenuity wireless SAW resonator (SAWR) based temperature sensing solution consists of a reader (RF Transceiver) RF or capacitively linked to one or more SAWR sensing elements as depicted in Figure 2.

The system operates in a range from 428 MHz to 439 MHz and allocates six distinct, 1.4 MHz wide, sub-channels to six distinct SAWR modules [21].

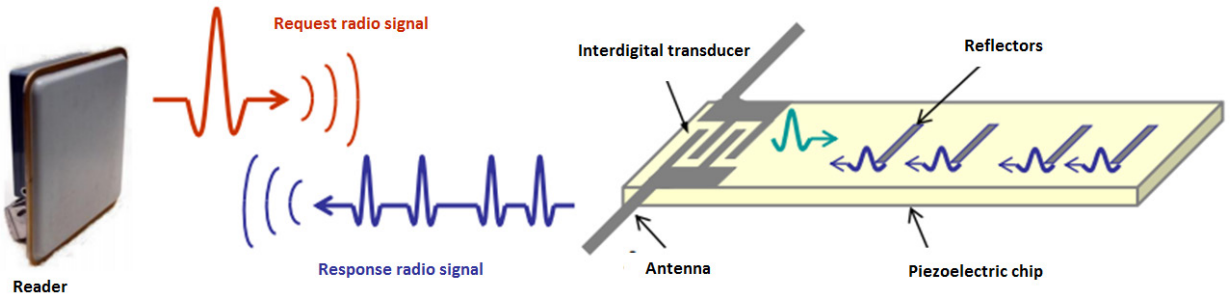

Figure 2 - Wireless SAW Temperature Sensing System [22]

SAW-based temperature sensing involves electrically inducing an acoustic wave into a piezoelectric material and then reconverting the energy of the wave (influenced by the temperature to which the sensing element is exposed) back into an electrical signal for temperature measurement. One significant advantage of SAW devices is their passive operation, which makes them very amenable to operation in harsh environments via wireless interrogation [22].

Conclusion

Thus, this system can ensure the safe operation of electrical equipment. Significant advantages of the system will be: high noise immunity, resistance to electromagnetic interference, long range of reading over the radio channel, durability (immutability of characteristics during operation), the system does not require maintenance. All of the above advantages make radio channel monitoring systems suitable for their use in troubleshooting Smart Grid systems.

References

1. Sorokin, A.V. Method of identification of passive radio frequency identification tags in conditions of high probability of collision / A.V. Sorokin, A.P. Shepeta, Yu.F. Podoplekin // Marine Radio Electronics No. 1 (59) March 2017, p. 34.
2. Sorokin, A.V. Anti-collision passive radio frequency tag with time-frequency information signs / A.V. Sorokin, A.P. Shepeta, Yu.F. Podoplekin // Marine Radio Electronics No. 1 (59) March 2016, p. 41.
3. Sorokin, A.V.. The main approaches used in coding passive radio frequency tags on surfactants / A.V. Sorokin, A.P. Shepeta, Yu.F. Podoplekin // Marine Radio Electronics No. 4 (62) December 2017, pp. 34-45
4. Sorokin, A.V. Passive acousto-electronic radio frequency temperature sensors for monitoring electric power facilities / A.V. Sorokin, A.P. Shepeta, Yu.F. Podoplekin // Marine Radio Electronics No. 3(61), 2017, pp. 12-18
5. Sorokin, A.V. Increasing the accuracy of positioning of railway transport based on RFID surfactants/ A.V. Sorokin //Radio Electronics Issues, General Technical Series (OT) No. 2, 2015, pp. 187-197
6. Sorokin, A.V. Application of acousto-electronic sensors on surfactants in industrial Internet of Things systems for monitoring the state of technogenic objects/A.V. Sorokin, V.V. Leontiev, V.A. Nenashev, G.M. Vattimena//Modern science: actual problems of theory and practice. Series: Natural and Technical Sciences. 2019. No. 11-2. pp. 61-66.
7. Sorokin, A.V. Passive anti-collision radio frequency identification tag on surface acoustic waves with time-frequency difference/ A.V. Sorokin, A.P. Shepeta, Yu.G Smirnov. Patent for invention No. 2616342, published: 14.04.2017, Byul. No. 11
8. Sorokin, A.V. Method of anti-collision radio frequency identification on surface acoustic waves and a system for its implementation" / A.V. Sorokin, A.P. Shepeta, Yu.G. Smirnov / Patent for invention No. 2634308. Published: 25.10.2017, Byul. No. 30
9. Sorokin, A.V. Passive anti-collision radio frequency identification tag on surface acoustic waves with a time-frequency difference"/A.V. Sorokin, A.P. Shepeta, Yu.G. Smirnov // Patent for utility model No. 160481, published: 20.03.2016, Issue No. 8.

10. Sorokin, A.V. Passive anti-collision temperature sensor on surface acoustic waves with a time-frequency code difference" / A.V. Sorokin, A.P. Shepeta, G. B. Vattimena // Patent for utility model No. 179933, published: 05/29/2018, Issue No. 16.

11. Sorokin, A.V. Passive anti-collision temperature sensor on surface acoustic waves with a time-frequency code difference"/ A.V. Sorokin, A.P. Shepeta, G. B. Vattimena // Patent for utility model No. 2665496, Published: 30.08.2018 Byul. No. 25

12. Sorokin, A.V. Anticollision processing of signals from passive radio frequency identification tags on surface acoustic waves"/A.V. Sorokin, A.P. Shepeta // State registration of a computer program //Certificate No. 2017619221, published on 08/16/2017.

13. Sorokin, A. V. Anti-collision radio-frequency identification system using passive SAW tags /A.V. Sorokin, A. P. Shepeta //Smart Sensors, Actuators, and MEMS VIII. – 2017. – T. 10246. – C. 1024613.

14. Sorokin, A.V. Wireless SAW passive tag temperature measurement in the collision case / A.V. Sorokin, A.P. Shepeta, M.G. Wattimena //Journal of Physics: Conference Series. – IOP Publishing, 2018. – T. 1008. – №. 1. – C. 012015.

15. Sorokin, A.V. Encoding of Passive Anticollision Radio Frequency Identification Surface Acoustic Waves Tags / A.V. Sorokin, A.P. Shepeta, M. G. Wattimena //Proceeding of the Electrical Engineering Computer Science and Informatics. – 2017. – T. 4. – C. 605-609.

16. Sorokin, A. V. Comparative characteristics of anti-collision processing of radio signal from identification tags on surface acoustic waves / A.V. Sorokin , A. P. Shepeta, V. A. Nenashev, G. M. Wattimena //Информационно-управляющие системы, 2019, No 1,с. 48–56. doi:10.31799/1684-8853-2019-1-48-56

17. Sorokin, A. V. Time-Frequency Approach to Anti-Collision Signal Processing for RFID SAW Tags/ A. V. Sorokin, D. A. Shepeta/ *2019 Wave Electronics and its Application in Information and Telecommunication Systems (WECONF)*, Saint-Petersburg, Russia, 2019, pp. 1-4.doi: 10.1109/WECONF.2019.8840631

18. Sorokin, A. V. Signal Detection of SAW RFID Tags under the Impact of Strong Industrial Noise/ A. V. Sorokin, A. P. Shepeta/*2020 Wave Electronics and its Application in Information and Telecommunication Systems (WECONF)*, Saint-Petersburg, Russia, 2020, pp. 1-6.doi: 10.1109/WECONF48837.2020.9131462

19. Sorokin, A.V. Identification of Orthogonal frequency coded SAW RFID tags in collision case/ A. V. Sorokin //Bulletin of the UNESCO department «Distance education in engineering» of the SUAI: Collection of the papers. St. Petersburg, Issue 1. -SPb.:SUAI, 2016. -p.77 ISBN 978-5-8088-1099-0

20. Sorokin, A.V. Possible solutions to the problem of collision of labels on surface acoustic waves/ A.V. Sorokin // Materials of the Third All-Russian Scientific and practical Conference "Solution - 2014", Perm. National. research. Polytech. Un-t, 2014, p. 169, ISBN 978-5-398-01301-6

21. Sorokin, A.V. Modeling of identification system SAW tags/ A. V. Sorokin// Modern information society formation – problems, perspectives, innovation approaches, XV international forum 1-5 June,2014 p. 63-66., SUAI, 2014, ISBN 978-5-8088-0906-2

22. Sorokin, A.V. Optimization of passive identification acousto-electronic tags for industrial control systems for the movement of parts/A.V. Sorokin // Higher School: scientific research. Materials of the Inter-university Scientific Congress (Moscow, September 14, 2019). - Moscow: Infiniti Publishing House, 2019, p. 177, ISBN 978-5-905695-56-8

CAR PARKING: A SMART WAY TO SIMPLIFY PARKINGS

Moreno Gabriele Libro, Emanuele Irti

Computer Engineering and Networks Laboratory – Kore University of Enna - Italy
morenogabriele.libro@unikorestudent.it
emanuele.irti@unikorestudent.it

Abstract
The following project aims to simulate the automatic management of an underground car park, located below a public square, containing a total of twenty cars. During the Simulink simulation, it was possible to observe how the system allocates and frees resources, indicated through displays, positioned at the entrance of the structure, the number of available parks and other useful information. In addition to the management of incoming and outgoing movements from the aforementioned car park, two sensors were placed inside the basement, used to detect air quality and temperature, to simulate the operation of the ventilation system controller.

Introduction

Making an everyday part of a driver's life automatic is an ambitious challenge. Some of the solutions on the market include, for example, different types of parking fully or partly automated.
A first type of fully automated car parks are the layered depots where the user is not expected to perform any manoeuvre except placing the vehicle on a treadmill controlled by the system, which, once verified the presence of a possible free place inside the structure, assigns and transports the vehicle to the free slot available at that time.

A second solution is obtained by leaving the user the freedom to drive by simply indicating the number of parking spaces available inside, thus avoiding wasting any time looking for a non-available parking spot. The Car Parking project aims to simulate the management of a partially automated car park using Matlab and Simulink. It was possible to realize the control system with wired networks for the parking system and wireless for ventilation control.

RELATED WORKS

Smart car parks appeared several years ago, in fact the first appearance of the concept of an automated car park took place in Paris, at the Garage Rue du Ponthieu in 1905 [1]; this system, however, required workers to sort the cars, placed inside an elevator, into the respective parking lots. Nowadays there are different methods to make an automated parking, for example, in 2018 an automated parking system was developed supported by the use of a network of cameras [2]. Smart car parks have benefits in various respects, allowing a smoother traffic flow and reducing driver's stress [3].

THE PROPOSED APPROACH

This proposal uses a wired network with CSMA/CD technology and a wireless network based on IEEE 802.15.4 (Zigbee). Makes use of five wired nodes and three wireless nodes, a gateway is connected to both networks.

The first wired node, called "Main Gateway", is the node in common between the two networks. It plays a retransmission role for the first Ethernet network. It receives data from the nodes connected to the bollards, namely [1:2] and [1:3], indicating the possible entry or exit of vehicles from the parking lot, which it forwards to the Manager Display Node [1:4] and Parking Manager Node [1:5].

For the second network, the Main Gateway node receives temperature and air quality index data from the nodes connected to the respective sensors, AQI Sensor Node [2:2] and Temperature Sensor Node [2:3]. It also performs the role of actuator, sending the previously mentioned data to a Fuzzy controller that manages the power level of the ventilation system.

The second and third wired node, named "Entry Bollard Node" and "Exit Bollard Node" have the task of sending any transits made in the parking to the node Main Gateway.

The fourth wired node, called "Display Manager Node", receives from the Main Gateway the transit signals of the vehicles, updating the displays located at the entrance of the parking lot. Outside it's possible to

see the number of places available, divided into classic parking lots and parking spaces for people with disabilities; it is also possible to look how many vehicles have made a stop and how many have left the parking lot.

Speaking of the fifth and last wired node, "Parking Manager Node", it receives data from the Main Gateway node regarding the entry and exit of vehicles from the parking, thus sequentially associating the entry of a vehicle to the first parking available; the entry and the consequent liberation of a parking lot will be randomly generated.

The two wireless nodes, "AQI Sensor Node" and "Temperature Sensor Node", will play the role of data transmission to the Main Gateway node, sending samples every 60 seconds. For temperature detection was chosen the "Alta" sensor produced by the company "Monnit Corporation", powered by a rechargeable 1500 mAh lithium battery. To take samples of air quality it has been chosen the "PM2.5" produced by "Nova Fitness Co.", connected to a microcontroller with module WiFi "ESP8266EX" by "Espressif Systems", both powered with a 21900 mAh battery pack consisting of three 7300 mAh rechargeable lithium batteries.

Down below are indicated all the consumption data related to the sensors:

"Alta" Wireless Temperature Sensor

- Battery: 1500 mAh rechargeable
- Power Consumption: 5.5 mA (*RX Mode Radio*), 0.57 mA (*MCU Idle*)
- Estimated autonomy: 272.72 Hours (*Radio RX Mode*)
- Consumption per second: 0.0015 mA (*Radio RX Mode*), 0.0001 mA (*MCU Idle*)
- Consumption per minute: 0.0900 mA (*Radio RX Mode*), 0.0060 mA (*MCU Idle*)

AQI sensor "PM2.5" with Wireless Microcontroller "ESP8266EX"

- Battery: 3x 7300 mAh rechargeable
- Consumption: 240 mA (70 mA + 170 mA) [*Active*], 18 mA (3 mA + 15 mA) [*Sleep*]
- Estimated autonomy: 91.15 Hours (*Radio RX Mode*)
- Consumption per second: 0.0015 mA (*Radio RX Mode*), 0.0001 mA (*MCU Idle*)
- Consumption per minute: 0.0900 mA (*Radio RX Mode*), 0.0060 mA (*MCU Idle*)

SCENARIO

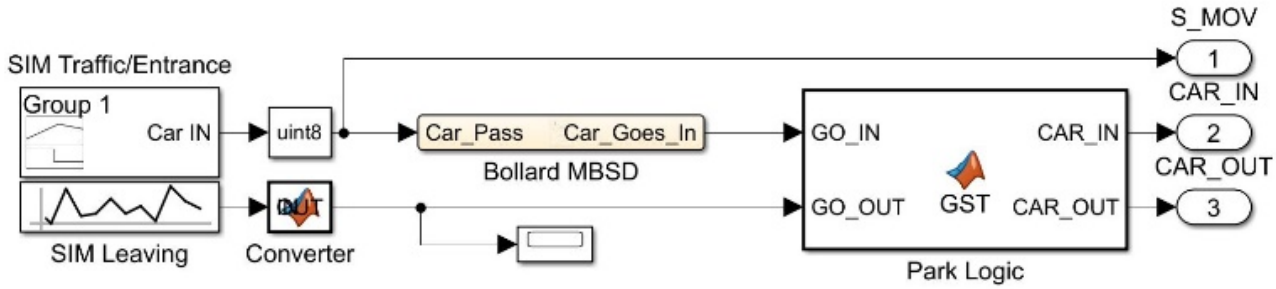

Figure 1: "Tollbooth" subsystem.

PARKING MANAGEMENT

The signal builder block "SIM Traffic/Entrance" contains a random generated signal, representing the data detected by a motion sensor. Through the MBSD scheme, when a signal persists for more than 3 seconds the request of access is made to the Matlab Function "Park Logic"; if there are parking spaces available, then the car will enter and occupy a slot (the possibility of a driver with a disability is obtained within Park Logic).

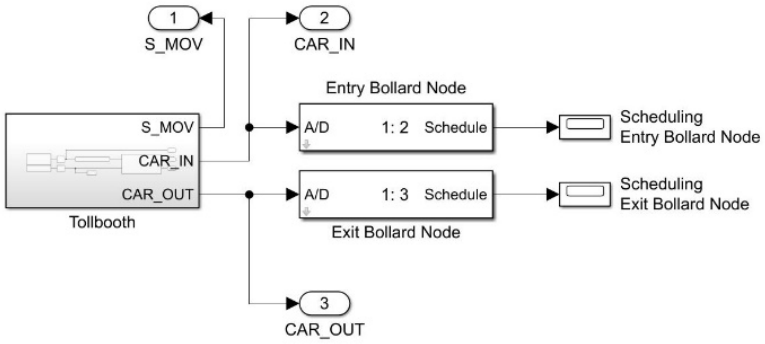

Figure 2: "Bollard and Tollbooth" subsystem.

The Random Uniform Number block "SIM Leaving", with the Matlab Function "Converter" will carry out the random generation of a vehicle leaving the parking lot. In detail, the function "CNV" contained in the Converter, will check if the value received in input from SIM Leaving is greater or less than 0.5 every 40 seconds, if it is greater, it will make a leaving request to Park Logic. If there are no parking spaces to empty, the request is ignored by the system. The variable "signal_to_go" indicates the temporal instant of the simulation, it is incremented by 1 every round.

Therefore, every 40 seconds there is a 50% chance of emptying a parking space. By changing the value for which signal_to_go is divided, the sample time for the chance of vehicles to leave will be increased or reduced.

When a vehicle is accepted by the system, whether it is entering or leaving, a signal is sent to the corresponding bollard. This signal through the nodes "Entry Bollard Node" and "Exit Bollard Node" will be forwarded to the Main Gateway. Data sent from nodes [1:2] and [1:3] reaches the Main Gateway, which redirects them to the "Parking Manager Node" and "Display Manager Node". The first node communicates directly with parking resources, filling them sequentially. The Matlab Function named "Car Parks Updater" empties parking spaces, using calculations with random values to make the simulation as true to reality as possible.

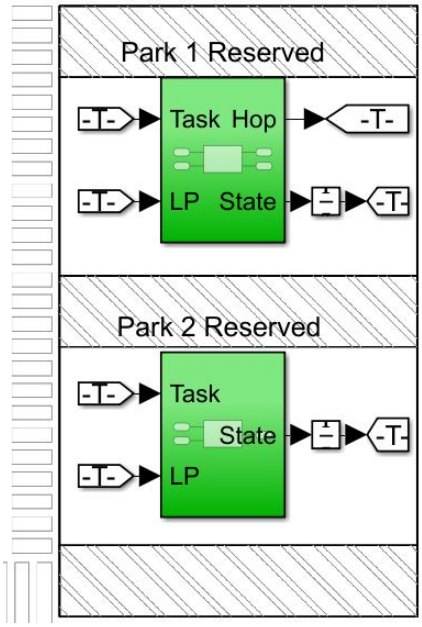

Figure 3: "Park" subsystem.

Parking spaces are subsystems that have two inputs and two outputs. The input "Task" defines the task of filling the parking lots.

If it is 0 there is no incoming car, otherwise if it is 1 the system is checking the possibility of resource allocation. If Task's value is 1, the status of the parking lot is checked: if it is free then it will

change to busy, vice versa, it will send through the output "Hop" the value 1. This output is directly linked to the input "Task" of the next parking lot. It keeps working like this until the first free slot is found.

The output "State" indicates the current state of the parking space and is connected to the Matlab Function "Car Parks Updater", which is used to empty the parking spaces.

The input "LP" instead, receives from Car Parks Updater any request for release of the parking.

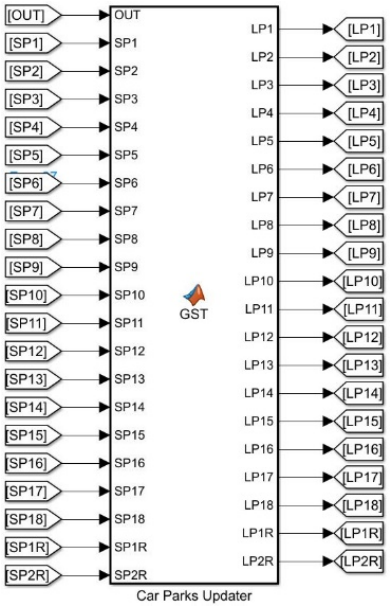

Figure 4: "Car Parks Updater" Matlab Function.

The Matlab Function "Parking Update Manager" receives as inputs "SP*" the values related to the real-time status of parking spaces. "OUT" on the other hand send the request to release a car, sent by Parking Manager Node. After randomly selecting the parking to be emptied, Car Parks Updater sends out in the respective output "LP*" the request to release, which is received in the selected parking lot's input "LP".

If "OUT" is 1, the leaving request is related to a classic car park, if it is "1.5", it is necessary to release a parking lot for disabled people.

The parking to be freed is randomly chosen within the following block: assuming the release of a classic parking lot, an 18 slots array will be generated, containing unique values in an interval between 1 and 18. The number contained in the first position of the array is checked, it will represent the parking to be analysed. If the relevant parking space is busy, it will be emptied; if it is already empty, the next position of the array will be checked until the first busy parking space is found.

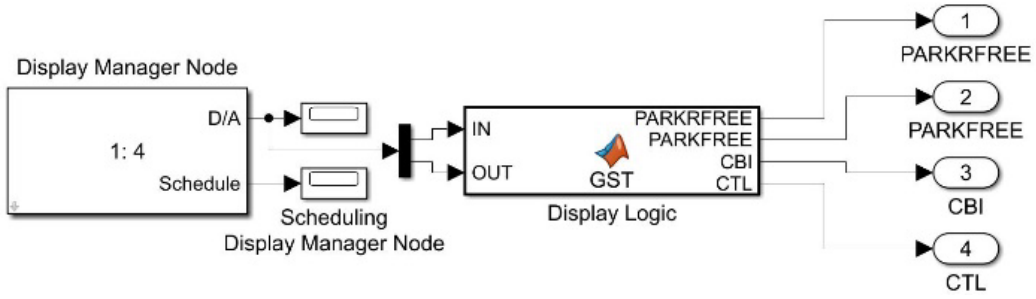

Figure 5: "Display" Subsystem

The second node, using a Matlab Function named "Display Logic", updates the values shown at the parking entrance displays.

VENTILATION MANAGEMENT

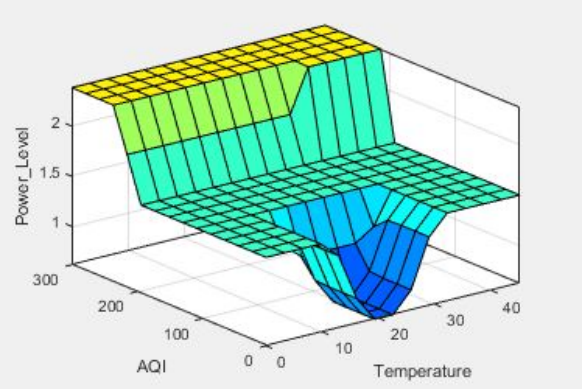

Figure 6: Fuzzy logic surface.

Both nodes Temperature Sensor Node and AQI Sensor Node receive incoming values obtained by the sensors, every 60 seconds the obtained samples are sent to the Main Gateway. The data is received by the Main Gateway, the actuator forwards them to the Fuzzy controller to determine the relative power level of the ventilation system.

PERFORMANCE EVALUATION

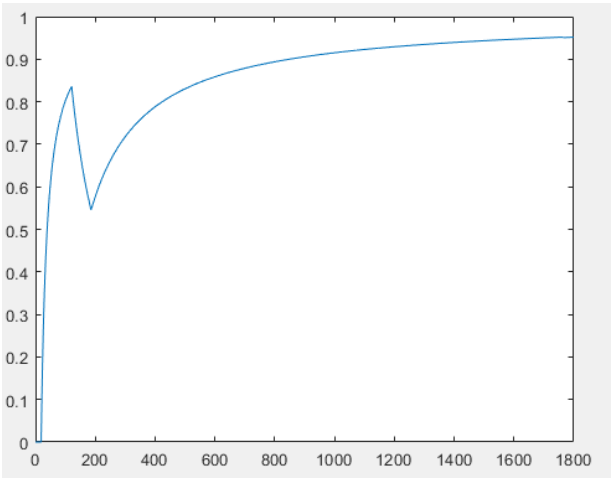

Figure 7: Park 1 usage time plotted.

All the data is obtained from a test simulation lasting 1800 seconds.

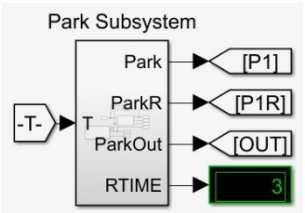

Figure 8: response time displayed.

The first performance metric represents the usage time of a specific resource, in this case it's about the total usage of the first park subsystem, "Park 1". It represents the ratio between the park busy time and the total simulation time.

Response time is the second performance metric, calculated as the time between the passing of a car through the entry bollard and the allocation of parking in the system.

Conclusions

The design of the parking management system involves several aspects and needs. First of all, it is necessary to assess how many parking spaces must be accommodated and, how many of these, are intended for special categories, such as, for example, parking spaces for disabled people, parking spaces reserved for emergency vehicles or, again, for taxis. Having considered only two types of parking (classic and disabled parking), the code developed and the devices used can manage the simulated data, allowing to display the available parking spaces within the structure, divided according to the two categories. The project, while being theoretical and verified on twenty parking spaces in Simulink, is also applicable to real situations, whether they are similar or larger and different.

References

[**1**] Shannon Sanders McDonald, The Parking Garage as the Undocumented Search for Modernism. Available: https://www.acsa-arch.org/proceedings/International%20Proceedings/ACSA.Intl.2005/ACSA.Intl.2005.49.pdf (2005).

[**2**] K. Hammoudi, et al.: Towards a Model of Car Parking Assistance System Using Camera Networks: Slot Analysis and Communication Management. IEEE International Conference on Smart City. Available: 10.1109/hpcc/smartcity/dss.2018.00210 (2018).

[**3**] Kalašová, A.; Culík, K.; ˇ Poliak, M.; Otahálová, Z. Smart Parking Applications and Its Efficiency. Sustainability 2021, 13, 6031. Available: https://doi.org/10.3390/su13116031 (2021).

IMAGE COMPRESSION METHOD IN SPATIALLY DISTRIBUTED SYSTEM OF INTENSIVE INFORMATION EXCHANGE

Sergey Nenashev, Konstantin Ryzhov

St. Petersburg State University of Aerospace Instrumentation,
Saint-Petersburg, Russia.
E-mail: nenashev_sergey178@mail.ru konstantin.r02.27@gmail.com

Annotation
Currently, the tasks of developing and improving new ways of representing, compressing, storing and noise-correcting coding of high-resolution images with a common mathematical basis are relevant. Most of the information transformation procedures are based on the use of bases, in particular, orthogonal and quasi-orthogonal matrices. The results of the application of such bases are presented and methods for the synthesis of quasi-orthoanal matrices for image compression problems that meet the formulated modern requirements are presented.
Keywords: image compression, complex processing systems, digital visual information, orthogonal bases, quasi-orthogonal matrices, error-correcting data coding.

INTRODUCTION

Today, in the field of digital visual information processing (DVI) algorithms, the use of a matrix apparatus and orthogonal transformations is of great interest. This applies mainly to symmetric algorithms based on the use of orthogonal or quasi-orthogonal matrices, for example, in compression/decompression of images, or error-correcting coding/decoding in data transmission over wireless channels of distributed systems, etc.

On the one hand, the size of the DVI is constantly growing - this is, firstly, the satisfaction of the consumer in the desire to have more formed personnel, and, secondly, the constant progress in the technology of manufacturers of video matrices and monitoring devices, for example, televisions.

Of particular interest are high-resolution images used in monitoring the earth's surface, in particular, in the search for minerals, in mountainous areas, agriculture, in agricultural areas, in search and rescue operations carried out from a group of small aircraft (SA), combined into a single network [1]. Due to the significantly lower cost of creating and operating SA with equal efficiency of the tasks performed compared to controlled SA, the production of SA has recently become a widespread and economically viable direction. Low cost, availability and ease of use have led to the emergence of a huge number of MAVs operated by civilian users in certain industries and services [2].

In spatially distributed airborne complexes and between individual SA, an intensive exchange of images, for example, thermal imaging images, is carried out. In this case, before data is transmitted to the channel, the input image is converted into a noise-like form. Then the converted image is broadcast over the air, during this period of time it is required that the amount of transmitted data be minimal. On the receiving side, in turn, when receiving the transformed image, decompression (calculation of the inverse transformation) is performed, which consists of DCT transformation with threshold quantization, “zigzag scanning”, as well as a group coding method. The ongoing restoration of the image is converted to its original form. In this case, the transmitted data must be protected from unauthorized access, for which it is necessary to allocate additional computing resources for cryptographic methods, especially in real-time systems [3].

Due to the fact that the quality of recorded information is of fundamental importance in SA, the issue of choosing the most appropriate compression method for thermal imaging images requires separate consideration. The developed method of image compression should not only solve the problem of long-term recording in a limited amount of memory, but also provide the necessary compression ratio and the minimum level of transmission losses, as well as take into account the specifics and features of working with thermal imagers, separately.

Thus, at present, there is a growing need to develop specialized algorithms for the representation, compression, and error-correcting coding of DVI in a spatially distributed complex for monitoring the earth's surface.

DISTRIBUTED SYSTEM FOR PROCESSING AND INTEGRATING INFORMATION

Development of a wireless high-performance network, the subscribers of which are SA and a ground station, capable of transmitting, processing and integrating the following types of information: high-resolution thermal imaging images, images obtained from optical location systems (video frames), navigation information, etc. At the same time, such systems require that the specified information be compressed, during its transmission within the considered distributed system.

The indicated processes of processing and transmission of information are planned to be carried out on the basis of the application of a new theory of quasi-orthogonal matrices. In general, the formation of a new extended basis of quasi-orthogonal matrices that differ from those used today, which can lead to significant development, improvement and, possibly, revision of the theory of DVI processing.

To solve the problems of surveying vast territories, searching for objects of interest, in environmental monitoring, in search and rescue operations, and in monitoring hard-to-reach places, SA or their group are used [4]. But the main criterion for guaranteeing the fulfillment of the task is the implementation of the real-time mode, which requires high-speed computing resources and fast algorithms for processing information received and transmitted within the system. In addition, in such systems, it is required to provide a reliable noise-resistant wireless channel for transmitting information between several users under the conditions of possible destructive influences [5-6].

To implement the exchange in such spatially distributed systems, it is first necessary to determine the type of information collected from location devices based on board the SA: as a rule, these are high-resolution images obtained from optical location systems taken in the visible or infrared range, thermal imaging images, etc. So basically it's a DVI, which is a matrix structure or a set of matrix structures.

The control center and complex processing of a distributed system of SA from several sides receives images of the observed territories from different angles, which makes it possible in the future, with the complex processing of these images of various nature, to solve the problems of mapping and classifying zones and objects on them with the required accuracy and reliability [7] . Figure 1 schematically shows a distributed system for processing and integrating information, where the subscribers of the distributed system are SA and the control and complex processing center of the DVI.

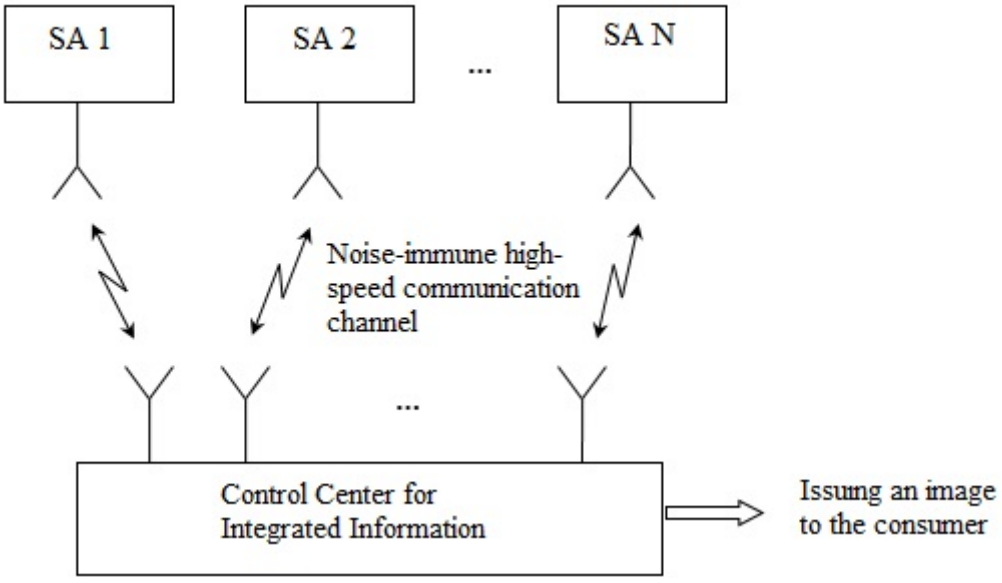

Figure 1 – Distributed system for processing and integrating information

However, this requires the simultaneous implementation of specialized compression algorithms and error-correcting image coding for their intensive exchange in a high-speed distributed system, which is formed by SA, as well as a control center for complex information processing.

WAYS TO COMPRESS THERMAL IMAGES

It is worth noting several features about the thermal imaging method of compression. Images obtained from a thermal imager contain a large amount of redundant information. This leads to a decrease in the speed

of processing and data transfer. Therefore, the task is to consider a lossless image compression method, namely, to find ways to implement efficient data conversion and subsequent decompression of data received from onboard monitoring systems. There are many ways to compress thermal images: processing in the spatial domain, using a covariance matrix, contour coding, wavelet compression, and so on. [8]. Also known are compression methods based on the use of orthogonal matrices using discrete cosine transform (DCT). Let's consider the latter in more detail.

IMPLEMENTATION OF THE COMPRESSION PROCESS

One of the ways to solve the problem of high-quality image processing with high resolution is the creation and use of new and modified compression methods, new noise-correcting coding algorithms based on the use of orthogonal and quasi-orthogonal matrices of various sizes. At the same time, in order to fulfill the requirements for the quality of the transmitted image on the one hand, as well as to implement high-speed exchange on the other hand, it is proposed to evaluate the compressed image with quality metrics on board the SA before transmitting it.

Of particular interest for individual problems of image processing [9-11] are the symmetrical constructions of the Hadamard-Walsh matrices obtained from the classical Hadamard matrices by ordering the columns by frequency (according to the number of sign changes of their elements). It is known that the lossy compression procedure, as the most promising, allows obtaining high compression ratios compared to lossless compression. At the same time, using lossy compression, it is possible to achieve a compromise between the requirements for image quality and the degree of compression, which makes it possible to develop a compression algorithm for a specific application.

In the course of experimental studies, the possibility of replacing the DCT in the JPEG algorithm in the chain of transformations with an orthogonal transformation with special matrices was considered. However, in contrast to the use of two-level symmetric Mersenne matrices, it is proposed to use four-level matrices, in the search for which, according to the formulas given in [7], the coefficients are not fixed, a = 1.

In the experiments carried out in the work, it is these four-level quasi-orthogonal Walsh-sorted Mersenne matrices, namely, the symmetric four-level Mersenne-Walsh matrices [4, 7], that performed better.

Figure 2 shows a color portrait of such matrices of order 7, 15, and 31. Obviously, when it is used in image transformation, unlike DCT, low frequencies are in the lower right corner [12].

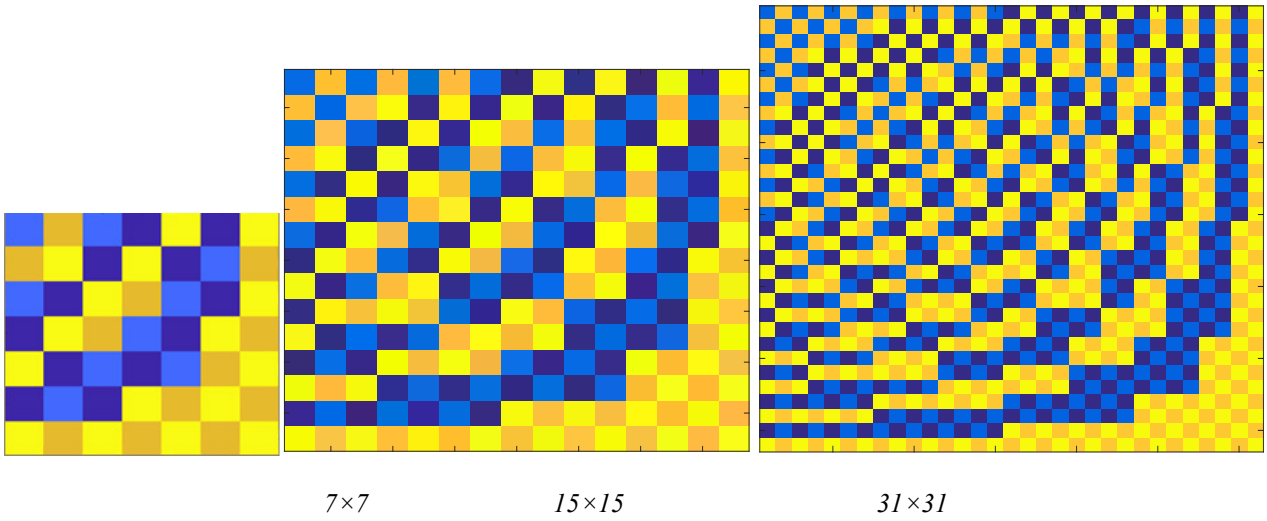

Figure 2 – Portraits of four-level Mersen-Walsh matrices

For the equivalence of experiments on image compression with DCT and Mersenne-Walsh matrices, the same compression ratios were set, the value of which is related to the quantization threshold. The test image generated by the equipment of thermal imaging systems on board the SA is shown in Figure 3.

As an example, Figure 4 shows the reconstructed image after compression for the cases of transformation with DCT (dimensions 8x8, 16x16, 32x32) and with the Mersenne-Walsh matrices shown in Figure 2, respectively.

Figure 3 – Test image generated by the equipment of thermal imaging systems on board SA

	DCT		Mersenne-Walsh
8x8		7x7	
16x16		15x15	
32x32		31x31	

Figure 4 – Restored images obtained by the decoded method, on the left using the JPEG method, and on the right using the Mersenne-Walsh matrix.

After converting an 8x8 matrix consisting of 64 elements into a vector using the zigzag scanning method, we apply the run-length encoding (RLE) technique [13-14], after which we calculate the compression ratio in Table 1.

Having calculated the number of transmitted bits, it also calculates how many times this algorithm has compressed. And then the compressed images are compared by the JPEG and Mersen-Walsh algorithm.

Table 1

Image compression ratio

	JPEG		Mersen-Walsh	
	Before compression, bit	After compression, bit	Before compression, bit	After compression, bit
1. Thermal image of the earth's surface	11 627 304	4 870 632	11 627 304	6 396 936

Comparison of the original image formed in the process of SA monitoring and the image obtained in the process of modeling the compression algorithm shows that when compressed by 1.8 times in the case of using Mersen-Walsh matrices, the reconstructed image is more consistent with the quality of the original. And in the case of JPEG only 1.5 times.

Table 2

Image quality metrics (restored) after compression

Orthogonal/ quasi-orthogonal transformation	Calculated Metric Values	
	PSNR – method	SSIM – method
DCT 8×8	38.1516	52.8571
MMW 7×7	41.5741	55.5135

Also, to compare the original image and the reconstructed image, the image quality metrics [15-16] are calculated in Table 2.

Conclusions

The results of experimental studies have confirmed the possibility of implementing a high-resolution image compression algorithm for a distributed system consisting of SA. Based on the results of the experiments, recommendations were formulated for adjusting the software for processing large-volume matrix structures in real time. The developed set of algorithms is applicable for the implementation of on-board algorithms for high-speed exchange. The results of the work are easily adapted for testing compression algorithms, encoding generated images recorded in real tests of a different type.

Bibliographic List

1. M. G. Wattimena, V. A. Nenashev, A. A. Sentsov and A. P. Shepeta, "On-Board Unlimited Aircraft Complex of Environmental Monitoring," 2018 Wave Electronics and its Application in Information and Telecommunication Systems (WECONF), 2018, pp. 1-5, doi: 10.1109/WECONF.2018.8604382.

2. A. A. Sentsov, V. B. Polyakov and N. A. Gladkii, "Electronic Methods to Protect Unmanned Aerial Vehicles from Seizing Control," 2018 Wave Electronics and its Application in Information and Telecommunication Systems (WECONF), 2018, pp. 1-4, doi: 10.1109/WECONF.2018.8604463.

3. Konakhovich G.F., Puzyrenko A.Yu. Computer steganography. Theory and practice. -M.: MK-Press, 2006. - 288 p.

4. V. A. Nenashev, A. A. Sentsov and A. P. Shepeta, "Formation of Radar Image the Earth's Surface in the Front Zone Review Two-Position Systems Airborne Radar," 2019 Wave Electronics and its Application

in Information and Telecommunication Systems (WECONF), 2019, pp. 1-5, doi: 10.1109/WECONF.2019.8840641.

5. Ryabinin Yury Evgenievich, and Finko Oleg Anatolyevich. "Mathematical model of covert, noise-resistant transmission of information presented in a modular code" Science. Innovation. Technologies, no. 2, 2017, pp. 53-62.

6. Speransky Valentin Sergeevich, Abramov Stepan Vladimirovich, Klintsov Oleg Ivanovich, and Shuvalov Viktor Mikhailovich. "Features of analog and digital transmission of radio signals over fiber" T-Comm - Telecommunications and Transport, vol. 10, no. 9, 2016, pp. 38-42.

7. Balonin N.A., Vostrikov A.A., Sergeev M.B. Mersenne-Walsh matrices for image processing. In: Damiani E, Howlett R, Jain L, Gallo L, De Pietro G, editors, Intelligent Interactive Multimedia Systems and Services. Springer International Publishing Switzerland; 2015. vol. 40 SIST, p. 141-147.

8. Buzylev, Fedor Nikolaevich. Methods and algorithms for digital processing and correction of thermal imaging images: dissertation... PhD: 05.12.04 / Buzylev Fedor Nikolaevich; [Place of protection: Mosk. state Institute of Electronics and Mathematics]. - Moscow, 2010. - 158 p. : ill.

9. Ekaterina Kapranova A., Vadim A. Nenashev, Mikhail B. Sergeev, Compression and coding of images for satellite systems of Earth remote sensing based on quasi-orthogonal matrices // Proc. of SPIE, Image and Signal Processing for Remote Sensing XXIV. Berlin, Germany. 2018. Vol. 10789. PP. 1078923-1 - 1078923-6; doi: 10.1117/12.2324249.

10. Guterman, A. New matrix partial order based on spectrally orthogonal matrix decomposition/ A. Guterman, A. Herrero, N. Thome, // Linear and Multilinear Algebra 64(3):1-13 May 2015.

11. Fiedler, M. More on G-matrices/ M. Fiedler, T. L. Markham // Linear Algebra and its Applications 438(1), January 2013, pp:231–241

12. Vostrikov A.A., Sergeev A.M. Expansion of the Quasi-orthogonal Basis to Mask Images // Smart Innovation, Systems and Technologies. 2015. vol. 40. pp. 161-168. DOI: 10.1007/978-3-319-19830-9_15.

13. Samokhvalov A.V. "Complex use of the run-length coding algorithm and arithmetic coding for image compression" Proceedings of the International Symposium "Reliability and Quality", vol. 1, 2008, pp. 237-240.

14. Kobozeva A.A., and Sokolov A.V. Efficient group signal coding in steganosystems with multiple access. Problems of Regional Energy, no. 2 (50), 2021, pp. 101-113.

15. Shubnikov Vladislav Germanovich, and Belyaev Sergey Yurievich. "Noise Reduction and Image Difference Evaluation" Computer Science, Telecommunications and Control, no. 3 (174), 2013, pp. 58-66.

16. Chervyakov Nikolai Ivanovich, Lyakhov Pavel Alekseevich, and Orazaev Anzor Ruslanovich. "New methods for adaptive median filtering of impulsive noise in images" Computer Optics, vol. 42, no. 4, 2018, pp. 667-678. doi:10.18287/2412-6179-2018-42-4-667-678.

AUTOMATIOФN OF THE PROCESS OF FLAW DETECTION OF ADDITIVE PRODUCTS

Maria Rassykhaeva

Saint-Petersburg State University of Aerospace Instrumentation,
Saint-Petersburg, Russia
E-mail: mitschiru@gmail.com

Annotation
The current transformation of production is based on the automation of all production and auxiliary processes. When developing and implementing automated flaw detection systems for production, it is necessary to take into account both the current level of process automation and already used software systems, information systems to ensure information compatibility

The main technical and operational and structural and technological characteristics of the automated flaw detection complex are selected taking into account the specifics of production. Additive manufacturing refers to technological processes with a discrete nature, since the evaluation is a piece product or batches of products. Whereas the process of layer-by-layer deposition refers to continuous processes. The structure of the measurements performed within the production processes also depends on this characteristic of the process.

Table 1

The ratio of controlled parameters

Options	Share of total number of measurements, %	
	Discrete processes	Nevernые Processes
Temperature	8	50
Amount of substance	5	5
Substance consumption	4	15
Devalenie	4	10
Уровень	4	6
Number of products	25	
Length (dimensions, position, distance)	25	
It's time	15	4
Composition of the substance	-	4
Other	10	6

When solving the problem of detecting defects in additive polymer products, it is now possible to predict the locations of defects by analyzing the process of layer-by-layer synthesis, since thread breakage, displacement of the print object, and some other defects that will be hidden after printing are visible when considering each of the layers during printing.

However, this method requires automation and modernization of the installation. Now cameras are not installed in print chambers. Photo or video materials received from the camera will be large, since printing of one small part can take up to 8 hours, and the number of printed layers can be in the hundreds.

The analysis of print data requires the use of machine vision to compare each layer with the STL file from which the object was printed.

When analyzing the incoming information in real time, it is possible to identify critical errors in layer-by-layer synthesis even during the process, which will allow it to be interrupted and save the resources that would be required to complete the print and then detect defects.

Figure 1 shows the scheme of the additive complex. At the moment, due to the specificity of the production process, the operator is in most cases involved in flaw detection of additive products. This factor leads to high requirements for the qualification of the operator and an increase in the risk of human error.

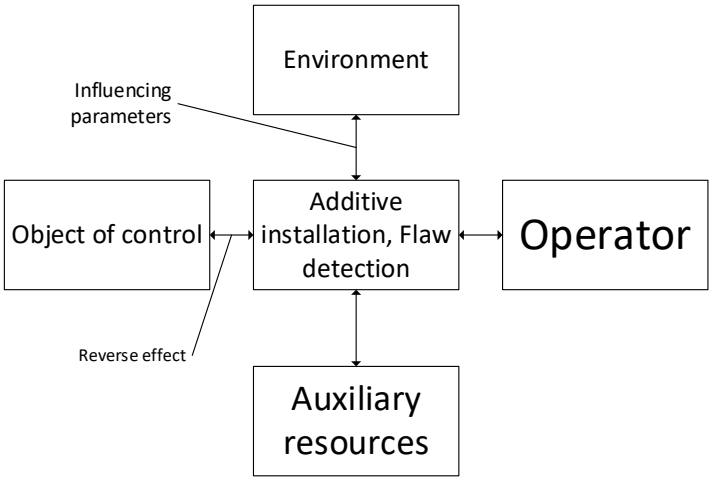

Figure 1. Work of additive complex control

The control and corrective elements of automation perform the functions of generating control signals for the executive elements of the system. In order to form these effects, various operations can be used: amplification of input signals, storage, transmission and further transformation according to the accepted algorithm.

Often, simple control elements are used to automatically control simple objects: amplifiers, relays, and logic devices. To implement more complex control algorithms (proportional-integral PI, proportional-integral differential - PID), various corrective elements are used in the feedback circuit of an electronic amplifier, for example. Corrective elements may not be part of control elements. Further improvement of control (implementation of adaptation functions, logical operations when starting and stopping an object, multistage protection, etc.) involves the use of aggregated automation complexes provided for by the nomenclature, as well as control computers.

As control elements, you can use microcontrollers and microprocessor systems made in the form of large integrated circuits (LSI), characterized by a number of technical and operational advantages.

The output stages of the control elements are power amplifiers. Non-contact power amplifiers are thyristor or magnetic.

The output stages of the control elements can also be hydraulic or pneumatic amplifiers.

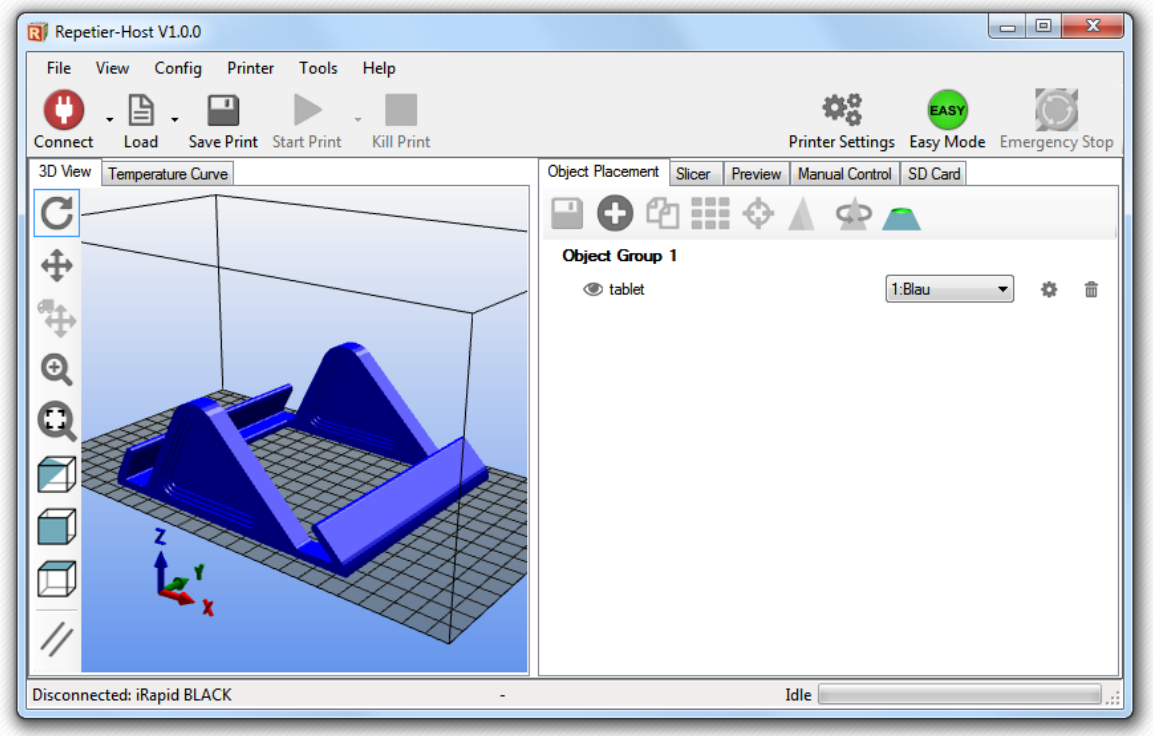

Figure 2 below shows the process of designing an additive product.

In industries with continuous technological processes, including chemical-technological ones, various operations are carried out continuously in time on the starting materials (raw materials and reagents) in apparatuses connected by technological lines. These operations are aimed at changing the physicochemical properties of the composition or state of the starting materials. As a result of the process, finished products of a given range and quality are obtained.

The need of the industry for measuring, analytical, testing instruments, means of automation and computer technology is extremely high in the world.

In the course of applied research, work was carried out with an additive installation. The results of the work are shown in Figure 3.

The simplest way to determine some characteristics of PCM is the so-called rule of mixtures (or the law of additivity). According to the rule of mixtures, a certain characteristic of PCM is defined as the sum of the products of a given characteristic of a matrix and its volume fraction and a given characteristic of a filler and its volume fraction.

$$X_к = X_м V_м + X_н V_н,$$

where $X_к$ $X_м$, $X_н$ - some characteristic, matrix and filler, respectively; $V_м$ and $V_н$ are the volume fraction of the matrix (binder) and filler, respectively, of the polymer.

Figure 3. Window of the information system for ensuring layer-by-layer synthesis

In these products, there is a distortion of geometry.

In this paper, we consider the possibility of automation in flow flaw detection for products of complex geometry.

Next, the products were tested for deformation of the layers (Figure 4).

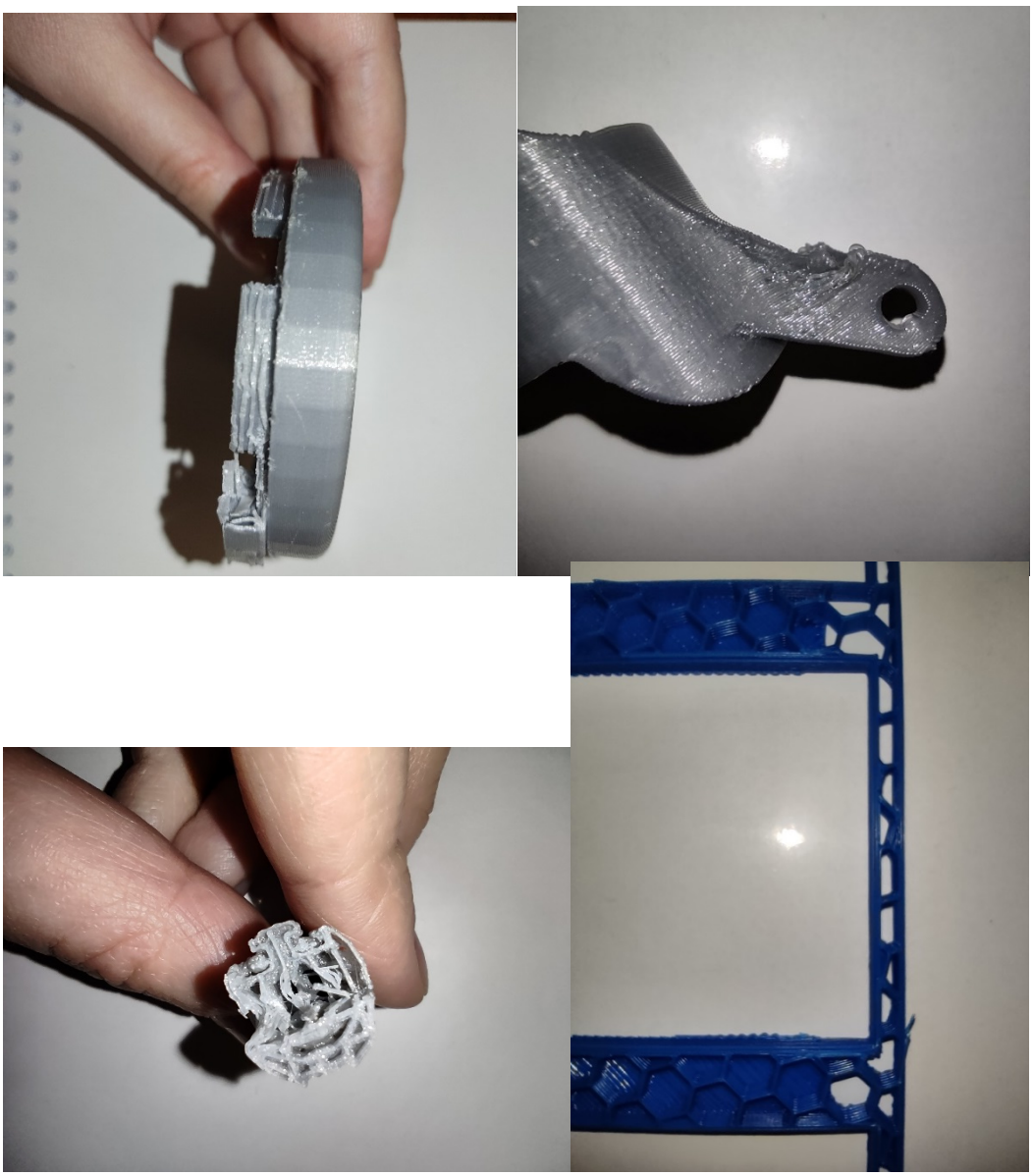

Figure 4. Deformation of additive glands

The State System of Industrial Instruments and Means of Automation (GSP) was created in order to provide technical means for the system of control, regulation and management of technological processes in various industries.

At present, the system of industrial devices is an operationally, informationally, energetically, metrologically and constructively organized set of products intended for use as means of automatic and automated systems for monitoring, measuring, regulating technological processes, as well as information-measuring systems. The system of industrial devices has become the technical basis for the creation of automated systems in industry. Its development and application contributed to the formalization of the design process, the transition to machine design.

The creation and improvement of systems of industrial devices are based on the following system engineering principles: typification and minimization of the variety of functions of automatic control, regulation and control; minimization of the range of technical means; block-modular construction of instruments and devices; aggregate construction of control systems based on unified instruments and devices; compatibility of instruments and devices.

According to the functional feature, all products of industrial instrumentation systems are divided into devices:

1) obtaining information about the state of the process or object;
2) receiving, converting and transmitting information via communication channels;
3) transformation, storage and processing of information, formation of control commands;

4) use of command information.

The first group of devices, depending on the method of information presentation, includes sensors that normalize converters that form a unified communication signal, devices that provide the presentation of measurement information in a form accessible for direct perception by the observer, and alphanumeric information devices entered manually by the operator. Means of obtaining information are the most numerous group of products of the state system of industrial instruments and automation equipment, more than half of the nomenclature of all technical means.

The second group of devices contains measuring circuit switches, signal and code converters, encoders and decoders, matching devices, means of telesignaling, telemetry and telecontrol. These devices are used to convert both measuring and control signals.

The third group consists of signal analyzers, functional and operational converters, logic and memory devices, controllers, regulators, control computing devices and complexes.

The fourth group includes actuators: electric, pneumatic, hydraulic or combined actuators, power amplifiers, auxiliary information presentation devices.

Minimization of the range of control and management tools is implemented on the basis of two ideas: the unification of devices of the same functional purpose based on the parametric range of these products and the aggregation of a set of technical means for solving large functional problems.

The minimization process begins with the selection of some basic parameters of instruments and devices, the selection of the main parameter from among them and the establishment of the minimum required number of devices to cover the entire range of the main parameter. At the same time, the transition from the range of use of one device to the range of use of another is subject to certain patterns. Predominantly a geometric progression based on a set of preferred numbers is used. The whole set of products of the same functional purpose is called a parametric range.

Conclusion

At present, parametric series of pressure, flow, level and electrical measuring instruments have been developed. Nevertheless, their optimization continues according to technical and economic indicators, for example, according to the criterion of the minimum total cost to meet the given needs. This criterion is based on the contradiction between the interests of the consumer and the manufacturer: the fewer devices in the series, the lower the development and mastering costs, the larger batches they are produced, which also reduces the manufacturer's costs. Increasing the number of devices in a row saves the consumer through more efficient use of the capabilities of the devices or due to more accurate compliance with the process regime.

Referens

1. Chabanenko A V, Kurlov A V 2021 Control the quality of polymers based on the model of Dzeno Journal of Physics: Conference Series

2. Chabanenko A V, Kurlov A V and Tour A C 2020 Model to improve the quality of additive production by forming competencies in training for high-tech industries *J. Phys.: Conf. Ser.* 1515 052065.

3. Chabanenko A V and Yastrebov A P 2018 Quality Assurance of Hull Elements of Radio-Electronic Equipment by Means of Control System *J. Phys.: Conf. Ser.* 1515 052065.

4. Chabanenko A V, Kurlov A V 2019 Construction of mathematical model of training and professional development of personnel support of additive production of REA IOP Conference Series: Materials Science and Engineering

5. Quality management of additive products / A. V. Chabanenko // RIA: Journal.: «Standards and quality». 2018. №2. S. 90-94.

6. Implementation of the PLM information system in the organization of Rassykhaeva M.D., Chabanenko A.V. In the collection: Selected scientific works of the twentieth International Scientific and Practical Conference "Quality Management". Moscow, 2021. S. 285-289.

7. Assessment of plasticity with combined hardening for the study of deformation processes of structural materials under various modes of low-cycle loads Chabanenko Alexander Valeryevich, Rassykhaeva Maria Dmitrievna Certificate of registration of the computer program 2021619545, 11.06.2021. Application No. 2021618914 dated 11.06.2021.

PROPERTIES OF THE COMPOSITION EULER TOTIENT FUNCTION Φ(N) AND THEIR APPLICATION TO CRYPTOGRAPHY

Maxim Rusanov

Saint-Petersburg State University of Aerospace Instrumentation,
Saint-Petersburg, Russia
E-mail: hatrue.max@gmail.com

Abstract

In this paper, we consider the solution of the equation with Euler's function:

$$\varphi_{\circ} k(n) = 1$$

And in this regard, an algorithm for searching the number *k* for a given n, as well as searching the number n for a given k, is being built. It is shown, that these algorithms have logarithmic and exponential complexity, respectively.

Also, for the sake of clarity of the research, the next dynamics of dependencies was built: Graph of the Euler's function; Dependence of the amount of compositions k on the argument n; Inverse dependence, that is, a graph of the amount of numbers n that satisfy the equation for a given *k*. The computational part of the work was performed using Python version 3.9.7.

At the end of paper, the idea of an encryption method is presented. It is based on the complexity of finding solutions to the equation:

$$\varphi_{\circ} k(n) = m$$

For various pairs of parameters.

Introduction

The Euler's function φ(*n*) is defined as a multiplicative arithmetic function showing the amount of natural numbers not exceeding n and coprime with it, that is [1]:

$$\varphi(n) = \sum_{\substack{k \le n \\ gcd(k,n)=1}} 1,$$

Where summation is kept for all numbers *k*, smaller or equal *n*, and coprime with *n*. Here the function gcd(*k*, *n*) is the greatest common divisor.

The most commonly used in practice (basic properties) Euler's function allow [1]:

1. Multiplicativity: $\varphi(n \cdot m) = \varphi(n) \cdot \varphi(m)$, if gcd(n, m) = 1, where, the numbers n and m are coprime (have no common divisors).

2. Calculation by factorization: $\varphi(n) = n \cdot \prod_{p \mid n} \left(1 - \frac{1}{p}\right)$, where p – prime and product is kept for all prime divisors of *n*.

3. Calculation at $n = p^{\alpha}$: $\varphi\left(p^{\alpha}\right) = p^{\alpha} - p^{\alpha-1} = p^{\alpha-1}(p-1)$

4. Elementary inequality: $\sqrt{n} \le \varphi(n) \le n$, for all natural numbers *n*.

5. Argument is an odd number: $\varphi(2m)=\begin{cases}2\varphi(m), & m=2k\\ \varphi(m), & m=2k-1\end{cases}, k\in \boldsymbol{N}$.

All these properties are widely used in both pure mathematics (the theory of divisibility and residues, number theory, group theory) and applied mathematics. Particularly in cryptography.

FORMULATION OF THE PROBLEM

Since the subject of this work is the consideration of the composition Euler function, for brevity, we will denote the function k times nested in itself as follows:

$$\varphi\Big(\varphi\big(\ldots\varphi\big(\varphi(n)\big)\ldots\big)\Big)=\varphi_{\circ}k(n)$$

Now consider the equation:

$$\varphi_{\circ}k(n)=1. \tag{1}$$

The problem is to find, for a given number n, the minimum number k sufficient to turn equation (1) into an equality. An algorithm for finding such a number k in logarithmic time will be constructed below.

PLOTING OF THE EULER FUNCTION AND THE DEPENDENCE OF THE AMOUNT OF COMPOSITIONS ON THE ARGUMENT

The first step in solving the problem was writing a program that would plot the dependence of the number of compositions k in equation (1) on the argument n. That is, the solution of equation (1) on a computer. In the future, using visual representations of the dependence, proceed to the mathematical justification of the algorithm.

Python 3.9.7 was used to write a program that plots the dependence of the number k on the argument n. The following algorithms were written: finding the number k given n; plotting the Euler function; plotting the dependence of the number of compositions k on the argument n; building an inverse relationship, that is, plot of the amount of numbers n that satisfy equation (1) for a given k.

This is followed by a description of the algorithms and the pictures dependency graphs.

By definition $\varphi(1) = 1$. This can be shown by using, for example, property 5. This is followed by an optimization block for large arguments. For small n, the function performs calculations equally fast both with and without the optimization block. The variable d is a power of two, the exponent of which, after calculations, is one less than in the factorization of n. Thus the variable phi calculates the Euler function only in $n / (2^{k-1})$, where k is a power of two in the expansion of *n*. This is followed by a calculation by counting all coprimes with n. The answer of the function will be the product of the numbers d and phi.

Using properties 1, 3 and 5 of the Euler function, you can derive similar properties for other prime numbers, for example, formula (2), thereby further optimizing the program, however, for the purposes of the work, it is enough to use property 5.

Example for numbers as $n = 3^w m$, where $\gcd(3, m) = 1$:

$$\varphi\left(3^w m\right)=\begin{cases}2\varphi(m), & w=1\\ 2\cdot 3^{w-1}\cdot\varphi(m), & w>1\end{cases}, k\in \boldsymbol{N}. \tag{2}$$

Code snippet of phi function in Python:

```
def phi(n):
    '''
    Euler's arithmetical function
    n: argument of function phi
    '''
    if n == 1:
```

```
    return 1

d = 1
phi = 1

# Optimization to big n
while (n % 2 == 0):
    n //= 2
    if (n % 2 == 0):
        d *= 2

for x in range(2, n + 1):
    if gcd(x, n) == 1:
        phi += 1
return d*phi
```

Using this function, it is not difficult to plot the following graph of the Euler function:

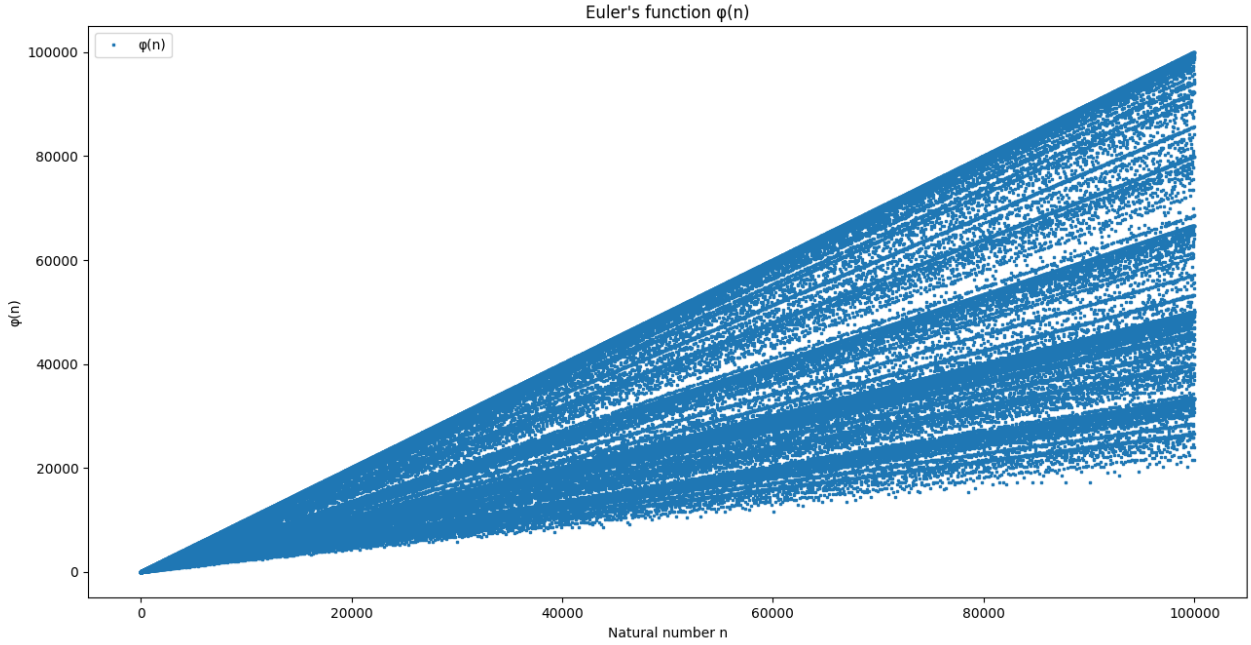

Figure 1 - Euler function φ(n), for n from 1 to 10^5

Using the function phi, one can numerically find the solution of equation (1). To do this, a code is written that applies the phi function to a given number n until the sequential composition gives one.Фрагмент кода решения уравнения на языке Python:

```
# Exact calculation of the number of compositions k,
# sufficient to bring the number to one
i = 1
while N != 1:
    print(str(i) + "-> φ(" + str(N) + ") = " + str(phi(N)))
    N = phi(N)
    i+=1
```

An example of execution for n = 10^8 was made with and without optimization to clearly show how effective it is to use the properties of a function when calculating it.

```
C:\Users\hatru\Desktop\Z+\Теория чисел\Y_function>python euler_func_composition.py 100000000 calc
1-> ϕ(100000000) = 40000000
2-> ϕ(40000000) = 16000000
3-> ϕ(16000000) = 6400000
4-> ϕ(6400000) = 2560000
5-> ϕ(2560000) = 1024000
6-> ϕ(1024000) = 409600
7-> ϕ(409600) = 163840
8-> ϕ(163840) = 65536
9-> ϕ(65536) = 32768
10-> ϕ(32768) = 16384
11-> ϕ(16384) = 8192
12-> ϕ(8192) = 4096
13-> ϕ(4096) = 2048
14-> ϕ(2048) = 1024
15-> ϕ(1024) = 512
16-> ϕ(512) = 256
17-> ϕ(256) = 128
18-> ϕ(128) = 64
19-> ϕ(64) = 32
20-> ϕ(32) = 16
21-> ϕ(16) = 8
22-> ϕ(8) = 4
23-> ϕ(4) = 2
24-> ϕ(2) = 1
--- 66.86628007888794 seconds ---
```

Figure 2 – Solution of equation (1) at $n = 10^8$ without optimization

```
C:\Users\hatru\Desktop\Z+\Теория чисел\Y_function>python euler_func_composition.py 100000000 calc
1-> ϕ(100000000) = 40000000
2-> ϕ(40000000) = 16000000
3-> ϕ(16000000) = 6400000
4-> ϕ(6400000) = 2560000
5-> ϕ(2560000) = 1024000
6-> ϕ(1024000) = 409600
7-> ϕ(409600) = 163840
8-> ϕ(163840) = 65536
9-> ϕ(65536) = 32768
10-> ϕ(32768) = 16384
11-> ϕ(16384) = 8192
12-> ϕ(8192) = 4096
13-> ϕ(4096) = 2048
14-> ϕ(2048) = 1024
15-> ϕ(1024) = 512
16-> ϕ(512) = 256
17-> ϕ(256) = 128
18-> ϕ(128) = 64
19-> ϕ(64) = 32
20-> ϕ(32) = 16
21-> ϕ(16) = 8
22-> ϕ(8) = 4
23-> ϕ(4) = 2
24-> ϕ(2) = 1
--- 0.35312342643737793 seconds ---
```

Figure 3 – Solution of equation (1) at $n = 10^8$ with optimization

It can be seen that when using property 5, we got an increase in execution speed by almost 190 times.

Algorithm for ploting values of k depending on n. The k_phi_arr array stores the k values for each n in the given interval. The calculation is the following. Since the values of the Euler function in the interval were calculated at the previous step, the corresponding value phi is searched for the number n, after which the value phi is assigned to the variable n and the counter k is increased by 1. The process continues until n is not equal to one.

Code fragment of the algorithm described above:

```
# Calculation of the dependence
# of the number of compositions k on the number n
k_phi_arr = []
for i in X:
```

```
k = 0
n = i
while n != 1:
    n = phi_arr[n - 1]
    k += 1
k_phi_arr.append(k)
```

Using the data in the k_phi_arr array, a dependency graph is built:

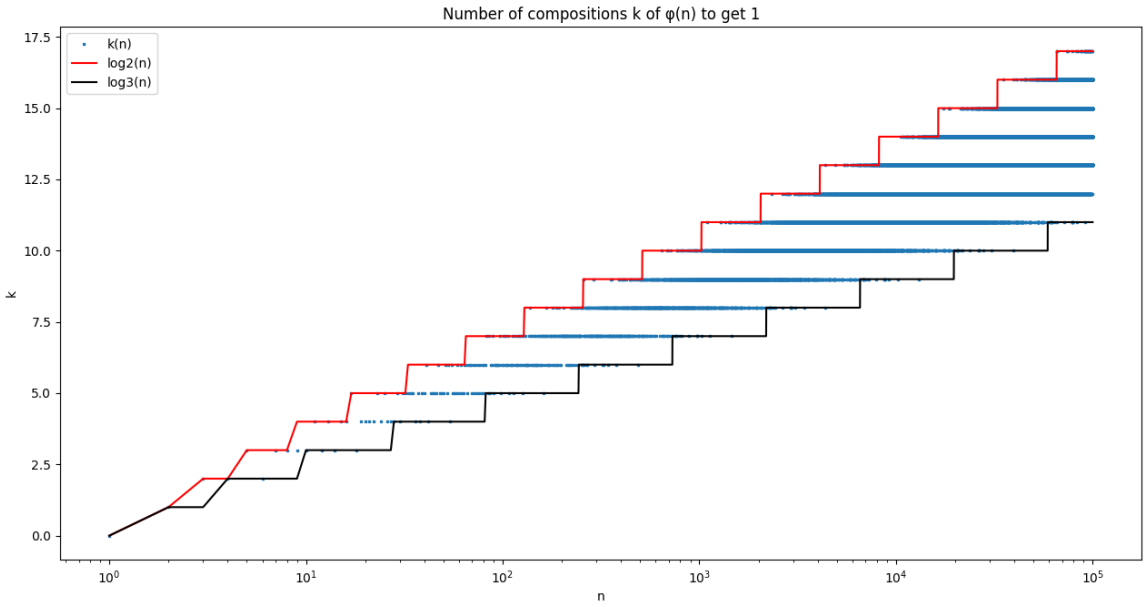

Figure 4 – The dependence of the number k on n, for n from 1 to 10^5 on a logarithmic scale along the x axis

The figure shows that the number of compositions k in equation (1) depends logarithmically on n. A complete mathematical justification of the boundaries shown in Figures 4 and 5 will be given later in the work in the section "Computational complexity of solving the equation".

The problem was also set to find the number of solutions to equation (1) for a given k and an unknown n [3]. The formal solution is also contained in the paper below. Provided that for each n its number k is known (array k_phi_arr), then the construction of the above dependence is trivial. Here's a dependency graph.

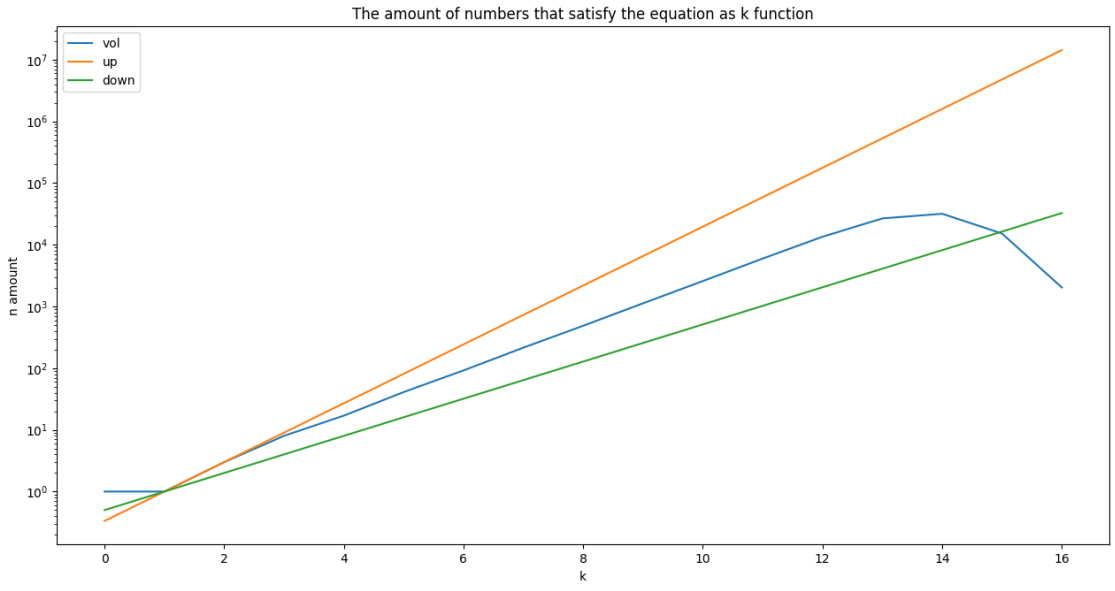

Figure 5 – The number of solutions to equation (1) for a given k and unknown n for n from 1 to 10^5 on a logarithmic scale along the y axis

Figure 5 shows that the number of solutions to equation (1) for a given k grows exponentially as k grows. The decrease in the dependence on the graph, starting from k = 13, can be explained by the fact that, starting from a given k, not all solutions of the equation are contained in the range from 1 to 10^5. However, as will be shown below, if this graph is continued indefinitely, then it will indeed have an exponential growth rate.

COMPUTATIONAL COMPLEXITY OF SOLVING THE EQUATION

Let's return to the consideration of the equation, but from an analytical point of view:

$$\varphi\left(\varphi\left(\ldots\varphi\left(\varphi\left(n\right)\right)\ldots\right)\right)=\varphi_{\circ}k\left(n\right)=1 \tag{3}$$

Considering the graph in Figure 4, as well as using the properties 1 – 5 of the Euler function, one can notice the following pattern. Jumps in values at the boundaries (outlined by red and black lines) occur at powers of two and three.

This remark can be substantiated by reducing the solution of the equation to the following dual problems: what is the smallest/largest number n in equation (3), where k is given. Thus, one can determine the upper and lower bounds for k and find the complexity of the search algorithm.

For k = 1 we have the following::

$$\varphi\left(n\right)=1 \quad \rightarrow \quad n_{\min}=1, n_{\max}=2$$

For k = 2:

$$\varphi\left(\varphi\left(n\right)\right)=1 \quad \rightarrow \quad n_{\min}=3, n_{\max}=6.$$

Consideration of special cases does not provide any guidance for solving the problem, or there are needs too many special cases to consider.

Therefore, we use the following relatively obvious arguments to find the upper bound for k. If φ(n) = 1, then it is clear that at the next step also φ(φ(n)) = 1. However, it can be noted that the minimum number n is not equal to one and satisfies the conditions above is n = 2.

Now, if the argument φ(*n*) contains a power of two, then the result will also be a power of two, but of a smaller order. Namely:

$$\varphi\left(2^m\right)=2^{m-1}$$

Further, if $n = 2^m$ in equation (3), then we get the following chain of calculations:

$$\varphi\left(2^m\right)=2^{m-1}\rightarrow\varphi\left(\varphi\left(2^m\right)\right)=\varphi\left(2^{m-1}\right)=2^{m-2}\rightarrow\varphi\left(\varphi\left(\varphi\left(2^m\right)\right)\right)=2^{m-3}$$

Thus, after m compositions we get the solution:

$$\varphi_{\circ}m\left(2^m\right)=1 \tag{4}$$

This is already enough to get the required goal.

Note that any number can be represented in terms of the binary logarithm as a power of two. That is, it is true that $n = 2^{\log_2 n}$. Solution (4) shows that in this case the solution to equation (3) will be $k = \log_2 n$. But the number $\log_2 n$ is not an integer for any n, and a non-integer number of compositions is excluded. Then we can say for sure, based on if φ(*n*) = 1, then also φ(φ(*n*)) = 1:

$$k \le \log_2 n, \ \textit{where } x - \textit{round up operation of number } x. \tag{5}$$

Thus, for any n, the solution to equation (3) is no greater than $\log_2 n.$.

For a more accurate estimate and to improve the efficiency of the search for the number *k*, we will find the lower bound. We use a similar fact as in the previous argument. It is necessary to determine the minimum

number not equal to one, for which $\varphi(n) \neq 1$, but at the next step $\varphi(\varphi(n)) = 1$. This number is n = 3. Indeed, $\varphi(3) = 2 \neq 1$, but $\varphi(\varphi(3)) = \varphi(2) = 1$.

Now, if the argument φ(n) contains a power of three, then the result will be the power of three multiplied by two, but of a smaller order. Namely:

$$\varphi\left(3^m\right) = 2 \cdot 3^{m-1}$$

Using the multiplicativity of the Euler function, consider the following chain of calculations:

$$\varphi\left(3^m\right) = 2 \cdot 3^{m-1} \rightarrow \varphi\left(\varphi\left(3^m\right)\right) = \varphi\left(2 \cdot 3^{m-1}\right) = \varphi(2) \cdot \varphi\left(3^{m-1}\right) = 2 \cdot 3^{m-2}.$$

Thus, after m steps we obtain the following:

$$\varphi_{\circ} m\left(3^m\right) = 2 \quad (6)$$

Since $\varphi(2) = 1$, then applying the Euler function to relation (6) we obtain the solution:

$$\varphi_{\circ}\left(m+1\right)\left(3^m\right) = 1 \quad (7)$$

Next, we apply the same reasoning to the number n as in the upper estimate, namely, that any number can be represented in terms of a ternary logarithm as a power of three. More precisely, $n = 3^{\log_3 n}$. It can be seen from solution (7) that in this case the solution to equation (3) exceeds $\log_3 n$. But not for any n the number $\log_3 n$ is an integer, but a non-integer number of compositions is excluded. Then we can say for sure that:

$$\log_3 n \leq k, where\, x - round\, down\, operation\, of\, number\, x \quad (8)$$

As a result, we have the following bounds for the number k in the equation (3):

$$\log_3 n \leq k \leq \log_2 n\ . \quad (9)$$

It is also clear from the reasoning that the same inequality will hold if the rounding operations are removed. We get a slightly stronger inequality, but due to the fact that the number k is an integer, this is not essential.

$$\log_3 n \leq k \leq \log_2 n\ . \quad (10)$$

Inequality (10) can be used to efficiently search for a solution to equation (3). Since the boundaries of the search are known, it is possible to set the maximum number of steps $T_k(n)$ that the algorithm performs in the worst case. This number will be the difference between the upper and lower bounds:

$$T\left(n\right) = \log_2 n - \log_3 n = \ln\left(n\right) \cdot \left(\frac{1}{\ln 2} - \frac{1}{\ln 3}\right) \approx 0.54 \cdot \ln\left(n\right). \quad (11)$$

Thus, it is established that the solution of equation (3) for a given k can be found in logarithmic time.

From inequality (10) it is also possible to establish the search boundaries and the maximum number of steps $T_n(k)$ that will be required to solve equation (3), for given k and unknown n.

Having carried out simple transformations in inequality (10), we can obtain the bounds of the number n:

$$2^k \leq n \leq 3^k \quad (12)$$

Thus, it has been established that the algorithm for finding a solution to equation (3) for a given n has exponential complexity.

DESCRIPTION OF THE IDEA OF ENCRYPTION BASED ON THE PROPERTIES OF SEARCHING FOR SOLUTIONS OF THE EQUATION

As a further vector of researches, we can consider the search for solutions to the following equation:

$$\varphi\left(\varphi\left(\ldots\varphi\left(\varphi\left(n\right)\right)\ldots\right)\right) = \varphi_{\circ} k\left(n\right) = m, \quad (13)$$

where the numbers k and m are given and m is an even number (from the range properties of the Euler function).

Then, as applied to cryptography problems, equation (13) can be interpreted as the process of encrypting the original message n with the key k, where m is the encrypted message. This process satisfies the necessary conditions for encryption, since the following complexity diagram for k, n and m is true:

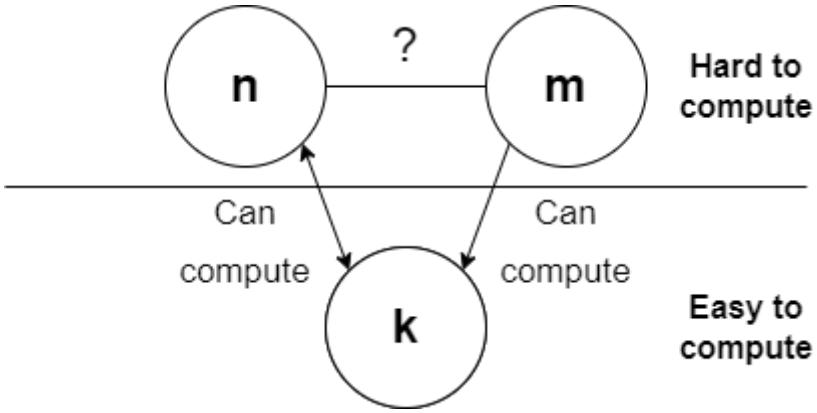

Figure 6 – Calculation complexity diagram

Here, a difficulty may arise in that the inverse Euler function $\varphi^{-1}(m) = n$ is multi-valued, that is, decoding can occur ambiguously [3]. However, this can be circumvented by constructing the original message in such a way that the dimension of values of the inverse Euler function is equal to a sufficiently small number.

Such cases in the encrypted message exist, since the K. Ford theorem about the number of dimensions of the Euler function is true:

$$\forall k \geq 2, \exists m \mid \dim\left(\varphi^{-1}(m)\right) = k$$

It remains only in the future to build the number n according to the given numbers k and m, then sorting through a relatively small number of values to get the original message.

Formally, the encryption process have the next steps:

1) Encryption of the original message n with the key k: $\varphi_{\circ} k(n) = m$
2) Send encrypted message *m*
3) Decryption of the received message using the key and determination of the initial value from the set: $\varphi^{-1}{}_{\circ} k(m) = n$

This idea are planned to be developed in future works.

References

[1] Changa M. E. / Methods of the Analytical Theory of Numbers. / M.: MCNMO, 2019. – 208 c. – ISBN 978-5-4439-1394-0

[2] Gupta H. / Euler's Totient Function and its Inverse. / Panjab University, Chandigarh 160014 (1980)

[3] Ford K. / The number of solutions of φ(x) = m. / Annals of Mathematics, 150 (1999), 1 – 29

THE IMPACT OF AUTOMATION ON MANUFACTURING

Rostislav Savenko

Saint-Petersburg State University of Aerospace Instrumentation,
Saint-Petersburg, Russia
E-mail: rosoops@mail.ru

Annotation
Some of the challenges facing business today include shortage of labour, declining unemployment rates and high staff turnover. The impact of these trends can be expected to intensify in the future with the global trend of population aging. Here we share a perspective showing how automation can address these challenges.
There is a perception that with automation and robotics come job losses. Here we consider this along with new job creation. The debate is not whether automation has a positive or negative impact on jobs; the debate is the magnitude of the impact of automation on jobs.
In a well-designed automated solution there will be benefits of productivity and yield improvements. These topics are well researched and here we provide several case-studies.
The impact of automation on health and safety on a macro level is not as well studied as its impact on jobs or productivity but in some industries the incident rates have been decreasing as automation has been increasing. Furthermore, automation allows staff to be removed from high hazard work environments.
For the benefits of automation to be realised however, the work place needs to adapt. There is agreement among some scholars and stakeholders that a smooth adoption of more automation calls for:
- Investing in R&D and human capital such as highly skilled mechanics, engineers, and big data personnel
- Redesigning workflow and workspace to facilitate human-machine collaboration
- Actively setting and implementing digital safety standards including data security, privacy, and malicious use etc.

Introduction

Labour shortage, high staff turnover, and work related accidents/injuries are some of the issues the manufacturing sectors face. Some regions (e.g., Europe, North America, and Japan) and industries (e.g., meat processers and fruit growers) are more affected than others. As a result, automation is being increasingly used in the production process.

This white paper summarises the results of recent research on a macro level, and provides some examples of real word applications and effects of automation. The aim is to inform on the labour force challenges we face, the benefits of automation as a solution, and the required steps companies may take to smoothly transition towards greater automation.

This paper deals with the current labour force situation and population aging estimations (Section 3), the impact of automation on jobs (Section 4), on productivity and profitability (Section 5), on yield and quality (Section 6), on workers' health and safety (Section 7) and the steps required for a frictionless transition to automation (Section 8).

Labour shortage, high staff turnover and population aging

An increase in population and material demand has led to a shortage of labour, with a workforce that can no longer keep up with consumption. Some regions and industries are worse affected than others. Globally, using data from the World Bank, Fig. 1 (right) shows that between 1991 and 2017,

- The growth rate of the labour force is generally decreasing for all country groups,
- In general, the unemployment rates are lower post 2000, and
- High income countries have experienced a negative annual unemployment rate of change since 2010.

The combination of declining unemployment rates in a declining labour market presents a serious challenge. When there is limited labour, competition for staff will increase and in certain industries high staff turnover is becoming the norm. In the U.S. meat and poultry processing industry, for example, labour turnover has increased from an historical 1-1.5% per week to 2-2.5% in recent years. The cost of replacement could add up to 4% of total processing cost, which is equivalent to hundreds of millions of profit loss (McCracken, 2018).

This shortage in labour and high staff turnover will almost certainly intensify in the future due to population aging.

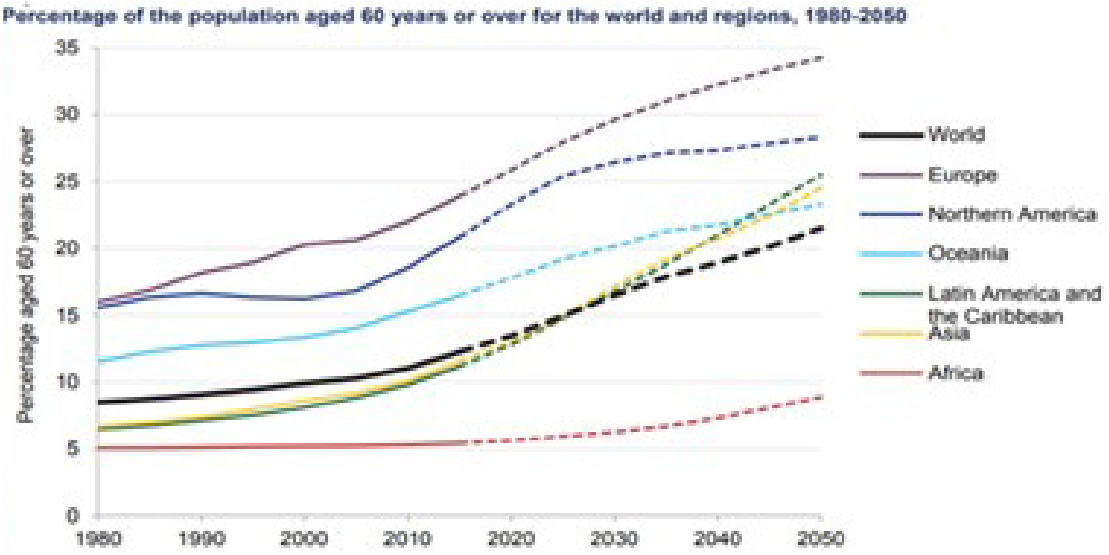

Figure 2. Population estimation of 60 years or over Worldwide. Source: UN (2015, 2017)

According to the UN (2015, 2017), 'the number of 60 years + people is expected to more than double by 2050 and to more than triple by 2100, rising from 962 million globally in 2017 to 2.1 billion in 2050 and 3.2 billion in 2100. Globally, population aged 60 or over is growing faster than all younger age groups' (Fig. 2 LHS).

Population aging is particularly concerning for developed regions. In Europe, approximately 25% of the population were over 60 years old in 2015, this number will increase to nearly 35% in 2050. Worldwide, approximately 12% of all people are over 60 years old in 2015, this number will increase to 21% in 2050 (Fig. 2 RHS).

Jobs

Job loss seems to be the first thing that comes to mind when it comes to automation and robotics; yet job creation is also an aspect brought by the same technology.

Autor (2015) commented that '(a)utomation does indeed substitute for labor—as it is typically intended to do … journalists and even expert commentators tend to overstate the extent of machine substitution for human labor and ignore the strong complementarities between automation and labor that increase productivity, raise earnings, and augment demand for labor'.

PwC (2018) noted that '… new technologies … will create many new jobs. Some of these new jobs will relate directly to these new technologies, but most will just result from the general boost to productivity, incomes and wealth that these technologies will bring. As these additional incomes are spent, this will generate additional demand for labour and so new jobs, as such technologies have done throughout history…'

The debate here is not whether automation has a positive or negative impact on jobs; the debate here is the magnitude of the impact of automation on jobs. This lack of clarity is captured in Winick (2018), which summarised a small part of job loss/creation estimation studies (Table 1). The author noted that '…these predictions are made by dozens of global experts in economics and technology, no one seems to be on the same page. There is really only one meaningful conclusion: we have no idea how many jobs will actually be lost to the march of technological progress.'

For example, on the job loss front, Thomas Frey (2012) suggested that 2 billion jobs worldwide could be automated by 2030, while McKinsey reported (2017b) the number should be 400 million to 800 and Graetz and Michaels (2015) suggested that there is no relationship between the use of robots and manufacturing job loss for the studied countries between 1996 and 2012.

Predicted Jobs Automation Will Create and Destroy

When	Where	Jobs Destroyed	Jobs Created	Predictor
2016	worldwide		900,000 to 1,500,000	Metra Martech
2018	US jobs	13,852,530*	3,078,340*	Forrester
2020	worldwide		1,000,000–2,000,000	Metra Martech
2020	worldwide	1,800,000	2,300,000	Gartner
2020	sampling of 15 countries	7,100,000	2,000,000	World Economic Forum (WEF)
2021	worldwide		1,900,000–3,500,000	The International Federation of Robotics
2021	US jobs	9,108,900*		Forrester
2022	worldwide	1,000,000,000		Thomas Frey
2025	US jobs	24,186,240*	13,604,760*	Forrester
2025	US jobs	3,400,000		ScienceAlert
2027	US jobs	24,700,000	14,900,000	Forrester
2030	worldwide	2,000,000,000		Thomas Frey
2030	worldwide	400,000,000–800,000,000	555,000,000–890,000,000	McKinsey
2030	US jobs	58,164,320*		PWC
2035	US jobs	80,000,000		Bank of England
2035	UK jobs	15,000,000		Bank of England
No Date	US jobs	13,594,320*		OECD
No Date	UK jobs	13,700,000		IPPR

Table 1. Examples of job estimation by different sources Source: Winick (2018)

Similarly, predictions on the number of jobs created worldwide through automation differ significantly. The estimated range differs from 2 million jobs (Martech, 2013 and Gartner, 2017) to U.S. 555-890 million (McKinsey, 2017b). PWC (2018) suggested that 'the net long term effect on employment in advanced economies like the US and the EU may be broadly neutral …'

According to IFR (2017), the automotive industry in the U.S. had accumulated an additional 52,000 units of the operational industrial robots between 2010 and 2016. During the same period, 260,600 jobs were added in the sector. Similarly, in the German automotive industry, which is renowned for its robot density (300 per 10,000 workers1), 72,313 jobs were added between 2010 and 2016 (data from EUROSTAT2, 2018).

Productivity and Profitability

The productivity-boost effect of automation is well supported by research.

Graetz and Michaels (2015) studied the impact of robotics on productivity using macroeconomic research. Using panel data from 14 industries in 17 countries between 1993 and 2007, the study found that the use of robots raised countries' average GDP growth rates by about 0.37 percentage points and productivity growth by about 0.36 percentage points respectively. These figures represents 12% of total GDP growth and 18% of labour productivity growth for the 17 countries over that time period.

Ceber (2017) studied the impact of automation on economic development (GDP per capita and labour productivity) in 23 OECD countries between 1993 and 2015. The study found 'a positive association between robotics density and labour productivity; … a one-unit increase in robotics density growth is associated with a 0.04% increase in labour productivity'. And, '… a positive relationship between robotics automation and economic development … a 1% increase robotics investment is associated with a long-run increase in GDP per capita of 0.03%.'

McKinsey Global Institute (2017a) estimated that 'automation could raise productivity growth globally by 0.8 to 1.4 percent annually'. Berg, Buffie, and Zanna (2018) suggested that '… even a small increase in the level of robot productivity can increase output enormously if the robots and humans are sufficiently close substitutes…'

According to Gollschewski (Rio Tinto's Pilbara Mines Managing director) (Fig. 3), the mine sites equipped with autonomous trucks and drills out-performed the manned sites for the investigated period; and the level of performance of the automated sites were improving with time.

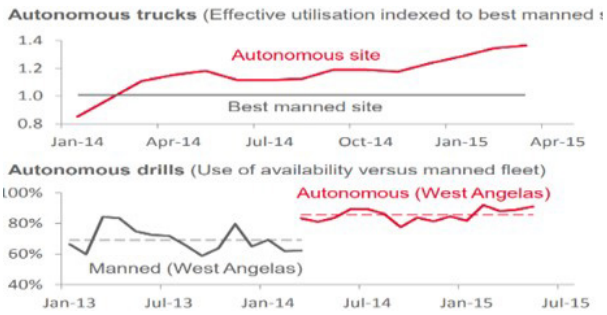

Figure 4. Rio Tinto Pilbara mine site performance, autonomous vs manned 2013-15 Source: Gollschewski (2015)

DHL (the global third-party logistics provider) suggested that, by using virtual reality and heads-up display, the staff are able to locate items faster. Their Ohio facility achieved a 10% productivity improvement during the trial period (Trebilcock, 2018).

Yield and quality

Yield improvement is another benefit of automation. McKinsey (2017a) suggested that the magnitude of the benefit varies substantially based on individual use case. One such example is hydroponic farms that are operated by automated systems. New Jersey based Bowery farm (Fig. 4 on the right) was suggested to be much more productive than average farmlands (Kowitt, 2018). This is because this indoor farming facility is mainly automated. Sensors control and set optimal temperature and moisture levels, leading to faster growth, more crop cycles, and higher yield per crop cycle (Fain, cited in Kowitt, 2018). Furthermore, this way of farming requires less water and no pesticides, which minimises water wastage and enhances crop flavour (Bloomberg, 2018)

In another example even small scale beef boning automation in the meat processing industry can effectively increase the amount of meat in primal cuts. Greenleaf (2009) found that these units can provide an average yield savings of approximately 0.40% (0.63 kgs)/carcass, for three different types of cattle, which was equivalent to AU $3.04/carcass on average, based on 2009 cattle prices.

Figure 5. Bowery farm Source: Kowitt, 2018

In addition to the increased profit/carcass, the otherwise wasted meat becomes available for consumption. If the beef boning unit was used in all Australia beef processing facilities, the additional yield would have put approximately 4,510 tonnes of beef on the dinner table in 2017.

Health and Safety

The impact of automation on health and safety on a macro level is not as well studied as its impact on jobs or productivity. Levert and Héry (2018) presented two sides of the coin: automation might be a contributing factor to work load intensification but it can also reduce physical demands and repetitive tasks.

While the report suggested that work load intensification could be the reason for an increase in work-related incidents, this theoretical hypothesis is not well matched by real world statistics. The occupational incidence rate in the U.S. private sector (Fig. 5) and U.S. poultry industry (Fig. 6) has been falling in the past 15 years, which coincided with the intensification of automation in general.

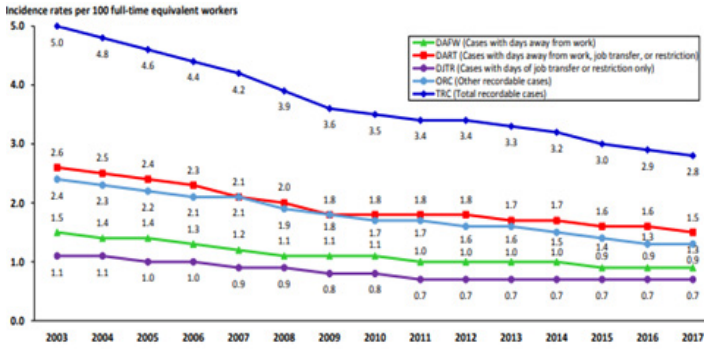

Figure 6. US occupational incidence rates, 2003-17 Source: BLS (Nov, 2018)

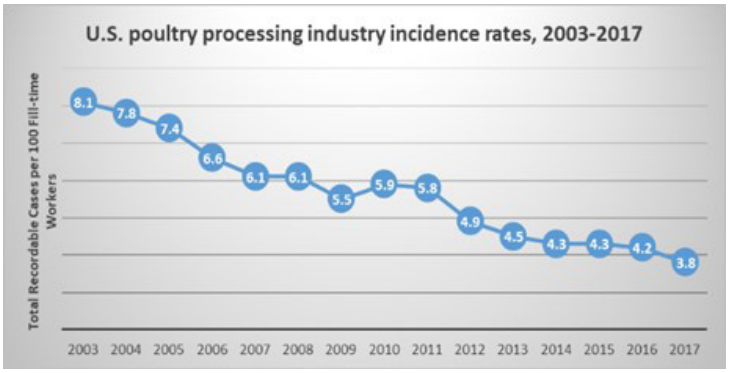

Figure 7. US Poultry industry incidence rates, 2003-17 Source: BLS Incidence rates—detailed industry level 2003-173

Beyond statistics, automation systems and robotics are seen at the most hazardous work places substituting repetitive and risky tasks. Automated welding systems, fully or collaborative, minimise operators' exposure to metal fumes and ultraviolet (UV) radiation while eliminating injuries such as burns, eye damage, electric shocks, cuts, and injury to toes and fingers typically associated with manual welding.

Another real world example is the use of cobots by German chainsaw maker STIHL in their cut-off production. According to IFR (2018a), Cobots were introduced to STIHL's cut-off machine inspection and packaging line because the lifting of a unit (weighs around 10 kg) by human operators had proven to be a considerable burden. During inspection, cobots remove the cut-off machine from a suspended conveyor, carry out the shake test, and keep it suspended until a final visual inspection is completed (Fig. 7 on the right); the packing line staff were involved from the outset interacting with the cobots for final inspection. Not only did the cobots help reduce the physical strain on human operators, it made the process more efficient.

Figure 8. Cobots holding STIHL cut-off machine for oper-ators to inspect Source: IFR (2018a)

Another example is Saint Gobain, a French specialist glass maker, who use a collaborative robot to polish glass. They reported that the cobots not only freed operators from the constant vibration of polishing, but they also reduced production time by one third (IFR, 2018b).

The Transition towards Production Automation

There is agreement among some scholars and stakeholders (e.g., Autor (2015), Bessen (2016); PwC (2016); IFR (2017), McCracken (2018), and McKinsey (2018)) that the smooth transition towards automation need to be coordinated amongst governments, industries, and companies.

Summarising from cited experts, a governments' role in this transition is to provide fit-for-purpose education systems to prepare and retrain the work force, creating dynamic labour market search/match plate forms and implement policies to allow the adoption of automation. While companies are suggested to:

- Invest in R&D and human capital such as highly skilled mechanics, engineers, and big data personnel
- Redesign workflow and workspace to facilitate human-machine collaboration
- Actively set and implement digital safety standards including data security, privacy, and malicious use.

Conclusion

Automation and robotics is here, just like steam power in the 1780s, electricity in the 1870s, and computing systems in the 1960s. The evidence supporting the argument that automation increases productivity, helps to address population aging and labour shortage, and improves work place health & safety cannot be ignored. While there might be short-term negative social impact, stopping or scaling back automation or robotics is not the answer. A company, industry or nation runs the risk of losing competitiveness altogether should the progress of automation be halted. It is therefore paramount that the collaboration between governments and industries make this transition safe and beneficial for all.

List of used literature:

1. Gartner (2019). Gartner Says By 2020, Artificial Intelligence Will Create More Jobs Than It Eliminates Retrieved from https://www.gartner.com

2. Bloombery. (2020). This High-Tech Farmer Grows Kale in a Factory.

3. Winick E. (2021). Every study we could find on what automation will do to jobs, in one chart. MIT Technology Review. Retrieved from https://www.technologyreview.com

4. McKinsey Global Institute. (2022). AI, Automation, and the future of work: ten things to solve for.

5. The Automation Advantage: Embrace the Future of Productivity and Improve Speed, Quality, and Customer Experience Through AI

by Bhaskar Ghosh , Rajendra Prasad

DIFFRACTION SPECTRAL INSTRUMENT IN A MULTIPLE ALTERNATIVE SYSTEM OF AUTOMATIC CONTROL BASED ON THE RADIO-OPTICAL APPROACH

Ksenia Serdiuk

Saint-Petersburg State University of Aerospace Instrumentation
Saint-Petersburg, Russia
E-mail: kserdiuk@yandex.ru

Abstract
On the basis of multi-channel automatic control, the possibility of multi-alternative automatic control of physical and physico-chemical processes accompanied by the optical emission is considered. The output vector is formed by means of spectral measurements with a diffraction prism spectral device, the action of which is considered in the framework of an alternative approach based on the signaling theory and the linear systems theory.
***Keywords*:** multi-alternative automatic control system; output vector; spectral measurements; spectroscopic information; diffraction prism spectral device; instrument function.

Introduction

In physics and engineering, spectral analysis methods and devices are among the most common, and harmonic spectrum analysis refers to the number of the most important physical measurements. The role of harmonic analysis is particularly important in spectroscopy, where the information obtained is contained in the function of electromagnetic radiation energy distribution through frequencies.

In spectroscopic measurements, spectral devices study electromagnetic radiation as a signal sent by matter and carrying information about the chemical composition of a substance, about the physical and physico-chemical processes occurring, along with the physical properties of the medium through which the radiation propagates. Thus, the spectral devices largely represent the tools for the microcosm study. These spectral measurements are characterized by obtaining spectroscopic information in the form of a continuous frequency function (wavelength).

Thus, the main task of the theory of spectral measurements is to establish a connection between the spectrum in the mathematical sense and the instrumental spectrum, i.e. registered as a result of spectral measurements [1], in other words, the input-output connection of the spectral device. Within the framework of the theory of optical spectral measurements, a solution to this problem was proposed in [2], where, on the basis of heuristic reasoning, a linear integral operator in the form of a convolution was obtained, which initially describes the measurement of energy spectra. It's the connection between the input and output of the spectral device in the form of a convolution that served as the basis for solving the inverse problem, i.e. reduction to an ideal spectral instrument. The ideology of the work [2] has firmly taken a place in the known manuals on optical spectroscopy techniques [3, 4, 5, 6, 7]. It should be emphasized that article [2] notes a change in resolution within the analyzed wavelength band, which is contrary to the folding operation.

Characteristically, in the mentioned manuals [3, 4, 5, 6, 7] the core of the integral operator, i.e. the instrumental function of the spectral device, is not directly related to the parameters of the dispersing systems of diffraction spectral devices. For lattice spectral devices, the issue of direct connection of the instrumental function with the parameters of the diffraction grating is to a certain extent solved in papers [8, 9, 10, 11]. In this paper, an attempt has been made to solve the issue of connecting a instrumental function with the parameters of a dispersing system for a prism spectral device within the framework of establishing an input-output connection of a spectral device for complex spectra of optical radiation.

In the paper [12], a fundamentally new direction of optical spectroscopy methods application is defined. We are talking about multi-alternative automatic control [13] of physical or physico-chemical processes accompanied by electromagnetic radiation in the optical range, while the error signal is formed by spectroscopic measurements. If a spectral device is used as a measuring device in multi-alternative automatic control systems, spectroscopic information must be provided in the form of reference values of the measured spectrum, i.e. in matrix form. For this purpose, a multi-channel optical spectral device that implements the resonant multi-channel principle of spectrum measurement and belongs to the new ones [14] is quite suitable.

This device is characterized by obtaining spectroscopic information in the form of reference values of the measured spectrum, which constitute the output vector $\{y'_k\}$ of a multi-channel automatic control system. The vector values $\{y'_k\}$ are determined by the controlled spectroscopic variables that are defined by the results of the spectrum measurement.

The use of well-established diffraction, spectral devices, in this case – prism one, for the formation of the output vector $\{y'_k\}$ is possible if the CCD is used for reading spectroscopic information.

During the automatic control system operation, the information, the carriers of which are dynamic signals, is processed. Here such signals are being optical radiation, their description and processing must be performed in terms of signaling theory and the linear systems theory. The traditional theory of diffraction optical spectral devices, for example [4, 5, 6], relies on the principles of geometric optics, and it is not possible to apply its results to solve the set task. In this regard, an alternative theory of the diffraction prism spectral device (DPSD) used in this work is proposed. Its prerequisites are proposed in the paper [15], within which the properties of the output vector are obtained .Within this theory the properties of the output vector $\{y'_k\}$ are obtained.

Multi-alternative automatic control system

The functional scheme of a multi-channel automatic control system (ACS) [16], which is shown in Fig.1., is adopted as the basis of the functional scheme of a multi-alternative automatic control system, where the error signal is proposed to be formed based on the spectroscopic measurements results.

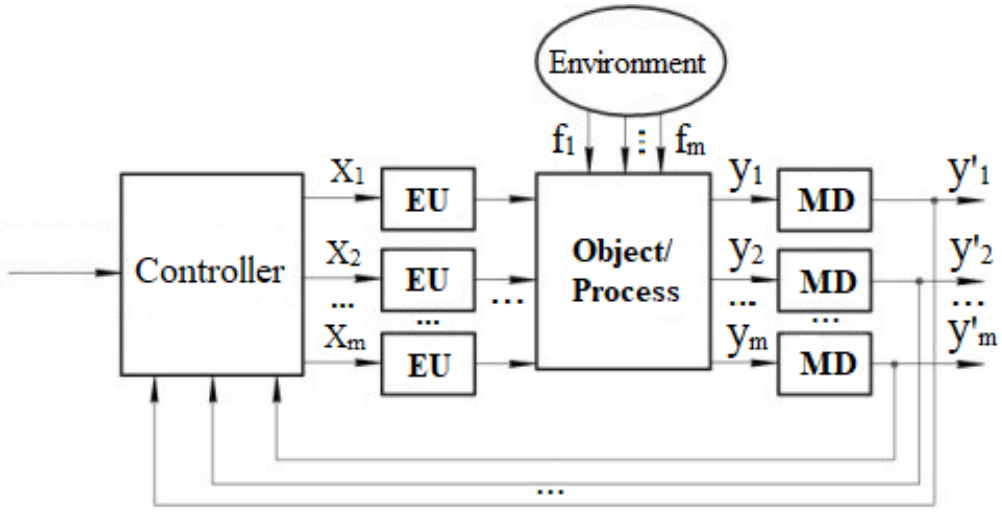

Fig.1. Functional scheme of the ACS

In this scheme, the following signs are introduced: Controller – control system; x_k - input variables; EU- execution units; Environment – external environment; f_k – disturbing influences; Object/Process - object/process; y_k – regulated devices; MD - measuring devices; y'_k – output variables that are combined in the output vector $\{y'_k\}$.

Transition from the diagram shown in Fig.1, to the scheme of multi-alternative ACS is as follows:

1) measuring device system {EU} is replaced by a single measuring device DPSD, on the input of which falls the optical radiation. The radiation, generated by a controlled physical or physico-chemical process, carries information about the development of the latest and replaces the system of vectors $\{y_j\}$; the formation of the output vector $\{y'_k\}$ is performed by reading out spectroscopic information using a CCD, this information is extracted using pixels corresponding to those narrow-band spectrum sections, which are controlled;

2) the control device is supplemented with a device for prioritizing control by a particular output vector component $\{y'\}$.

The corresponding functional diagram of a multi-alternative automatic control system is represented in Fig.2.

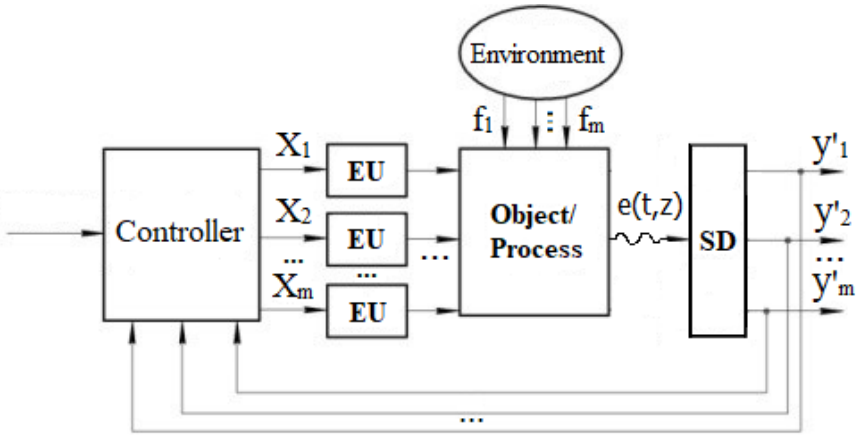

Fig.2. Functional scheme of the multi-alternative ACS

In contrast to Fig.1, in Fig.2 the following designations are introduced: $e(t,z)$ – optical radiation that carries spectroscopic information about the object/control process; SD- optical spectral device.

Functional scheme of a diffraction spectral instrument using the radio-optical approach

The general functional scheme of the diffraction prism spectral device [7] is shown in Fig.1, it consists of two parts: the collimating system (A) and the analyzing (resolving) system (B). The collimating system (A) generates the analyzed signal in the form of a uniform plane wave beam. The analyzing system (B) includes a dispersing system (DS), an optical system consisting of two layers of free space and a positive lens between them and a recording device. The recording device performs photodetection and temporal integration of its results and ultimately provides the recipient with spectroscopic information in the form of an energy spectrum.

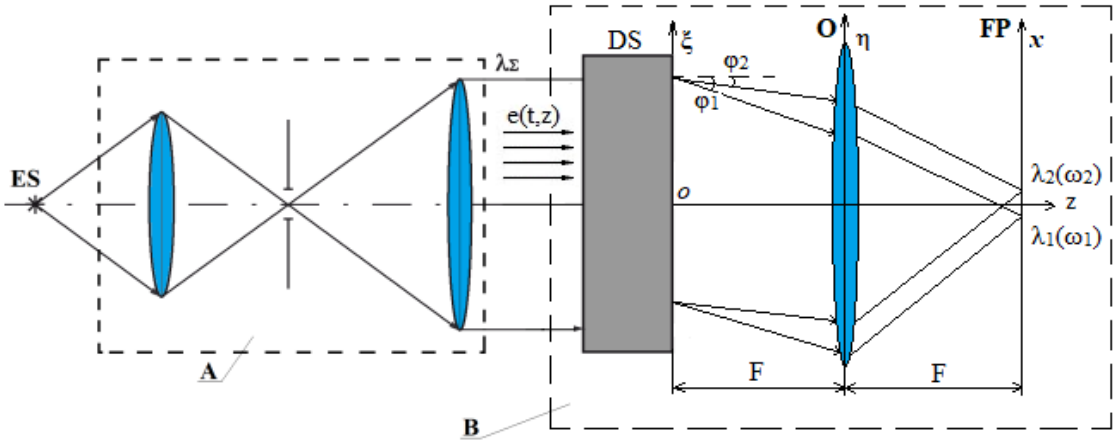

Fig.3. Optical scheme of the diffraction prism spectral device

The dispersing system, as a one-dimensional transparency [17], introduces the analyzed optical radiation into the analyzing system, which includes two layers of free space and an ideal thin positive lens with a focal length F between them. Within the framework of the radio-optical approach [18], it was shown that an optical system including in the following order: a layer of free space with an extension F, an ideal thin positive lens with a focal length F, and a layer of free space with an extension F. When illuminating this optical system with a uniform flat monochromatic light wave, a spatial transformation of the function $f(\xi, z=0)$ is performed in the form [19]:

$$S_s(\omega_x,\omega') = \sqrt{\frac{2\pi c_0 F}{\omega'}} \cdot \exp(i\pi/4) \cdot \hat{F}[f(\xi,z=0)] = \sqrt{\frac{2\pi c_0 F}{\omega'}} \cdot \exp(i\pi/4) \cdot \int_L f(\xi,z=0)\exp(-i\omega_x\xi)d\xi, \quad (1)$$

Where $S_s(\omega_x,\omega')$ - spectrum of spatial frequencies; $\hat{F}$ - direct fourier transform operator; $\omega_x = \dfrac{\omega' x}{c_0 \mathrm{F}}$ - spatial frequency; c_0 - скорость света в вакууме; F - focal length of the ideal thin lens; ω' - angular frequency of uniform flat monochromatic wave incident on dispersing system:

$$e(z,t) = \dot{E}_0 \exp[i(\omega' t - k' z)], \tag{2}$$

where $\dot{E}_0$ - complex amplitude; t - current time; k' - wave number; z - direction of wave motion $e(z,t)$.

Spectrum of spatial frequencies $S_s(\omega_x,\omega')$ is formed in plane (fp) $z = 2\mathrm{F}$ on sensitive surface of photodetector as spatial modulation of space-time signal

$$s(x,t) = \dot{E}_0 \exp(i\omega' t) \cdot S_s(\omega_x,\omega'). \tag{3}$$

In this case, the function $f(\xi, z=0)$ is the result of spatial modulation of a uniform flat monochromatic wave (2) by a dispersing system, which is considered a one-dimensional placard. According to the definition of the transparency transmission function [14], in what follows, we mean

$$f(\xi, z=0) = \mathrm{T}(\xi). \tag{4}$$

Performing the spatial fourier transform (1) served as a basis to call such a system an optical coherent fourier processor [20].

The dispersing system of the prism spectral device is a prism, here it is a straight triangular prism with a base in the form of an isosceles triangle. The cross section of the prism is shown in Fig. 2.

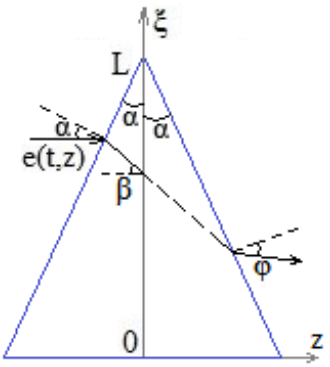

Fig.4. Optical scheme of the dispersive system of a prism spectral device

The diffraction prism spectral device analyzing system under illumination by a flat homogeneous monochromatic light wave is considered as an optical coherent Fourier processor [19], where the input device for the processed signal is a prism.

The main prism parameters are: the size of its input aperture L, the angle of the prism α, and the refractive index of the prism material $n(\cdot)$, attenuation in the prism material is not taken into account. Through these parameters, the transmission function of the prism as a phase transparency, takes the form of [7]:

$$\dot{\mathrm{T}}(\xi,\nu) = \exp[(i\nu n(\nu)\xi tg\alpha / c_0], \tag{5}$$

where $\nu -$ is the time circular frequency of a monochromatic light wave; c_0 – the speed of light.

The action of an optical coherent Fourier processor is described by the ratio [19]:

$$S_x(\omega_x) = \alpha \int_L f(\xi) \exp(-i\omega_x \xi) d\xi, \tag{6}$$

where $S_x(\omega_x) -$ is the spatial frequency spectrum; $\omega_x = \nu x / c_0 \mathrm{F}$- is the spatial frequency; $\alpha = \sqrt{2\pi c_0 F / \nu}$; $f(\xi) -$ spatial signal in the input plane.

The most important relation of the linear systems theory is the «input $x(\cdot)$ - output $y(\cdot)$ » ratio of a linear system [21]

$$y(\lambda) = \hat{\mathrm{L}}\, x(\lambda) = y(\lambda) = \int_{\Lambda} H(\lambda,\lambda')x d\lambda' , \tag{7}$$

where $\hat{\mathrm{L}}-$ is a linear bounded operator; $H(\lambda,\lambda')-$ is the instrument function; the meaning of variables λ,λ' and the interval of integration Λ are determined by the current tusk.

The relation (7) is a von Neumann problem, representing a linear operator in the form of an integral [22]; in relation to the linear systems theory, its solution is proposed in [8], where the meaning of the integral transform of the linear integral operator (7) is defined in the form:

$$H(\lambda,\lambda') = \hat{\mathrm{L}}\,\delta(\lambda-\lambda') . \tag{8}$$

When performing spectral measurements, this $\delta-$effect is represented by a spectral function $\delta(\omega-\nu)$ that has no physical interpretation, however, the following expression has a clear physical meaning:

When performing spectral measurements, such an effect is represented by the spectral function that does not have a physical interpretation, however, a clear physical meaning is reflected by a harmonic vibration, under the influence of which the instrument function of a spectral device that performs measurements of the spectrum of oscillatory processes is determined:

$$\hat{\mathrm{F}}^{-1}\,\delta(\omega-\nu) = \exp(i\nu t), \tag{9}$$

where $\hat{\mathrm{F}}^{-1}-$ is the inverse Fourier transform operator; $\omega-$ is the circular time spectral frequency.

The complex spectrum spread function of the diffraction prism spectral device, as a wave analyzer, is determined when its analyzing system is exposed to a homogeneous plane monochromatic light wave, which can be represented in a scalar form characteristic of optical spectrometry:

$$e(z,t) = \exp(i(\nu t - kz)) = \hat{\mathrm{V}}\hat{\mathrm{F}}^{-1}\exp(i\nu t) , \tag{10}$$

where $k = \nu / c_o -$ is the wave number;

$$\hat{\mathrm{V}} = \int_{-\infty}^{\infty} e(t')\delta((z/c_0)-t-t')dt' . \tag{11}$$

If the analyzing system action is described by a linear bounded operator $\hat{\mathrm{A}}$, then the result of complex spectrum measurement, according to (7), has the form:

$$S_a(\omega) = \int_{-\infty}^{\infty} H(\omega,\nu)S_0(\nu)d\nu , S_0(\nu) = \hat{\mathrm{F}}\,e(t) , \tag{12}$$

where $\hat{\mathrm{F}}-$ is the direct Fourier transform operator; the complex instrument function

$$H(\omega,\nu) = \hat{\mathrm{A}}\hat{\mathrm{V}}\hat{\mathrm{F}}^{-1}\,\delta(\omega-\nu) = \hat{\mathrm{L}}\,\delta(\omega-\nu) \tag{13}$$

satisfies the definition (8).

When a homogeneous plane monochromatic light wave falls on a prism, a spatial-temporal signal acts on the output face of the prism, i.e., on the input of an optical coherent Fourier processor

$$s(t,\xi,z=0) = \exp(i\nu t)\cdot\dot{\mathrm{T}}(\xi,\nu) , \tag{14}$$

which, according to the ratio (6) is converted by an optical coherent Fourier processor to the form:

$$\mathrm{S}(\omega_x,t) = \exp(i\nu t)\int_0^L \dot{\mathrm{T}}(\xi,\nu)\exp(-i\omega_x\xi)d\xi , \tag{15}$$

where $\mathrm{S}(\omega_x,t)$ - is the spatial-temporal signal in the output plane of an optical coherent Fourier processor.

In the paper [11] it is demonstrated that the complex spectrum spread function is a necessary and sufficient condition for calculating the complex instantaneous spectrum, the definition of which is proposed in the

paper [23], i.e., a complex instantaneous spectrum of optical vibration $e(t)$ is formed in the output plane of a diffraction prism spectral device.

In the output plane of the diffraction prism spectral device acts a spatial-temporal optical signal

$$e(t, z = 2\mathrm{F}) = \exp(i\omega t) \cdot S_a(\omega, t), \tag{16}$$

which is subject to photodetection, which results in a characteristic for optical spectral measurements' energy spectrum. The energy spectrum measurement $\bar{G}(\omega)$ includes [11] the operation of the function calculating $|S_a(\omega,t)|^2$ and the operation of its time-averaging over the interval $[-T_R, T_R]$, i.e.

$$\bar{G}(\omega) = \frac{1}{2T_R} \int_{-T_R}^{T_R} S_a(\omega,t) S_a^*(\omega,t) dt. \tag{17}$$

Integration of the expression (17) demonstrated [24] that there is an energy spectrum estimation with the Bartlett spectral window.

As noted previously, to form the output vector, it is necessary to read out the spectrometric information using the CCD, the conditional scheme f which is shown in Fig.5.

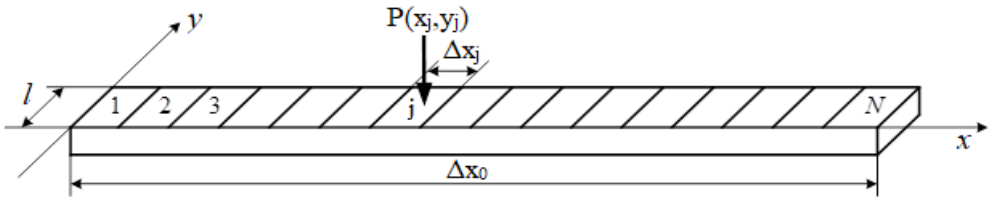

Fig.5. CCD (j-th element)

Since the frequency interval associated with the j-th pixel, $\Delta\omega_j << \Delta\nu$, we assume zero approximations in the series involved in the calculations of functions [11], which are not given here.

Electric current in the $j-$ th pixel

$$i_j = \gamma \frac{q_e p}{\hbar \nu_j}, \tag{18}$$

where $\gamma-$ is the quantum efficiency; $p-$ the optical radiation power incident on the sensitive surface of the $j-$th pixel ; $\hbar-$ Planck's constant.

The power p is given by the ratio:

$$p = \iint_{\Delta S_j} \mathrm{P} ds, \tag{19}$$

where P - the Poynting vector; $\Delta S_j = \Delta x_j l$ - the sensitive surface area of the CCD $j-$th pixel.

The Poynting vector

$$\mathrm{P} = \mathrm{E} \times \mathrm{H} = |\mathrm{E} \times \mathrm{H}| s = \sqrt{\varepsilon / \mu} \cdot |\mathrm{E}|^2 s = \sqrt{\mu / \varepsilon} \cdot |\mathrm{H}|^2 s, \tag{20}$$

where E, H - are the electric and magnetic vectors, respectively, s - is the unit vector; ε, μ - are the permittivity and permeability, respectively.

Comparison of expressions demonstrates that the values of the energy spectrum $\bar{G}(\omega)$ are proportional to the power p. Therefore, the current from the CCD j-th pixel is given by the ratio:

$$i_j = \beta l \int_{\Delta\omega_j} \bar{G}(\omega) d\omega, \tag{21}$$

where β - is the coefficient of proportionality; $\Delta\omega_j = \Delta x_j / \mathrm{F} n'(\nu_j)$.

The currents i_j allow to form output vectors $\{y'_k\}$ and thus to realize the possibility of multi-alternative automatic control of physical and physico-chemical processes accompanied by optical radiation.

Input-output ratio of a prism spectral device for complex spectra

The input-output ratio of a spectral device for complex spectra is given in the form of a linear integral operator [23]:

$$\dot{S}_a(\omega,t) = \int_{\Delta\Omega} \dot{K}(\omega,\omega',t)\cdot\dot{S}_0(\omega')d\omega', \tag{22}$$

where $\dot{S}_a(\omega,t)$ - instrumental complex spectrum; ω - current temporal angular spectral frequency; $\Delta\Omega$ - - the band of the analyzed frequencies; $\dot{K}(\omega,\omega',t)$ - complex instrumental function; $\dot{S}_0(\omega')$ - complex mathematical spectrum of the analyzed optical vibration $e(t)$, i.e.

$$\dot{S}_0(\omega) = \hat{F}[e(t)] = \int_{T_s} e(t)\exp(-i\omega t)dt, \tag{23}$$

where T_s - signal duration $e(t)$.

The apparatus function, according to the definition of the general theory of linear systems, is the response of a linear system to $\delta-$action, the meaning of which is determined by the problem being solved; in the case of measuring a complex spectrum, the $\delta-$action is a spectral function $\delta(\omega-\omega')$. Then the complex instrumental function of the spectral device is given by the expression:

$$\dot{K}(\omega,\omega',t) = \hat{L}[\delta(\omega-\omega')], \tag{24}$$

where $\hat{L}$ - some linear bounded operator, which in general form establishes the transformation of the spectral function (23) when performing spectral measurements.

The complex instrumental spectrum when measured with a prism spectral device is described by the expression:

$$\dot{S}_a(\omega,t) = \int_{\Delta\Omega} \frac{\sin\left[(\omega-\omega')\frac{T_a}{2}\right]}{\omega-\omega'}\cdot\exp(i\omega' t)\cdot\dot{S}'(\omega')d\omega'. \tag{25}$$

The complex instrumental function establishes a time-varying complex spectrum and is a necessary and sufficient condition for measuring the instantaneous complex spectrum of the signal $e(t)$ [11], the definition of which (instantaneous spectrum) was proposed in [23].

In expression (25), the quantity

$$\omega = \omega(x,\omega') = \frac{\omega' x}{2n(\omega')F\,\mathrm{tg}\,\alpha} \tag{26}$$

is the current temporal spectral angular frequency, which is expressed as a non-linear function of the coordinate x, since the refractive index of the prism material $n(\omega')$ is described by a non-linear function. Further, the quantity

$$T_a(\omega') = \frac{n(\omega')L\,\mathrm{tg}\,\alpha}{c_0}, \tag{27}$$

having the dimension of time, is interpreted as "analysis time", since it determines the resolution of the prism spectral instrument when measuring the instantaneous spectrum.

When measuring the spectra of optical radiation, i.e. signals of the optical range of electromagnetic phenomena, the recipient of the spectroscopic information is given energy spectra.

When measuring the complex instantaneous spectrum, the energy spectral function is understood as the energy spectrum $G_a(\omega)$ as a result of performing the following operations [11]:

$$G_a(\omega) = \frac{1}{T_R} \int_{T_R} \left| \dot{S}_a(\omega, t) \right|^2 dt, \tag{28}$$

where the time integration of the photodetection result is presented.

The integration in expression (28) was performed in [23, 11], as a result, the relation:

$$G_a(\omega) = M \cdot \int_{\Delta\Omega} \frac{\sin^2\left[(\omega - \omega') \frac{T_a}{2} \right]}{(\omega - \omega')^2} \cdot G'(\omega') d\omega', \tag{29}$$

where $G'(\omega') = \left| \dot{S}'(\omega') \right|^2$; $M = const$.

Relations (28) and (29) indicate that the phase-frequency distortions of the complex spectrum caused by the function $\arg \dot{H}(\omega')$ do not affect the measurement result of the energy spectrum, while the amplitude-frequency distortions described by the function $\left| \dot{H}(\omega') \right|$ distort the measurement result of the energy spectrum.

Relation (29) is not a usual convolution, since the temporal spectral angular frequency ω is a function ω'; moreover, the quantity T_a is also a function ω' and is not a constant. This is the internal difference between the integral operator (29) and the corresponding integral operator introduced in [2].

Conclusion

This paper is a continuation of the application of the radio-optical approach in the theory of diffractive optical spectral devices. Earlier, radio optics methods were used to describe the operation of a grating spectral device [8, 10, 11], which made it possible to give a consistent description of the conversion of the optical radiation spectrum from the input aperture of the spectral device to the issuance of spectroscopic information to the recipient in the form of an energy spectrum. The intermediate result is the statement of the complex spectrum of optical radiation.

In this paper, the use of radio-optical ideas also made it possible to show the processing of the optical radiation spectrum from the entrance aperture of a prism spectral device to obtain an energy spectrum and also to state the complex instrumental spectra in spectroscopic measurements in the optical range with a prism spectral device.

It should be emphasized that the noted specific errors in spectral measurements in the optical range can hardly be established within the framework of the existing methodology of optical spectrometry based on the principles of geometric optics.

The possibility of multi-alternative automatic control of physical and physicochemical processes accompanied by optical radiation by forming output vectors based on spectroscopic measurements with a diffraction prism spectral device is demonstrated. These measurements provide spectroscopic information about the various sides of the above-mentioned processes' development, which can be used for multi-alternative automatic control.

The use of a diffraction prism spectral device as an integral part of a multi-alternative automatic control system required the development of an alternative description of the operation of such a device, seeing that it is necessary to describe the process of output vectors forming and their properties. In the framework of a new approach to the DPSD action description, it is demonstrated that a complex instantaneous spectrum of optical radiation vibrations is formed in the input plane of this device. Further transformations of this spectrum allowed us to establish that the output vectors are being formed on the basis of an estimate of the energy spectrum with a Bartlett spectral window.

ACKNOWLEDGMENT

The work was carried out with the financial support of the Ministry of Science and Higher Education of the Russian Federation, Agreement No. FSRF-2020-0004, "Scientific foundations for the construction of architecture and communication systems of on-board information and computing complexes of a new generation for aviation, space systems and unmanned vehicles".

References

[1] G.S. Gorelik Oscillations and waves / Moscow: Fizmatlit, 2007.

[2] S. G. Rautian Real spectral devices / S. G. Rautian // Advances in physical sciences, 1958. T. 66. №. 3. pp. 475-517.

[3] V. I. Malyshev Introduction to experimental spectroscopy / Moscow: Nauka, 1979. 480 p.

[4] K. I. Tarasov, Spectral devices / K.I. Tarasov, edition 2-nd L .: Machine building, Leningrad Branch, 1977. 367 p.

[5] V.V. Lebedeva, Optical spectroscopy technique, 2-d edition, Publishing house of Moscow University, Moscow University, 1992. 352 p.

[6] Yu.M. Belyakov, N.K. Pavlycheva, Spectral instruments, Kazan: Izd-vo Kazan. state tech. un-ta, 2007. 203 p.

[7] A.N. Zaidel, G.V. Ostrovskaya, Yu.I. Ostrovsky Technique and practice of spectroscopy / Moscow: Nauka, 1978. 392 p.

[8] Moskaletz O.D. Classical and quantum approach to power spectrum measurement by diffractional methods. Proc. SPIE // Vol. 3900, P. 297-308. 1999.

[9] V.I. Kazakov, O.D. Moskaletz Complex spectra in a diffraction grating spectral device // Radioindustry. - 2016. - № 4. pp. 32-37.

[10] Kazakov V.I., Moskaletz O.D. Alternative theory of diffraction grating spectral device and its application for calculation of convolution and correlation of optical pulse signals // Proc. SPIE 10680, Optical Sensing and Detection V, p. 1068025, 2018/

[11] Kazakov V.I., Kuryleva A.S., Moskaletz D.O., Moskaletz O.D. Instantaneous spectra in spectral and correlation processing of dynamic signal devices of radio and optical ranges and their linear and nonlinear transformations // Proc. SPIE 10680, Optical Sensing and Detection V, p. 1068025, 2018/

[12] M.A. Vaganov, O.D.Moskaletz. Application of contactless optical spectroscopy in problems of multi-alternative automatic control of physical and physico-chemical processes // Sensors and systems. 2019. №11. C. 5 - 10.

[13] S.L.Podvalniy, E.M.Vasiliev Intelligent systems of multi-alternative management: principles of construction and ways of implementation. // All-Russian meeting on management problems. AMMI 2014. Moscow, 16 - 19 Juli 2014. p.996 – 1007.

[14] Patent 86734 RF, IPC8 G 01 J 3/26. The parallel spectrum analyzer of optical signals range / I. N. Archipov, M. A. Vaganov, S. V. Kulakov, O. D. Moskaletz, L. N. Preslenev, V. N. Prokashev (RF). № 2009116195/22 // Inventions and utility models. 2009. № 25. 2 p.

[15] Moskaletz .O.D., Serdiuk K.V Complex spectra in a prizm optical spectrum device. // XX International Conference for Young Researches. Wave Electronics and Its Applications in the Information and Telecommunication Systems. Saint - Petersburg, 26 - 30 June 2017. P. 175 – 179.

[16] I.V. Miroshnik Automatic control theory. Linear systems / St.-P.: Piter. 2005. 336 p.

[17] Born M., Wolf E.. *Principles of optics*. Second (revised) edition. PERGAMON PRESS. Oxford-London- New York-Paris-Frankfurt, 1964. 856 p.

[18] Zverev, N.S. Stepanov, Foreword of editors, Experimental radiooptics / Moscow: Nauka, 1979, pp. 6-10.

[19] Papoulis A. Systems and Transforms with Applications in Optic. McGRAW - HILL BOOK COMPANY. New York - St. Louis - San Francisco - Toronto - London – Sydney, 1968

[20] Kendall Preston, Jr. Coherent optical computers. McGraw-Hill Book Company, 1972. 400 p.

[21] Khurgin Yu.I., Yakovlev V.P., Finite functions in physics and engineering. Ed. 2nd, ext. M .: Book House "LIBROKOM", 2010.

[22] B. V. Korotkov Integral operators. Novosibirsk: Nauka. Siberian branch. 1983. 224 p.

[23] Moskaletz .O.D. Dynamic signals and spectral measurements // Progress in modern radio-electronics. 2013. №2. C. 152-158.

[24] Moskaletz D O., Moskaletz O.D. Complex and Energy Spectra in Optical Diffraction Spectral Devices // Electronic ISBN: 978-1-7281-2288-5 Print on Demand(PoD) ISBN: 978-1-7281-2289-2 INSPEC Accession Number: 19058550

REVIEW OF EXISTING APPROACHES TO THE TASK OF AUTOMATIC EMOTION RECOGNITION

Ksenia Sokolova

Saint-Petersburg State University of Aerospace Instrumentation, Saint-Petersburg, Russia
E-mail: ksusha.so-va@yandex.ru

Abstract
The article discusses the main approaches to the analysis of photo and video data in order to extract information about the emotional state of the people depicted on them, analyses the current state of the market for affective computing systems and provides information on the main commercial products offered on the market.
Keywords: affective computing, emotion recognition, image processing algorithms, machine learning.

There are numerous operational tasks related to facial recognition and analysis of human emotions nowadays. Various human-interacting systems based on user emotional response are being developed. Assistant robots recognize the psychological state of a person and react in an appropriate way.

Psychologists, doctors, criminologists, proctors, advertising and marketing specialists, entertainment industry workers use emotion recognition by facial expressions in their work. Technologies that automate this process are constantly being improved. Scientific fields related to construction of automated algorithms that understand human emotions and demonstrate a suitable response are being actively developed. There is a high demand for commercial products, the functionality of which includes automated recognition and analysis of emotions based on images, video data, and audio information. However, the recognition accuracy that developers manage to achieve is still far from ideal. Some of these systems use physiological data - heart rate, respiration, body temperature. These systems could provide accurate information however they are expensive and non-ergonomic. The development and optimization of systems and algorithms for detecting human emotions will not lose its relevance for many years.

Let us consider some approaches to the problem of automatic emotion recognition and retrieve an overview of various types of data, on which the analysis of the emotional state of a person is executed.

Emotions play substantial role in the interaction between people. The expression of emotions can vary from person to person. The way of emotion demonstration depends on cultural and national features. However, there are a number of basic emotions that are understandable by absolutely any person, regardless of his belonging to any culture. Basic emotions include:

- fear,
- anger,
- disgust,
- joy,
- sadness,
- surprise,
- contempt.

This list of universal emotions was derived by Paul Ekman during a study of isolated tribes' nonverbal behavior. He also developed Facial Action Coding System (FACS) that allows to record facial expressions as a sequence of symbols. This system has found its application in psychiatry and forensic science. Some algorithms for automatic recognition of emotions based on the Ekman system will be discussed in this article.

Numbers from one to forty-six (with the exception of the number 40) in FACS indicate the facial muscles involved in the expression of a particular emotional state. The number zero indicates a neutral, relaxed facial expression. Figure 1 shows the codes of FACS assigned to certain muscles.

The numbers from 51 to 60 code for head movements, from 61 to 69 for eye movements. There are codes for non-verbal behavior, gestures, body turns, nervous trembling, and so on. Letter codes reflect the intensity of motor activity and its symmetry. There are also a number of codes to reflect a particular face part visibility for the analysis of non-verbal behavior. For example, contempt according to the Ekman system is coded as "R12A + R14A", a sincere smile as "6 + 12" [1].

It is generally accepted that any complex emotion can be represented as a combination of basic emotions. A human being has a wide range of emotions that could be expressed with different intensities.

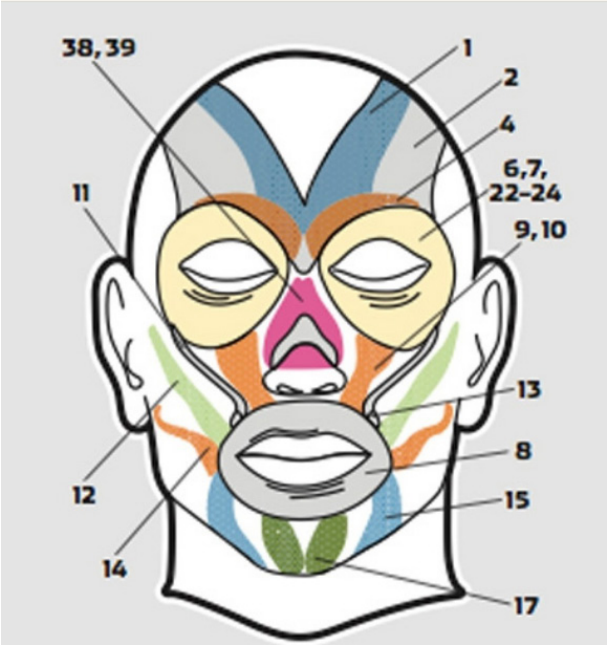

Figure 1 – Codes of facial muscles according to the Paul Ekman system

In addition to discrete models, continuous ones have been developed to evaluate the extant of expression. One of such models is the D. Russell system which represents a two-dimensional basis. In this system, each emotion is described by such parameters as "valence" and "intensity". Figure 2 is a schematic representation of Russell's model. The “sign” (valence) of emotional experience is measured along the horizontal axis, and its intensity along the vertical axis.

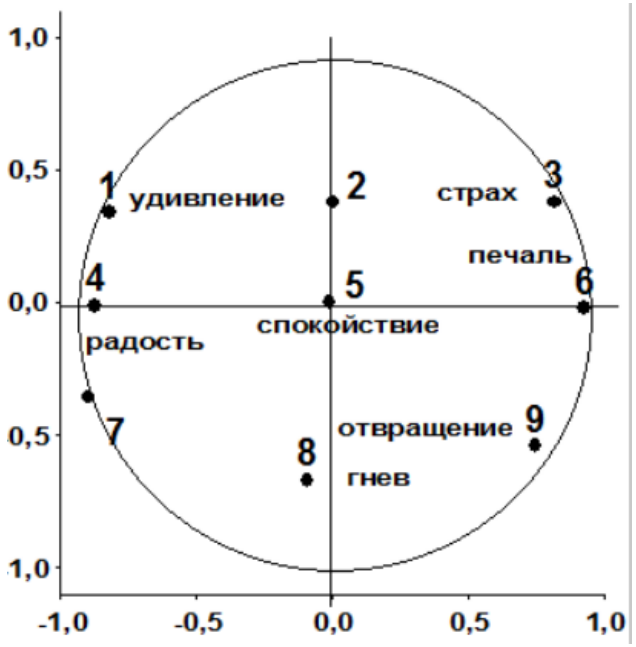

Figure 2 - Schematic representation of the Russell model

The Russell model has become widely used in solving problems of automatic recognition due to its conciseness [2].

Most of modern automatic emotional state detection systems analeses several types of data simultaneously. This could increase the probability of getting the right decision. The most common types of information used for processing are:

- photo images,

- frame sequences,
- audio recordings,
- video data,
- physiological data (heart rate, respiration, perspiration, etc.) obtained using medical equipment or specialized electronic sensors.

Sometimes it is necessary to consider the context and dynamics emotional state to identify it correctly. The same facial expressions can often be characteristic of several mutually exclusive emotions. Therefore, a single face image is not enough for an unambiguous solution. It is also necessary to examine the body position. That is why various types of data should be analyzed to build classifiers. A number of studies show the importance of context in interpretation of emotions by photographs. An example from a by Ronak Kosti study is demonstrated below [3]. Figure 3.a shows an image that is disconnected from the context, what creates difficulties in interpreting the emotional state of the child. Figure 3.b gives "clues" that could clarify the situation.

Figure 3 – Evaluation of the emotional state of the child: a) – without context, b) – context

Similar results are given in the study by L.F. Barret [4]. The figure below shows an example presented in her paper "Context in Emotion Perception". It can be assumed that the woman at figure 4.a, is in great pain. However, when considering the image in context (figure 4.b), her emotion can be described as “the joy of victory.”

Figure 4 – An example of the influence of an external context on the perception of a person's emotional state, given in the study by L. Barrett

There are two main approaches to solving the problem of automatic detection of human emotions based on visual data analysis. In the first case, information is processed by a classifier constructed using key points. One of the tasks to be solved in his approach is face detection. Ehe open computer vision library "OpenCV" is one of the examples of such solutions. [5]. The image is marked using a special algorithm, then the coordinates of the points attached to the face parts are analyzed. Thus, facial expressions can be considered and according to the Ekman system. It should be borne in mind that in this case the image should be aligned and static. Figure 5 shows the process of marking up an image using the control point method, followed by binding the points to coordinates in space.

Figure 5 – Attaching points to a coordinate system [6]

The advantages of the key point method are:

- implementation simplicity,
- the presence of algorithms for determining the position of the face in the image, identifying key points and linking them to coordinates.
- The disadvantages of this approach include:
- relatively low accuracy of recognition (when recognizing facial expressions by points, a significant part of the information is lost, which leads to errors);
- the requirement that the position of the face be aligned.

The second method is based on the Machine Learning. There are many opportunities for building a classifier based on a neural network. The sources of initial information about the external manifestations of emotions are specialized data sets marked according to the required parameters. Such sets are usually available in the public domain.

- The advantages of this approach include:
- Ability to use different source data (set of frames / video sequence / sound);
- a large number of signs for reconciliation;
- the ability to track emotions in dynamics;

- higher recognition accuracy (due to the possibility of analyzing a larger number of features).
- The disadvantages of the considered method are:
- high requirements for the computing power of the equipment when using the system;
- labor intensity in comparison with the method of control points.

Let us consider some of the automatic emotion recognition systems on the market. The comparative characteristics of these systems are represented in Table 1.

Table 1

Overview of the market for automatic emotion recognition systems

Product name	Developer	Application	Data type	Functions	Technology
FaceReader [8]	Noldus (Netherlands)	Commercial use	Video sequence	7 categories of emotions, gender, age, nationality	Key points grid overlay
EmoDetect [9]	«Neurobotics» (Russia)	Marketing research, criminology	Photo and video data	Ability to track the emotional state in dynamics, 6 categories of emotions	Not specified by the manufacturer
Neurodata Lab [10]	Neurodata Lab (Russia)	Marketing, banking services	Video and audio recordings	Analysis of the emotional state by movements and gestures, assessment of physiological parameters (pulse, breathing) without using physical sensors	A neural network trained for specific tasks
The Face Analysis System [11]	MMER-Systems (Germany)	Commercial use	Video sequence	Gender, age, nationality, 6 emotional states	Superimposing a deformable mesh with key areas
eMotion Software [12]	Visual Recognition (Netherlands)	The system is designed for a wide range of commercial tasks. Details are not specified by the manufacturer.	Photo images	Identification of 6 emotions	Creating a 3D model of a face, followed by highlighting the key areas
CompanionMX [13]	Cognito	Healthcare	Audio recording	Identification of signs of anxiety, anxiety, assessment of the psychological state of the patient	

Most modern recognition systems use several classifiers built using different approaches at once. Several types of data are used for detection to reducing the likelihood of an erroneous determination of the emotional state. By combining the results obtained using different methods, it is possible to achieve recognition accuracy.

As a result of an analytical review of the market of goods and services that provide emotion detection capabilities, it was found that there is a high demand for affective computing systems in different fields and for various tasks. A high potential for the development of such systems and algorithms has been revealed. Affective computing is a relatively new and rapidly developing branch of computer technology. Systems that interact with a person by means of determining emotions and demonstrating an appropriate response will enter our daily routine in next few years.

References

1. Петров А. Н. По ту сторону слов // Популярная механика. №3. 2012.

2. Russell, J. A. A circumplex model of aiiect //Journal of Personality and Social Psychology – 1980.

3. Ronak Kosti, Jose M. Alvarez, Adria Recasens, Agata Lapedriza. Context Based Emotion Recognition using EMOTIC Dataset // IEEE TRANSACTIONS ON PATTERN ANALYSIS AND MACHINE INTELLIGENCE – 2020.

4. Lisa Feldman Barrett. Context in Emotion Perception // Psychological Science № 5. 2011.

5. Программа Open CV https://opencv.org/opencv-4-5-4 (дата обращения 05.12.21).

6. Введение в задачу распознавания эмоций// Блог компании «Центр речевых технологий» URL: https://habr.com/ru/company/speechpro/blog/418151

7. Архив публикаций MIT Affective computing https://www.media.mit.edu/groups/affective-computing/publications (дата обращения 05.12.21).

8. Программное обеспечение FaceReader URL: https://www.noldus.com/facereader (дата обращения 28.11.21).

9. Сервис Emodetect URL: https://emodetect.ru (дата обращения 16.02.22).

10. Описание сервиса Neurodata Lab URL: https://vc.ru/services/93624-ocenivaet-puls-i-dyhanie-po-video-chtoby-ponyat-emocii-klienta-istoriya-rossiyskoy-razrabotki-neurodata-lab (дата обращения 16.02.22).

11. Программное обеспечение MMER URL: http://ww17.mmer-systems.eu/

12. Программное обеспечение eMotion http://www.visual-recognition.nl/eMotion.html (дата обращения 16.02.22).

13. От понимания к проявлению: способен ли ИИ испытывать эмоции URL: https://hub.forklog.com/ot-ponimaniya-k-proyavleniyu-sposoben-li-ii-ispytyvat-emotsii/ (дата обращения 16.02.22).

COMPARATIVE ANALYSIS OF METHODS FOR ASSIGNING PARAMETERS TO END DEVICES IN LORAWAN

Nikita Stepanov

Saint-Petersburg State University of Aerospace Instrumentation,
B.Morskaya 67, 190000, Saint-Petersburg, Russia
E-mail: Leos29-07@yandex.ru

Abstract
We present a comparative analysis of LoRaWAN network studies for three typical scenarios (one base station, several base stations and several providers). We focus on LoRaWAN end devices parameter assignment algorithms. We identify and formulate typical optimization problems.
Keywords*:* wireless connection, LoRaWAN, IoT, optimization problems, multiple access.

Introduction

Nowadays, Internet of Things (IoT) devices are increasingly common in everyday life. An increase in the performance of communication systems is already associated with the specifics of the environment, adjusting algorithms to the needs of services, a load of systems due to a large number of smartphones, the spreading of IoT sensors, and transport in loaded areas. All of these cases lead us to the problem of scaling

This paper provides an overview of the existing methods for assigning LoRaWAN parameters to increase performance. LoRaWAN is one of the most popular low-power wide-area networks (LPWAN). Most of them are listed in the excellent survey [1]. However, here in this work, we will focus on the network parameter assignment topic. The research of parameters assignment is a widespread topic since it has already been shown that in particular cases, a specific set of the parameters for end devices (ED) can increase the network performance several times [2]. The network performance is defined as the ability of the base station to receive messages from a large number of devices, which is achieved by increasing the packet delivery rate (PDR) and device density. However, the question of a network configuration for the general case during the deployment phase remains open. The next section describes different scenarios for LoRaWAN network; further provides an overview of existing parameters assignment methods; the next section provides a comparison analysis; finally, further gives typical formulations of optimization problems. The last section provides a conclusion.

Scenarios for LoRaWAN

A scenario with one base station will be called scenario A below. The main idea of the scenario is the presence of one base station and devices located around it at a certain radius. The system has fixed parameters as several frequency channels, bandwidth, message payload size, message frequency. All messages are sent without acknowledgement.

A scenario with several base stations will be called scenario B below. In this scenario, a message can be successfully received at one base station, even if a messages collision occurred while receiving at another base station.

A scenario with several base stations belong to different operators will be called scenario C below. The most realistic scenario is the coexistence of several LoRaWAN operators. Moreover, there may be the same or a different number of operator base stations in each operator's network in a specific area.

Related work

Let's review the works in which the scenarios described above are investigated. The results of this review are presented in Table 1.

Summing up the consideration of various scenarios of the network operation, it can be noted that most of the works are based on scenarios of types A and B. In most cases, the authors try to consider a slightly more general version of the scenario, in which one of the assumptions will be absent, for which a new solution is proposed. The result of the review made it possible to identify several types of optimization problems.

Table 1

Comparison of network simulation scenarios

Reference	*Payload size*	*Coverage radius*	*Number of devices*	*Scenario type*	*Explicit formulation of the optimization problem*
[2]	8 byte	1 km	5000 –10000	A	
[3]	10 byte	1–3 km	1000 –3000	A	+
[4]	20 byte	5 km	200 ED/km^2 – 1000 ED/ km^2	A	+
[5]	20 byte	100 m	–	A	-
[6]	10-50 byte	1–20 km	100 – 1250 per network (400–5000 total))	C	-
[7]	60 byte	3–10 km	100 – 1000	A,B	+
[8]	30 byte	7.5 km	500 – 4000	A	-
[9]	20-169 byte	50–130 m	500	A	-
[10]	51 byte	100–1500 m	100 – 3500	A,B	-
[11]	20 byte	4 × 4 km	1000–5000	A,B	-
[12]	20 byte	99 m and 350 m	100 – 1500	A,B	-

Formulation of optimization problems and goals

The works often describe the problem of network parameters assignment or a specific scenario that requires some approach to the distribution of certain system resources. However, below are still two optimization problems that could be used in most works with some clarifications. The use of such optimization problems makes it possible to compare the presented algorithms with the optimal values obtained as a result of solving the problems.

Optimization problem of maximizing the packet delivery rate [3]:

$$\max_{n_i} \sum_{i=7}^{12} \frac{n_i e^{-\lambda t_i n_i}}{N}$$

$$subject\,to \sum_{i=7}^{12} n_i = N$$

$$n_i \geq 0, i = 7,\ldots,12,$$

where n_i is number of devices with SF_i, t_i is air time of SF_i, λ is message frequency coefficient, N is total number of devices. This optimization problem was solved using the Lagrange multiplier method:

$$n_i = \frac{\prod_{j=k_{min}, j\neq i}^{k_{max}} t_j}{\sum_{l=k_{min}}^{k_{max}} \prod_{j=k_{min}, j\neq l}^{k_{max}} t_j} \cdot N$$

The presented solution equalize PDRs on each SF to maximize the overall probability of successful delivery, i.e. $n_7 e^{-\lambda t_7 n_7} = n_8 e^{-\lambda t_8 n_8} = \ldots = n_{12} e^{-\lambda t_{12} n_{12}}$. However, with an increase in the number of devices, the problem becomes non-convex. In this case, the proposed solution finds a local optimum and finding the numerical optimal solution requires significant computational costs. Moreover, the optimal solution for the non-convex case will drop some SFs and not assign them to any devices.

To eliminate this drawback, an optimization problem was formulated in [6] in terms of the sum of logarithms. In our article, we give the wording using other notations than ours. The optimization problem of assigning the optimal SF coefficient:

$$G_s = \sum_{i=1}^{N} \left(\lambda p_s^i N_c^i \right) T_s,$$

where N_c^i is the number of nodes belonging to operator *i.* The normalized ALOHA bandwidth on each SF can be selected as $G_s \exp\left(-2G_s\right)$. Normalized network bandwidth becomes:

$$\tau = \sum_{s=1}^{S} G_s \exp\left(-2G_s\right),$$

The problem of finding the optimal coefficients of the assignment ratios SF p_s can be formulated as follows:

$$\underset{p_s}{\text{Maximize}} \sum_{s=1}^{S} log\left(G_s \exp\left(-2G_s\right)\right)$$

Subject to

$$\sum_{s=1}^{S} p_s \le 1,$$

$$\sum_{k=1}^{s} p_k \le \sum_{k=1}^{s} \frac{N_k}{N_c}, \forall s = 1, \ldots, S$$

Furthermore, although this formulation solves the above issues, it still requires an expensive numerical solution. Therefore, in practice, the proposed solution by the Lagrange multiplier method [3] is more suitable since all SF are covered and equalize PDRs.

The optimization problem of minimizing the load of each subchannel presented in [12]. The goal is to minimize thedifference between the utilization coefficients for each pair of frequency channels (CF) and SF, defined as $U_{cf,sf}$, which minimizes the load.

$$\sum_{cfi \in CF} \sum_{sfj \in sf} \left(U_{sfi,sfj} - U_{sfl,sfk} \right)$$

$$cfl : cfl \in CF \wedge cfi \neq cfl;$$

$$sfk : sfk \in SF \wedge sfj \neq sfk,$$

where

$$U_{cfi,sfj} = N_{cfi,sfj} \times airtime\left(\xi, sfi\right) \times \lambda;$$

$$U_{cfl,sfk} = N_{cfl,sfk} \times airtime\left(\xi, sfk\right) \times \lambda;$$

and

$$N_{cfi,sfj} = \sum_{i}^{n} cf_{i,cfi} \times sf_{i,sfj}$$

$$N_{cfl,sfk} = \sum_{i}^{n} cf_{i,cfl} \times sf_{i,sfk},$$

Subject to

$$\sum_{cf \in CF} \left(cf_{i,cf} \right) = 1 \forall i : 1..n$$

$$\sum_{sf \in SF} \left(sf_{i,sf} \right) = 1 \forall i : 1..n,$$

where number of devices $N = \{N_1, N_2, N_3 \dots N_n\}$ with CF and SF; λ is message frequency coefficient, average packet size ξ byte; function $airtime(\xi, sf)$ calculates transmission time according to SF, CR, BW parameters and payload size.

General case of the optimization problem for delivery probability maximization, based on a model from [13].

$$\{k_0, SF_0, R_0, B_0\} = \begin{cases} \arg \max\limits_{k,(SF,R,B)} p_d(\cdot), & p_d(\cdot) \le p_O \\ \arg \min\limits_{k,(SF,R,B)} |\, p_d(\cdot) - p_O \,|, & p_d(\cdot) > p_O \end{cases}$$

where $p_d(\cdot) = p_d(k, SF, R, B)$; k_0 and k is the initial and chosen number of re-transmissions, respectively, R is the transmission rate, B is the bandwidth, p_d is delivery probability and p_O is the target value of the delivery probability.

Conclusion

The paper describes three typical scenarios, reviewed the works in which one or more of these typical scenarios are considered, and algorithms for assigning parameters of end devices to maximize some evaluation metrics of the efficiency of the network operation are considered. In the course of a comparative analysis of the works, three types of formulations of optimization problems have been identified. These optimization problems can be used to develop algorithms for the functioning of real systems. These optimization problems provide boundaries to strive for.

References

[1] F. S. Dantas Silva et al., "A Survey on Long-Range Wide-Area Network Technology Optimizations," IEEE Access, 2021.

[2] Tiurlikova, Aleksandra, Nikita Stepanov, and Konstantin Mikhaylov, "Method of assigning spreading factor to improve the scalability of the LoRaWAN wide area network," 2018 10th International Congress on Ultra Modern Telecommunications and Control Systems and Workshops (ICUMT). IEEE, 2018, pp. 1–4.

[3] Gusev, Oleg, et al., "Data delivery efficient spreading factor allocation in dense LoRaWAN deployments," 2019 XVI International Symposium "Problems of Redundancy in Information and Control Systems"(REDUNDANCY). IEEE, 2019, pp. 199–204.

[4] M. El-Aasser, T. Elshabrawy and M. Ashour, "Joint Spreading Factor and Coding Rate Assignment in LoRaWAN Networks," 2018 IEEE Global Conference on Internet of Things (GCIoT), 2018, pp. 1–7.

[5] Zorbas, Dimitrios, et al., "Improving LoRa network capacity using multiple spreading factor configurations," 2018 25th International Conference on Telecommunications (ICT). IEEE, 2018, pp. 516–520.

[6] Fawaz, Hassan, et al., "Cooperation for spreading factor assignment in a multioperator lorawan deployment," IEEE internet of things journal 8.7 (2020): 5544-5557.

[7] Yatagan, Tugrul, and Sema Oktug. "Smart spreading factor assignment for lorawans," 2019 IEEE Symposium on Computers and Communications (ISCC). IEEE, pp. 1–7, 2019.

[8] Farhad, Arshad, et al., "Interference-aware spreading factor assignment scheme for the massive LoRaWAN network," 2019 International Conference on Electronics, Information, and Communication (ICEIC). IEEE, pp. 1–2, 2019.

[9] Cuomo, Francesca, et al., "Towards traffic-oriented spreading factor allocations in LoRaWAN systems," 2018 17th Annual Mediterranean Ad Hoc Networking Workshop (Med-Hoc-Net). IEEE, pp. 1–8, 2018.

[10] Reynders, Brecht, et al., "Improving reliability and scalability of LoRaWANs through lightweight scheduling," IEEE Internet of Things Journal 5.3 (2018): 1830-1842.

[11] Lima, Eduardo, et al., "Adaptive priority-aware LoRaWAN resource allocation for Internet of Things applications," Ad Hoc Networks (2021):102598.

[12] E. Sallum, N. Pereira, M. Alves and M. Santos, "Improving quality-ofservice in LoRa low-power wide-area networks through optimized radio resource management," Journal of Sensor and Actuator Networks, 9(1), 10.

FORMATION OF A CONSOLIDATED NOMENCLATURE OF REQUIREMENTS FOR VARIOUS TYPES OF PRODUCTS OF THE RADIO-ELECTRONIC INDUSTRY

Albina Tur

Saint Petersburg State University of Aerospace Instrumentation
E-mail: Liona1996@yandex.ru

Annotation
The sale of inauthentic products prevails in most developing countries and becomes widespread in developed countries. In this regard, it is important to establish requirements for the effectiveness of authentication tools designed to counter the circulation of counterfeit and counterfeit products at the national and international level. The purpose of the work was to formulate a range of requirements for products of the radio-electronic industry, in accordance with the standards governing detection methods, reducing the risks of use and decisions on the use of falsified and counterfeit products. As a result of the analysis of regulatory documents, a nomenclature of requirements for products of the radio-electronic industry was formed. The practical significance of the research results lies in the formation of the nomenclature of requirements for the products of the radio-electronic industry, in accordance with the standards governing the tools for ensuring the control of authentic components.

Illicit trade and circulation of non-authentic components cause significant damage to manufacturers, suppliers, consumers and distributors. To achieve effective protection, rational integration of organizational and technical measures is necessary, taking into account the unique characteristics of each type of product and organization. [1]. Product traceability is one of the most important indicators of quality assurance, safety of use, and countering the circulation of non-authentic products. The use of an effective traceability system makes it possible to define tools for controlling the authenticity of components, documents and assessing security risks and countering the circulation of non-authentic products.

Comparative analysis of standards

The increase in non-authentic products is a problem for most electronic component manufacturers. Organizations widely use authentication methods to secure their products. However, it is necessary to define requirements for the effectiveness of authentication methods used to combat the distribution and receipt of non-authentic electronic components at the national and international levels.

Table 1

Comparative table of standards governing the production of authentic products

Standard						
	GOST R 57880-2017 [2]	GOST R 58634-2019 [3]	GOST R 58635-2019 [4]	GOST R 58636-2019 [5]	GOST R 58637-2019 [6]	GOST R 58924-2020 [7]
Name	System of protection against falsifications and counterfeit. Electronic products. Obtaining prevention, detection methods, application risk reduction and solutions for the use of falsified	System of protection against falsifications and counterfeit. Authentic materials. Acquisition Methods	System of protection against falsifications and counterfeit. Methods for ensuring control of the authenticity of products and documents. General	System of protection against falsifications and counterfeit. Traceability of product turnover. General requirements	System of protection against falsifications and counterfeit. Criteria for the effectiveness of authentication solutions used to combat counterfeiting	System of protection against falsifications and counterfeit. Electronic products. Distributor Risk Assessment Methods

Standard						
	GOST R 57880-2017 [2]	GOST R 58634-2019 [3]	GOST R 58635-2019 [4]	GOST R 58636-2019 [5]	GOST R 58637-2019 [6]	GOST R 58924-2020 [7]
	and counterfeit products		provisions			
Territoriality	National	National	National	National	National	National
Destination	organizations that procure and integrate electronic products and assemblies [2]	organizations that carry out activities in the framework of the procurement of material objects of industrial production at any stage of the product life cycle	organizations, whose purpose is to provide an appropriate level of confidence in the authentic products they produce	organizations that carry out activities within the framework of product turnover throughout the entire life cycle of products	all types of organizations that require product authentication	the standard is not specialized to a particular industry
Mandatory performance	The rules for the application of this standard are established in Article 26 of the Federal Law of June 29, 2015 No. 162-FZ "On Standardization in the Russian Federation".	The rules for the application of this standard are established in Article 26 of the Federal Law of June 29, 2015 No. 162-FZ "On Standardization in the Russian Federation".	Not required	Not required	Not required	The rules for the application of this standard are established in Article 26 of the Federal Law of June 29, 2015 No. 162-FZ "On Standardization in the Russian Federation".
Target	This standard has been developed to reduce the risk of acquiring non-authentic electronic components, as well as to create a unified toolkit to reduce the risk of receiving non-authentic products.	This standard has been developed with the aim of maximizing the share of authentic materials throughout the product life cycle. [3].	This standard has been developed to ensure the authenticity of products, documentation and risk assessment based on an effective traceability system. [4].	This standard has been developed with the aim of improving the performance of products in the fight against the circulation of non-authentic components and the management of life cycle problems with a better use of resources.	This International Standard has been developed to integrate performance requirements for authentication methods into the life cycle of products. [6].	This standard has been developed with the aim of improving the quality of products and services through the effective application of a risk management system, including processes and methods for risk assessment as its main component. [7].
Requirements	1.development and application of a control plan to identify non-	1.development and application of a plan for guaranteeing the	1.assessment of threats associated with illegal actions; 2.	1. compliance of product characteristics with mandatory and	1.assessment of tools that reveal the authenticity of products 2.	1. identification of key factors that form risks, vulnerabilities of

Standard						
	GOST R 57880-2017 [2]	GOST R 58634-2019 [3]	GOST R 58635-2019 [4]	GOST R 58636-2019 [5]	GOST R 58637-2019 [6]	GOST R 58924-2020 [7]
	authentic radio-electronic components; 2. Establishment of the process of verification of electronic components; 3. control of non-conforming products to prevent them from entering the supply chain; 4. purchase of electronic products only from authorized suppliers 5. staff training to identify risks and implement actions in relation to non-authentic products; 6.Ensuring the authenticity of purchased radio components.	purchase of authentic materials; 2.supply chain tracking; 3.determining the criticality of products by evaluating the materials used; 4. control of non-compliant materials to avoid getting into the supply chain by fraud 5. control of non-authentic materials to avoid re-entering the supply network; 6.assessment of sources of supply.	list of measures to protect products; 3.control about the characteristics of products in the labeling of the product; 4. control over signs of falsification; 5.traceability of measurements of product characteristics; 6.determination of the necessary criteria for protection measures; 7. approve the concept of protection; 8. implementation of protection measures in practic	additional requirements [5]; 2. implementation of metrological traceability to the production stage; 3.monitoring measurements at all stages of the product life cycle; 4. the use of special identifications at all stages of the life cycle; 5.end-to-end traceability throughout the life cycle	open items to detect counterfeit must be complex; 3. the control process must include physical observation; 4.hidden means of authentication should be designed only in production conditions; 5. control tools must ensure the issuance of an opinion on the spot	the organization and its systems in the processes of supply, pricing in domestic and foreign markets; 2. selection of risk treatment methods that will reduce the risk to an appropriate level; 3. prevention of incidents by analyzing the consequences of previous ones; 4.assessment of risks at the stage of life cycle; 5.assessment of corruption risk; 6. identification of risks; 7. analysis of deviations caused by natural and political factors.
Reporting documentation	1.certificates, declarations of conformity; 2. information on the traceability of deliveries, 3. manufacturer's data; 4. specifications for components; 5. Reports on products that have been in use, repaired, but presented as new products	1.purchase agreements; 2. register of suppliers; 3.packing lists	1. design documentation; 2.technological documentation; 3.operational documentation; 4.repair documentation 5.accompanying documentation	1. route map; 2.technological passport; 3.accompanying ticket.	1.documented information on internal audits; 2.route maps	1. Records on the composition of the marking and operational documentation; 2. contracts for purchases and deliveries; 3.list of measures to minimize damage; 4.records on the origin of products and their conformity 5.records of personnel training to identify counterfeit products.

Conclusion

Thanks to the development of new standards, it is possible to reduce the risks of manufacturers and suppliers, to ensure a high level of consumer confidence in the authenticity of the manufacturer's products and in the reliability of documents and data associated with it.

Referens

1. Sidorov V.O., Shchenikov Ya.A., Tur A.S. *Model vybora metodov vyyavleniya falsificirovannyh elektronnyh komponentov* [Model for the selection of methods for detecting counterfeit electronic components] // SPbGUAP: Metrologicheskoe obespechenie innovacionnyh tekhnologij Mezhdunarodnyj forum. 2020. S. 82-83.

2. GOST R 57880-2017. Sistema zashchity ot falsifikacij i kontrafakta. Izdeliya elektronnye. Predotvrashchenie polucheniya, metody obnaruzheniya, sokrashchenie riskov primeneniya i resheniya po ispolzovaniyu falsificirovannoj i kontrafaktnoj produkcii [Anti-falsification and counterfeit protection system. Electronic products. Prevention of receipt, detection methods, reduction of risks of use and solutions for the use of falsified and counterfeit products] M.: Standartinform, 2017. 46 s.

3. GOST R 58634-2019. Sistema zashchity ot falsifikacij i kontrafakta. Autentichnye materialy. Metody priobreteniya [Anti-falsification and counterfeit protection system. Authentic content. Acquisition methods] M.: Standartinform, 2019. 28 s.

4. GOST R 58635-2019. Sistema zashchity ot falsifikacij i kontrafakta. Metody obespecheniya kontrolya autentichnosti produkcii i dokumentov. Obshchie polozheniya [Anti-falsification and counterfeit protection system. Methods for ensuring control over the authenticity of products and documents. General Provisions] M.: Standartinform, 2019. 28 s.

5. GOST R 58636-2019. Sistema zashchity ot falsifikacij i kontrafakta. Proslezhivaemost oborota produkcii. Obshchie trebovaniya [Anti-falsification and counterfeit protection system. Traceability of product turnover. General requirements] M.: Standartinform, 2019. 12 s.

6. GOST R 58637-2019. Sistema zashchity ot falsifikacij i kontrafakta. Kriterii effektivnosti reshenij po autentifikacii, primenyaemyh dlya borby s kontrafaktnoj produkciej [Anti-falsification and counterfeit protection system. Performance Criteria for Anti-Counterfeiting Authentication Solutions] M.: Standartinform, 2019. 36 s.

7. GOST R 58924-2020. Sistema zashchity ot falsifikacij i kontrafakta. Elektronnye izdeliya. Metody ocenki riska distribyutorov [Anti-falsification and counterfeit protection system. Electronic products. Distributor risk assessment methods] M.: Standartinform, 2019. 19 s.

MATHEMATICAL MODELS OF LOCATION SIGNALS, REFLECTED FROM THE UNDERLYING SURFACES OF THE LAND AND SEA

Violetta Tyurinova

Saint-Petersburg State University of Aerospace Instrumentation,
Saint-Petersburg, Russia
E-mail: viletteee@yandex.ru

Abstract
When designing complex on-board systems of aircraft, methods of simulation modeling of designed systems on computers are widely used, which reduces the number of semi-natural and full-scale tests of the designed equipment [1]. At the same time, the adequacy of modeling the operating conditions of the equipment to the real conditions of its operation is extremely important, in particular, the adequacy of the input signals of on-board systems to real signals. Therefore, models based on the empirical characteristics of input signals are used as mathematical models of input signals, which most accurately approximates the simulation conditions to the conditions of real testing of equipment in full-scale experiments [2]. The paper considers algorithms for simulation of input signals of on-board systems of aircraft, due to reflections of location signals from the underlying surfaces of the earth and sea.
Keywords: complex system, mathematical modeling, pseudo-random sequence, locating signal, underlying land and sea surfaces, density of distribution, correlation function, Markov model.

INTRODUCTION

At present, one of the most important vital tasks is the task of ecological monitoring of the environment. This task is solved by organizing monitoring with the help of unmanned small aircraft (UAVs), equipped with appropriate equipment, since in this case it is possible to organize monitoring in an automated mode. When solving the task of monitoring, information can be collected from special sensors, and the observation of possible contamination, and the change in the outlines of the coastal edge, etc. [3] In all these cases, at the inputs of the receivers of the on-board equipment of the UAV, there are information or interfering signals due to the reflection of request signals or probing signals from underlying surfaces, which are reflections from the earth and water surfaces, in particular from the sea surface. Therefore, the construction of efficient algorithms for simulating such signals is an important aspect in the development and design of on-board environmental monitoring equipment.

In this paper, we solve a particular problem of synthesizing algorithms for modeling radar signals due to reflections of probing signals from UAV onboard radar stations from the underlying surfaces of the earth and sea. A similar problem is solved when determining the coastal outlines, which are currently changing due to global warming, leading to a change in the level of the world's oceans, and due to volcanic eruptions, in which even new islands arise, and due to hurricanes leading to landslides, etc. At the same time, the parameters of the synthesized algorithms are determined by empirical formulas, which makes it possible to bring the statistical characteristics of the simulated signals closer to the real statistical characteristics of echo signals observed during the operation of on-board systems.

MATHEMATICAL MODELS OF ECHO SIGNALS UNDERLYING LAND AND SEA SURFACES

When choosing mathematical models of the underlying surfaces of the earth and the sea, we will use the information given in the works [4]. Same as in works [3,5] confine ourselves to considering one track of range, but unlike the works [3,5], take into account the spatial correlation of echo signals, which cannot be eliminated [6]. We will rely on empirical formulas for determining the parameters of the laws of distribution of the envelope of echo signals, and with a pulsed probing signal, соответственно, on the laws of distribution of fluctuations of amplitudes, reflected probe pulses.

Under these conditions, as statistical models of fluctuations, one should use the logarithmic-normal distribution law for reflections from the sea surface and the Weibull distribution law, for different values of the shape parameter, for reflections from the underlying earth surface [5]. Regarding the correlation-spectral characteristics of echo signals, we restrict ourselves to taking into account the width of the energy spectrum or, which is equivalent, taking into account the width of the duration of the normalized correlation function

at the level of 0.5, since only for this parameter of the correlation function there are empirical dependencies on the conditions for observing the underlying surfaces.

Under these conditions, it is enough to use only one-dimensional laws of distribution of fluctuations of amplitudes of location signals and normalized correlation functions. Using the appropriate form of correlation functions and two-dimensional distribution laws of fluctuations, it is possible, after calculating the transition probabilities, to limit ourselves to modeling Markov processes [7].

ONE-DIMENSIONAL PROBABILITY DISTRIBUTION DENSITIES OF FLUCTUATIONS IN THE AMPLITUDES OF ECHO-SIGNALS OF THE UNDERLYING SEA AND LAND SURFACES

Probability distribution densities of fluctuations in amplitudes of sea surface echoes

For the statistical description of fluctuations of the sea surface, we use the logarithmic-normal distribution [5]

$$f_L(A) = \frac{1}{\sqrt{2\pi}\sigma_L A}\exp\left[-\frac{\left(\ln A - \ln \overline{A}_L\right)^2}{2\sigma_L^2}\right], x > 0, \quad (1)$$

where σ_L and $\ln \overline{A}_L$ – distribution parameters (1), related to expectation and variance distribution D_L correlation

$$\begin{cases} m_L = M(A) = \overline{A}_L \cdot \exp\left(\dfrac{\sigma_L^2}{2}\right), \\ D_L = D(A) = \overline{A}_L{}^2 \cdot \exp\left(\sigma_L^2\right) \cdot \left(\exp\left(\sigma_L^2\right) - 1\right), \end{cases} \quad (2)$$

where $M(A)$ and $D(A)$ expected and variance operators.

When determining the distribution parameters to calculate the parameters of modeling algorithms, it is necessary to use the data that are used in practice. Actually, this is the coefficient of variation K_L, which is equal to the ratio of the standard deviation to the expected value of the distribution

$$K_L = \sqrt{D(A)} / M(A) = \sqrt{D_L} / m_L = \sqrt{\exp(\sigma_L^2) - 1}, \quad (3)$$

and the average power of the reflected radio pulses, determined by the parameters of the on-board equipment, the conditions of observation of the sea surface and the effective specific reflectivity of the underlying surface [8]. Considering that we determine the power of the radio pulse, the average power of the reflected pulses is equal to half the second initial moment of distribution

$$\tilde{P}_L = 0.5 \cdot \int_0^\infty A^2 \cdot f_L(A) \cdot dA = 0.5\overline{A}_L^2 \exp(2\sigma_L^2). \quad (4)$$

From the expressions (3) and (4) we get

$$\begin{cases} \sigma_L = \sqrt{\ln\left(1 + K_L^2\right)}, \\ \overline{A}_L = \dfrac{\sqrt{2\tilde{P}_L}}{\left(1 + K_L^2\right)}. \end{cases} \quad (5)$$

Numerical values of the variation coefficient K_L can be found in [5], and the average power of the reflected pulses shall be calculated from the expressions given, inter alia, for the case under consideration, in [8].

Probability distribution densities of fluctuations in the amplitudes of echo signals of the earth's surface

For the statistical description of the fluctuations of the earth's surface, we use the Weibull distribution [3]

$$f_W(A) = \alpha_W \lambda_W A^{\alpha_W - 1} \exp\left(-\lambda_W A^{\alpha_W}\right), x > 0, \tag{6}$$

where α_W and λ_W – distribution parameters associated with the mathematical expectation and variance by the relations:

$$\begin{cases} m_W = M(A) = \dfrac{\lambda_W^{-\frac{1}{\alpha_W}}}{\alpha_W} \cdot \Gamma\left(\dfrac{1}{\alpha_W}\right), \\ D_W = D(A) = \lambda_W^{-\frac{2}{\alpha_W}} \cdot \left[\dfrac{2}{\alpha_W}\Gamma\left(\dfrac{2}{\alpha_W}\right) - \dfrac{1}{\alpha_W^2}\Gamma^2\left(\dfrac{1}{\alpha_W}\right)\right], \end{cases} \tag{7}$$

where $\Gamma(\cdot)$ – gamma function.

Just like the log-normal distribution, when determining the distribution parameters for the Weibull calculation of the parameters of modeling algorithms, it is necessary to use those data, that are being used in practice. This is the coefficient of variation, which is equal to the ratio of the standard deviation to the expected value of the distribution

$$K_W = \frac{\sqrt{D(A)}}{M(A)} = \frac{\sqrt{D_W}}{m_W} = \sqrt{2\alpha_W \cdot \frac{\Gamma\left(\dfrac{2}{\alpha_W}\right)}{\Gamma^2\left(\dfrac{1}{\alpha_W}\right)} - 1}, \tag{8}$$

and the average power of the reflected radio pulses $\tilde{P}_W$, determined in the same way as above, by the parameters of the on-board equipment, the conditions of observation of the earth's surface and the effective specific reflectivity of the earth [8]. The average power of the reflected pulses is also equal to half of the second initial moment of distribution, which for the Weibull distribution is calculated by the expression

$$\tilde{P}_W = 0.5 \cdot \int_0^\infty A^2 \cdot f_W(A) \cdot dA = \lambda^{-2/\alpha_W} \cdot \Gamma\left(\frac{2}{\alpha_W} + 1\right). \tag{9}$$

From expressions (8) and (9) it is possible to obtain the values of the Weibull distribution parameters α_W and λ_W, but in general, with an arbitrary value of the form parameter α_W, these values are only obtained by numerical methods.

In one particular case, when the form parameter $\alpha_W = 2$, Weibull distribution passes into Rayleigh distribution

$$f_W(A) = 2\lambda_W A \exp\left(-\lambda_W A^2\right) = f_R(A) = \frac{A}{\sigma_R^2} \cdot \exp\left(-\frac{A^2}{2\sigma_R^2}\right), \; x > 0, \tag{10}$$

in which, as follows from (9) or (10), $\sigma_R^2 = \tilde{P}_W = 1/(2\lambda_W)$. The Rayleigh distribution, as opposed to the two-parameter Weibull distribution, being a special case of the Weibull distribution, is one-parametric. Therefore, to determine its parameter, it is enough to know only the coefficient of variation, which for this distribution is constant and equal to $K_R = \sqrt{(4-\pi)/\pi} \approx 0.52$. It is this distribution, the Rayleigh distribution, that is most commonly used to approximate the density of the probability distribution of location pulses reflected from the earth's surface.

TWO-DIMENSIONAL DISTRIBUTION DENSITIES OF FLUCTUATIONS OF AMPLITUDES OF ECHO SIGNALS OF THE UNDERLYING SEA AND LAND SURFACES

Since, as indicated earlier, we restrict ourselves to considering only the width of the energy spectrum of fluctuations of echo signals, or, equivalently, taking into account the width of the correlation function of fluctuations in the amplitudes reflected from the underlying surfaces of the probing pulses, then it is enough for us to use models described only by two-dimensional laws of amplitude distribution.

Same as in work [3,5] we will confine ourselves to considering only one range track and at the same time we will assume that the conditions for observing the resolution elements of the range track are the same for all elements, which, in practice, is fulfilled with sufficient accuracy.

Density of distribution of probabilities of fluctuations of the amplitudes of the sea surface echo signals

The two-dimensional log-normal distribution density, subject to the restrictions introduced above, is written as [9]

$$f_L\left(A_i, A_j\right) = \frac{1}{2\pi\sigma_L^2 A_i A_j \sqrt{1-r_{Lij}^2}} \exp\left\{-\frac{1}{2\left(1-r_{Lij}^2\right)\sigma_L^2}\cdot \right.$$
$$\left.\cdot\left[\ln^2\frac{A_i}{\overline{A}_L} + \ln^2\frac{A_j}{\overline{A}_L} - 2r_{Lij}\ln\frac{A_i}{\overline{A}_L}\cdot\ln\frac{A_j}{\overline{A}_L}\right]\right\},\ A_i > 0,\ A_j > 0, \tag{11}$$

where parameter r_{Lij} the correlation coefficient of the logarithms of the amplitudes of the probing pulses reflected from *i*-той и *j*-той range paths. This parameter determines the width of the fluctuation spectrum of echo signal amplitudes.

Amplitude correlation coefficient R_{Lij} location pulses reflected from *i*-той и *j*-той distance tracks, is equal to

$$R_{Lij} = \frac{1}{D_L}\int_0^\infty\int_0^\infty \left(A_i - m_W\right)\left(A_j - m_W\right)\cdot f_L\left(A_i, A_j\right)\cdot dA_i \cdot dA_j = \frac{1}{K_L^2}\left(\left(1+K_L^2\right)^{r_{Lij}} - 1\right). \tag{12}$$

In the general case, the normalized correlation function of location signals reflected from the underlying sea surface is written in the form

$$R_L(\tau) = \frac{1}{K_L^2}\left(\left(1+K_L^2\right)^{r_L(\tau)} - 1\right), \tag{13}$$

where $R_L(\tau)$ correlation coefficient between samples of the envelope of the reflected signal, separated in time by τ, or in field $l = c\tau/2$, c - the speed of light. Duration $\tau_{0.5}$ normalized correlation function at the level of 0.5 is found from the equation

$$R_L(\tau_{0.5}) = \frac{1}{K_L^2}\left(\left(1+K_L^2\right)^{r_L(\tau_{0.5})} - 1\right) = 0.5, \tag{14}$$

which allows, when specifying the functional form of the correlation function of the logarithms of the amplitudes $r_L(\tau)$ and values $\tau_{0.5}$ define parameters $r_L(\tau)$ and, accordingly, the parameters of the amplitude correlation function $R_L(\tau)$.

When limited to Markov processes, as the correlation function of the logarithms of the amplitudes, it is necessary to take the exponential function [9]

$$r_L(\tau) = \exp\left(-\alpha_L|\tau|\right), \tag{14}$$

Then the correlation function of the amplitudes $R(\tau)$ determined by the expression

$$R_L(\tau)=\frac{1}{K_L^2}\left(\left(1+K_L^2\right)^{\exp(-\alpha_L|\tau|}-1\right), \tag{15}$$

out of which, knowing $\tau_{0.5}$ and K_L compute α_L

$$\alpha_L=\frac{1}{\tau_{0.5}}\ln\frac{\ln\left(1+0.5\cdot K_L^2\right)}{\ln\left(1+K_L^2\right)}. \tag{16}$$

Expressions (11), (15) and (16) determine the Markov model of fluctuations of amplitudes of location signals reflected from the underlying sea surface, in this case, the probability distribution density and the width of the energy spectrum of fluctuations of the amplitudes are approximated quite accurately, inversely proportional to the duration of the normalized amplitude correlation function at the level 0.5.

Density of distribution of probabilities of fluctuations of the amplitudes of the sea surface echo signals

As a two-dimensional distribution density of the amplitudes of the echo signals of the earth's surface, we take a special case of the Weibull distribution Rayleigh's two-dimensional probability distribution density, which, in the notation introduced above, can be written as [10]

$$f_W(A_i,A_i)=\frac{A_i\cdot A_j}{\sigma_W^4(1-r_{Wij}^2)}\exp\left\{\frac{A_i^2+A_j^2}{2\sigma_W^2(1-r_{Wij}^2)}\right\}\times I_0\left[\frac{r_{Wij}\cdot A_i\cdot A_j}{\sigma_W^2(1-r_{Wij}^2)}\right],\quad A_i>0,\quad A_j>0, \tag{17}$$

where the parameter r_{Wij} coefficient of correlation of sine and cosine quadratures, probing radio pulses reflected from *i*-той and *j*-той range paths. This parameter, as well as above, determines the width of the spectrum of fluctuations in the amplitudes of echo signals reflected from the earth's surface.

Amplitude correlation factor R_{Wij} location impulses, reflected from *i*-той and *j*-той distance tracks, is equal to [10]

$$\begin{aligned}R_{Wij}&=\frac{1}{D_W}\int_0^\infty\int_0^\infty\left(A_i-m_W\right)\left(A_j-m_W\right)\cdot f_W\left(A_i,A_j\right)\cdot dA_i\cdot dA_j=\\&=\frac{\pi}{4(4-\pi)}\left[r_{Wij}^2+\sum_{n=2}^{\infty}\frac{\left[(2n-3)!!\right]^2}{2^{2n-2}(n!)^2}r_{Wij}^{2n}\right].\end{aligned} \tag{18}$$

In the general case, the normalized correlation function of location signals reflected from the underlying ground surface is written as

$$R_W(\tau)=\frac{\pi}{4(4-\pi)}\left[r_W^2(\tau)+\sum_{n=2}^{\infty}\frac{\left[(2n-3)!!\right]^2}{2^{2n-2}(n!)^2}r_W^{2n}(\tau)\right], \tag{19}$$

where $R_W(\tau)$ correlation coefficient between samples of the envelope of the signal reflected from the earth's surface, spaced, as above, in time by τ, and in field $l=c\tau/2$, c - the speed of light. $\tau_{0.5}$ normalized correlation function at the level of 0.5 is found from the equation

$$R_W(\tau_{0.5})=\frac{\pi}{4(4-\pi)}\left[r_W^2(\tau_{0.5})+\sum_{n=2}^{\infty}\frac{\left[(2n-3)!!\right]^2}{2^{2n-2}(n!)^2}r_W^{2n}(\tau_{0.5})\right]=0.5, \tag{20}$$

which allows, when specifying the functional form of the correlation function of the quadratures of the amplitudes of the radio pulses $r_W(\tau)$ and values $\tau_{0.5}$ define parameters $r_W(\tau)$ and, accordingly, the param-

eters of the correlation function of amplitudes $R_W(\tau)$. In contrast to the previous case, here the computation $\tau_{0.5}$ only possible with numerical methods.

When limited to Markov processes, as the correlation function of quadratures of the amplitudes of radio pulses $r_W(\tau)$ you need to take the exponential function

$$r_W(\tau) = \exp(-\beta_W|\tau|), \tag{21}$$

then the amplitude correlation function $R(\tau)$ is defined by the expression

$$R_W(\tau) = \frac{\pi}{4(4-\pi)}\left[e^{-2\beta_W|\tau|} + \sum_{n=2}^{\infty}\frac{[(2n-3)!!]^2}{2^{2n-2}(n!)^2}e^{-2n\beta_W|\tau|}\right]. \tag{22}$$

Expressions (17), (21) и (22) determine the Markov model of fluctuations of the amplitudes of location signals reflected from the underlying earth's surface, while approximating the probability distribution density and the width of the energy spectrum of amplitude fluctuations, inversely proportional to the duration of the normalized amplitude correlation function at the level 0.5.

Conclusion

The paper presents analytical expressions defining Markov mathematical models of fluctuations in the amplitudes of probing pulses from the underlying surfaces of the earth and the sea. The models allow taking into account the density of the distribution of echo signals, which are approximated using the log-normal distribution for reflections from the sea surface and the Rayleigh distribution for reflections from the earth's surface. The models also take into account the energy spectra of the corresponding echo signals, but not the functional form of the spectra themselves, but only their width at a level of 0.5 from the maximum. The width of the spectra is inversely proportional to the duration of the normalized correlation functions at the level of 0.5, which is used in the work by choosing the appropriate functional representations of the normalized correlation functions corresponding to Markov processes.

References

1. Izrantsev V.V., Shepeta D.A. Modeling of external signals of onboard instrument complexes of fifth-generation aircraft // Scientific instrumentation. 2000. Vol. 10. No. 2. pp. 14-19.
2. Ivanova M.S., Isakov V.I., Shepeta D.A. Simulation models of input signals of information processing systems synthesized from empirical data // 2020 Wave Electronics and its Application in Information and Telecommunication Systems, WECONF 2020. 2020. C. 913-1164.
3. Wattimena G.M., Shepeta D.A., Isakov V.I. Determination of the coastal edge using on-board radar // Determination of the coastal edge using on-board radar. Proc. SPIE 11914, SPIE Future Sensing Technologies 2021, 119140D.
4. Semin A.E., Shepeta D.A. Mathematical model of echo signals of the sea surface observed by onboard locators of aircraft // Information and control systems. 2010. No. 2 (45). pp. 21-25.
5. Isakov V.I., Shepeta D.A. Power distribution density of the envelope of location signals reflected from the land-sea edge //Processing, transmission and protection of information in computer systems '21. International Scientific Conference: collection of reports. St. Petersburg, 2021. pp. 25-28.
6. Shepeta A.P., Makhlin A.M. Decorrelation of echo signals of the sea surface during the restructuring of the carrier frequency of the onboard radar // Marine radioelectronics. 2020. No. 1 (71). pp. 36-38.
7. Wattimena G. M., Bozhenko V.V, Tyurinova V.A. Modeling fluctuations of echo signals sea surface when determining the coastal edge // Proceedings of the International Conference “Scientific research of the SCO countries: synergy and integration”. C. 245–252.
8. Blaunstein N.S., Sergeev M.B., Shepeta A.P. Applied aspects of electrodynamics. St. Petersburg, 2016– - 272 p.
9. Shepeta D.A. Development of mathematical models and synthesis of algorithms for modeling input signals of on-board information processing and control systems. dissertation for the degree of Candidate of Technical Sciences: 05.13.14 - St. Petersburg, 2000 - 16 p.
10. Levin B.R. Theoretical foundations of statistical radio engineering. M.: Radio and Communications, 1989. 656 p.

CONTENTS

GREETINGS

PROFESSIONALS SPEAKING

THE EIGHTEENTH ISA EUROPEAN STUDENTS PAPER COMPETITION (ESPC-2022) WINNERS

The scientific edition

ИЗВЕСТИЯ КАФЕДРЫ UNESCO ГУАП «ДИСТАНЦИОННОЕ ИНЖЕНЕРНОЕ ОБРАЗОВАНИЕ»

Сборник статей

Выпуск 7

BULLETIN OF THE UNESCO DEPARTMENT “DISTANCE EDUCATION IN ENGINEERING” OF THE SUAI

Collection of the papers

Issue 7

ISBN: 978-5-8088-1709-8

9 785808 817098

Computer imposition
Papers are publish in author's edition

Подписано в печать 07.04.2022. Дата выхода в свет: 12.04.2022. Формат 60×84 1/8.
Усл. печ. л. 20,7. Тираж 150 экз. Заказ № 154.

Редакционно-издательский центр ГУАП
190000, г. Санкт-Петербург, ул. Б. Морская, 67, лит. А

Распространяется бесплатно

Submitted for publication 07.04.2022. Passed for printing 12.04.2022.
Format 60×84 1/8.

Department of operative polygraphy SUAI
67A, B. Morskaia, 190000, Saint Petersburg, Russia

Free distribution